Conceptual Design of a 1000-MW(e) Heterogeneous Oxide LMFBR
Volume 1

NP-1616, Volume 1
Research Project 620-32

Final Report, November 1980
Work Completed, August 1980

Prepared by

SCIENCE APPLICATIONS, INC.
1211 West 22nd Street, Suite 901
Oak Brook, Illinois 60521

Principal Investigators
W. P. Barthold
C. P. Tzanos

With Contributions by
F. Gunnison
N. Hanan
R. Jarka
P. Lam
R. May
B. Singer

Prepared for

Electric Power Research Institute
3412 Hillview Avenue
Palo Alto, California 94304

EPRI Project Manager
R. K. Winkleblack

Developing Applications and Technology Program
Nuclear Power Division

ORDERING INFORMATION

Requests for copies of this report should be directed to Research Reports Center (RRC), Box 50490, Palo Alto, CA 94303, (415) 965-4081. There is no charge for reports requested by EPRI member utilities and affiliates, contributing nonmembers, U.S. utility associations, U.S. government agencies (federal, state, and local), media, and foreign organizations with which EPRI has an information exchange agreement. On request, RRC will send a catalog of EPRI reports.

NOTICE

Prepared by
Science Applications, Inc.
Oak Brook, Illinois

EPRI PERSPECTIVE

PROJECT DESCRIPTION

The work reported herein, under RP620-32, is a follow-on to that reported in EPRI Interim Report NP-1000. Related work is reported in EPRI Final Reports NP-1615, Core Restraint and Seismic Analysis of a Large Heterogeneous Free-Flowering Core Design; and NP-1617, Hardware Concepts for a Large Low-Energetics LMFBR Core. These two reports and NP-1616 are the final reports of the project.

PROJECT OBJECTIVE

The objective of this project is to show the feasibility and practicality of large liquid metal fast breeder reactor cores that have significantly reduced sodium void coefficients of reactivity due to the placement of blanket subassemblies at strategic locations within the core assembly. Such cores will have characteristics that will reduce the energetics of a hypothetical core disruptive accident to a very low value such that the impact on the vessel head would be tolerable.

PROJECT RESULTS

The objective has been accomplished. The reference core design is shown by analysis to be a sound basis for final development of a safe, licensable, reliable, and efficient breeder core. Further improvements may be made in final engineering and experimental verification. This reference design will be an excellent "yardstick" with which to measure whether future refinements truly represent real improvements in such areas as excess plutonium production, low energetics, full-power days of power produced between shutdowns for refueling, peak clad temperatures, maximum-to-average ratio of sodium temperature at the fuel and blanket subassemblies outlets, maximum-to-average burnup ratios, and other factors of merit.

This report is directed to LMFBR core designers, neutronics and thermohydraulic analysts.

R. K. Winkleblack, Project Manager
Nuclear Power Division

ABSTRACT

A numerical core/blanket design is presented for a large--1000-MW(e)--liquid metal fast breeder reactor (LMFBR) that has a much lower sodium void coefficient of reactivity than would be the case for a core assembly made up entirely of fuel subassemblies with an appropriate number of control rods. Blanket subassemblies are placed among the fuel subassemblies to form a "heterogeneous" core/blanket assembly that would have low energetics in case of a hypothetical core disruptive accident (HCDA) but still retains good thermohydraulic performance, good breeding gain, and a reasonable fuel cycle.

TABLE OF CONTENTS

ILLUSTRATIONS

XX

TABLES

SUMMARY

Sodium void reactivity is one of the main parameters of concern in LMFBR safety. Sodium voiding during an unprotected loss-of-flow transient in large homogeneous LMFBRs introduces high ramp rates of positive reactivity. As a consequence, such a transient has the potential to lead to energy releases that may challenge the integrity of the containment. Thus, there is a strong incentive for developing designs of large LMFBRs that have low sodium void reactivities. Heterogeneous designs that consist of successive core and blanket zones, in the radial direction, have the potential of achieving low sodium void reactivities. Previous analyses of large heterogeneous LMFBRs have indicated that a sodium void reactivity of $2.50 or less is sufficient to assure a low energetics potential in the event of a core disruptive accident. This reactivity refers to voiding the core plus upper axial blanket part of the core fuel assemblies. The purpose of this research project was to develop a conceptual design of a 1000 MWe heterogeneous oxide LMFBR that is mainly constrained by a sodium void reactivity of about $2.50, and has the following performance characteristics:

1. Acceptable Doppler coefficient and assured voiding incoherence.
2. High fissile material gain/cycle and doubling time of 15-16 years.
3. Conservative technology base in regard to:
    a. peak cladding temperatures
    b. fuel linear heat rating
    c. peak-to-average outlet temperature ratio over the total reactor.

To develop this conceptual design, trade-off and sensitivity studies, optimization studies and design analyses were performed. In these studies and analyses a set of common basic assumptions and ground rules were used which leaned heavily on the ground rules developed for the Proliferation Resistant Preconceptual Core Design Study (PRLCDS).

The core configuration is a central blanket heterogeneous configuration developed

in an earlier core layout optimization study (EPRI-NP-1000). It is a compromise between low sodium void reactivity, reasonable neutronic coupling between core fuel regions and reasonable flat power distribution. It consists of four internal blanket regions and three core fuel regions.

The selection of the final design parameters was based on certain performance constraints and performance measures. The performance constraints were:

- sodium void reactivity of $\leq$ \$2.50
- doubling time of 15-16 years or less.

The performance measures were:

- fissile material gain per cycle
- fissile inventory
- burnup swing per cycle
- peak discharge burnup
- power peaking factor
- relative fuel cycle cost.

Using these performance constraints and measures, optimization and sensitivity studies were performed to select the axial blanket thickness, the radial blanket residence time, the fuel cycle length, the number of enrichment zones, the fuel pin diameter, and the plenum length. Based on these studies the following selections were made:

- An axial blanket thickness of 15 inches
- A radial blanket residence time of 5 cycles
- A core and internal blanket fuel residence time of three cycles consistent with a cycle length of 255.5 full-power days
- A core fuel pin diameter of 0.28 inches
- Two enrichment zones
- A fission gas plenum length of 30 inches.

After these parameters were fixed, a final assembly design and final nuclear thermal-hydraulic and fuel life analyses as well as a limited transient analysis were carried out.

The main assembly design parameters are as follows. The fuel assembly contains 271 pins with a pin pitch-to-diameter ratio of 1.171. The assembly design is consistent with a fuel bundle pressure drop of 60.1 psi. The duct wall thickness is 0.100 in. The inside flat-to-flat distance is 5.482 in. and the assembly pitch is 5.907 in. The peak stress in the duct corner is 38,783 psi which is well below the maximum allowable stress for 20% CW316SS. The fuel pins are wire-wrapped with a helical pitch of 12 in. and a wire diameter of 0.047 in. The cladding thickness is 0.014 in.and the fuel inside the cladding tube has a smear density of 88% T.D. The total bundle length is 100 in.,i.e., 40 in. of active core height, 30 in. of axial blanket,and 30 in. of plenum.

The blanket assembly duct has the same dimensions as the fuel assembly duct. It contains 127 pins with a pitch-to-diameter ratio of 1.07. The blanket pin diameter is 0.447 in., the cladding thickness is 0.013 in.,and the fuel smear density is 90% T.D. The wire wrapped around the pin has a diameter of 0.030 in. and a helical pitch of 6 in.

No specific design for a control assembly was developed at this stage. The assumption was made that the control assembly of this reactor is a linearly enlarged CRBRP control assembly, which yields the same material volume fractions as the CRBRP control assembly. An EBR-II type control system, that uses natural boron control rods with fuel assembly followers, was also briefly evaluated.

The nuclear performance and thermal-hydraulic analyses were carried out for the first cycle and an equilibrium cycle where fresh and irradiated fuel were homogenized for the neutronic calculations. To obtain a measure for the differences between this approach and a discrete fuel management, a limited discrete fuel management analysis was performed for the first four cycles. As previously mentioned, for the reference fuel management a cycle length equal to 255.5 full power days and residence times of three cycles for the core and internal blanket assemblies and five cycles for the radial blanket assemblies were chosen. At the end of each cycle, one third of the core and internal blanket assemblies and one fifth of the radial blanket assemblies were replaced with fresh fuel assemblies in a scatter refueling approach. Since, reactor performance characteristics such as:

a. fissile inventory
b. fissile gain
c. doubling time

d. fuel cycle cost
e. sodium void reactivity and
f. cladding temperatures

are dependent on fuel management, in addition to this reference fuel management scheme, nuclear and thermal-hydraulic performance analyses were carried out for:

a. two and three-year straight burn of the core and internal blanket fuel.
b. refueling every year; core and internal blanket fuel residence time of two years.

The analyses based on the first cycle and the equilibrium cycle, with the reference fuel management scheme, will be discussed first, and then the discussion on the discrete fuel management and on the additional fuel management schemes will follow.

The nuclear performance of the reactor can be summarized as follows:

1. The average core fuel enrichment is 17.12% at BOL and 16.46% at BOEC.
2. The total reactor fissile inventory is 4261 kg at BOL and 4762 kg at BOEC.
3. The fraction of power produced in the core decreases from 89.96% at BOL to 74.83% at EOEC while the fraction of power produced in the internal blankets increases from 6.35% at BOL to 17.77% at EOEC.
4. The core peaking factor is 1.484 at BOL and 1.482 at EOEC.
5. The nominal peak linear power rating in the core is equal to 14.2 kW/ft and occurs at BOL. The linear power ratings of the internal and radial blankets peak at EOL and are 16.4 kW/ft and 9.6 kW/ft, respectively. Both peak linear power ratings in the core and the blankets are below the design limiting values of 15 kW/ft and 16.5 kW/ft, respectively.
6. The peak total flux is 5.3×10^{15} n/cm^2-sec at BOL, and 5.2×10^{15} n/cm^2-sec at EOEC.
7. The peak fast fluence is 2.06×10^{23} n/cm^2 in the core, 1.77×10^{23} n/cm^2 in the internal blankets, and 1.94×10^{23} n/cm^2 in the radial blankets.
8. The peak discharge burnup (pellet) is 107,349 MWD/T for the core, 33,660 MWD/T for the internal blankets, and 21,690 MWD/T for the radial blanket.
9. The burnup swing is 0.35%Δk.
10. If the PRLCDS ground rules are used to establish control system requirements, then 60% and 90% enriched BC_4 primary and secondary, respectively, control rods are needed. However, if more realistic assumptions are used to calculate the

control system requirements, then natural boron can be used in both control systems. Finally, the PRLCDS control requirements are easily satisfied by EBR-II type primary and secondary systems that consist of natural boron control rods with fuel assembly followers.

11. The Compound System Doubling Time (CSDT) depends on the parked position of the secondary system control rods. Doubling time improves as the parked position of the control rods moves closer to the top of the upper axial blanket. Thus, the CSDT is 15.17 years if the secondary system is parked at the top of the upper axial blanket and 16.25 years if this system is parked at the core-upper axial blanket interface.
12. Voiding of the flowing sodium (sodium within the assembly) in the core and the upper axial blanket gives a reactivity of $1.32 at BOL and $2.58 at EOEC.
13. The core isothermal Doppler coefficient at BOL is 0.0055 for sodium-in and 0.0039 for sodium-out conditions and decreases to 0.0046 and 0.0029, respectively, at the EOEC. The internal blanket isothermal Doppler coeffcient is 0.0048 and 0.0040 at BOL for sodium-in and sodium-out, respectively, and increases to 0.0059 and 0.0044 at EOEC.
14. For two rows of radial reflector assemblies the thirty-year fast fluence at the outer surface of the radial reflector is 8.97×10^{21} n/cm^2. This is well below the limiting values of 2×10^{22} n/cm^2.
15. At BOL, the uniform axial fuel expansion coefficient is -0.07 cents/mil and the uniform radial expansion coefficient is -0.151 cents/mil.
16. Since sodium void reactivity is the main constraint of this conceptual design, a review of a wide range of sodium void reactivity experiments was carried out to evaluate computed vs. measured sodium void reactivities. This review has shown that, in general, computed sodium void reactivity values are larger than the measured values. Thus, the calculated void reactivity of $2.58 for this EPRI conceptual design is expected to be conservative.

The orificing of LMFBRs is based on considerations such as: a) assembly lifetime, b) transient limitations, c) impact on upper internals structure, d) assembly power-to-flow ratio, and e) cooling requirements of other components than assemblies. These considerations can be translated into constraints on the cladding midwall temperature. The coolant flow allocation to orificing zones is then determined such that these constraints are satisfied.

Since transient analysis as well as analysis of the upper internal structure was not carried out at this stage of the project, reactor orificing was based on either equalizing peak coolant temperature rises or peak cladding midwall temperatures.

The assignment of assemblies to orificing zones was based either on assembly power or assembly peak pin power. Thus, the following four orificing strategies were used

1. Orificing based on assembly power and equal peak assembly coolant temperatures.
2. Orificing based on assembly power and equal peak cladding midwall temperatures.
3. Orificing based on assembly peak pin power and equal peak assembly coolant temperatures.
4. Orificing based on assembly peak pin power and equal peak cladding midwall temperatures.

The peak coolant and cladding temperatures occur at BOL conditions for the core fuel assemblies and at EOL conditions for the blanket assemblies. Thus, for the core assemblies, the BOL assembly power, peak assembly coolant temperature, assembly peak pin power and peak cladding midwall temperature are used. For the blanket assemblies the EOL values of the same quantitites are used.

A total of nine orificing zones have been used;i.e., three for the core, four for the internal and radial blankets, one for the radial reflector and one for the control assemblies. To avoid inadvertent misplacement of an assembly (core, blanket, control, reflector) these nine orificing zones and the two enrichment zones require 12 discriminator zones.

To guarantee that adequate margins are provided so that design limits and requirements are not exceeded, the CRBRP hot channel factors have been used to account for analytical and experimental uncertainties, instrumentation accuracy, manufacturing tolerances, and uncertainties in physical properties and correlations.

The accurate determination of coolant pressure drops and temperature distributions in wire-wrapped LMFBR core and blanket assemblies is dependent upon the use of correlations that accurately predict the assembly average friction factor and the subchannel flow splits. The Novendstern correlations are presently utilized by LMFBR core design codes to determine these assembly parameters. Recently, Chiu, Todreas, and Rohsenow have developed new correlations for predicting bundle coolant flow split parameters and bundle average friction factors. An evaluation of these two methodologies was performed that lead to the conclusion that the correlations developed by Chiu et al. are more accurate. Thus, the Chiu et al. correlations were used in the thermal-hydraulic analysis.

The analysis of the thermal-hydraulic performance of the reactor was based on the following plant conditions:

- Total reactor power 3084 MW (thermal).
- Reactor coolant inlet temperature of 595^{o} F.
- Reactor coolant outlet temperature of 875^{o} F.
- A 5% of the total flow is used as a cold by-pass flow.

The results of this analysis can be summerized as follows:

1. The total reactor flow rate, not including the cold by-pass flow, is equal to 116,463,258 lb/hr. The flow split among the different reactor regions depends slightly on the orificing strategy. Thus, the core flow fraction varies from 70.5% to 72.1%, the flow fraction allocated to the blanket varies from 27.4% to 28.9%,and the flow fractions allocated to control and shield assemblies is equal to 0.6%. The maximum assembly average coolant velocity depends also on the orificing strategy and varies from 22.0 ft/sec to 23.1 ft/sec.
2. The orificing strategies that equalize the peak cladding midwall temperatures yield lower 2σ power cladding midwall temperatures and between them, the one that is based on pin power yields the lowest 2σ peak cladding midwall temperature which is 1220^{o} F. If orificing is based on assembly power and equal peak assembly coolant temperatures, the 2σ peak cladding midwall temperature is raised to 1300^{o} F.
3. The orificing strategies that equalize the peak assembly coolant temperatures yield lower assembly coolant temperatures and between them, the one that is based on assembly power yields the lowest peak assembly coolant temperature which is 990^{o} F. However, the difference between the lowest and maximum peak assembly coolant temperatures,that results from the four orificing strategies,is 16^{o} F.
4. The maximum duct wall temperatures and duct wall temperature differences are functions of the reactor region. Also, there is a small variation in these maximum values as the orificing strategy varies. The largest of these maximum duct wall temperatures is 923.1^{o} F (BOL) in the core, 847.6^{o} F (EOEC) in the internal blankets,and 833.1^{o} F (EOEC) in the radial blanket. Similarly, the largest of these maximum duct wall temperature differences is 161.3^{o} F (BOL) in the core, 133.8^{o} F (BOL) in the internal blankets,and 151.6^{o} F (BOL) in the radial blanket.
5. The maximum pressure drops are provided either by the first core orificing

zone (it includes the maximum power core assembly), or by the first blanket orificing zone (it includes the maximum power blanket assembly), and they vary with the orificing strategy from 51.0 psi to 53.2 psi. The pressure drop used to design the fuel assembly is well above these values to accomodate calculational uncertainties.

In heterogeneous reactor designs, the buildup of fissile material in the internal blankets, during burnup, results in a power swing from the core zones to the internal blankets as burnup proceeds. To avoid excessive peak cladding temperatures in the internal blanket assemblies at EOL, these assemblies must be overcooled and core assemblies must be undercooled at BOL. Thus, peak cladding temperatures are higher in heterogeneous than equivalent homogeneous LMFBR designs. This difference in peak cladding temperatures can be reduced, if the flow allocated to core and blanket assemblies can be adjusted as burnup proceeds, such that the flow matches the power as closely as possible.

Simple analytical models were developed to evaluate the reduction in peak coolant temperature (and consequently, peak cladding temperature), that can be achieved by continuously adjusting the flow split between the core and blanket assemblies. Continuous adjustment of the flow split between the core and blanket assemblies reduces the peak assembly coolant temperature. This reduction is small ($\sim 10^{0}$ F) if the reactor is partially refueled every year. If a straight burn fuel management is used, the reduction in peak assembly coolant temperature depends on the residence time of the radial blanket fuel. The maximum reduction, $\sim 32^{0}$ F, is achieved if all the fuel in the reactor (core, internal and radial blanket) has the same residence time.

These reductions were obtained under the assumption that the power of all core assemblies decreases uniformly with burnup. Since there are a few core assemblies for which power either increases or changes very little with burnup, the analysis has shown that these reductions can be retained if the flow feed of these core assemblies is connected with the flow feed of the blanket assemblies.

The fuel element performance parameters such as fission gas release and pressure, gap closure, fuel-cladding mechanical interaction, cladding stresses and strains were determined using the LIFE-III code. The release of fission gas from the fuel pellets into the plenum, and consequently,the concentration of fission gas in the plenum, increases as fuel irradiation proceeds. Thus, 50 hours after startup, 12.5%

of the total fission gas produced has been released and the corresponding concentration of fission gas in the plenum is 0.5%. At 1753 hours, 68.4% of the total fission gas produced has been released and the corresponding concentration of fission gas in the plenum is 64.6%. Both, the fission gas release and the concentration of fission gas in the plenum slowly approach their respective asymtoptic values of 90 and 96%.

The plenum pressure increases linearly with respect to irriadiation time. It starts with a value of 43.4 psia at 50 hours after startup, and increases to 1030.9 psia at 18,050 hours (EOL).

The radial gap between the fuel pellet and the cladding, which is 3.5 mils, starts to close at approximately 63 hours after startup at 20 inches above the bottom of the active fuel. At 8,000 hours the gap is closed in the active fuel part of the pin. After 8,800 hours the gap starts to reopen at 28 inches above the bottom of the active fuel. At EOL (18,050 hours) the gap is open for the part of the active fuel pin above the core mid-plane

The cladding hoop stresses reach local peak values of 6,500 and 4,000 psia, respectively, at 28 and 36 inches above the bottom of the active fuel before the fuel-cladding gaps reopen at 8,800 hours. After reopening of the gaps, the cladding hoop stresses rise monotonically to peak values of 8,500 and 9,000 psia, respectively, at the 28 and 36 inch locations.

There is an incubation period of approximately 8,000 hours for both the diametral change and inelastic strain. The maximum diametral change increases slowly from 0.96% at 50 hours after startup to 1.50% at 8,000 hours. Then, it increases more rapidly to 6.16% at 18,050 hours. Similarly, the inelastic strain increases slowly from a zero value to 0.4% at 8,000 hours and then accelerates to 1.96% at 18,050 hours. Using either a 6% total cladding diametral change or a 2% inelastic strain as a tentative fuel failure criterion, the reference fuel pin will not fail.

As mentioned earlier, moving the parked position of the secondary control system from the core-upper axial blanket interface to the top of the upper axial blanket reduces the CSDT by about one year. However, this change in the parked position of the secondary system affects the transient performance of the reactor. The time delay between a protection system scram signal and the entry of the secondary control

rods into the core, is increased by the time needed for the control rods to cross the upper axial blanket thickness. To determine the impact that the parked position of the secondary control system has on the transient perrmance of the reactor, uncontrolled rod withdrawal transients have been analyzed for two secondary system parked positions, i.e., control rods parked at the core-upper axial blanket interface and control rods parked at the top of the upper axial blanket. In these analyses the same trip points and delay times were used as in CRBRP.

The results of these analyses show the following. Moving the parked position of the secondary control system from the top of the core to the top of the upper axial blanket delays the insertion of the rods into the core by 400 msec. This delay increases the 3σ maximum cladding midwall temperature, during an unprotected control rod withdrawal transient, by 50^{0} F. If the pump trip is delayed by 400 msec - to compensate for the delay of the insertion of the control rods - the increase in the 3σ maximum cladding midwall temperature, during the transient, is reduced by $\sim$60%,i.e., from $\sim 50^{0}$ F to 20^{0} F.

Large heterogenous LMFBRs are attractive because they have significantly lower core sodium void reactivities than equivalent homogeneous LMFBRs. However, the total reactivity resulting from voiding the core and the internal blankets of a heterogeneous LMFBR is comparable to the sodium void reactivity of an equivalent homogeneous LMFBR. Thus, if boiling occurs simultaneously in the core and the internal blankets, the safety advantage of the low core sodium void reactivity is lost.

The assembly coolant temperature rise is a function of the assembly power-to-flow ratio. If the power-to-flow ratio is the main parameter that determines the coolant temperature rise during a transient, then the incoherence in sodium boiling, between core and internal blanket, can be improved by lowering the power-to-flow ratio in the internal blanket assemblies.

The effect of the power-to-flow ratio on the incoherence of sodium boiling has been investigated by analyzing an unprotected loss-of-flow accident with different power-to-flow ratios. The analysis has shown that two pin channels which either have the same pin design, but different power ratings, or have different pin diameters, will not boil coherently even if they have the same power-to-flow ratio at steady-state (and consequently,the same coolant outlet temperature at steady-state). Thus, even if the hottest core and blanket channels have the same power-to-flow

ratio at steady-state, at initiation of sodium boiling in the core the outlet coolant temperature in the hottest blanket channel is significantly below boiling. Decreasing the blanket power-to-flow ratio increases the temperature difference between the hottest core and blanket channels, at initiation of boiling in the core, but this increase is only a fraction of the difference that is inherently present.

As mentioned earlier, the nuclear and the thermal-hydraulic performances, of the reactor analyzed in this report, are based on the first cycle and on an equilibrium cycle where fresh and irradiated fuel are homogenized for the neutronic calculations. To obtain a measure for the differences between this approach and a discrete fuel management, a limited discrete fuel management analysis has been performed for the first four cycles. This discrete fuel management has not been optimized.

The results of the nuclear analysis show that average fuel enrichments, fissile inventories and fissile gain as well as breeding ratios in the core, internal blanket, and radial blanket converge to their equilibrium values as we proceed from the first to the fourth cycle. The rate of convergence increases as we move from the radial blanket to the internal blanket, to the core, and the whole reactor. The maximum peak discharge burnup in the core is ~19% higher than the value determined from the equilibrium cycle analysis. The maximum peak discharge burnup in the internal blanket is ~12% lower than the values determined from the equilibrium cycle analysis.

The comparison of the results obtained from a thermal-hydraulic analysis of the reactor based on discrete fuel management with the results obtained from the analysis that was based on BOL and equilibrium cycle conditions shows that:

1. The assignment of assemblies to orificing zones is different for 16% of the core and blanket assemblies.
2. The discrete fuel management analysis gives about 4% higher maximum assembly bundle average pressure drop.
3. The difference in peak assembly coolant temperatures is negligible.
4. The difference in peak nominal cladding midwall temperatures is small ($\sim 10^{\circ}$ F).
5. The difference in the highest duct wall temperatures and duct wall temperature differences is $\sim 11^{\circ}$ F and $\sim 13^{\circ}$ F, respectively.

6. If individual cycle information is not needed, the homogenized equilibrium cycle analysis is adequate and requires much less manpower and computation time than the discrete fuel management analysis.

To investigate the impact of the fuel management scheme on the performance of the reactor, in addition to the reference scheme, the nuclear and the thermal-hydraulic performances of the reactor were analyzed for the following schemes:

a. two and three-year straight burn of the core and internal blanket fuel.
b. refueling every year; core and internal blanket fuel residence time of two years.

In the first case, the radial blanket fuel residence time was six years. At the end of each cycle one third, for two-year straight burn, and one half, for the three-year straight burn, of the irradiated radial blanket fuel were replaced with fresh fuel. In the second case, the radial blanket fuel had a residence time of five years, and at the end of each cycle one fifth of it was replaced with fresh fuel. In all cases the assembly design was the same as for the reference design, which was based on core and internal blanket fuel residence times of three years, radial blanket fuel residence time of five year, refueling every year. The capacity factor was 70% for the partial core refueling case, 77.5% and 80% for the two-year and three-year straight burn cores, respectively. The following conclusions have been derived from the analysis.

The equilibrium cycle fresh fuel feed enrichment increases with core fuel residence time. The two-year fuel residence time core with refueling every year, has the lowest fresh fuel feed enrichment, 17.06% and the three-year fuel residence time core with straight burn, has the highest fresh fuel feed enrichment, 17.35%. The straight burn reactors have lower BOEC inventories than the corresponding partial refueling reactors. The three-year core fuel residence time reactor with straight burn, had the lowest BOEC fissile inventory, 4573.7 kg, and its corresponding partial refueling reactor, has the highest BOEC fissile inventory, 4,761.6 kg.

The power swing from the core zones to the internal blanket zones increases with fuel residence time and with switching from partial refueling to straight burn. Thus, the two-year fuel residence time core with refueling every year, has the smallest swing and the three-year straight burn core has the largest swing. In the first case, the fraction of power produced in the internal blankets increases

from 6.35% at BOL to 15.19% at EOEC. In the second case, the fraction of power produced in the internal blankets increases from 5.99% at BOEC to 23.59% at EOEC.

The core fuel peak discharge burnup increases with fuel residence time and with switching from partial refueling to straight burn. Thus, the two-year fuel residence time core with refueling every year, has the lowest peak discharge burnup, 72,724 MWD/T, and the three-year straight burn core has the maximum peak discharge burnup, 121,409 MWD/T. The internal blanket fuel peak discharge burnup follows the same trend and varies from 17,610 MWD/T to 38,414 MWD/T, respectively.

The average breeding ratio of the equilibrium cycle decreases with core fuel residence time and with switching from partial refueling to straight burn. The reactor which has a two-year core and internal blanket fuel residence time with refueling every year has the largest equilibrium cycle average breeding ratio, 1.431, and the three-year straight burn reactor has the smallest equilibrium cycle average breeding ratio, 1.386. In the case of partial core refueling every year, the BOEC fissile inventory increases with core fuel residence time. The fissile gain shows the opposite trend. For straight burn, the BOEC fissile inventory decreases and the fissile gain increases with core fuel residence time. Finally, for the same refueling scheme, the compound system doubling time decreases as the core fuel residence time increases. The straight burn reactors have lower compound system doubling times than the partially refueled reactors and the three-years straight burn reactor has the lowest compound system doubling time, 13.07 years.

Fuel cycle cost decreases as the core fuel residence time increases, and as partial refueling is replaced by straight burn. Thus, the reactor that has two-year core fuel residence time with refueling every year, has the highest fuel cycle cost, and the three-year straight burn reactor has the lowest fuel cycle cost.

Both straight burn reactors have higher EOEC sodium void reactivities than the partially refueled reactors. Especially, the three-year straight burn reactor has an EOEC sodium void reacitivity of $3.22, which is much higher than the design objective of $2.50. The reactor with two-year core fuel residence time and refueling every year, has the lowest EOEC sodium void reactivity, $2.37. Since the sodium void reactivity of the three-year straight burn option is much higher than the design objective of $2.50, this option was not anlayzed any further.

The peak assembly coolant temperatures are practically the same for all three fuel

management schemes examined. Since the power swing from the core to the blanket assemblies increases as the core and internal blanket fuel residence time increases, the reference design, which has a core and internal blanket fuel residence time of three years, has a peak 2σ cladding midwall temperature that is 18^{o} F and 35^{o} F, respectively, higher than the corresponding temperature in the two years straight burn reactor and the reactor that is refueled every year and has a two-year core and internal blanket fuel residence time.

A summary of the values of the main reactor performance parameters, obtained from the different fuel management schemes, i.e., fissile inventory, fissile gain, doubling time, fuel cycle cost, sodium void reactivity, and peak cladding temperature, is given in Table 1. The reactor with a three-year core fuel residence time and refueling every year,i.e., the reference design, is the best compromise.

Breeding performance can be improved if the duct wall thickness is reduced. Such a reduction can be achieved if the pressure drop across the assembly duct wall is reduced by "venting" the duct. A parametric study was performed to assess the incentives for "venting" the assembly ducts. The results of this study can be summarized as follows.

A 10 mil reduction in duct wall thickness reduces doubling time by slightly less than six months. The same reduction in sodium gap reduces the doubling time by less than one month. A reduction in sodium gap size of 60 mils is equivalent to a 10 mil reduction in duct wall thickness in regard to doubling time.

A 10 mil reduction in duct wall thickness requires a pressure drop reduction of approximately 20%. This pressure drop reduction is the equivalent of a 20 inch reduction in effective length of the fuel bundle. A one year reduction in doubling time requires a 20 mil reduction in duct wall thickness. This in turn requires a 40% reduction in pressure drop, which is the equivalent of a 40 inch effective length reduction for the bundle. For the design under consideration this must be considered the upper limit in improving breeding performance.

TABLE 1

FISSILE INVENTORY, FISSILE GAIN, COMPOUND SYSTEM DOUBLING TIME,
FUEL CYCLE COST AND CORE PLUS UPPER AXIAL BLANKET FLOWING SODIUM VOID REACTIVITY

	Refueling Every Year					
	Core Fuel Residence Time of Two Years		Core Fuel Residence Time of Three Years		Two-Year Straight Burn	
	BOEC	EOEC	BOEC	EOEC	BOEC	EOEC
Fissile Inventory (kg)	4661.3	4988.1	4761.6	5072.3	4609.6	5303.5
Fissile Gain (kg)	326.8		310.7		693.9	
CSDT (Years)	16.30		15.7		14.46	
Relative Fuel Cycle Cost	1.00		0.72		0.86	
Sodium Void Reactivity ($)		2.37		2.58		2.74
2σ Peak Cladding Midwall Temperature (° F)	1185		1220		1202	

1.0 INTRODUCTION

Radially heterogeneous core configurations are effective means to reduce sodium void reactivity. This reduction results, in principle, from an increase in the neutron leakage, with respect to a homogeneous core, due to the placement of blanket assemblies or blanket regions into the fuel region. While one can correlate the number of internal blanket assemblies to a reduction in sodium void reactivity the arrangement of those internal blanket assemblies in the core is of great significance. In general, radially heterogeneous cores can be designed as tightly or loosely coupled cores with center core or center blanket arrangements. Core height, the number of core regions and the number of fuel pins per assembly are additional variables in an optimization of basic heterogeneous core configurations.

Earlier, an extensive study was carried out to develop core configurations for 1000 MWe LMFBRs[1] which were constrained by an upper sodium void reactivity limit of $2.50 and a doubling time of approximately 15-16 years or less. All cores were subject to a common set of nuclear, mechanical and thermal-hydraulic design assumptions. Figures of merit were specific inventory, peak clad temperature, maximum discharge burnup, control requirements,and fuel cycle cost. This study led to a center blanket configuration where the inner core regions were tightly coupled and the outer core regions were loosely coupled.

1.1 OBJECTIVE

The objective of this activity was to develop a conceptual design of a 1000 MWe heterogeneous oxide LMFBR based on the central blanket configuration selected in the earlier study. The major constraint for this design was the sodium void reactivity limit of about $2.50. The desired performance characteristics are:

1. acceptable Doppler coefficient and assured voiding incoherence

2. high fissile material gain/cycle and doubling time of 15-18 years
3. conservative technology base in regard to
    a. peak cladding temperatures
    b. linear heat rating for fuel
    c. low peak-to-average outlet temperature ratio over the total reactor

To assure feasibility of the design it was necessary to analyze the performance of this reactor not only for an equilibrium cycle but for the first four consecutive cycles of operation too. The control system was assumed to be similar to the system used for CRBRP. However, an EBR-II type control system that uses natural boron control rods with fuel assembly followers was also briefly evaluated.

1.2 OUTLINE OF STUDY

The work described in this report consisted of

- trade-off and sensitivity studies
- optimization studies
- design analyses

To put these activities into proper perspective, Section 2.0 of this report will describe the general approach taken in this study. Design assumptions and ground rules are listed and the methodology is described. This section is followed by a description of the various assemblies and the core layout. Section 4.0 discusses the results of the core performance analysis and consists of four segments describing the nuclear, thermal-hydraulic, fuel life,and transient analyses. The results of the various trade-off, sensitivity,and optimization studies are discussed in the Appendices.

2.0 APPROACH

2.1 ASSUMPTIONS AND GROUND RULES

The assumptions and ground rules used for this design effort are very similar to those used during the earlier phase[1] which in turn leaned heavily on the ground rules developed for the Proliferation Resistant Preconceptual Core Design Study (PRLCDS) project[2].

The general parameters for the reactor are:

- Reactor lifetime, years.	30
- Reactor power, MWth	3000
- Thermal efficiency*, %	32
- Reactor inlet temperature, ^{o}F	595
- Reactor outlet temperature, ^{o}F	875
- Cladding and duct material	Improved 20% CW316SS

The limiting fuel assembly parameters are:

- Spacer Type	Wire
- Spacer Pitch, inches	12
- Minimum Cladding Thickness, mils	12
- Minimum Cladding Thickness-to-o.d. Ratio	0.039
- Minimum Driver Pin Pitch-to-Diameter Ratio	1.15
- Nominal Peak Linear Power, kW/ft	15.0
- Plenum Location	Top
- Maximum Nominal Subassembly Outlet Temperature, ^{o}F	1075^{o}F

*This value is defined as the ratio of gross electric power (turbine-generator output) to gross thermal power (reactor power plus pumping heat input).

- Smear Density, % of Theoretical — 90.0

The limiting blanket assembly parameters are:

- Minimum Cladding Thickness, mils — 12
- Minimum Cladding Thickness-to-o.d. Ratio — 0.0229
- Pin Pitch-to-Diameter Ratio — 1.07
- Maximum Smear Density, % of Theoretical — 90.0
- Nominal Peak Linear Power, kW/ft — 16.5

The flow parameters are:

- Hot Channel Factors — Tables 4.2.3.1, 4.2.3.2, 4.2.3.3 and 4.2.3.4.
- Maximum Number of Discriminator Zones — 15
- Maximum Pin Bundle Coolant Velocity — 35 ft/sec
  This value represents a moderate advance in technology.
- Maximum Pin Bundle Pressure Drop — 90 psi
  Exclusive of entry and exit losses
- Bypass Flow — 5%
  This fraction of the total flow is unheated; the remainder is available for cooling driver and blanket assemblies.

The limiting conditions are:

- Fuel Pin Limits
  1. Total Mechanical Strain, % — <2
  2. Cladding temperature — 2σ at midwall

- Duct Limits
  Maximum duct-duct interaction — 0
  Interaction is measured as distance by which duct wall exceeds pitch line, neglecting axial duct bowing and elastic wall deformation.

The material properties are shown in Tables 2.1.1, 2.1.2,and 2.1.3.

The following assumptions were made for the physics analysis:

- Heavy Metal Composition[3]

1.	Feed Plutonium, % wt	^{238}Pu	0.997
		^{239}Pu	67.272
		^{240}Pu	19.209
		^{241}Pu	10.127
		^{242}Pu	2.395
2.	Fertile Uranium. % wt	^{235}U	0.2
		^{238}U	99.8

- Radial Reflector[4]

1. Composition (atoms/barn-cm)

a.	Fe	1.63106×10^{-2}
b.	Ni	4.40411×10^{-2}
c.	Cr	1.30353×10^{-2}
d.	Mo	0.02772×10^{-2}
e.	Mn	0.06274×10^{-2}
f.	Na	0.31284×10^{-2}

2. Thickness
   Use a minimum of two rows and add whatever thickness is necessary for fixed shield fluence limit considerations.

The fuel management is governed by the following ground rules:

- Plant Capacity Factor	70%
- Refueling Interval	Multiples of 6 months
- Number of Core Batches	Open
- Residence Time	
1. Driver Fuel Assemblies	Open
2. Blanket Assemblies	$\leq$6 years
- Number of Enrichment Zones	Open
- Out-of-Reactor Time	
Plutonium Fissile	1.00 year
- Combined Fabrication/Reprocessing Losses	0.01

TABLE 2.1.1.

Improved SS316 Irradiation Induced Swelling

Stress Free Swelling

$$\text{Swelling} = S = (0.01)\, R\left[\phi t + \frac{1}{\alpha} \ln\left\{\frac{1 + \exp\,\alpha(\tau - \phi t)}{1 + \exp\,(\alpha\tau)}\right\}\right]$$

$$\text{Fractional Volume Change} = \frac{\Delta V}{V_o} = \frac{S}{1-S}$$

ϕt = neutron fluence in units of 10^{22} n/cm^2 (E>0.1 MeV)

$R(T) = \exp\,(0.0419 + 1.498\Delta + 0.122\Delta^2 - 0.332\Delta^3 - 0.441\Delta^4) \times 0.7$

$\Delta = (T - 500)/100$ and T is the temperature in ^oC

$\alpha = 0.75$

$\tau_{(\text{nominal})} = 9.0$

Stress Effect on Swelling

$$\frac{\dot{\Delta V}}{V_o} = \left(\frac{\dot{\Delta V}}{V_o}\right)_o \left[1 + P\sigma_{HYD}\right]$$

$\dot{\Delta V}/V_o$ = swelling rate

$(\dot{\Delta V}/V_o)_o$ = stress-free swelling rate

σ_{HYD} = hydrostatic component of stress, psi

$$P = \left(\frac{T_{^oF} - 700.00}{100}\right) \times 2 \times 10^{-5}\ \text{psi}^{-1}$$

$T_{^oF}$ = temperature, ^oF

TABLE 2.1.2

Irradiation Induced Creep

Rate Equation Form

$$\dot{\bar{\varepsilon}}/\bar{\sigma} = \frac{A\phi}{\tau_{tr}} \exp(-\phi t/\tau_{tr}) + DR\phi G(\phi t) + B_o\phi$$

Integrated Form (Constant Stress)

$$\bar{\varepsilon}/\bar{\sigma} = A\left[1 - \exp(-\phi t/\tau_{tr})\right] + DR\phi t\left[1 - \frac{\Omega}{\phi t}G(\phi t)\right] + B_o\phi t$$

where

$\bar{\varepsilon}$, $\bar{\sigma}$ = effective strain and stress (ε is fractional and σ has units of psi).

$\dot{\bar{\varepsilon}}$ = effective strain rate (sec^{-1})

ϕ = neutron flux, n/cm^2 sec (E>0.1 MeV)

ϕt = neutron flucence, n/cm^2 (E>0.1 MeV)

$G(\phi t) = 1 - \exp(-\phi t/\Omega)$

$\Omega = 0.753\ \tau$ (n/cm^2, E>0.1 MeV)

$R(T) = \exp(0.0419 + 1.498\Delta + 0.122\Delta^2 - 0.332\Delta^3 - 0.441\Delta^4) \times 10^{-22} \times 0.7$

$\Delta = (T - 500)/100$ and T is the temperature in ^oC

$B_o = 3 \times 10^{-30}\ psi^{-1}\ n^{-1}\ cm^2$

$\tau_{(nominal)} = 9.0 \times 10^{22}\ n/cm^2$

$D = 2 \times 10^{-5}\ psi^{-1}$

$A = 1 \times 10^{-8}\ psi^{-1}$

$\tau_{tr} = 0.2 \times 10^{22}\ n/cm^2$

TABLE 2.1.3

Improved SS316 Stress Rupture

$$\log_{10} t_r = -15.2420 + 18910.4/T_{^oK} + 7.39226 \log_{10}\left(10g_{10}\,(90/\sigma_{ksi})\right)$$

where: t_r = time to rupture, hours

$T_{^oK}$ = temperature, ^oK

σ_{ksi} = rupture stress, ksi

- Cross Sections — ENDF/B-IV
- Fission Gas Yields
  ^{238}U, Pu — 0.249 atoms/fission
- Fission Gas Release (%) — 90
- Fission Energy
  Use 207 MeV/fission deposited heat for all isotopes.
- Uncontrolled End-of-Cycle Reactivity
  Designs shall confirm to an end-of-cycle effective multiplication factor of 1.000 with all control rods withdrawn from the core.
- Fluence Limits
  Fixed Shield — 2×10^{22} nvt (E > 0.1 MeV)
- Controls
  1. Model
     a. Park controls in upper axial blanket during burn and
     b. Use 92% enriched B_4C, if necessary.
  2. Requirements
     a. Primary system shall be able to maintain shutdown with one withdrawn control rod and the following conditions:
        (1) Hot-to-cold shift
        (2) Reactivity fault
        (3) Excess reactivity at BOEC
        (4) Criticality uncertainty
        (5) Fissile tolerance
     b. Secondary system shall be able to maintain shutdown with one withdrawn control rod and the following conditions:
        (1) Hot-to-cold shift
        (2) Reactivity fault
  3. Briefly evaluate EBR-II type control rods

A variety of figures of merit were considered, among them:

- Sodium Void Worth
- Doppler Coefficient
  Isothermal Doppler Coefficient
- Fissile Gain per Cycle
- Doubling time
  Calculate individual reactor Compound System Doubling Time (CSDT) using the ANL method[5].
- Breeding Ratio/Breeding Gain
- Specific Fissile Inventory
- Discharge Exposure

2.2 METHODOLOGY

The basis for this conceptual design effort on core layout and fuel pin and assembly designs was developed during the earlier phase[1]. To assure optimality of the finally selected design parameters, the following types of analyses were carried out:

- trade-off studies
- sensitivity studies
- optimization studies

All preliminary analyses were carried out for the core layout shown in Fig. 2.2.1 and fuel and blanket pins and assembly design described in Table 2.2.1.

Both detailed rigorous methods as well as approximate methods were employed in the design analyses presented in this report. Up to the selection of the reference design, approximate methods dominated the nuclear and thermal-hydraulic design analyses. For the final design analyses, the more detailed rigorous methods were used for both nuclear and thermal design. The nuclear analysis was based upon NSMH[6] properties with minor modifications. The irradiation induced swelling correlation is derived from the NSMH Rev. 7 correlation by increasing the incubation period τ from 6.3 to 9.0. The steady-state swelling rate R is reduced to 0.7 R. The irradiation induced creep calculation is based upon the nominal proposed MSMH Rev. 4 correlation using only 70% of the steady-state swelling rate and τ = 9.0. The stress rupture properties for steady-state analysis are the ones for nominal unirradiated N-lot steel.

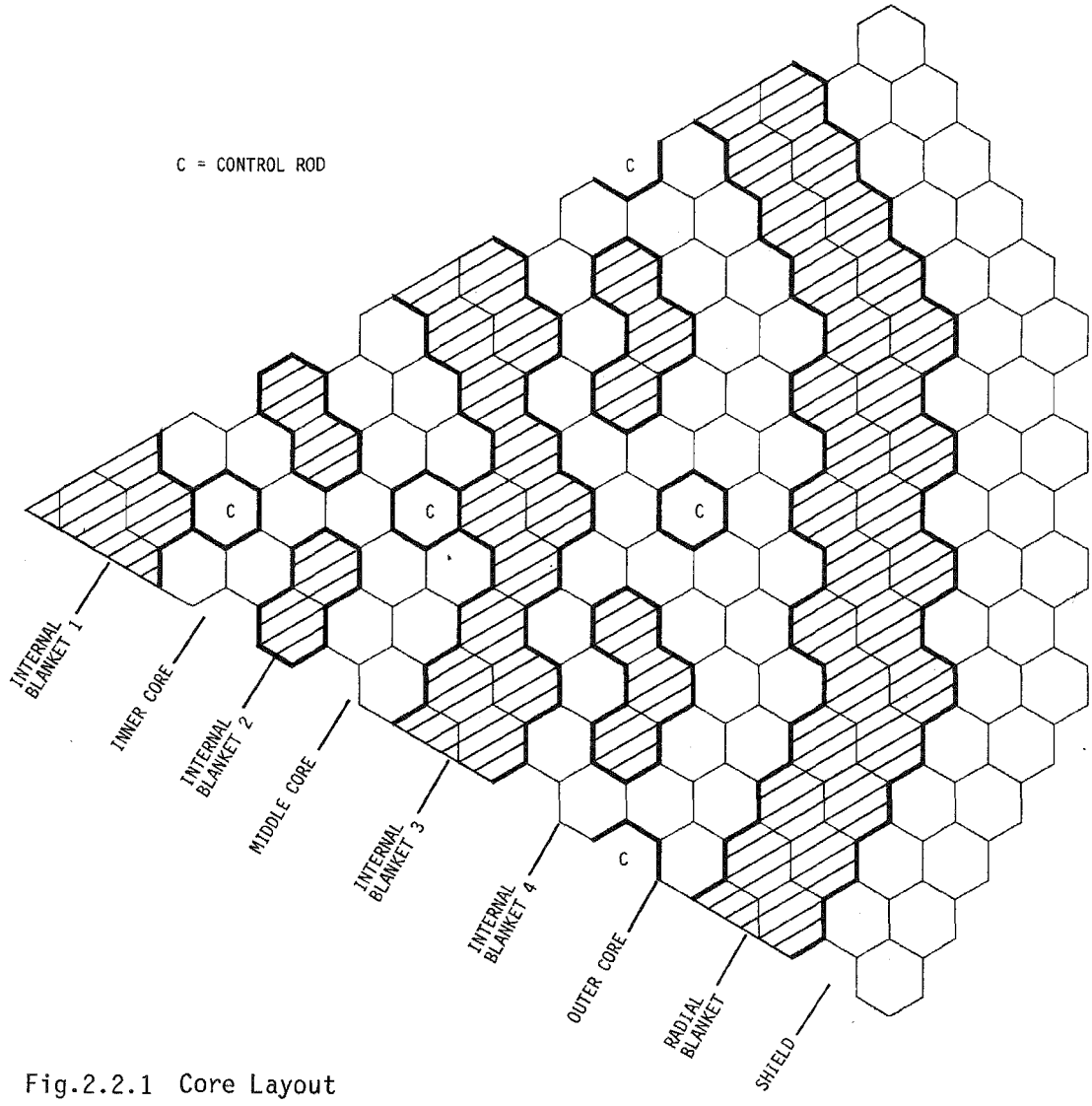

Fig.2.2.1 Core Layout

TABLE 2.2.1

Design Parameters for Preliminary Analysis

Fuel Pin/Blanket Pin	
Cladding O.D., in.	0.26/0.425
Cladding Thickness, in.	0.013/0.013
Fuel Smear Density, % T.D.	88/90
Fuel Assembly/Blanket Assembly	
Pins Per Assembly	271/127
p/d	1.197/1.070
Lattice Pitch, in.	5.653/5.653
Duct Thickness, in.	0.113/0.113
Interassembly Gap, in.	0.215/0.215
Nominal Peak Linear Heat Rating, kW/ft	
Core	13.4
Internal Blanket	12.8
Radial Blanket	8.7
Number of Assemblies	
Inner Core	36
Middle Core	72
Outer core	222
Internal Blanket 1	19
Internal Blanket 2	24
Internal Blanket 3	78
Internal Blanket 4	36
Control	24
Radial Blanket	174
Shield	198

The design analysis flow sheet is presented in Fig. 2.2.2. It shows schematically the various steps in the design evolution.

Performance Estimates: Estimates are required on clad and duct temperatures, fluence and power distribution.

Fuel Pin Design: Based on the design ground rules, the following fuel pin design parameters are fixed for the preliminary analyses: cladding o.d., cladding thickness, fuel smear density, peak linear heat rating, plenum location and length. The final fuel pin design is based on LIFE-III[7] calculations.

Fuel Assembly Design (NIFD Code[8]): The following design parameters are calculated: duct diameter, duct wall thickness, creep and swelling dilation of the duct as a function of axial position, fuel pitch/diameter ratio, assembly pitch, pressure drop, spacer wire thickness. The code furthermore calculates bundle-duct-interaction (BDI), number of subassemblies required, flow requirements, as well as the following blanket assembly parameters: pin diameter, pitch-to-diameter ratio, wire thickness, assembly dimensions.

The rigorous nuclear analysis of the first cycle and the equilibrium cycle was carried out with the REBUS[9] code package. The REBUS code package performs burnup calculations in 1D and 2D. The code system handles discrete burnup, equilibrium cycle analysis, homogenized fuel management, discrete fuel management, fuel shuffling as well as a large variety of fuel recycle options. DIF2D[10] is the 2-dimensional diffusion code used in REBUS. Burnup analysis was carried out using both RZ and hexagonal geometry options. Control rod worth calculations were carried out in hexagonal geometry using bucklings obtained from RZ geometry calculations. Criticality and sodium void worth as well as power distribution obtained from DIF2D were checked against the results obtained from DIF3D, a three-dimensional diffusion code.

PARC2D[11] is a two-dimensional perturbation code which was used for worth calculations in general and sodium void and Doppler reactivity distribution in particular.

After completion of the nuclear analysis, core layout, fuel management, and power distribution feed into the thermal analysis. The codes CORE-3D[12] and ENERGY[13] were used together with an orificing code for rigorous thermal analysis.

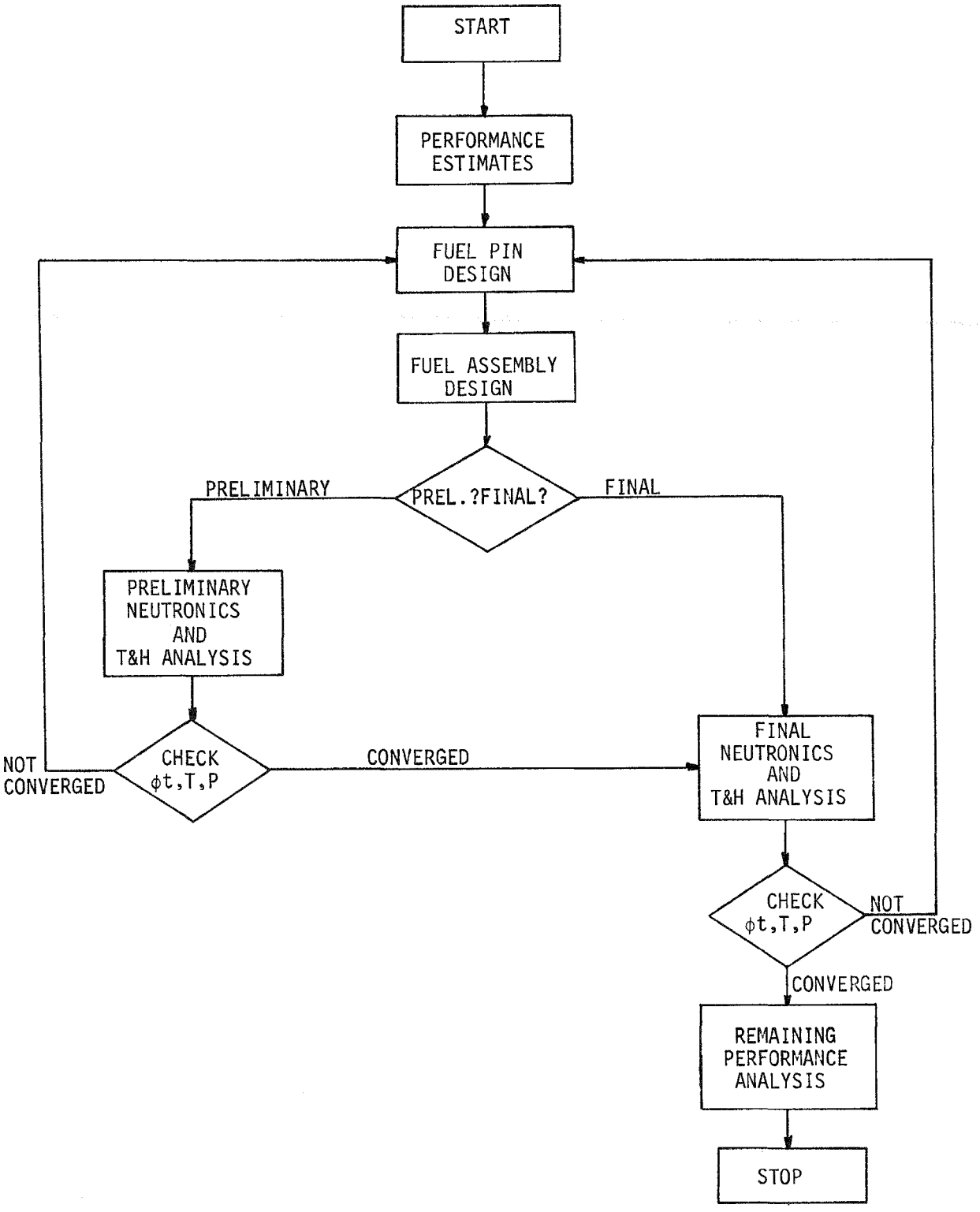

Fig. 2.2.2 Design Analysis Flow Sheet

The CORE-3D code determines steady-state core-wide temperature distributions. It is based on the ENERGY code and takes interassembly heat transfer into account without limiting the number of fuel assemblies of which the core consists. Fuel assemblies can be orificed individually. Coolant temperatures were calculated inside all fuel assemblies as well as duct temperatures and cladding hot-spot temperatures.

The ENERGY code determines the temperature distribution inside a fuel subassembly. The various mixing modes are lumped into an equivalent turbulent cross flow which is described by an effective eddy diffusivity. The code was used for a detailed thermal analysis of the design limiting assemblies

The LIFE-III[7] code was used to determine steady-state fuel pin performance.

3.0 CORE DESIGN

3.1 FUEL ASSEMBLY

As discussed in Appendix I, a near optimum fuel pin diameter equal to 0.28 in. has been selected. The fuel pin and assembly design parameters are summarized in Table 3.1.1. The total length of the bundle is 100 in. The active core height is equal to 40 in., the axial blanket thickness is equal to 15 in., and the plenum length is equal to 30 in. (Appendix H). A cladding thickness of 0.014 in. has been selected and the fuel inside the cladding tube has a fuel smear density of 88% T.D. The fuel pins are wire-wrapped with a helical pitch of 12 in. and a wire diameter of 0.047 in.

The fuel assembly contains 271 pins with a pin pitch-to-diameter ratio equal to 1.171. The assembly design is consistent with fuel bundle pressure drop of 60.1 psi. The duct wall thickness is 0.100 in. The inside flat-to-flat distance is 5.482 in. and the assembly pitch is 5.907 in. The peak stress in the duct corner is 38,783 psi which is well below the maximum allowable stress for 20% CW316SS.

3.2 BLANKET ASSEMBLY

The blanket assembly design parameters are summarized in Table 3.2.1. The fuel pin diameter is 0.447 in., the cladding thickness is 0.013 in., and the fuel smear density is 90% T.D. The wire wrapped around the pin has a diameter of 0.030 in. and a helical pitch of 6 in.

The blanket assembly duct has the same dimensions as the fuel assembly duct. It contains 127 pins with a pitch-to-diameter ratio of 1.07.

3.3 CONTROL ASSEMBLY

No specific design for a control assembly was developed at this stage. The assumption has been made that the control assembly of this reactor is a linearly

Table 3.1.1

FUEL ASSEMBLY DESIGN DATA

Fuel		$PuO_2 + UO_2$
Fuel Smear Density, %TD		88.0
Cladding Outside Diameter, in.		0.280
Cladding Wall Thickness, in.		0.014
Cladding Material		20% CW316SS
Bond Type		Helium
Overall Bundle Length, in.		100.0
Active Core Height, in.		40.0
Axial Blanket thickness, in.*		15.0
Plenum Location		Top
Plenum Length, in.		30.0
Pins per Assembly		271
Pin Pitch-to-Diameter Ratio		1.171
Spacer Concept		Wire wrap
Wire Wrap Diameter, in.		0.047
Spacer Pitch, in.		12.0
Lattice Pitch, in.		5.907
Duct Outside Width Across Flats, in.		5.682
Duct Wall Thickness, in.		0.100
Sodium Gap Between Assemblies, in.		0.225
Duct Material		20% CW316SS
Material Volume Fractions		
Fuel		0.447300
Coolant	0.293098	
Sodium in Gap	0.074730	
Total Sodium		0.367828
Total Structural		0.184872

*The same for upper and lower axial blanket.

Table 3.2.1

BLANKET ASSEMBLY DESIGN DATA

Fuel		Depleted UO_2
Fuel Smeared Density, %T.D.		90.0
Cladding Outside Diameter, in.		0.447
Cladding Wall Thickness, in.		0.013
Cladding Material		20%CW316SS
Bond Type		Helium
Overall Bundle Length, in.		100.0
Blanket Height, in.		70.0
Plenum Location		Top
Plenum Length, in.		30.0
Pins per Assembly		127
Pin Pitch-to-Diameter Ratio		1.070
Spacer Concept		Wire Wrap
Wire Wrap Diameter, in.		0.030
Spacer Pitch, in.		6.0
Lattice Pitch, in.		5.907
Duct Outside Width Across Flats, in.		5.682
Duct Wall Thickness, in.		0.100
Sodium Gap Between Assemblies, in.		0.225
Duct Material		20% CW316SS
Material Volume Fractions		
Fuel		0.585477
Coolant	0.198047	
Sodium in Gap	0.074730	
Total Sodium		0.272777
Total Structural		0.141746

enlarged CRBRP[3] control assembly which yields the same material volume fractions as the CRBR control assembly (Table 3.3.1). An EBR-II[14] type control system that uses natural boron control rods with fuel assembly followers was also briefly evaluated (Appendix L).

3.4 SHIELD ASSEMBLY

No specific design for a shield (radial reflector) assembly was developed in this work. Based on previous system studies[4], the assumption has been made that the shield assembly has the following volumetric composition: 0.6383 Inconel, 0.2216 20% CW316SS, 0.1401 Sodium.

3.5 CORE LAYOUT

The core configuration used in this conceptual design is shown in Figure 2.2.1 It is the result of a core layout optimization, performed in Reference 1,aiming to a compromise between low sodium void reactivity and reasonable neutronic coupling between core fuel regions. It is a central blanket heterogeneous configuration that consists of four internal blanket regions and three core fuel regions. The second internal blanket region is a one-row ring of assemblies that has been broken to improve coupling between the first and second core regions. Also, to improve coupling between the second and third core regions, the third internal blanket region consists of a one-row complete ring of assemblies plus another one-row ring that is broken. The fourth internal blanket region consists of small one-row thick clusters of assemblies that not only reduce the sodium void reactivity of the outer core region but also flatten the power distribution in this region. The number of assemblies per reactor region is given in Table 3.5.1.

Table 3.3.1

CONTROL ASSEMBLY COMPOSITION*

Control Rod Full In	Volume Fraction
B_4C Pellet	0.3174
Void	0.0216
Coolant	0.3323
Structure	0.3287
Control Rod Full Out	
Coolant	0.8842
Structure	0.1158

* The EBR-II type control assembly is discussed in Appendix L

Table 3.5.1

NUMBER OF ASSEMBLIES PER REACTOR REGION

Region	Number of Assemblies
Inner Core	36
Middle Core	72
Outer Core	222
Core	330
Internal Blanket 1	19
Internal Blanket 2	24
Internal Blanket 3	78
Internal Blanket 4	36
Internal Blankets	157
Control Assemblies	24
Radial Blanket	174
Shield Assemblies	198

4.0 CORE PERFORMANCE ANALYSIS

4.1 NUCLEAR ANALYSIS

4.1.1 Ground Rules

The major constraint in this conceptual design effort was the sodium void reactivity. This reactivity change should be equal to or less than $2.50 and is defined as the eigenvalue increase coming from the removal of the flowing sodium in the core and upper axial blanket section of fuel assemblies.

A detailed listing of assumptions for the nuclear design is shown in Chapter 2.1. The overall plant specifications led to the following ground rules for the nuclear design:

- total thermal power output of 3084 MWt
- plant capacity factor of 70%
- cycle length of 255.5 full power days
- no fuel assembly shifting and rotation
- The control assembly design is that of CRBRP ratioed up to the pitch calculated for this design (an EBR-II type control assembly has also been considered)
- two independent control assembly systems
- 271 fuel pins/fuel assembly and 127 pins/blanket assembly.

The constraints for fuel pin performance are:

- The peak nominal fuel rod should be less than 15 kW/ft to prevent fuel centerline melting.[2]
- The peak nominal blanket rod power should be less than 16.5 kW/ft to prevent pellet centerline melting.[2]

4.1.2 Figures of Merit

To measure the success in this nuclear design work certain figures of merit were identified. Some of them were constraints, others were performance measures and/or performance parameters to be optimized. The following is a listing of figures of merit considered in the completed design effort:

- sodium void reactivity
- Doppler coefficient
- fissile material gain per cycle
- doubling time
- fissile inventory
- burnup swing per cycle (reactivity)
- peak discharge burnup
- peak cladding temperature
- peak temperature difference across duct
- power peaking

The most important figure of merit, which also constrained the design, is the sodium void reactivity. A $2.50 limit was imposed on the reactivity change coming from the removal of the flowing sodium in fuel assemblies in the core and upper axial blanket region. The only other figure of merit constraining the design is the peak burnup. However, since the burnup is less than 13% this constraint never becomes active. The other figures of merit measure performance in a sense that performance is the better the smaller/greater the respective figure of merit is.

4.1.3 Nuclear Performance

4.1.3.1 Core and Blanket Fuel Management

From the analyses presented in Appendices C, D,and I, a cycle length equal to 255.5 full power days and residence times equal to three years for the core and internal blanket assemblies and five years for the radial blanket assemblies have been chosen. At the end of each cycle, one third of the core and internal blanket assemblies and one fifth of the radial blanket assemblies are replaced with fresh fuel assemblies in a scatter refueling approach. The nuclear performance and thermal-hydraulic analyses are based on the first cycle and an equilibrium cycle where fresh and irradiated fuel are homogenized for the neutronic calculations.

To obtain a measure for the differences between this approach and a discrete fuel management, a limited discrete fuel management analysis has been performed for the first four cycles. The results of this analysis are presented in Appendix J.

The nuclear and thermal-hydraulic performance of the 0.28 inch fuel pin diameter design has also been analyzed: a) for two and three years straight burn of the core and internal blanket fuel and b) for core and internal blanket fuel residence time of two years and refueling every year. This analysis is presented in Appendix K.

4.1.3.2 Fuel Enrichments and Inventories

The core fuel pins contain mixed plutonium-uranium oxide pellets in the core region and depleted uranium oxide pellets in the axial blanket regions. The blanket fuel pins contain depleted uranium oxide pellets. The isotopic fuel composition is given in Table 4.1.3.2.1.

Average fissile fuel enrichments for BOL, BOEC and EOEC conditions as well as fresh fuel feed enrichment for the BOEC are given in Table 4.1.3.2.2. Fissile inventories for the same conditions are presented in Table 4.1.3.2.3. These quantities have been determined from two-dimensional burnup calculations in RZ geometry using the REBUS[9] code with eight neutron group cross-sections and having all the control rods parked at the top of the upper axial blanket. The average core fuel enrichment is 17.12% and 16.46% at BOL and BOEC conditions, respectively. The total reactor fissile inventory at the same conditions is 4260.7 kg and 4761.6 kg.

4.1.3.3 Power Distribution

Exact predictions of the power distribution require multigroup three-dimensional calculations. Since such calculations are very expensive, two-dimensional calculations are used to synthesize a three-dimensional distribution. The power distribution in the radial and azimuthal directions is determined from two-dimensional calculations in hexagonal geometry. In these calculations an axial buckling is used to account for leakage in the axial direction. The power distribution in the axial direction as well as the fractions of power produced in the different reactor regions are determined from two-dimensional calculations in RZ geometry.

Table 4.1.3.2.1

ISOTOPIC COMPOSITION OF FEED FUEL (% wt)[α]

Plutonium	^{238}Pu	0.997
	^{239}Pu	67.272
	^{240}Pu	19.209
	^{241}Pu	10.127
	^{242}Pu	2.395
Uranium	^{235}U	0.2
	^{238}U	99.8

[α] From Reference 3

Table 4.1.3.2.2

AVERAGE FISSILE ENRICHMENTS[a] (%)

Reactor Region	BOL	BOEC[b]	EOEC
Core	17.12	16.46	15.82
Internal Blanket 1	0.0	1.08	2.07
Internal Blanket 2	0.0	1.51	2.84
Internal Blanket 3	0.0	1.35	2.55
Internal Blanket 4	0.0	1.33	2.51
Axial Blanket	0.0	0.61	1.18
Radial Blanket	0.0	0.98	1.43

[a] $\text{Enrichment} = \dfrac{^{239}\text{Pu} + ^{241}\text{Pu}}{^{239}\text{Pu} + ^{240}\text{Pu} + ^{241}\text{Pu} + ^{242}\text{Pu} + ^{235}\text{U} + ^{238}\text{U}} \dfrac{\text{kg}}{\text{kg}}$

[b] fresh fuel feed enrichment = 17.17 (equilibrium cycle).

Table 4.1.3.2.3

FISSILE INVENTORIES, kg.

Reactor Region	BOL	BOEC	EOEC
Inner Core	458.6	426.6	396.9
Middle Core	917.3	850.8	789.5
Outer Core	2884.8	2706.3	2536.9
Total Core	4260.7	3983.7	3723.3
Internal Blanket 1	0.0	35.9	68.6
Internal Blanket 2	0.0	63.3	118.3
Internal Blanket 3	0.0	183.7	346.1
Internal Blanket 4	0.0	83.5	157.2
Total Internal Blanket	0.0	366.4	690.2
Axial Blanket	0.0	114.6	223.7
Radial Blanket	0.0	296.9	435.1
Total Reactor	4260.7	4761.6	5072.3

The power shape in the radial and azimuthal directions depends on both the BOL enrichment distribution as well as the control rod programming. The objective of an optimum power shape and reactivity control strategy must be the determination of BOC enrichment distribution and control rod programming such that:

1. Reactor criticality and a minimum power peaking factor are retained throughout the cycle
2. The control rods are out at EOC

The BOC enrichment distribution and the control rod programming that satisfy such an optimum strategy can be determined by the computer code CYPRUS[15]. The results of the work presented in Ref. 16 indicate that, if only the BOL and EOEC power distributions that result in a minimum power peaking factor with the control rods out at the EOEC are needed, then a good approximation of the BOC enrichment and control rod distribution can be obtained as follows. Burnup calculations are performed with all the control rods removed to determine the BOC fresh fuel enrichment distribution that leads to an EOC power distribution having a minimum peaking factor. Then, this BOC fresh fuel enrichment distribution is used in static diffusion calculations to determine the control rod distribution that minimizes the power peaking factor at BOC. This simple procedure has been used in this work to determine BOL and EOEC power distributions.

The fractions of power produced in the different reactor regions for the first cycle and the equilibrium cycle are given in Table 4.1.3.3.1. In determining the power distribution, the assumption is made that the γ-rays are absorbed in the place they are produced.

The fraction of power produced in the core decreases from 89.96% at BOL to 74.83% at EOEC while the fraction of power produced in the internal blankets increases from 6.35% at BOL to 17.77% at EOEC.

Peak to average power density ratios for each reactor zone, as determined from RZ calculations are given in Table 4.1.3.3.2.

Typical axial power shapes in the core, internal blanket and radial blanket are shown in Figure 4.1.3.3.1. As it is discussed in Appendix E, for the shaping of the radial power distribution two enrichment zones are adequate. The second enrichment zone consists of the outer ring of core assemblies and the rest of the

Table 4.1.3.3.1

POWER DISTRIBUTION[a](%)

Reactor Region	First Cycle		Equilibrium Cycle	
	BOC	EOC	BOC	EOC
Inner Core	9.83	9.96	9.33	9.21
Middle Core	20.69	20.63	19.60	19.13
Outer Core	59.44	51.04	52.61	46.49
Total Core	89.96	81.63	81.54	74.83
Internal Blanket 1	0.43	0.96	0.88	1.39
Internal Blanket 2	1.21	2.66	2.37	3.50
Internal Blanket 3	2.77	6.20	5.79	8.72
Internal Blanket 4	1.94	3.35	3.22	4.16
Total Internal Blanket	6.35	13.17	12.26	17.77
Axial Blanket	1.36	2.09	2.05	2.78
Radial Blanket	2.12	2.90	3.93	4.39
Radial Reflector	0.21	0.21	0.22	0.23

[a] γ-heating included

Table 4.1.3.3.2

REGIONAL PEAK/AVERAGE POWER DENSITY RATIOS

Reactor Region	First Cycle		Equilibrium Cycle	
	BOC	EOC	BOC	EOC
Inner Core	1.328	1.301	1.302	1.279
Middle Core	1.348	1.310	1.308	1.272
Outer Core	1.439	1.450	1.428	1.456
Total Core	1.420	1.517	1.441	1.492
Internal Blanket 1[a]	3.600	3.110	3.095	2.830
Internal Blanket 2[a]	2.184	2.234	2.211	2.175
Internal Blanket 3[a]	2.599	2.414	2.398	2.326
Internal Blanket 4[a]	2.074	2.218	2.178	2.198
Axial Blanket[b]	3.068	3.203	2.931	3.160
Radial Blanket[a]	4.946	4.794	4.680	4.527

[a]over the total height of the region (70")

[b]above and below core

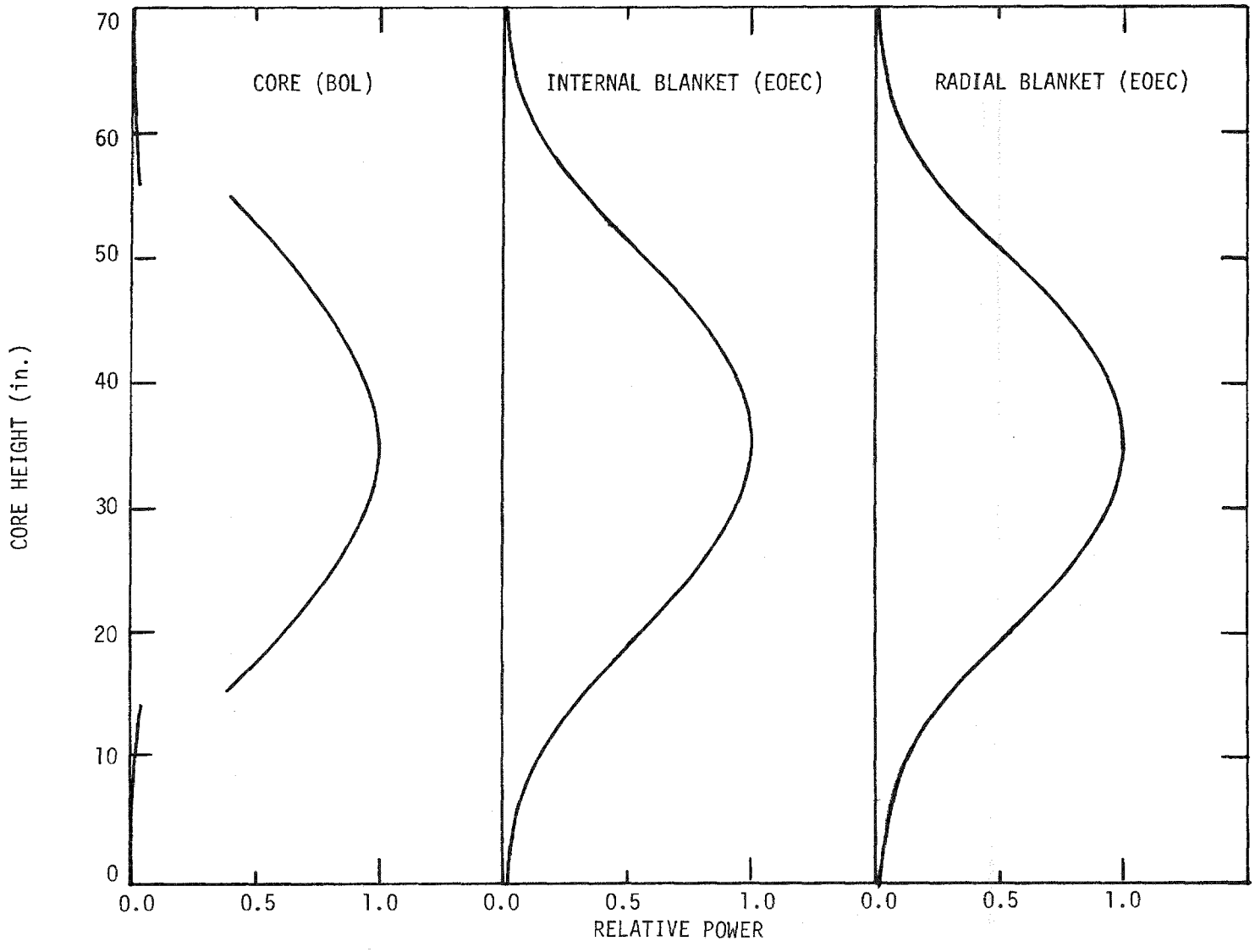

Figure 4.1.3.3.1. Typical Axial Power Shapes

core assemblies belong to the first enrichment zone. The fresh fuel enrichment and the BOL control rod distribution, that minimize the peaking factor at BOL and EOEC conditions, as well as the core power peaking factor at the same conditions are given in Table 4.1.3.3.3. As has already been mentioned, the data presented in Table 4.1.3.3.3 was determined from two-dimensional calculations in hexagonal geometry. In these calculations an axial buckling was used to account for leakage in the axial direction [17].

The core peaking factor is equal to 1.484 at BOL and 1.482 at EOEC. The true core power peaking factor will be higher due to fuel management power peaking. As shown in Appendix J, where the discrete fuel management analysis is presented, the maximum core peaking factor for the four cycles analyzed is equal to 1.670. In the analysis that follows, the core power peaking factor has not been corrected for fuel management power peaking.

The assembly average (over a hexagonal cell) and peak power density distributions at core midplane at BOL and EOEC, that result from the fuel enrichments and control rod distribution presented in Table 4.1.3.3.3, are shown in Figures 4.1.3.3.2 to 4.1.3.3.5. The overall peak power density is equal to 627.2 watts/cc at BOL and drops to 539.8 watts/cc at EOEC. These peaks correspond to peak linear power ratings of 14.2 kW/ft and 12.2 kW/ft, respectively.

4.1.3.4 Flux Distribution and Fluences

Assembly average and peak total neutron fluxes at core midplane for BOL and EOEC conditions are shown in Figures 4.1.3.4.1 to 4.1.3.4.4. These fluxes result from beginning of cycle enrichment and control rod distributions that minimize the peak to average power density (Table 4.1.3.3.3). The peak total flux is 5.3×10^{15} n/cm^2-sec at BOL and 5.2×10^{15} n/cm^2-sec at EOEC. A typical picture of the flux shape in the radial direction is shown in Figure 4.1.3.4.5. The flux peaks occur in the core regions and the flux valleys in the blanket and control rod regions. At BOL the row 7 and row 11 control rods are inserted in a ratio of row 11/row 7 equal to 9.873/1.0. At EOEC all control rods are removed.

Assembly peak fast (neutron energy > 0.1 Mev) fluences for a core and internal blanket residence time of three cycles, radial blanket residence time of five cycles and a cycle length of 255.5 days are shown in Figure 4.1.3.4.6. The peak fast fluence is 2.06×10^{23} n/cm^2 in the core, 1.77×10^{23} n/cm^2 in the internal blankets and 1.94×10^{23} n/cm^2 in the radial blankets.

Table 4.1.3.3.3

FRESH FUEL ENRICHMENTS[a], CONTROL ROD INSERTION PATTERN, AND PEAK/AVERAGE POWER DENSITY RATIOS

	BOL	Equilibrium Cycle
Fresh Fuel Enrichments Zone 1/ Zone 2	0.1702/0.1847	0.1716/0.1927
Control Rod Insertion Pattern[b] Row 11/ Row 7	9.873/1.0	
Peak/Average Power Density	1.484	1.482[c]

$$^{a}\text{Enrichment} = \frac{^{239}\text{Pu} + ^{241}\text{Pu}}{^{239}\text{Pu} + ^{240}\text{Pu} + ^{241}\text{Pu} + ^{235}\text{U} + ^{238}\text{U}} \quad \frac{(\text{kg})}{(\text{kg})}$$

[b]Normalized ratio of interest posion

[c]EOEC

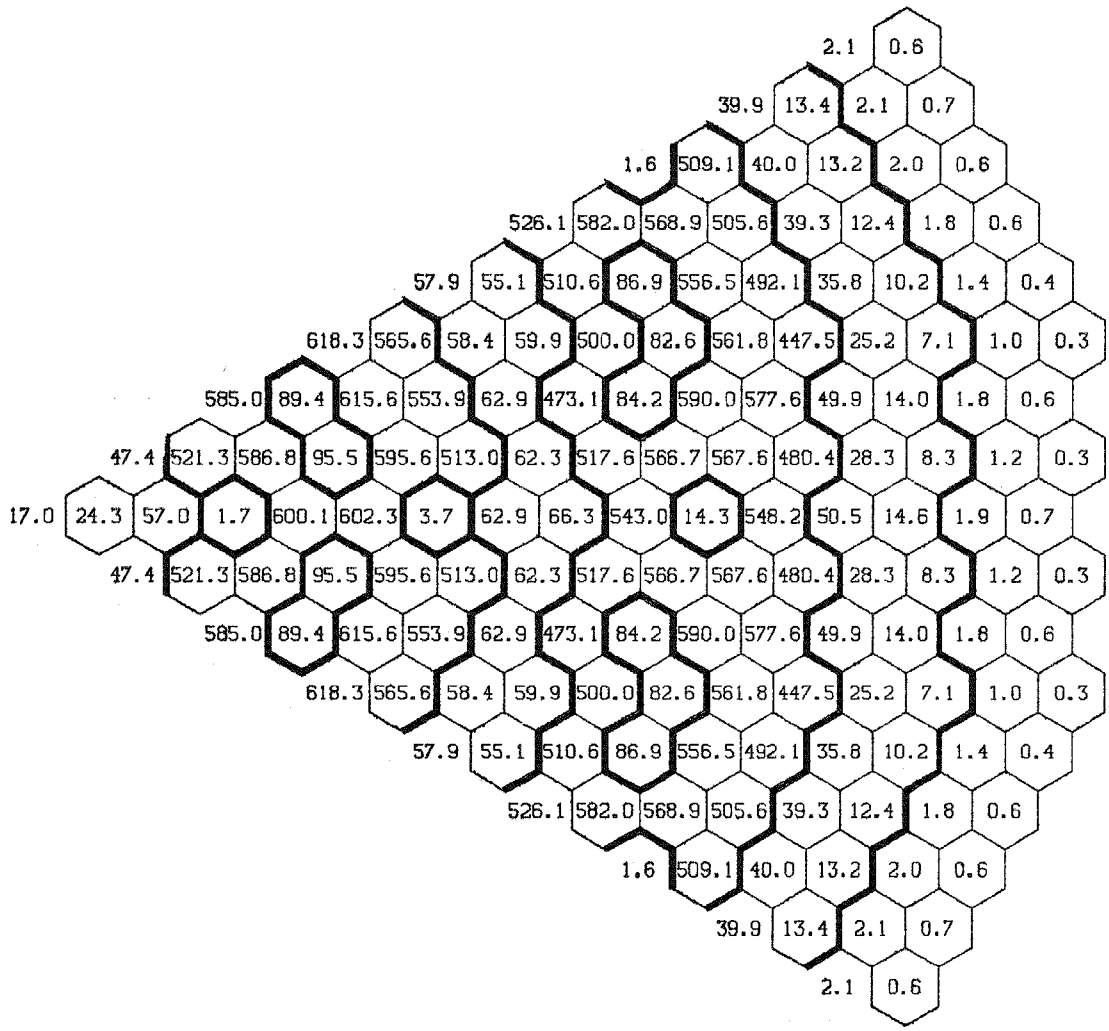

Figure 4.1.3.3.2. Assembly average power density (watts/cm^3) distribution at core midplane at BOL.

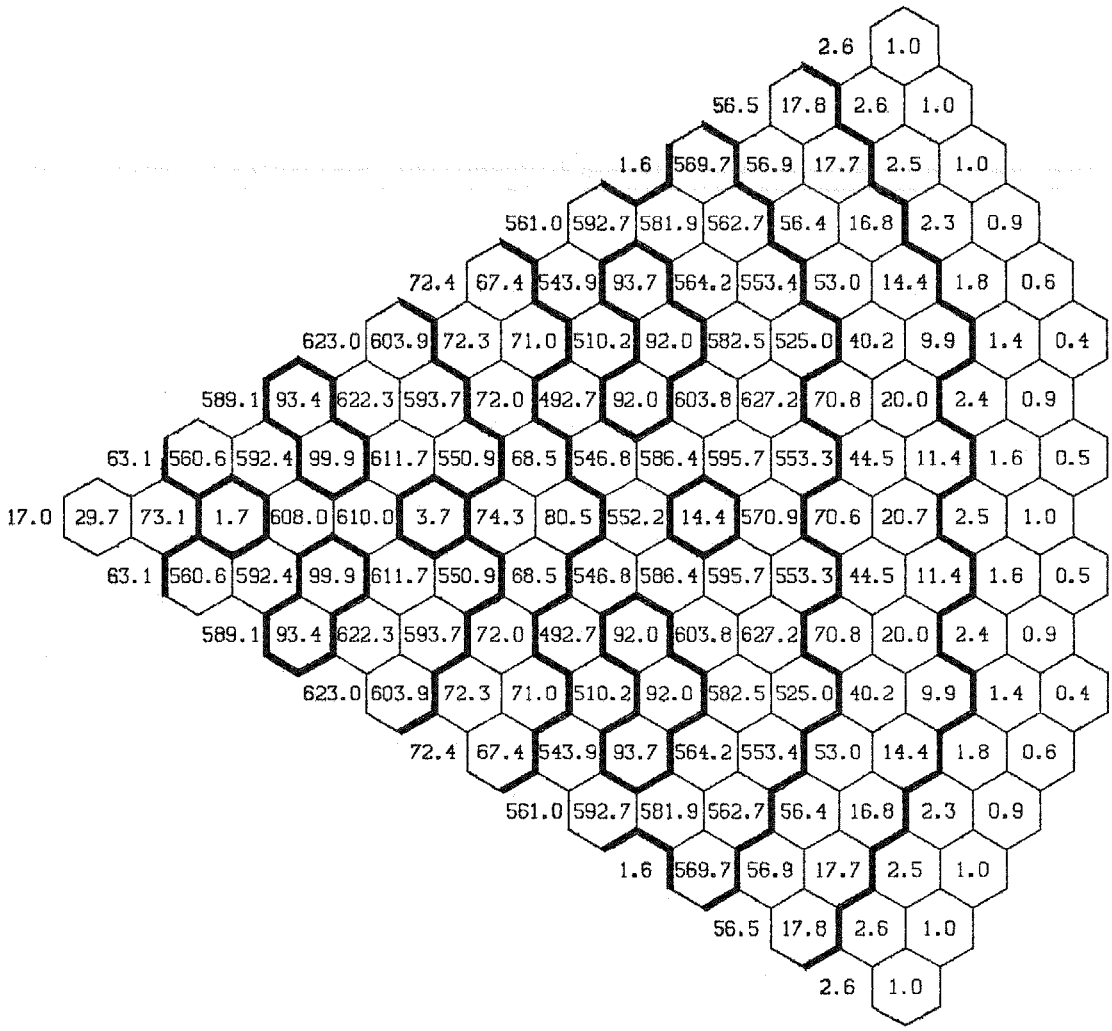

Figure 4.1.3.3.3. Assembly peak power density (watts/cm^3) distribution at BOL.

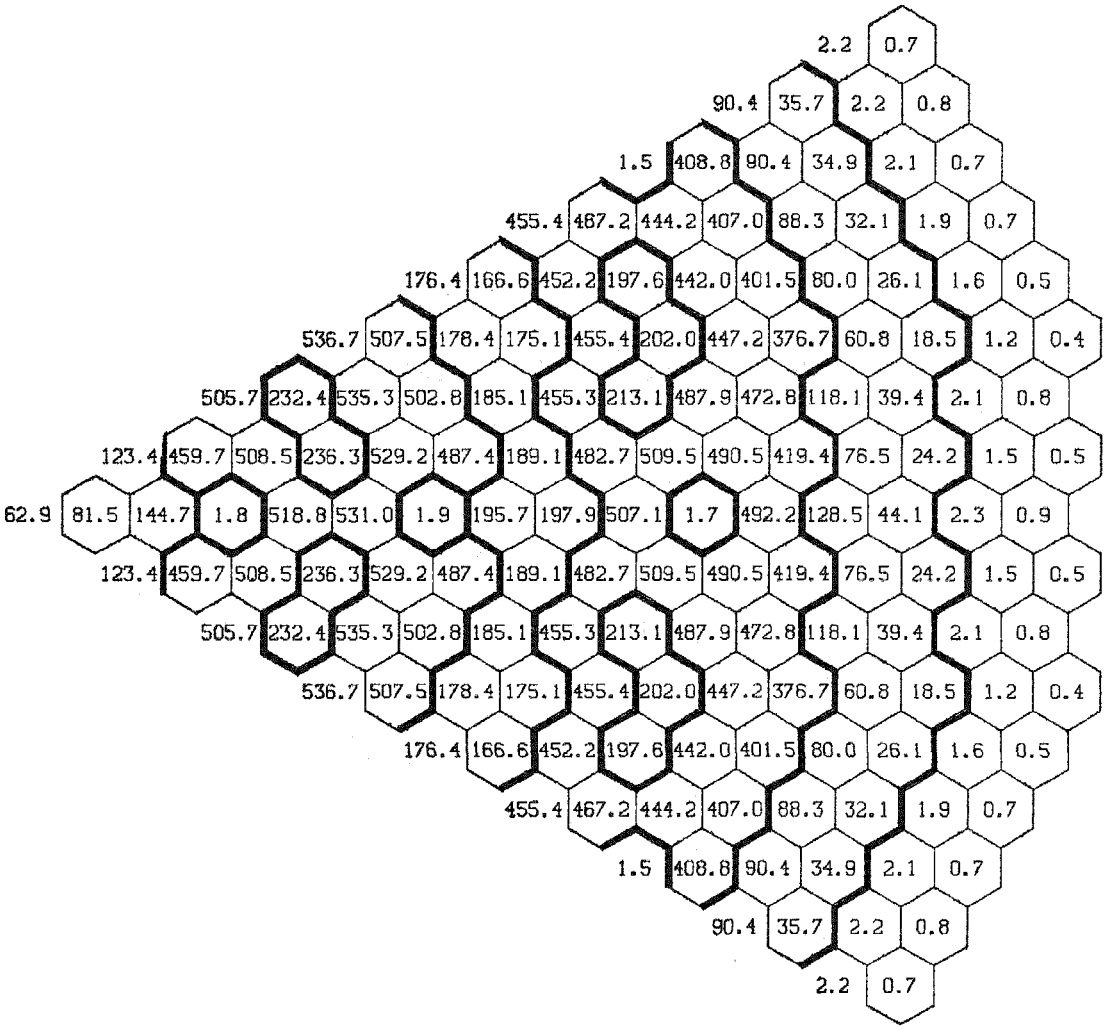

Figure 4.1.3.3.4. Assembly average power density (watts/cm^3) distribution at core midplane at EOEC.

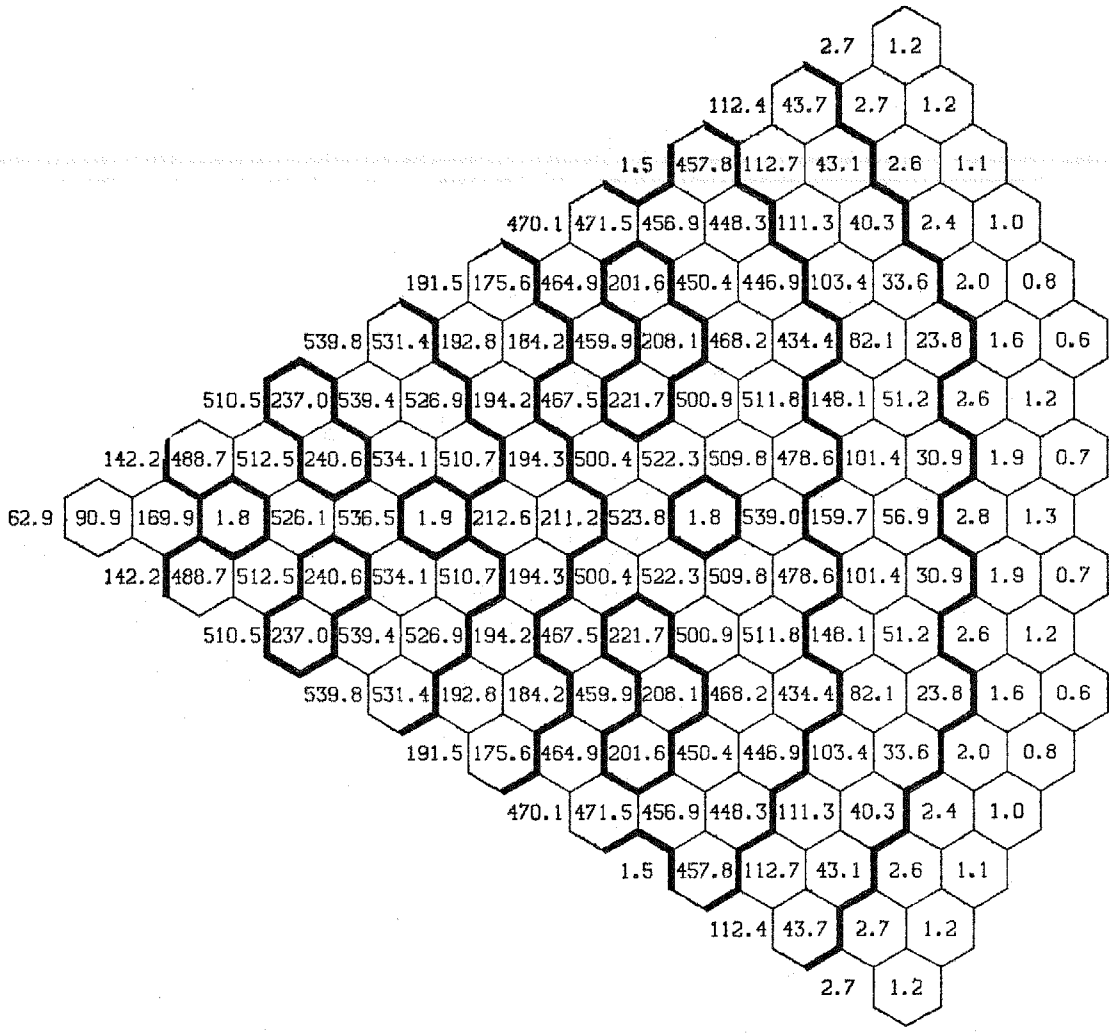

Figure 4.1.3.3.5. Assembly peak power density (watts/cm^3) distribution at EOEC.

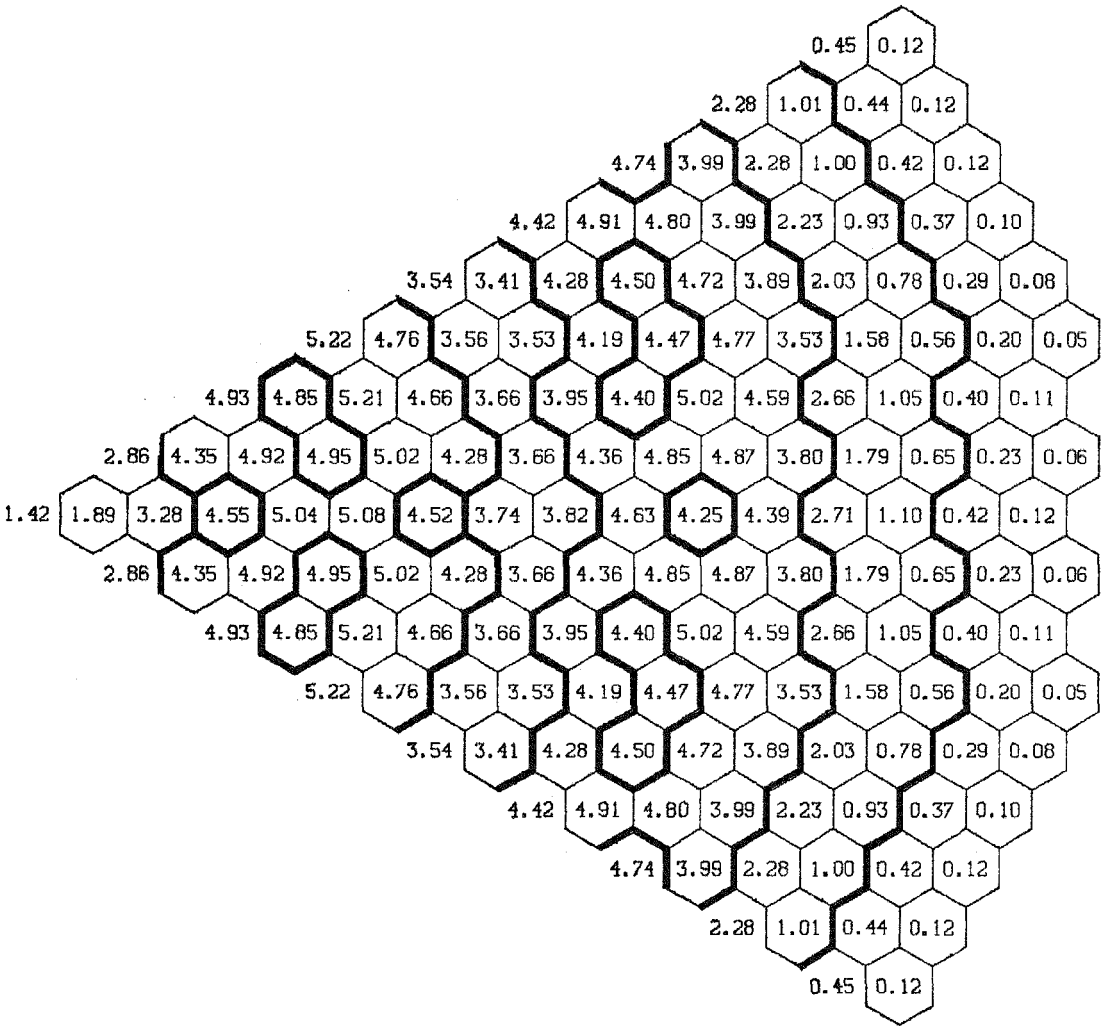

Figure 4.1.3.4.1. Assembly average total flux ($\frac{n}{cm^2.sec} \times 10^{-15}$) distribution at core midplane at BOL.

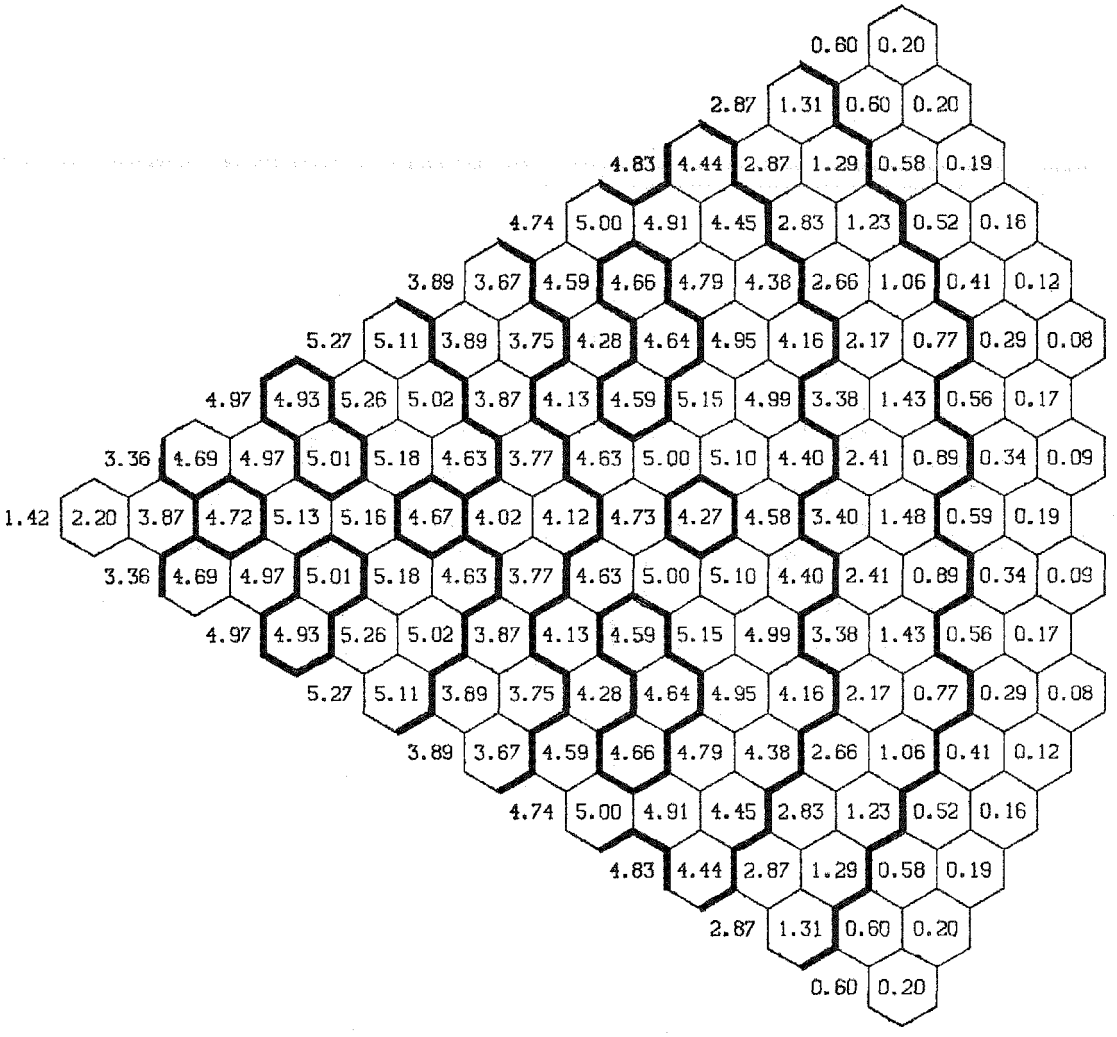

Figure 4.1.3.4.2. Assembly peak total flux ($\frac{n}{cm^2.sec} \times 10^{-15}$) distribution at BOL.

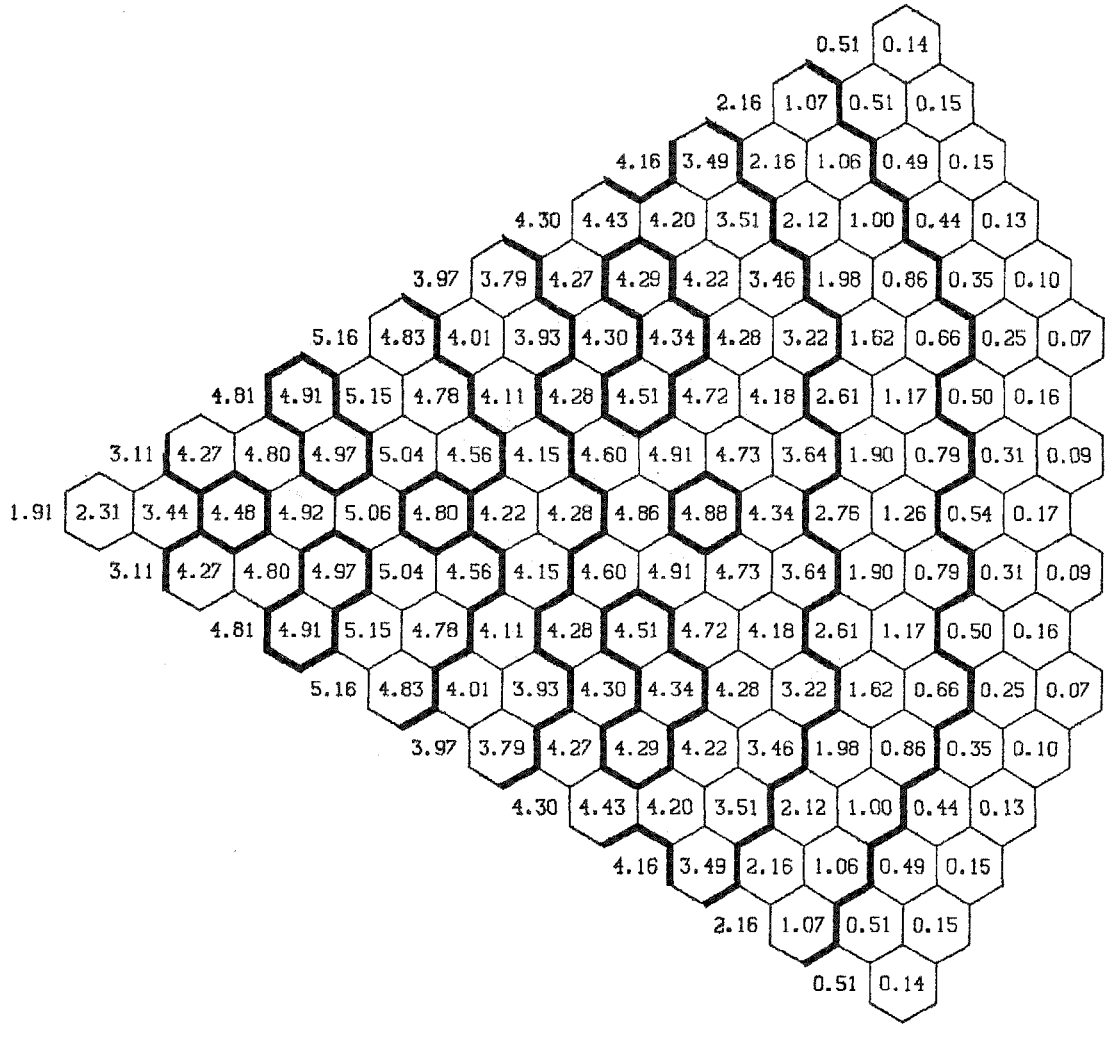

Figure 4.1.3.4.3. Assembly average total flux ($\frac{n}{cm^2.sec} \times 10^{-15}$) distribution at core midplane at EOEC.

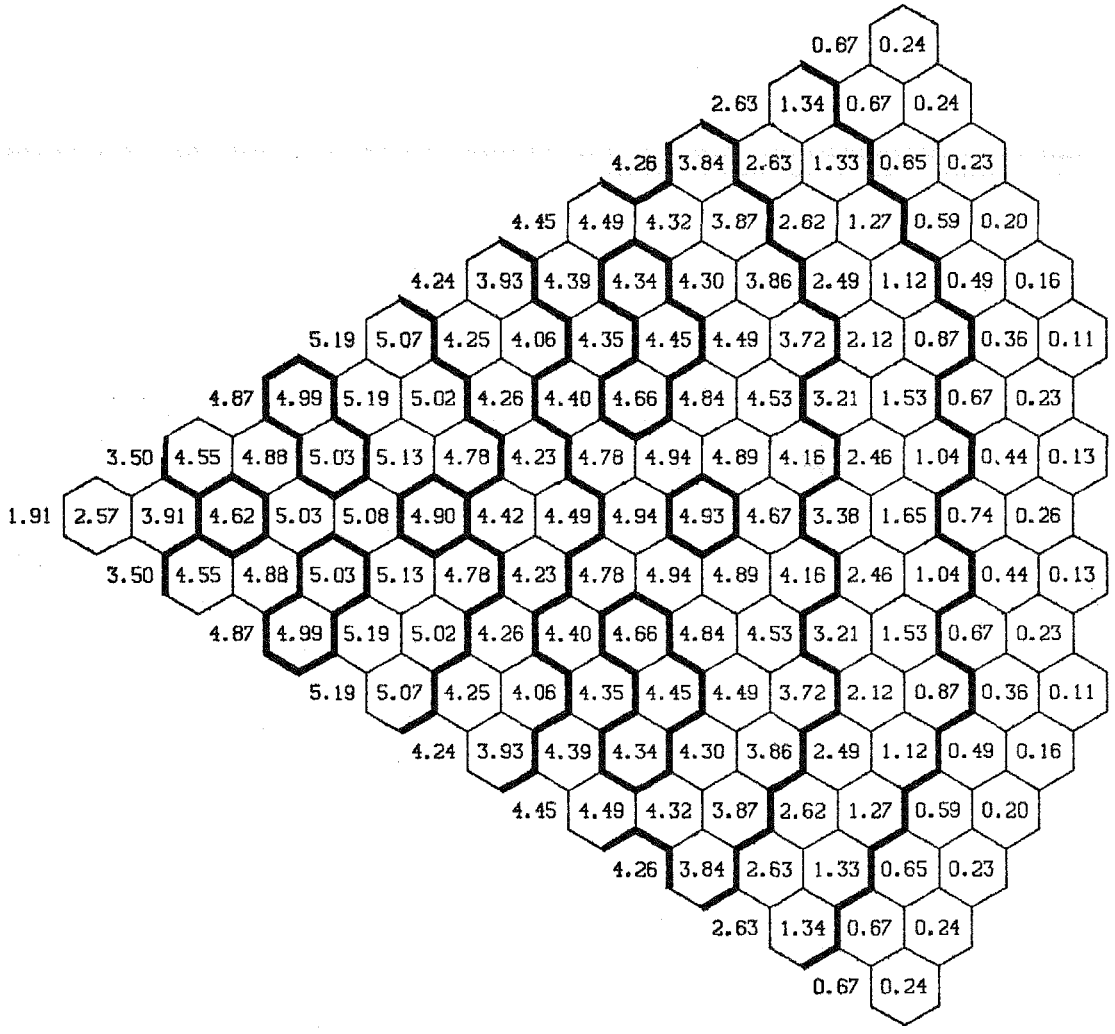

Figure 4.1.3.4.4. Assembly peak total flux ($\frac{n}{cm^2.sec} \times 10^{-15}$) at EOEC.

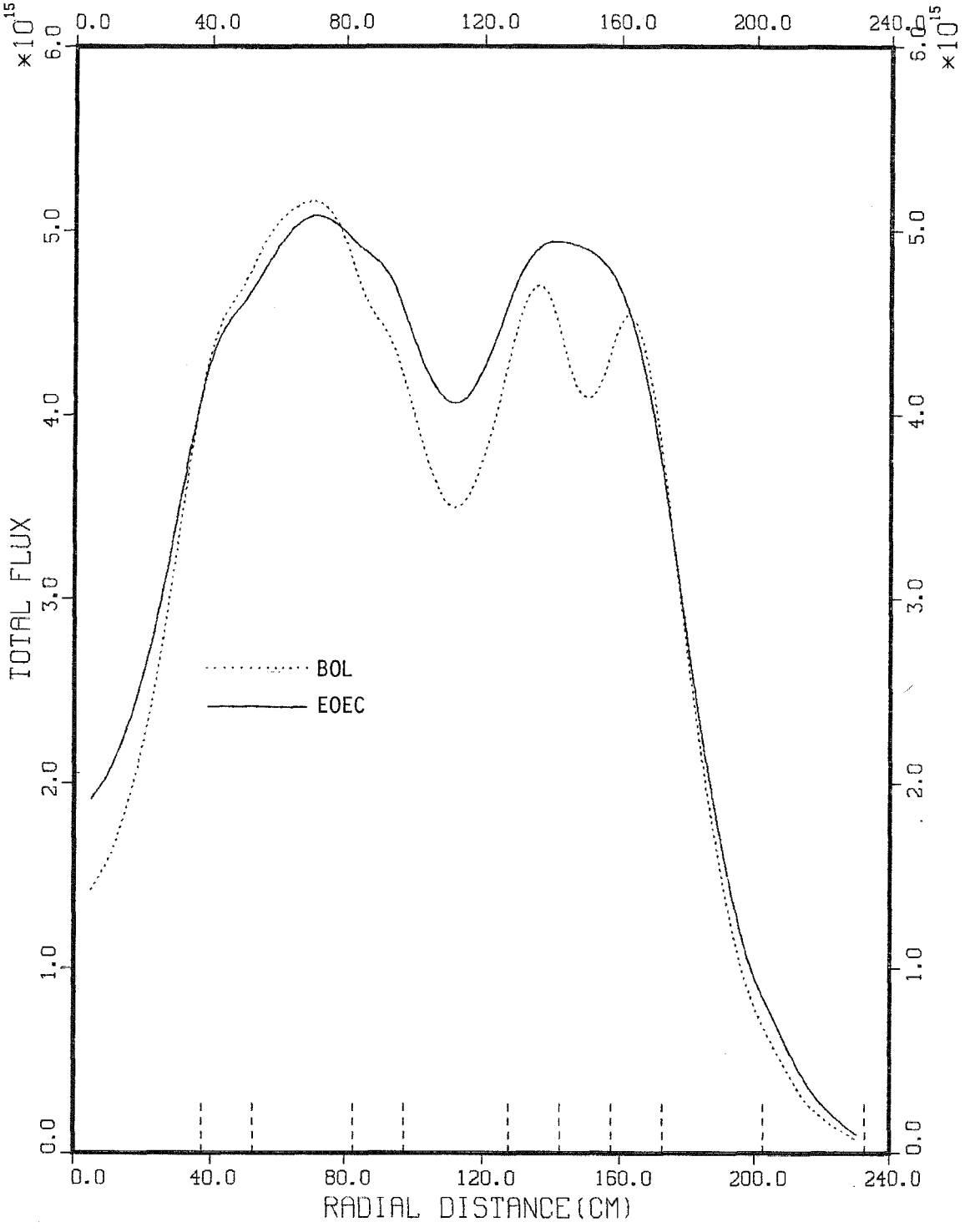

Figure 4.1.3.4.5. Total flux along the axis of symmetry of one-sixth of the reactor.

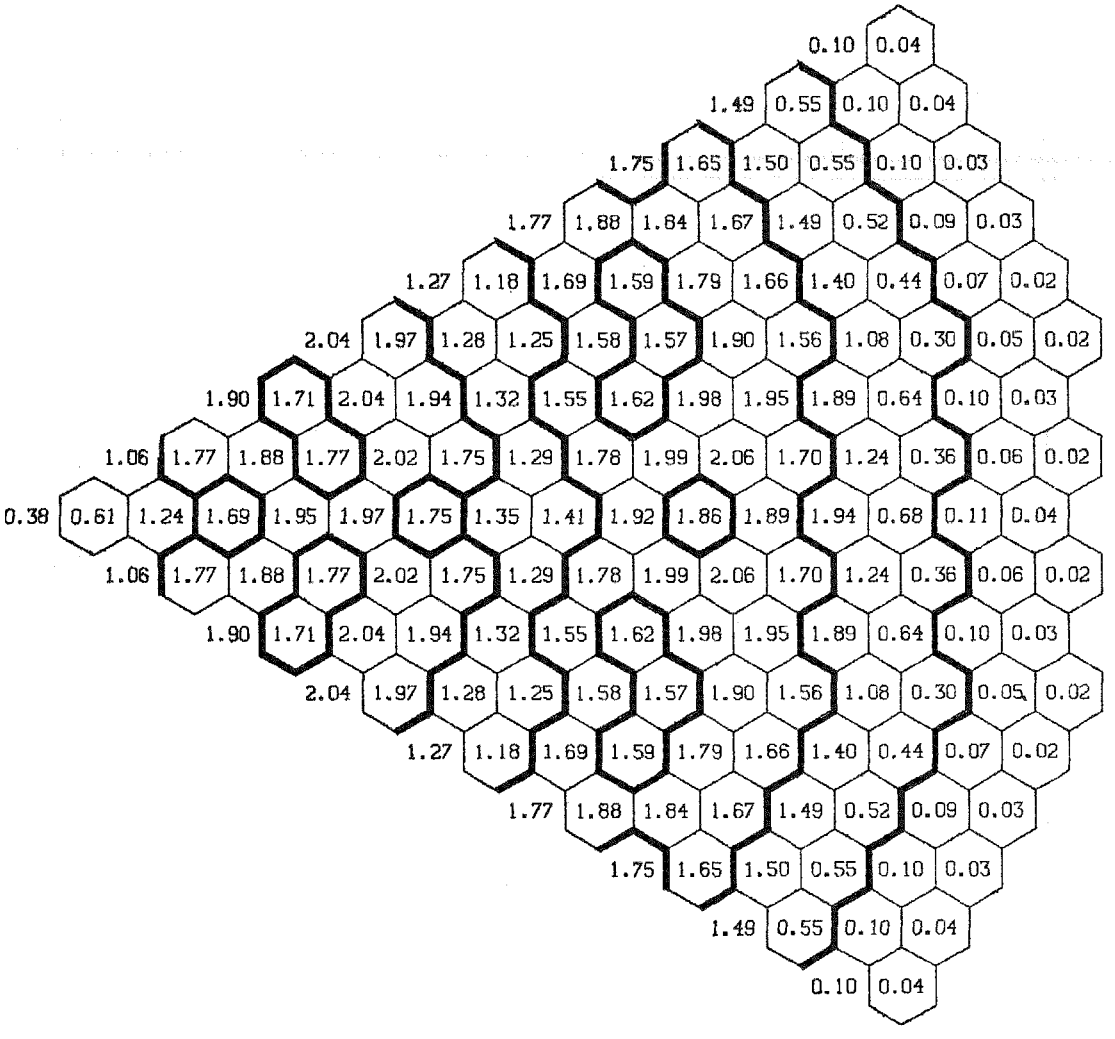

Figure 4.1.3.4.6. Fast fluence (10^{-23} x n/cm^2).

4.1.3.5 Burnup

Average and peak discharge burnups per reactor region are given in Table 4.1.3.5.1. The peak discharge burnup (pellet), is equal to 107340 MWD/T for the core assemblies, 33660 MWD/T for the internal blanket assemblies and 21690 MWD/T for the radial blanket assemblies.

4.1.3.6 Control System

To control reactivity, two independent control systems are used, i.e., the primary and the secondary. The primary system is also used for power shaping. There are 24 control assemblies. Twelve of them, located in rows 7 and 11, belong to the primary system and the other twelve, located in rows 4 and 13, form the secondary control system. Their locations are shown in Figure 2.2.1.

To allocate the control assemblies to the primary and secondary systems the following procedure has been used. The BOL power distribution is determined with all control rods removed. As it is shown in Figure 4.1.3.6.1 this distribution peaks in the outer core zone around the control assemblies located in row 11. Therefore, the row 11 control assemblies have to be assigned to the primary system. If the row 11 control assemblies are inserted to reduce the power peaking, then the power distribution peaks in the middle core zone. Therefore, the row 7 control assemblies have to be assigned to the primary system too. As shown in Figure 4.1.3.3.3, the insertion of control rows 11 and 7 with an insertion ratio, row 11/row 7, equal to 9.873/1 minimizes the BOL power peaking factor (both enrichment zones have the same peak power density).

4.1.3.6.1 Control requirements

4.1.3.6.1.1 Description of control requirements

The independent primary and secondary control systems described in Section 4.1.3.6 are designed to assure that specified acceptable fuel design limits are not exceeded as a result of any anticipated operational occurence or for any single malfunction of the control systems. The primary control system, as both an operational and safety system, must have enough worth at any time in life to shut down the reactor from any operating condition to the refueling temperature with one active member stuck in position[3]. The secondary control

Table 4.1.3.5.1

AVERAGE AND PEAK DISCHARGE BURNUPS
(MWD/T)

Reactor Region	Average	Peak
Core	73200	107340
Internal Blanket 1	7130	21120
Internal Blanket 2	15350	33660
Internal Blanket 3	11450	27040
Internal Blanket 4	12870	28620
Axial Blanket	2470	7520
Radial Blanket	4710	21690

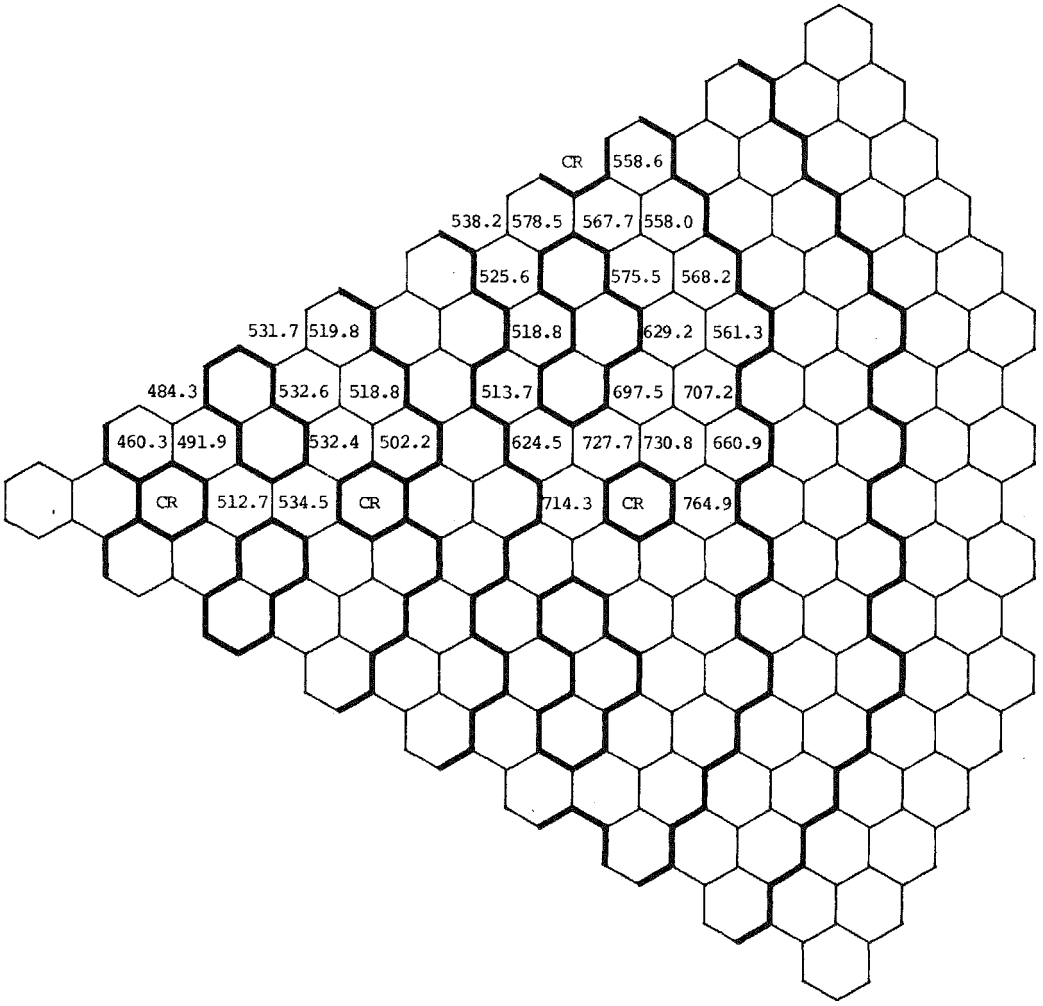

Figure 4.1.3.6.1. Peak power density distribution at BOL with all control rods removed.

system must have sufficient worth at any time in life to shut down the reactor from any operating condition to the hot shut down temperature of the coolant with one active member stuck in position.[3]

The various components of the primary and secondary control systems are listed in Table 4.1.3.6.1.1.1. A brief description of these contributing components to the worth requirements is given below.[3]

a. Hot-to-Cold Shift: The hot-to-cold component compensates for the net positive reactivity insertion due to Doppler effect, radial and axial core contraction, and sodium density changes during reactor shut down from full to zero power. The primary system is designed to take the reactor temperature down from hot-full-power (including 3σ temperature uncertainties and 15% overpower) to refueling temperature. The secondary system is designed to take the reactor temperatures from hot-full-power to standby temperature.
b. Reactivity Fault: The reactivity fault is defined as the reactivity worth of the highest worth inserted control rod running out from its furthest inserted position.
c. Excess Reactivity: This is the excess reactivity required at the beginning of cycle to insure that the reactor can maintain criticality throughout the cycle. Only the primary system is designed to compensate for this excess.
d. Criticality Uncertainty: Control margin is included, in the primary system only, to compensate for the uncertainty in k_{eff} calculation.
e. Fissile Tolerance: Control margin is required only in the primary system to cover the manufacturing uncertainty of the fuel pellets.

4.1.3.6.1.2 Assignment of values for the control requirements

Since the accurate prediction of the control system requirements requires very detailed core performance analysis, a simplified approach is often used in design studies. Both the PRLCDS (Proliferation Resistant Large Core Design Study)[2] and CDS (Conceptual Design Study) projects established a set of values for each of the five components in the control requirements. The basis for these data is the CRBRP-AFMS design. The values for these requirements are shown in Table 4.1.3.6.1.2.1. The hot-to-cold shift value for both the primary and secondary systems is set at 0.94% Δk. The reactivity fault for both the primary and secondary system is set also at 0.94% Δk. Both

Table 4.1.3.6.1.1.1

CONTROL SYSTEM REQUIREMENTS

Primary Control System	Secondary Control System
Hot-To-Cold Shift (To Refueling)	Hot-To-Cold Shift (To Standby)
Reactivity Fault	Reactivity Fault
Excess Reactivity	
Criticality Uncertainty	
Fissile Tolerance	

Table 4.1.3.6.1.2.1

CONTROL REQUIREMENTS FROM PRLCDS AND CDS GROUND RULES

	Primary Control Requirements, %Δk	Secondary Control Requirements, %Δk
Hot-to-Cold Shift	0.94	0.94
Reactivity Fault	0.94	0.94
Excess Reactivity	0.35	
Criticality Uncertainty	± 0.30	
Fissile Tolerance	+ 0.30	
Total	2.23 ± 0.42	1.88
Max. Total	2.65	1.88

criticality uncertainty and fissile tolerance are set by the ground rules to be $\pm$ 0.3% Δk.

However, a closer look at these worth requirements given by the ground rules reveals that, the 0.94% Δk for reactivity fault is an extremely conservative value derived from the CRBRP-AFMS design which has a large excess reactivity[18] (3.77% Δk), thus a large reactivity fault. A more realistic value (still very conservative) for the current design is estimated in the following fashion. The excess reactivity at the beginning-of-equilibrium cycle is 0.35% Δk. The fissile tolerance and criticality uncertainty is 0.30% Δk each. Combining all the uncertainties via their root mean squares with the excess reactivity value of 0.35% Δk in the table below gives:

excess reactivity	0.35
hot-to-cold uncertainty	$\pm$ 0.17
criticality uncertainty	$\pm$ 0.30
fissile tolerance	$\pm$ 0.30
Total system	0.35 $\pm$ 0.46 % Δk
Maximum Total System	0.81 % Δk
Maximum worth rod	$\frac{0.81}{12} \times 1.785 = 0.12\%\ \Delta k$

This gives a 0.12% Δk reactivity fault value. Then, as shown in Tables 4.1.3.6.1.2.1 and 4.1.3.6.1.2.2, the control requirements for both the primary and secondary systems are drastically reduced, from 2.65 to 1.85% Δk for the primary system and from 1.88 to 1.08% Δk for the secondary. Because of the reduced requirements, as shown in the next section, natural boron can be used for both the primary and secondary systems.

4.1.3.6.2 Control system worths

Table 4.1.3.6.2.1 gives the control worths without any uncertainties (2σ or stuck rod) for both the primary and secondary systems for various B-10 enrichments. These worths are computed from 2D hexagonal calculations. Going from natural (19.8%) to 90% B-10, the primary system worth increases from 2.66 to 4.28% Δk, while the secondary system worth increases from 1.60 to 2.46% Δk. Matching these values against the control requirements based on PRLCDS and CDS ground rules (Table 4.1.3.6.1.2.1) or based on current design

Table 4.1.3.6.1.2.2

REVISED CONTROL REQUIREMENTS BASED ON CURRENT DESIGN VALUE OF EXCESS REACTIVITY

	Primary Control Requirements, %Δk	Secondary Control Requirements, %Δk
Hot-to-Cold Shift	0.94	0.94
Reactivity Fault	0.14	0.14
Excess Reactivity	0.35	
Criticality Uncertainity	± 0.30	
Fissile Tolerance	± 0.30	
Total	1.43 ± 0.42	1.08
Max. Total	1.85	1.08

Table 4.1.3.6.2.1

CONTROL SYSTEM WORTHS WITHOUT ANY UNCERTAINTIES

B-10 Enrichment, %	Primary System Worth, % Δk	Secondary System Worth, % Δk
19.8 (Natural)	2.66	1.60
30	3.09	1.84
60	3.70	2.25
90	4.28	2.46

requirements (Table 4.1.3.6.1.2.2), it is necessary to use 60% and 90% B-10 enrichments, respectively, in the primary and secondary systems to meet the PRLCDS and CDS ground rule control requirements, but only natural boron in both the primary and secondary systems to satisfy the revised control requirements. These requirements are worths given in Tables 4.1.3.6.2.2 and 4.1.3.6.2.3. The $2\breve{\sigma}$ values used in the above two tables are unity bias values with $1\sigma = 4\%$. The interaction factor value of 1.785 is set by the PRLCDS and CDS ground rules and used also in the revised requirement estimates for the sake of conservatism. From Table 4.1.3.6.2.2, the PRLCDS-CDS requirements are 2.65 and 1.88% Δk, respectively, for the primary and secondare systems. A 60% B-10 primary system has a worth (-2σ and stuck rod) of 2.85% Δk and a 90% B-10 secondary system has a worth (-2σ and stuck rod) of 1.89%, thus satisfying the PRLCDS-CDS requirements. The revised requirements, based on the current design value of excess reactivity and its maximum fault, are 1.85 and 1.08% Δk, respectively, for the primary and secondary systems. Using natural boron, the primary and secondary systems have worths (-2σ and stuck rod) of 2.06 and 1.25% Δk, respectively. Therefore, natural boron can be used for both the primary and secondary systems to meet the revised requirements.

4.1.3.7 Breeding Performance

For the breeding performance analysis a two-dimensional RZ model and eight neutron-group cross-sections have been used. Two types of doubling time were calculated. In the first case, it was assumed that all the control rods were parked at the top of the upper axial blanket. A doubling time for a reactor without control rods is ficticious. Nevertheless, since it is a figure of merit calculated in other reactor design projects, it was calculated for purposes of comparison. In the second case, the presence of the primary control system in the upper axial blanket was taken into account. The impact of the control rods parked position on the reactor breeding and transient performance is discussed in detail in Appendix A and Section 4.4, respectively.

Region-wise breeding ratios, fissile inventories, fissile gains, and compound system doubling times are presented in Tables 4.1.3.7.1 and 4.1.3.7.2. The breeding ratio is defined as the ratio of the rate of production of atoms of the fissile isotopes ^{239}Pu and ^{241}Pu to the rate of destruction of atoms of the same isotopes. The compound system doubling time is determined from the relation[5]:

Table 4.1.3.6.2.2

CONTROL REQUIREMENTS DICTATED BY CDS GROUND RULES
AND CONTROL WORTHS OF 60% B-10 PRIMARY AND 90% SECONDARY SYSTEM

Primary Control Requirements, %Δk, CDS Ground Rules		
Hot-to-cold shift	0.94	
Reactivity fault	0.94	
Excess reactivity at BOEC	0.35	
Criticality uncertainty		± 0.30
Fissile tolerance		± 0.30
Total	2.23	± 0.42
Maximum Requirement	2.65	
Primary Control Worths, %Δk, 60% B-10		
Primary control	3.70	
-2σ values*	-0.30	
Stuck rod**	-0.55	
Total	2.85	
Secondary Control Requirements, %Δk, CDS Ground Rules		
Hot-to-cold shift	0.94	
Reactivity fault	0.94	
Total	1.88	
Maximum requirements	1.88	
Secondary Control Worths, %Δk, 90% B-10		
Secondary control	2.46	
-2σ values *	-0.20	
Stuck rod **	-0.37	
TOTAL	1.89	

* Unity bias, 1σ = 4%.
**Interaction factor = 1.785.

Table 4.1.3.6.2.3

CONTROL REQUIREMENTS BASED ON REACTIVITY FAULT ESTIMATES AND CONTROL WORTHS WITH NATURAL BORON

Primary Control Requirements, %Δk, as Estimated		
Hot-to-cold shift	0.94	
Reactivity fault	0.14	
Excess reactivity at BOEC	0.35	
Criticality uncertainty		± 0.30
Fissile tolerance		± 0.30
Total	1.43	± 0.42
Maximum Requirement	1.85	
Primary Control Worths, %Δk, Natural Boron		
Primary control	2.66	
-2σ values*	-0.21	
Stuck rod**	-0.39	
Total	2.06	
Secondary Control Requirements, %Δk, as Estimated		
Hot-to-cold shift	0.94	
Reactivity fault	0.14	
Total	1.08	
Maximum Requirements	1.08	
Primary Control Worths, %Δk, Natural Boron		
Secondary Control	1.60	
-2σ values*	-0.13	
Stuck rod**	-0.24	
Total	1.23	

*Unity bias, 1σ = 4%.
** Interaction factor = 1.785

Table 4.1.3.7.1

BREEDING RATIOS

Reactor Region	BOL	BOEC	EOEC
Inner Core	0.067	0.065	0.067
Middle Core	0.138	0.136	0.138
Outer Core	0.380	0.347	0.319
Total Core	0.585	0.548	0.524
Internal Blanket 1	0.046	0.047	0.051
Internal Blanket 2	0.093	0.090	0.091
Internal Blanket 3	0.266	0.260	0.260
Internal Blanket 4	0.138	0.124	0.114
Total Internal Blanket	0.543	0.521	0.516
Axial Blanket	0.151	0.149	0.151
Radial Blanket	0.230	0.213	0.192
Reactor Total	1.509	1.431	1.383

Table 4.1.3.7.2

FISSILE INVENTORY, FISSILE GAIN, AND
COMPOUND SYSTEM DOUBLING TIME

	A		B	
Fissile Inventory (kg)	BOEC	EOEC	BOEC	EOEC
Core	3,983.8	3,723.3	4,005.5	3,741.9
Internal Blanket	366.4	690.2	359.6	677.2
Axial Blanket	114.6	223.7	104.0	203.2
Radial Blanket	296.8	435.1	297.1	435.5
Total Reactor	4,761.6	5,072.3	4,766.2	5,057.8
Fissile Gain (kg)	310.7		291.7	
CSDT (years)	15.17		16.25	

[A] All control rods parked at the top of upper axial blanket

[B] Primary control rods are parked at core/upper axial blanket interface, secondary control rods are parked at the top of upper axial blanket

$$CSDT = 0.693 \times \frac{M_{in} + M_{ex}}{(G-L_p-L_d) \times (cycles/yr)}$$

where

M_{in} = in-reactor fissile inventory
M_{ex} = external cycle fissile inventory
G = fissile gain/cycle
L_p = processing loss
L_d = ^{241}Pu decay loss

The external cycle fissile inventory is determined from the relation

$$M_{ex} = M_{in} \times R.F \times \frac{T_{ex}}{T_{cycle}}$$

where

R.F. = refueling fraction
T_{ex} = external cycle time
T_{cycle} = cycle length

The processing losses have been taken as 1% and the external cycle time is equal to one year. The total reactor fissile inventory at BOEC is equal to 4761.6 kg, the fissile gain over the equilibrium cycle is equal to 310.7 kg and the CSDT is equal to 15.17 years. Since the primary control system is in the reactor during reactor operation, this doubling time has to be increased to 16.47 years (Appendix A). This value is well within the objective of a CSDT of 15-16 years (Section 1.1).

4.1.3.8 Safety Parameters

In this section, two of the main reactor safety parameters, i.e., sodium void reactivity and Doppler coefficient are presented.

A. Sodium Void Reactivity

As discussed in Section 1.1 the sodium void reactivity is the most important

design constraint for this reactor. A limit of $2.50 has been imposed on the reactivity change resulting from voiding the flowing sodium in the core and upper axial blanket.

Flowing sodium void reactivities for BOL and EOEC conditions are presented in Table 4.1.3.8.1. These reactivities have been calculated as follows. Perturbation calculations have been performed in two-dimensional RZ geometry to determine the reactivities resulting from voiding the different reactor regions. Then total sodium void reactivities have been determined for flowing sodium in the core and upper axial blanket from direct eigenvalue calculations. These calculations have shown that perturbation theory underpredicts the core plus upper axial blanket flowing sodium void reactivity by less than 15¢. Finally, as discussed in Appendix F, an additional correction must be made to account for the differences between two-dimensional RZ and three-dimensional hexagonal-Z calculations. The corrected core plus upper axial blanket sodium void reactivities presented in Table 4.1.3.8.1 include both these corrections. All sodium void reactivity calculations have been performed using twenty-one neutron-group cross-sections prepared for sodium-in and sodium-out configurations.

As Table 4.1.3.8.1 shows the flowing sodium void reactivity for core plus upper axial blanket sodium voiding is $1.32 at BOL and $2.58 at EOEC. The EOEC sodium void reactivity is slightly over the design limit of $2.50. However, as discussed in Appendix N, the calculated void reactivity of $2.58 is expected to be conservative.

B. Doppler Coefficient

Isothermal Doppler coefficients for BOL and EOEC conditions, for sodium-in and sodium-out configurations are shown in Table 4.1.3.8.2. Only the Doppler broading of ^{238}U resonances was considered. Sodium voiding hardens the neutron spectrum and reduces the Doppler coefficient. Burnup also reduces the core Doppler coefficient but increases the internal blanket Doppler coefficient. The total core Doppler coefficient at BOL is 0.0055 for sodium-in and 0.0039 for sodium-out conditions and decreases to 0.0046 and 0.0029, respectively, at the EOEC. The total internal blanket Doppler coefficient is 0.0048 and 0.0040 at BOL for sodium-in and sodium-out, respectively, and increases to 0.0059 and 0.0044 at EOEC.

The core Doppler coefficient of the heterogeneous design analyzed, is smaller

Table 4.1.3.8.1

FLOWING SODIUM VOID REACTIVITIES ($)

Reactor Region	BOL	EOEC
	Perturbation Results	
Inner Core	0.208	0.396
Middle Core	0.438	0.886
Outer Core	0.806	1.316
Total Core	1.452	2.598
Internal Blanket 1	0.006	0.041
Internal Blanket 2	0.204	0.268
Internal Blanket 3	0.406	0.553
Internal Blanket 4	0.266	0.247
Total Internal Blanket	0.882	1.109
Radial Blanket	-0.226	-0.140
Axial Blanket	-0.190	-0.178
Core and Upper Axial Blanket	1.357	2.509
	Corrected	
Core and Upper Axial Blanket	1.322	2.575

Table 4.1.3.8.2

ISOTHERMAL DOPPLER COEFFICIENTS ($-T \frac{dk}{dT} \times 10^4$)

	BOL		EOEC	
Reactor Region	Sodium In	All Sodium Out	Sodium In	All Sodium Out
Inner Core	6.329	5.510	6.657	4.025
Middle Core	13.741	11.175	13.925	8.959
Outer Core	35.394	22.363	25.618	16.364
Total Core	55.464	39.048	46.200	29.348
Internal Blanket 1	2.157	2.376	4.332	3.555
Internal Blanket 2	9.524	8.721	11.780	8.492
Internal Blanket 3	20.011	17.878	29.680	23.312
Internal Blanket 4	16.673	11.725	13.405	8.566
Total Internal Blanket	48.365	40.070	59.197	43.925
Radial Blanket	7.089	5.577	7.575	6.566
Axial Blanket	4.493	4.198	6.754	6.368

than the core Doppler coefficient of an equivalent homogeneous design. However, if the contribution of the internal blanket is taken into account, the total reactor Doppler coefficient will be higher than the core contribution alone. As burnup proceeds, the buildup of plutonium in the internal blanket increases the contribution of the internal blanket to the total reactor Doppler coefficient.

4.1.3.9 Expansion and Bowing Reactivities

A. Expansion Reactivity Coefficients

Temperature changes in a reactor result in reactor dimension changes which in turn introduce reactivity perturbations. The uniform axial fuel expansion reactivity coefficient is defined as the reactivity change that results from the expansion of the fuel pellet stack height by a unit of length. The uniform radial expansion reactivity coefficient is defined as the reactivity change that results from the uniform radial expansion of the lower core support plate by a unit of length.

Axial fuel and radial reactor expansion coefficients have been determined for BOL conditions, for the reactor analyzed in this report, from direct k_{eff} calculations. A 2D-RZ model and 21 neutron group cross-sections were used. In the axial expansion calculations the fuel pellet stack height was increased keeping the mass of the pellets constant. Similarly, in the radial expansion calculations the radius of the core support plate was increased keeping the mass of the fuel and structural material constant. The resulting reactivity expansion coefficients are -0.070 cents/mil for uniform axial fuel expansion and -0.151 cents/mil for uniform radial reactor expansion.

B. Radial Bowing Reactivity Coefficients

Fuel and blanket assembly bowing is a phenomenon dependent on both the temperature gradients across the fuel and blanket assemblies and the irradiation induced swelling of the structural material. For a given row of assemblies, the radial bowing reactivity coefficient at a given axial location is defined as the change in reactivity associated with the radial motion of fuel, structural and coolant materials per unit change of radial motion. To this end, material reactivity worths, resulting from addition of material, and their radial gradients across a row of assemblies on a row-by-row basis have been determined.

The reactivity worths of the fuel, structure and coolant at various locations in the core, internal and radial blankets have been determined for the reference reactor at the beginning-of-life condition. The reactor is divided into 17 cylindrical rings, as shown in Fig. 4.1.3.9.1. Each ring has 20 axial subdivisions, 10 in the core region 5 in the lower and 5 in the upper axial blanket. Perturbation calculations in RZ geometry are conducted for this analysis.

Tables 4.1.3.9.1, 4.1.3.9.2 and 4.1.3.9.3 tabulate the reactivity worth in ¢/kg for the fuel, structure, and coolant, respectively. For each region, the reactivity worths near-the-left and near-the-right radial boundaries are given. Specifically, a reactivity worth near-the-left radial boundary is the worth averaged over a volume adjacent to the left radial boundary having 5% of the total volume of the region being considered. A similar definition applies to the reactivity worth near-the-right radial boundary. The differences between the near-right and near-left boundary values of these material reactivity worths gives the worth gradients across a row of assemblies. These worth gradients can then be used to obtain the radial bowing reactivity coefficients.

As shown in Table 4.1.3.9.1, the fuel reactivity worth is positive in all the core regions, ranging from a maximum of 1.40¢/kg at the 7th row core mid-plane, to a minimum of 0.22¢/kg at the 15th row core axial-blanket interface. In the axial and radial blankets, the fuel reactivity worth can be either positive or negative, depending on its location. Furthermore, the worth of fuel in the axial and radial blankets is usually smaller than its worth in the core regions by two orders of magnitude. For example, the fuel reactivity worth in the axial blanket is -0.01¢/kg and +0.02¢/kg, respectively, at the 5th and 15th row core-axial blanket interfaces. The fuel reactivity worth is negative in all the internal blanket regions. It ranges in value from zero at 35 inches above the core mid-plane to -0.73¢/kg at the 6th row mid-plane location.

The reactivity worth of the structural material is negative in the core regions with the exception of the right boundary of the last core row. For example, from Table 4.1.3.9.2, the reactivity worth of the structural material varies from -0.23¢/kg to -0.51¢/kg at the core mid-plane location of all the core regions, except in the 15th row, when its near-the-right bound-

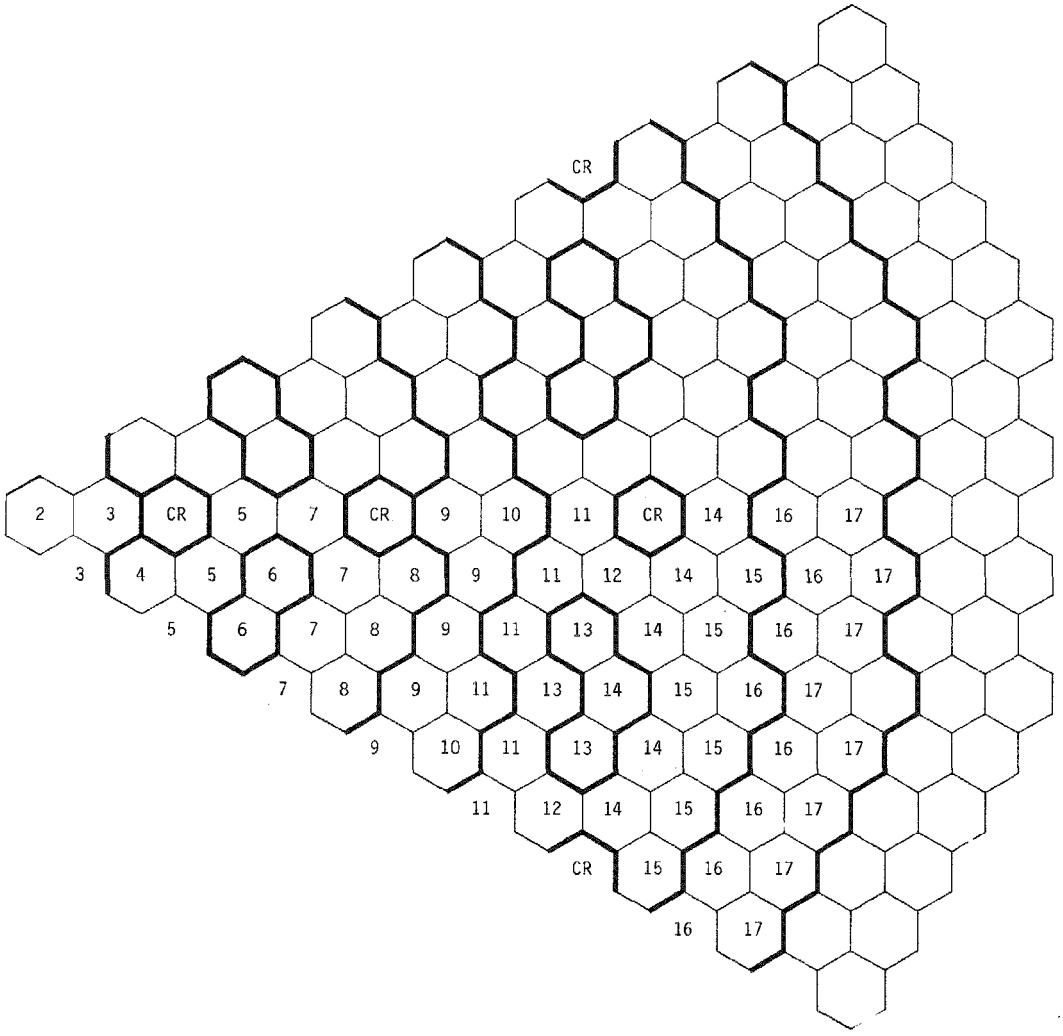

Figure 4.1.3.9.1 Assignment of Assemblies into Rings

Table 4.1.3.9.1

REACTIVITY WORTH OF FUEL

Axial Location (Inches Above Fuel Assembly Mid-Plane)		CENTS PER KILOGRAM X10^2															
		Row 2	Row 3	Row 4	Row 5	Row 6	Row 7	Row 8	Row 9	Row 10	Row 11	Row 12	Row 13	Row 14	Row 15	Row 16	Row 17
		Int. Blkt.	Int. Blkt.	Core	Core	Int. Blkt.	Core	Core	Int. Blkt.	Int. Blkt.	Core	Core	Int. Blkt.	Core	Core	Rad. Blkt.	Rad. Blkt.
Upper Axial Blanket	35	* 0.0	0.0	0.0	0.0	0.0	0.0	0.0	0.0	0.0	0.0	0.0	0.0	0.0	0.0	0.0	0.0
		** 0.0	0.0	0.0	0.0	0.0	0.0	0.0	0.0	0.0	0.0	0.0	0.0	0.0	0.0	0.0	0.0
	32	0.0	0.0	0.0	-0.1	-0.1	0.0	0.0	0.0	-0.1	0.0	0.0	-0.1	0.0	0.0	0.0	0.0
		0.0	0.0	0.0	0.0	-0.1	0.0	0.0	-0.1	0.0	0.0	0.0	-0.1	0.0	0.0	0.0	0.0
	29	-0.1	-0.1	0.0	-0.2	-0.3	0.0	0.0	-0.2	-0.2	0.0	0.0	-0.2	0.0	0.2	0.1	0.0
		-0.1	-0.1	-0.1	-0.1	-0.2	0.0	0.0	-0.2	-0.1	0.0	0.1	-0.2	0.1	0.1	0.0	0.0
	26	-0.2	-0.3	-0.1	-0.6	-0.9	-0.1	-0.1	-0.5	-0.7	0.0	0.0	-0.7	0.0	0.6	0.2	0.0
		-0.3	-0.3	-0.3	-0.3	-0.7	-0.1	0.1	-0.7	-0.4	0.1	-0.2	-0.7	0.5	0.4	0.0	0.0
	23	-0.5	-0.7	0.1	-1.4	-2.7	-0.4	0.2	-1.5	-2.2	0.2	0.3	-2.5	-0.5	1.9	0.7	0.0
		-0.7	-0.7	-0.8	-0.9	-2.4	-0.2	-0.1	-2.3	-1.2	0.5	-1.0	-2.4	1.7	1.5	0.1	0.0
Core Upper Half	20	-1.1	-1.8	30.1	38.6	-11.6	44.4	42.2	-5.8	-7.3	35.2	41.6	-10.7	39.1	34.5	2.1	0.1
		-1.7	-2.3	35.4	39.9	-11.0	44.5	34.3	-7.4	-5.6	41.7	40.8	-10.6	36.3	22.4	0.2	0.0
	16	-2.2	-4.0	49.2	61.9	-29.0	71.8	67.3	-15.3	-16.9	58.5	67.3	-27.0	64.0	56.9	2.4	0.1
		-3.5	-7.1	56.5	64.8	-28.4	72.0	56.5	-16.9	-15.6	67.4	66.7	-26.8	59.4	39.2	0.2	-0.1
	12																

Table 4.1.3.9.1

REACTIVITY WORTH OF FUEL (continued)

Axial Location (Inches Above Fuel Assembly Mid-Plane)	CENTS PER KILOGRAM X10^2															
	Row 2	Row 3	Row 4	Row 5	Row 6	Row 7	Row 8	Row 9	Row 10	Row 11	Row 12	Row 13	Row 14	Row 15	Row 16	Row 17
	Int. Blkt.	Int. Blkt.	Core	Core	Int. Blkt.	Core	Core	Int. Blkt.	Int. Blkt.	Core	Core	Int. Blkt.	Core	Core	Rad. Blkt.	Rad. Blkt.
12	-3.4	-6.5	69.9	86.8	-47.9	101.5	96.1	-25.9	-27.6	83.8	95.3	-45.1	90.8	81.0	2.4	0.1
	-5.7	-12.5	79.1	91.1	-47.4	101.4	80.7	-27.5	-26.6	95.4	94.6	-44.9	84.5	57.3	0.2	-0.1
8	-4.4	-8.6	87.0	107.6	-63.6	126.2	119.3	-34.8	-36.5	104.9	118.7	-60.4	113.3	101.2	2.3	0.0
Core Upper Half	-7.5	-17.1	97.9	113.1	-63.3	125.9	100.8	-36.3	-35.9	118.7	118.0	-60.2	105.4	72.3	0.1	-0.1
4	-5.0	-9.8	96.7	119.3	-72.5	140.2	132.6	-39.9	-41.6	116.9	131.9	-69.0	126.0	112.6	2.2	0.0
	-8.5	-19.7	108.5	125.6	-72.3	139.8	112.3	-41.4	-41.2	132.0	131.3	-68.9	117.2	80.8	0.1	-0.1
0	Legend: * Near-the-left boundary. ** Near-the-right boundary.															

Table 4.1.3.9.2

REACTIVITY WORTH OF STRUCTURAL MATERIAL

Axial Location (Inches above center of fuel assembly)	CENTS PER KILOGRAM X10^2															
	Row 2	Row 3	Row 4	Row 5	Row 6	Row 7	Row 8	Row 9	Row 10	Row 11	Row 12	Row 13	Row 14	Row 15	Row 16	Row 17
	Int. Blkt.	Int. Blkt.	Core	Core	Int. Blkt.	Core	Core	Int. Blkt.	Int. Blkt.	Core	Core	Int. Blkt.	Core	Core	Rad. Blkt.	Rad. Blkt.
35	0.0	0.0	0.1	0.1	0.0	0.1	0.1	0.0	0.0	0.0	0.1	0.1	0.1	0.1	0.0	0.0
	0.0	0.0	0.1	0.1	0.0	0.1	0.0	0.0	0.0	0.1	0.1	0.1	0.1	0.0	0.0	0.0
32	0.0	0.0	0.2	0.2	0.1	0.2	0.3	0.1	0.1	0.1	0.2	0.2	0.2	0.2	0.1	0.0
	0.0	0.1	0.2	0.2	0.1	0.2	0.2	0.0	0.1	0.2	0.2	0.2	0.2	0.1	0.0	0.0
29	0.0	0.1	0.5	0.6	0.4	0.7	0.8	0.3	0.1	0.5	0.7	0.4	0.7	0.7	0.3	0.0
	0.0	0.3	0.7	0.6	0.4	0.8	0.5	0.1	0.3	0.7	0.7	0.4	0.7	0.4	0.1	0.0
26	-0.1	0.2	1.3	1.5	0.9	1.9	2.2	0.7	0.3	1.4	1.9	1.0	1.8	2.0	0.8	0.1
	-0.1	0.8	1.8	1.6	1.1	2.1	1.4	0.2	0.8	2.0	1.7	1.0	2.1	1.2	0.2	0.0
23	-0.2	0.3	3.3	3.1	1.4	4.5	5.1	1.4	0.0	3.7	4.8	1.6	3.8	5.5	2.3	0.3
	0.1	2.0	3.6	3.6	2.0	4.9	3.4	-0.2	1.8	5.1	3.5	1.6	5.6	3.6	0.4	0.0
20	-0.5	0.2	3.9	-0.2	-4.6	-0.5	0.9	-0.5	-2.9	1.9	0.5	-3 3	-1.3	4.2	5.8	0.7
	-0.1	2.8	-0.4	-1.9	-3.5	1.0	2.0	-3.3	-0.2	0.9	-1.5	-3.7	3.4	7.2	1.0	0.1
16	-1.2	-0.4	0.7	-10.6	-18.0	-14.7	-11.5	-6.8	-9.3	-6.0	-13.1	-15.4	-14.4	-4.4	8.7	1.2
12	-0.7	1.0	-9.8	-15.9	-16.7	-12.1	-5.1	-9.7	-7.0	-12.7	-14.2	-16.1	-6.8	9.1	1.8	0.1

Upper Axial Blanket

Core Upper Half

Table 4.1.3.9.2

REACTIVITY WORTH OF STRUCTURAL MATERIAL (continued)

Axial Location (Inches above center of fuel assembly)	CENTS PER KILOGRAM X10^{-2}															
	Row 2	Row 3	Row 4	Row 5	Row 6	Row 7	Row 8	Row 9	Row 10	Row 11	Row 12	Row 13	Row 14	Row 15	Row 16	Row 17
	Int. Blkt.	Int. Blkt.	Core	Corw	Int. Blkt.	Core	Core	Int. Blkt.	Int. Blkt.	Core	Core	Int. Blkt.	Core	Core	Rad. Blkt.	Rad. Blkt.
12	-1.9	-1.3	-2.8	-22.2	-32.6	-30.2	-25.4	-13.9	-16.7	-14.7	-27.8	-29.2	-29.0	-13.7	11.5	1.7
	-1.5	-1.1	-20.4	-31.1	-31.2	-26.8	-12.9	-17-1	-14.6	-27.3	-28.7	-30.1	-17.8	10.8	2.5	0.1
Upper Axial Blanket 8	-2.5	-2.1	-5.9	-32.0	-44.8	-43.0	-37.0	-19.9	-22.9	-22.0	-40.2	-40.8	-41.4	-21.4	13.7	2.1
	-2.3	-2.9	-29.3	-43.7	-43.3	-39.1	-19.5	-23.3	-21.0	-39.6	-40.9	-41.9	-27.0	12.2	3.1	0.2
4	-2.9	-2.6	-7.6	-37.6	-51.7	-50.3	-43.6	-23.3	-26.5	-26.2	-47.2	-47.4	-48.4	-25.8	15.0	2.3
	-2.7	-4.0	-34.4	-50.8	-50.1	-46.1	-23.3	-26.8	-24.6	-46.6	-47.9	-48.6	-32.2	13.0	3.4	0.2
0	Legend: * Near-the-left boundary ** Near-the-right boundary															

Table 4.1.3.9.3

REACTIVITY WORTH OF SODIUM

Axial Location (Inches Above Fuel Assmebly Mid-Plane)	CENTS PER KILOGRAM X10^2															
	Row 2	Row 3	Row 4	Row 5	Row 6	Row 7	Row 8	Row 9	Row 10	Row 11	Row 12	Row 13	Row 14	Row 15	Row 16	Row 17
	Int. Blkt.	Int. Blkt.	Core	Core	Int. Blkt.	Core	Core	Int. Blkt.	Int. Blkt.	Core	Core	Int. Blkt.	Core	Core	Rad. Blkt.	Rad. Blkt.
35	0.0*	0.0	0.0	0.1	0.0	0.1	0.1	0.0	0.0	0.0	0.1	0.0	0.1	0.1	0.0	0.0
	-0.1**	0.0	0.1	0.0	0.0	0.1	0.0	0.0	0.0	0.1	0.1	0.0	0.1	0.0	0.0	0.0
32	-0.1	-0.1	0.2	0.2	0.0	0.2	0.3	0.0	0.0	0.1	0.3	0.1	0.3	0.3	0.1	0.0
	-0.1	0.0	0.2	0.2	0.0	0.3	0.2	0.0	0.0	0.2	0.3	0.1	0.3	0.2	0.0	0.0
29	-0.1	-0.1	0.6	0.7	0.0	0.8	1.2	0.1	-0.1	0.6	0.9	0.3	0.9	1.0	0.4	0.0
Upper Axial Blanket	-0.1	0.2	1.0	0.6	-0.2	1.1	0.6	-0.2	0.1	0.9	0.9	0.3	1.1	0.6	0.1	0.0
26	-0.4	-0.2	1.9	2.5	0.3	2.7	4.0	0.4	-0.5	2.1	3.1	1.0	2.8	3.7	1.3	0.1
	-0.3	0.8	3.1	1.9	0.7	3.7	1.9	-0.7	0.7	3.2	2.6	1.0	3.7	2.3	0.2	0.0
23	-1.0	-0.6	6.6	7.6	1.1	8.7	11.9	1.6	-2.3	7.3	10.4	2.2	7.8	12.4	4.6	0.4
	-0.7	3.3	8.6	6.5	2.4	11.5	6.5	-2.8	2.7	11.2	6.8	2.2	12.6	7.7	0.6	0.0
20	-2.2	-1.6	14.8	10.0	-6.7	9.0	13.8	1.6	-9.8	12.3	12.2	-3.6	5.3	18.7	14.4	1.0
Core Upper Half	-2.0	9.0	8.5	4.6	-3.4	14.7	11.8	-11.1	3.6	13.8	4.2	-4.4	17.7	20.1	1.6	0.0
16	-4.5	-4.6	13.2	-4.1	-32.6	-13.7	-3.4	-9.2	-26.5	2.2	-8.1	-26.0	-15.9	7.8	22.9	1.7
	-4.9	8.2	-4.0	-18.8	-27.9	-3.8	3.1	-28.5	-6.8	-6.3	-17.0	-27.2	3.6	28.4	2.7	0.0
12																

Table 4.1.3.9.3

REACTIVITY WORTH OF SODIUM (continued)

Axial Location (Inches Above Fuel Assembly Mid-Plane)	CENTS PER KILOGRAM X10^2															
	Row 2	Row 3	Row 4	Row 5	Row 6	Row 7	Row 8	Row 9	Row 10	Row 11	Row 12	Row 13	Row 14	Row 15	Row 16	Row 17
	Int. Blkt.	Int. Blkt.	Core	Core	Int. Blkt.	Core	Core	Int. Blkt.	Int. Blkt.	Core	Core	Int. Blkt.	Core	Core	Rad. Blkt.	Rad. Blkt.
12	-7.1	-8.3	10.8	-20.8	-61.5	-38.9	-23.5	-22.0	-45.8	-9.6	-30.7	-52.3	-40.6	-4.2	31.0	2.3
	-8.4	6.3	-19.2	-44.6	-55.5	-25.3	-7.3	-48.4	-19.3	-28.3	-41.0	-54.0	-11.7	36.4	3.7	0.0
8	-9.3	-11.5	8.6	-35.1	-85.7	-59.8	-40.4	-32.9	-62.0	-19.5	-49.7	-74.6	-61.6	-14.2	37.6	2.7
	-11.5	4.6	-32.1	-66.2	-78.6	-43.3	-16.1	-65.2	-29.8	-46.7	-63.2	-76.7	-24.6	42.9	4.5	0.0
Core Upper Half 4	-10.5	-13.3	7.4	-43.2	-99.4	-71.7	-50.0	-39.1	-71.2	-25.1	-60.5	-87.3	-73.6	-19.9	41.3	3.0
	-13.2	3.6	-39.5	-78.3	-91.8	-53.6	-21.1	-74.7	-35.8	-57.2	-75.3	-89.6	-31.8	46.6	4.9	0.0
0	Legend: * Near the left boundary ** Near the right boundary															

ary value is +0.13¢/kg. The reactivity worth of the structural material in the axial, internal, and radial blankets varies from -0.00 to +0.15¢/kg.

The sodium reactivity worths (addition of sodium) is usually negative in the core regions. Its value ranges from -0.21 to -0.74¢/kg. The exceptions are the left boundary of the 4th row which is adjacent to the center internal blanket and the right boundary of the 15th row, which is adjacent to the radial blanket. There, the sodium reactivity worths are positive. For example, from Table 4.1.3.9.3, at the core mid-plane location, the sodium reactivity worth is +0.07¢/kg at the left boundary of the 4th row and +0.47¢/kg, at the right boundary of the 15th row. In the internal blankets, the sodium reactivity worths are in general more negative than those in the core regions. For example, at the core mid-plane locations at the 6th, 9th, 10th,and 13th row internal blankets, the sodium reactivity worths near-the-left boundaries are -0.99, -0.39, -0.71, and 0.87¢/kg, respectively, while as mentioned before, the sodium reactivity worths in the core vary from -0.21 to -0.74¢/kg. In the radial blankets, the sodium reactivity worth is positive and its value varies from 0.00 to +0.41¢/kg. The sodium reactivity worth in the axial blankets varies from 0.00 to +0.13¢/kg.

4.1.3.10 Shielding

To assure that irradiation damage to in-reactor structures from fast neutrons does not exceed design limits, selected shielding calculations have been performed to determine the total flux emerging from the outer radial reflector surface and the total flux incident on the upper surface of the reactor support grid plate. From diffusion calculations it was determined that the thirty year fast fluence (>0.1 Mev) at the outer surface of the radial reflector for a reflector thickness of one and two rows is 2.34×10^{22} and 8.97×10^{21} neutrons/cm^2, respectively. Since the design limit is equal to 2×10^{22} neutrons/cm^2 (Section 2.1), two rows of radial reflector assemblies were chosen.

At the time the shielding analysis was performed, no specific design had been developed for the part of the assembly below the lower axial blanket. Thus, to determine the neutron flux incident on the support grid plate, the assumption was made that the dimensions of the reactor regions below the lower axial blanket and their material compositions are the same as in FFTF.[19] These dimensions and compositions are shown in Figure 4.1.3.10.1 and Table 4.1.3.10.1,respectively.The total flux incident on the upper surface of the support grid plate was calculated

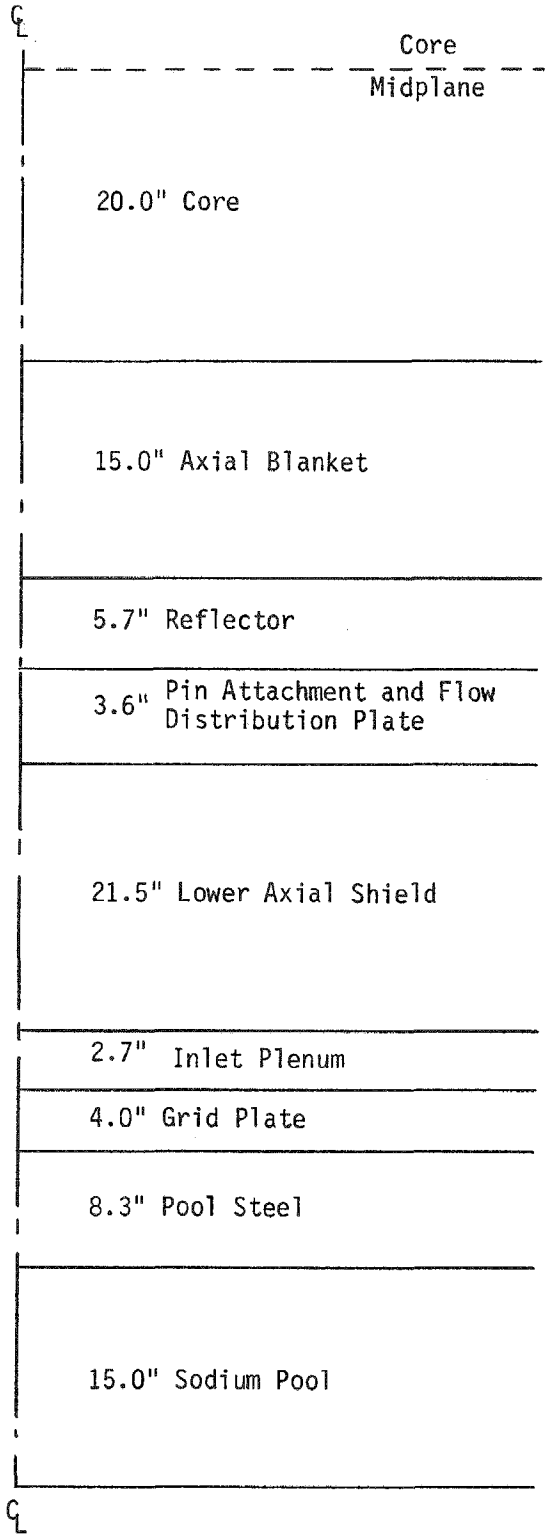

Figure 4.1.3.10.1 Reactor modeling for the lower axial shield calculations.

Table 4.1.3.10.1

MATERIAL COMPOSITIONS[α] FOR LOWER AXIAL SHIELD CALCULATIONS

Region	Material Volume Fractions			
	SS 316	Inconel	Sodium	Void
Axial Reflector	0.238	0.318	0.408	0.036
Pin Attachment and Flow Distribution Plate	0.545		0.455	
Lower Axial Shield	0.793		0.207	
Inlet Plenum	0.090		0.910	
Grid Plate	0.744		0.256	
Pool Steel	0.079		0.921	
Sodium Pool			1.000	

[α]FFTF (However, the lower core and subassemblies supports will be of much less expensive configuration.)

using diffusion theory. As shown in Figure 4.1.3.10.2., the total flux peaks at radial position 45.721 cm from the core center and its peak value is 1.16×10^{12} neutrons/cm^2. This value is only ~12% of the value calculated for FFTF. Therefore, the shielding used in this analysis for the support grid plate is adequate. The axial distribution of the total flux at position 54.721 cm is shown in Figure 4.1.3.10.3. A shielding design for the part of the assembly below the lower axial blanket was developed later by the ANL team (Volume 2). However, this design was not optimized.

4.1.3.11 Delayed Neutron Fraction and Prompt Neutron Lifetime

Effective delayed neutron fractions and decay constants for six groups of delayed neutron precursors are given in Table 4.1.3.11.1. This data is required to analyze the time-dependent behavior of the reactor. The total effective delayed neutron fraction is 0.00380 at BOL conditions and 0.00366 at EOEC conditions. The prompt neutron lifetime is 0.356×10^{-6} seconds at BOL and 0.363×10^{-6} seconds at EOEC conditions.

4.2 THERMAL-HYDRAULIC ANALYSIS

4.2.1 Plant Conditions

The total reactor power (fission and γ heating) is equal to 3084 MW (thermal). The reactor coolant inlet temperature is equal to 595° F and the reactor coolant outlet temperature is equal to 875° F. A fraction of the total flow equal to 5% is used as cold by-pass flow. The by-pass flow is expected to decrease as the details of hardware design evolve during final engineering.

4.2.2 Core Orificing

4.2.2.1 Orificing Strategies

In heterogeneous reactor designs, the buildup of fissile material in the internal blankets during burnup results in a power swing from the core zones to the internal blankets as burnup proceeds. This swing depends on the number of internal blanket assemblies, on their arrangement in the core, and on the residence time of the internal blankets.

Figure 4.2.2.1.1 shows the change in assembly power between BOL and EOEC condi-

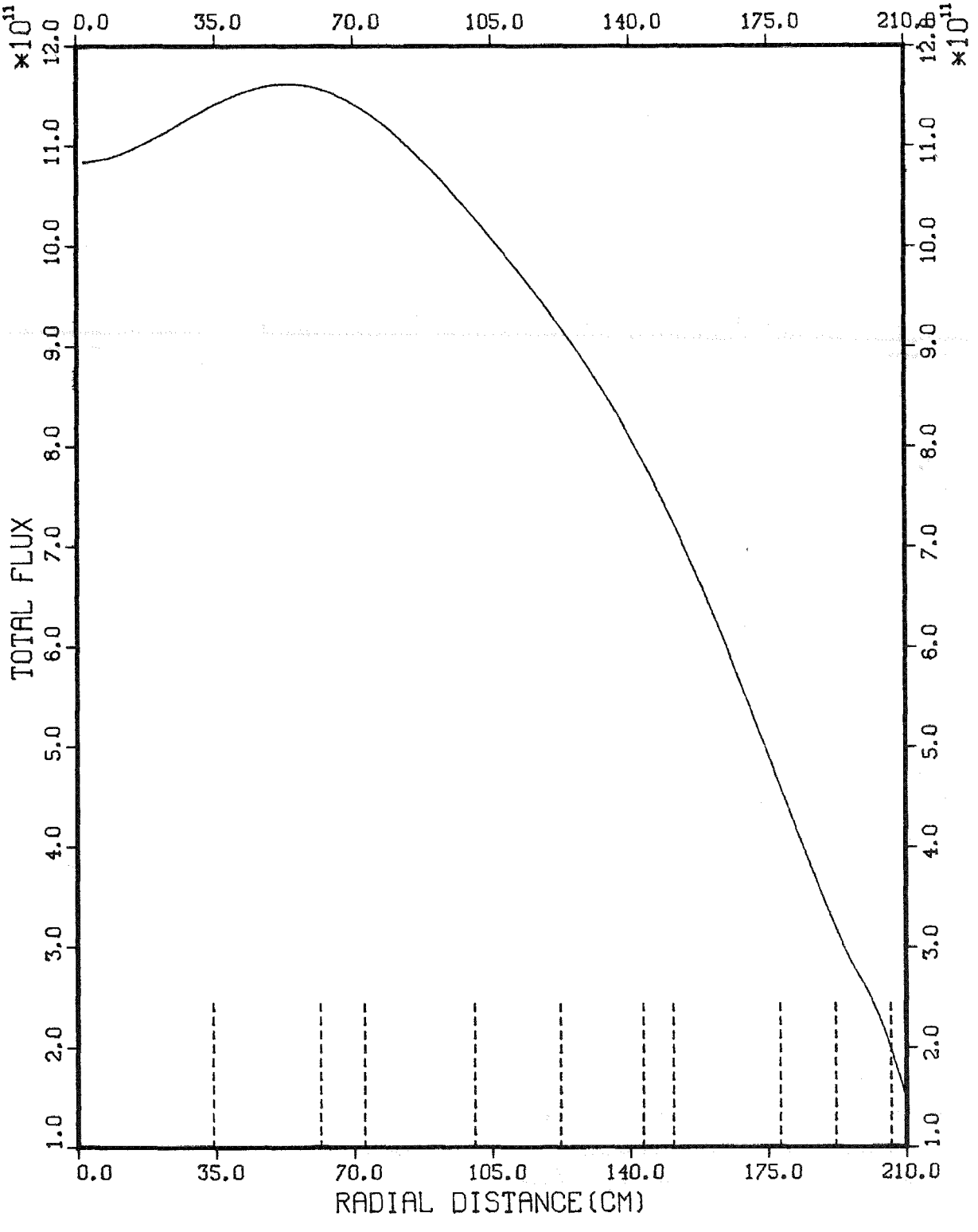

Figure 4.1.3.10.2. Radial distribution of the total flux incident on the support grid plate. The final design of hardware is expected to reduce this peak.

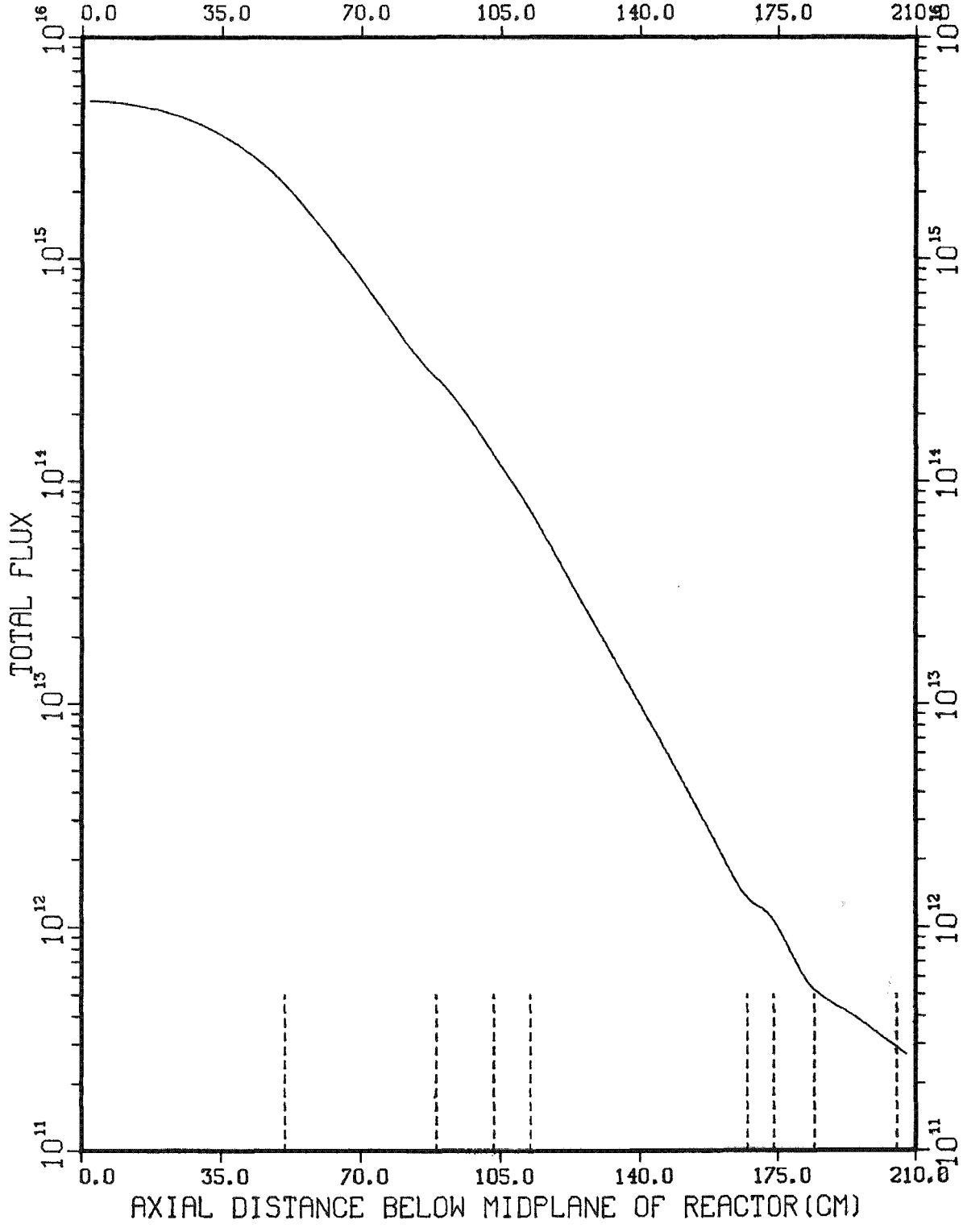

Figure 4.1.3.10.3. Axial distribution of the total flux at radial position 54.721 cm. (Three rings of removable reflector/shield subassemblies, instead of two rings, will be accommodated within the fixed radial neutron shield).

Table 4.1.3.11.1

DELAYED NEUTRON CONSTANTS

Delayed Neutron Precursor Group	Effective Delayed Neutron Fraction		Decay Constant (sec^{-1})
	BOL	EOEC	
1	8.025×10^{-5}	7.934×10^{-5}	0.0130
2	7.840×10^{-4}	7.546×10^{-4}	0.0314
3	6.925×10^{-4}	6.697×10^{-4}	0.1360
4	1.392×10^{-3}	1.334×10^{-3}	0.3400
5	6.572×10^{-4}	6.303×10^{-4}	1.3200
6	1.899×10^{-4}	1.894×10^{-4}	3.500
Total Effective Delayed Neutron Fraction	3.796×10^{-3}	3.657×10^{-3}	

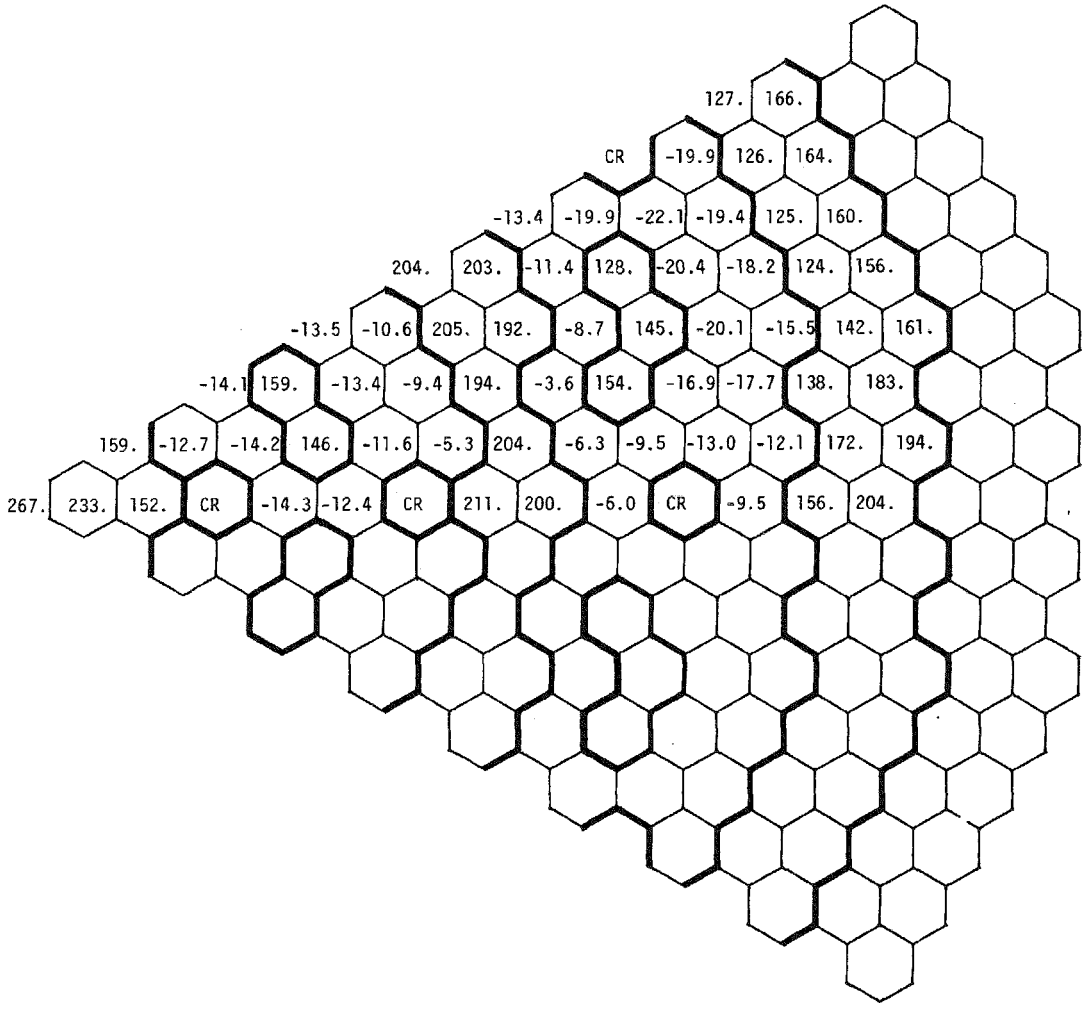

Figure 4.2.2.1.1. Power swing $\left(\frac{P_{EOEC} - P_{BOL}}{P_{BOL}} \times 100\right)$

tions. The core fuel assembly power decreases with burnup while the blanket assembly power increases. The maximum changes are -22.1% and 267% in the core and internal blanket assemblies, respectively. These changes will be even higher at EOL conditions.

From Figure 4.2.2.1.1 it is concluded that the peak coolant cladding temperatures will occur at BOL conditions for the core fuel assemblies and at the EOL conditions for the blanket assemblies. The magnitude of these temperatures depends on the number of orificing zones, and the criteria used to assign assemblies and coolant flow to orificing zones. The assignment of assemblies to orificing zones can be done according to: a) assembly power or b) assembly peak pin power. For the core fuel assemblies the power at BOL conditions is used and for the blanket assemblies the power at EOL conditions.

The allocation of coolant flow to the orificing zones of a LMFBR is based on considerations such as[20]: a) assembly lifetime, b) transient limitations, c) impact on upper internals structure, d) assembly power-to-flow ratio, and e) cooling requirements of components other than assemblies. These considerations can be translated into constraints on the cladding midwall temperatures. The coolant flow allocation to orificing zones is then determined such that these constraints are satisfied. To determine the assembly lifetime and the transient limitations that result from a given orificing scheme, transient analysis must be performed. Since such analysis is out of the work scope of this project, reactor orificing was based on either equalizing peak coolant temperature rises or peak cladding midwall temperatures. More specifically, the flow was allocated to orificing zones such that:

a. The maximum assembly coolant temperature rise is the same in all core orificing zones at BOL.
b. The maximum assembly coolant temperature rise is the same in all blanket orificing zones at EOL.
c. The maximum BOL assembly coolant temperature rise in the core is equal to the maximum EOL assembly coolant temperature rise in the blankets.

or

a. The peak cladding midwall temperature is the same in all core orificing zones at BOL.

b. The peak cladding midwall temperature is the same in all blanket orificing zones at EOL.
c. The BOL peak cladding midwall temperature in the core is equal to the EOL peak cladding midwall temperature in the blankets.

The combination of these two options used to assign assemblies to orificing zones with the two options used to distribute the flow to orificing zones, results in four orificing strategies ,i.e., orificing is based on:

1. Assembly power and equal peak assembly coolant temperatures.
2. Assembly power and equal peak cladding midwall temperatures.
3. Assembly peak pin power and equal peak assembly coolant temperatures.
4. Assembly peak pin power and equal peak cladding midwall temperatures.

Assembly coolant and cladding temperatures have been determined for all these orificing strategies.

The concept of continuously adjusting the flow allocated to core and blanket assemblies as burnup proceeds has also been analyzed. This analysis is presented in Appendix M.

4.2.2.2 Orificing Zone Arrangement

The assignment of assemblies to orificing zones according to assembly and peak assembly pin power are shown in Figures 4.2.2.2.1 and 4.2.2.2.2.

A total of nine orificing zones have been used ,i.e., three for the core, four for the internal and radial blankets, one for the radial reflector ,and one for the control assemblies. The use of more than nine orificing zones is not expected to reduce significantly the peak coolant and cladding temperatures[21]. To avoid inadvertent misplacement of an assembly (core, blanket, control reflector) these nine orificing zones and the two enrichment zones require 12 discriminator zones.

4.2.3 Hot Channel Factors

To guarantee that adequate margins are provided so that design limits and requirements are not exceeded, the CRBRP[3] hot channel factors have been used to account for theoretical and experimental analyses uncertainties, instrumentation accuracy,

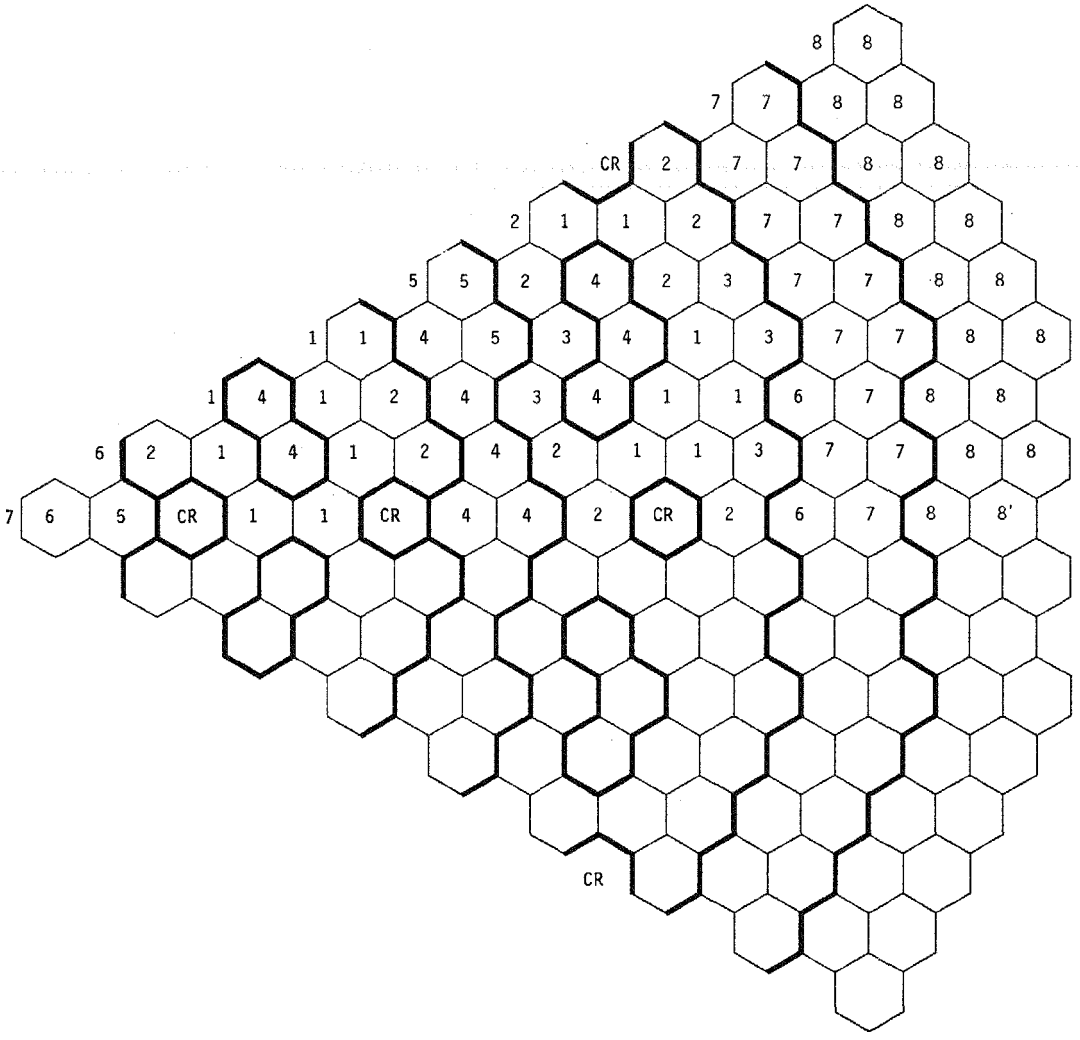

Figure 4.2.2.2.1. Assembly assignment to orificing zones according to assembly power.

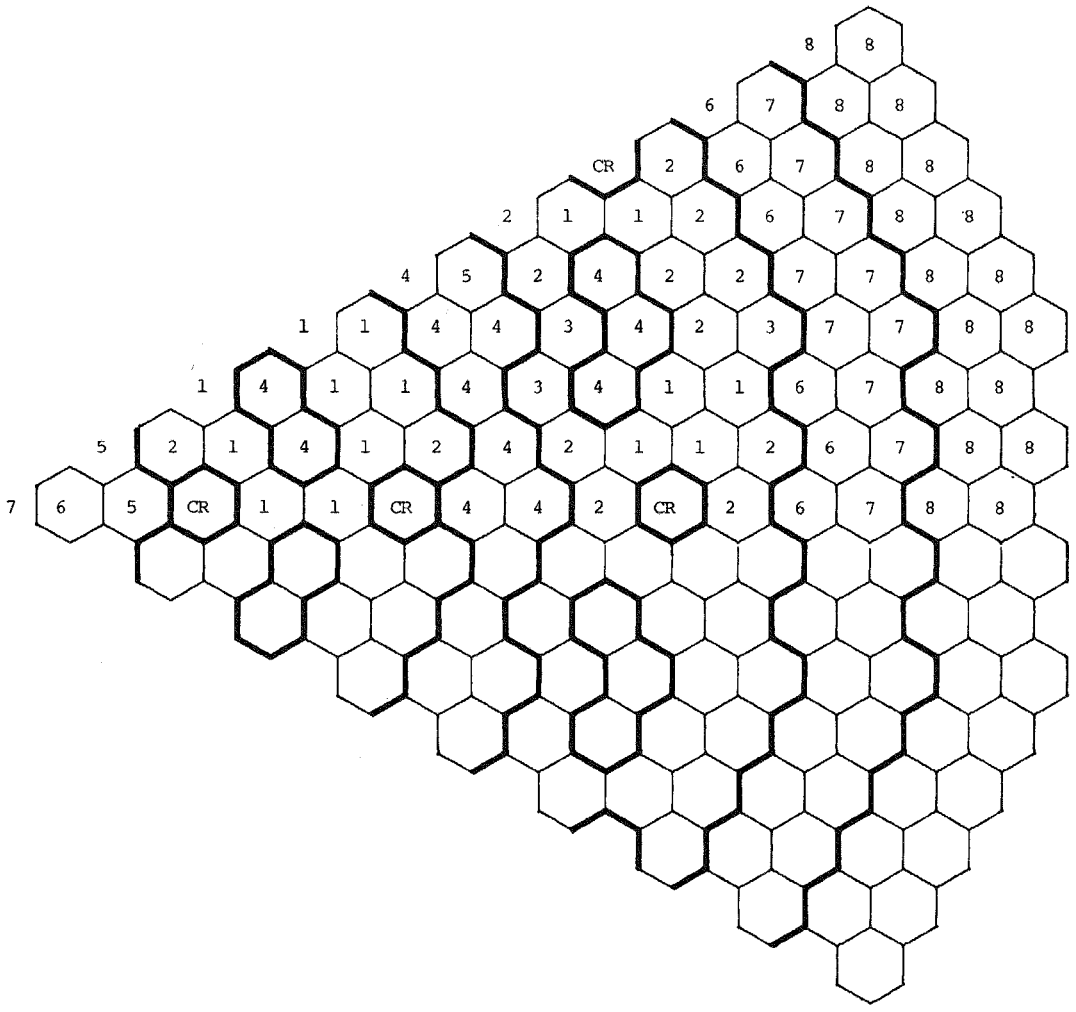

Figure 4.2.2.2.2. Assembly assignment to orificing zones according to assembly peak pin power.

manufacturing tolerances, and uncertainties in physical properties and correlations. To determine total hot channel factors the semi-statistical hot spot analysis method is used[3], i.e., random variables are combined statistically and together with the direct bias uncertainties, characterize a hot channel/spot as the one affected simultaneously by all uncertainties

The CRBRP temperature hot channel factors for core and blanket fuel rods are shown in Tables 4.2.3.1 and 4.2.3.2, respectively. The CRBRP plenum pressure hot channel factors for the core and blanket fuel assemblies are shown in Tables 4.2.3.3 and 4.2.3.4, respectively.

4.2.4 Steady State Thermal-Hydraulic Analysis

The methodology used in the thermal-hydraulic analysis is illustrated in Figure 4.2.4.1. The power distribution in the radial and azimuthal directions is determined from multigroup two-dimensional diffusion calculations in hexagonal geometry. The power distribution in the axial direction is determined from multigroup diffusion calculations in a two-dimensional RZ reactor model. These two distributions are synthesized to generate three-dimensional power distributions. Finally, from the three-dimensional distributions assembly and pin powers are generated which are used to orifice the reactor.

The orificing strategies discussed in Section 4.2.2.1 require the end-of-life (EOL) power distribution in the blanket zones. This power distribution is calculated from the beginning-of-life (BOL) and end-of-equilibrium-cycle (EOEC) power distributions assuming that power production in the blanket zones increases linearly with time.

To calculate the assembly average friction factor and the subchannel flow splits, the Novendstern[22] correlations are presently utilized in design codes. As shown in Appendix N, the Chiu et al.[23,24] correlations are more accurate than the Novendstern correlations. Thus, the Chiu et al. correlations have been used in this analysis.

Core-wide coolant and assembly wall temperatures are determined using the computer code CORE-3D. This code is based on the ENERGY code and includes the effect of interassembly heat transfer. Finally, cladding temperatures for the design limiting assemblies are calculated using the ENERGY code.

Table 4.2.3.1

CRBRP FUEL ASSEMBLY ROD TEMPERATURE HOT CHANNEL/SPOT FACTORS[1]

	Coolant	Film	Cladding	Gap	Fuel	Heat Flux
Direct[2]						
Power Level Measurement and Control System Dead Band	1.03					1.03
Inlet Flow Maldistribution	1.05	1.035				
Subassembly Flow Maldistribution Calculational Uncertainties	1.08					
Cladding Circumferential Temperature Variation		1.0[3]	1.0[3]	1.7[4]		
Statistical (3σ)[5]						
Inlet Temperature Variation	1.02[6]	1.0[7]				
Reactor ΔT Variation	1.04[6]	1.0[7]				
Nuclear Data	1.06					1.065
Fissile Fuel Maldistribution	1.01					1.035

Table 4.2.3.1 (continued)

	Coolant	Film	Cladding	Gap	Fuel	Heat Flux
Wire Wrap Orientation	1.01					
Subchannel Flow Area	1.028	1.0				
Film Heat Transfer Coefficient		1.12				
Pellet-Cladding Eccentricity		1.15	1.15			
Cladding Thickness and Conductivity			1.12			
Gap Conductance				1.48[8]		
Fuel Conductivity					1.10	
Coolant Properties	1.01					
TOTAL	2σ 1.232[6] 1.221[7]	1.168 1.986[4]	1.128			1.081
	3σ 1.264[6] 1.248[7]	1.234 2.101[4]	1.192	1.48	1.10	1.106

Table 4.2.3.1 (continued)

(1) Carelli, M.D. and Markley, R.A., "Preliminary Thermal-Hydraulic Design and Predicted Performance of the Clinch River Breeder Reactor Core," ASME Heat Transfer Conference, San Francisco, California, August 11-13, 1975.

(2) Uncertainties due to physics analysis calculational methods and control rod effects (4% on coolant enthalpy rise) are applied directly on nuclear radial peaking factors.

(3) For fuel temperature calculations.

(4) For cladding midwall temperature calculations. Applies to nominal temperature drop between cladding midwall and bulk coolant.

(5) In addition, the assembly inlet temperature will be increased by $16^{o}F$, to account for primary loop temperature control uncertainties.

(6) Applies to Plant Expected Operating Conditions.

(7) Applies to Plant T&H Design Conditions

(8) Applies to BOL conditions.

Table 4.2.3.2

RADIAL BLANKET ASSEMBLY ROD TEMPERATURE HOT CHANNEL/SPOT FACTORS

		Coolant	Film	Cladding	Gap	Fuel	Heat Flux
DIRECT(+)							
Power Level Measurement and Control System Dead Band		1.03					1.03
Inlet Flow Maldistribution		1.07					
Assembly Flow Maldistribution			1.05				
Calculational Uncertainties		1.1					
Cladding Circumferential Temperature Variation			$1.0^{(\Delta)}$ $2.2^{(*)}$	$1.0^{(\Delta)}$			
STATISTICAL $(3\sigma)^{(o)}$							
Inlet Temperature Variation		$1.02^{(\phi)}$ $1.0^{(\dagger)}$					
Reactor ΔT Variation		$1.04^{(\phi)}$ $1.0^{(\dagger)}$					
Nuclear Data		1.08					1.09
Fissile Fuel Maldistribution		1.01					1.01
Wire Wrap Orientation		1.01					
Subchannel Flow Area		1.035	1.0				
Film Heat Transfer Coefficient			1.21				
Pellet-Cladding Eccentricity			1.15	1.15			
Cladding Thickness & Conductivity				1.12			
Gap Conductance					1.48		
Fuel Conductivity						1.10	
Coolant Properties		1.01					
TOTAL	2σ	$1.292^{(\phi)}$ $1.284^{(\dagger)}$	1.231 $2.708^{(*)}$	1.128			1.092
	3σ	$1.332^{(\phi)}$ $1.320^{(\dagger)}$	1.321 $2.906^{(*)}$	1.192	1.48	1.10	1.123

+) Uncertainties due to physics analysis calculational methods and control rod effects are applied directly on nuclear radial peaking factors.

Table 4.2.3.2 (continued)

RADIAL BLANKET ASSEMBLY ROD TEMPERATURE HOT CHANNEL/SPOT FACTORS (cont.)

o) In addition, the assembly inlet temperature will be increased by $16^{o}F$, to account for primary loop temperature control uncertainties.

*) For cladding midwall temperature calculations. Applies to nominal temperature drop between cladding midwall and bulk coolant.

Δ) For fuel temperature calculations.

ϕ) Applies to Plant Expected Operating Conditions

+) Applies to Plant T & H Design Conditions.

Table 4.2.3.3

FUEL ASSEMBLY PLENUM PRESSURE HOT CHANNEL FACTORS

	Plenum Temperature	Burnup
DIRECT(+)		
Power Level Measurement	1.02	1.02
Inlet Flow Maldistribution	1.05	
Subassembly Flow Maldistribution Calculation Uncertainties	1.08	
STATISTICAL (3σ)(o)		
Inlet Temperature Variation	$1.02^{(\phi)}$ $1.0^{(\dagger)}$	
Reactor ΔT Variation	$1.04^{(\phi)}$ $1.0^{(\dagger)}$	
Nuclear Data	1.06	1.06
Fissile Fuel Maldistribution	1.01	1.01
Wire Wrap Orientation	1.01	
Coolant Properties	1.01	
TOTAL 2σ	$1.216^{(\phi)}$ $1.205^{(\dagger)}$	1.061
TOTAL 3σ	$1.246^{(\phi)}$ $1.229^{(\dagger)}$	1.082

(†) Uncertainties due to physics analysis calculational methods and control rod effects (4% for both plenum temperature and burnup) are applied directly on nuclear radial peaking factors.

(ϕ) Applies to Plant Expected Operating Conditions.

(†) Applies to Plant T&H Design Conditions.

(o) In addition, the assembly inlet temperature will be increased by $16^{o}F$ to account for primary loop temperature control uncertainties.

Table 4.2.3.4

RADIAL BLANKET ASSEMBLY PLENUM PRESSURE
HOT CHANNEL FACTORS

		Plenum Temperature	Burnup
DIRECT(*)			
Power Level Measurement		1.02	1.02
Inlet Flow Maldistribution		1.07	
Assembly Flow Maldistribution Calculations Uncertainties		1.10	
STATISTICAL (3σ)(o)			
Inlet Temperature Variation		$1.02^{(\phi)}$ $1.0^{(\dagger)}$	
Reactor ΔT Variation		$1.04^{(\phi)}$ $1.0^{(\dagger)}$	
Nuclear Data		1.08	1.08
Fissile Fuel Maldistribution		1.01	1.01
Wire Wrap Orientation		1.01	
Coolant Properties		1.01	
TOTAL	2σ	$1.275^{(\phi)}$ $1.266^{(\dagger)}$	1.075
	3σ	$1.313^{(\phi)}$ $1.299^{(\dagger)}$	1.102

(*) Uncertainties due to physics analysis calculational methods and control rod effects are applied directly on nuclear radial peaking factors.

(ϕ) Applied to Plant Expected Operating Conditions.

($\dagger$) Applied to Plant T&H Design Conditions.

(o) In addition, the assembly inlet temperature will be increased by $16^{o}F$ to account for primary loop temperature control uncertainties.

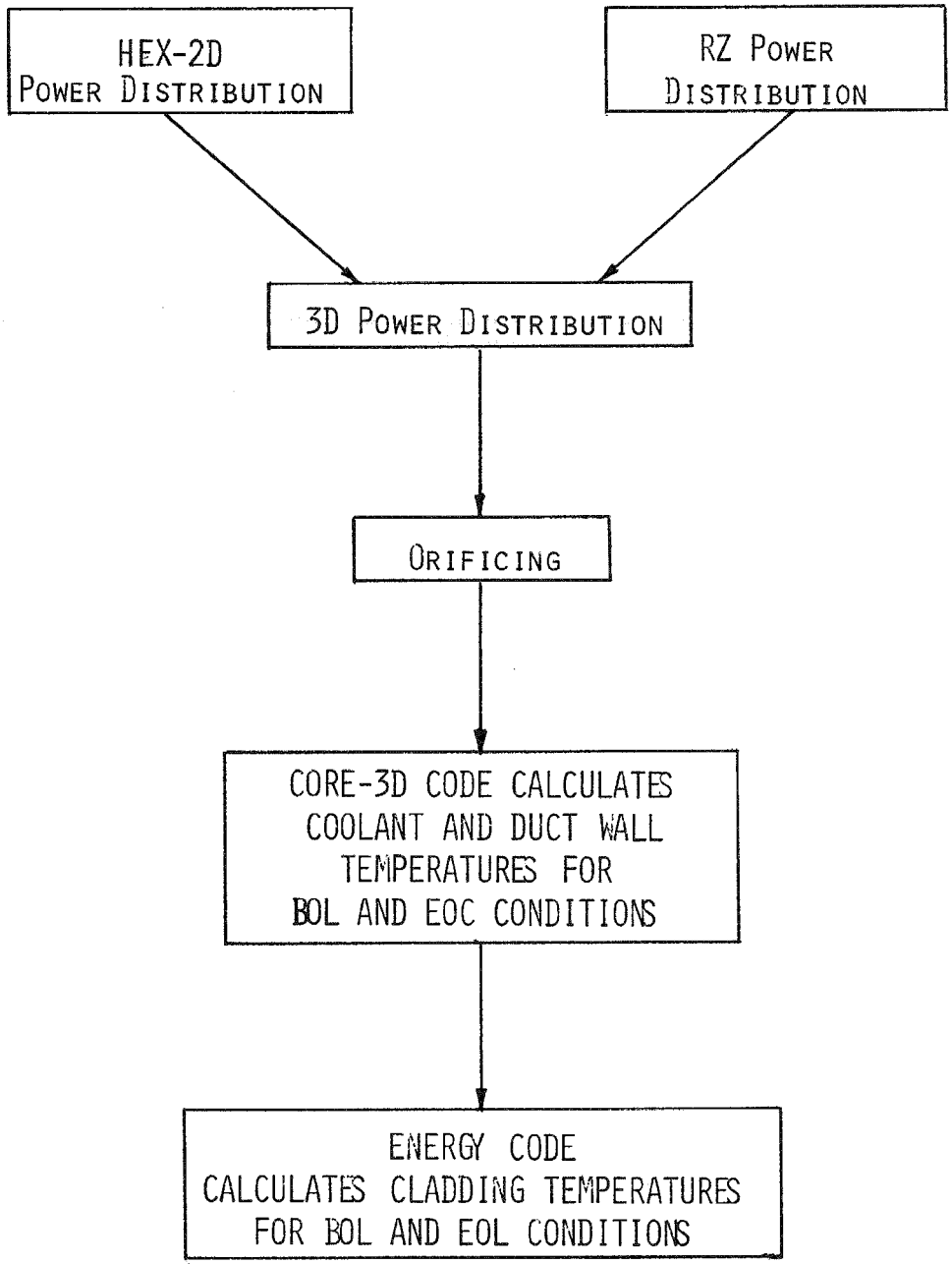

Figure 4.2.4.1. Calculational method for thermal-hydraulic analysis.

4.2.4.1 Assembly Flow Rates

Assembly flow rates for the four orificing strategies discussed in Section 4.2.2.1 are given in Table 4.2.4.1.1. The corresponding coolant velocities are given in Table 4.2.4.1.2. The total flow rate, not including the cold by-pass flow, is equal to 116,463,258 lb/hr. The flow split among the different reactor regions depends slightly on the orificing strategy. Thus, the core flow fraction varies from 70.5% to 72.1%, the flow fraction allocated to the blankets varies from 27.4% to 28.9% and the flow fraction allocated to control and shield assemblies is equal to 0.6%. The maximum assembly average coolant velocity depends on the orificing strategy too and varies from 22.0 ft/sec to 23.1 ft/sec.

Assembly power to flow ratios are presented in Appendix O.

4.2.4.2 Linear Power Ratings

Nominal peak linear power ratings for BOL and EOL conditions are given in Table 4.2.4.2.1. The nominal peak linear power rating in the core is equal to 14.2 kW/ft and occurs at BOL. The linear power ratings of the internal and radial blankets peak at EOL and are equal to 16.4 kW/ft and 9.6 kW/ft, respectively. Both peak linear power ratings in the core and the blankets are below the design limiting values of 15 kW/ft and 16.5 kW/ft, respectively (Section 2.1).

4.2.4.3 Cladding Temperatures

Axial distributions of the nominal and 2σ cladding midwall temperatures in the hot pin of each orificing zone are shown in Figures 4.2.4.3.1 to 4.2.4.3.28. In the same figures are also presented axial distributions of the average coolant,duct,and bundle temperatures for the assembly that contains the hot pin in each orificing zone. These temperatures have been calculated by the ENERGY code and therefore interassembly heat transfer has not been taken into account. Cladding midwall temperatures in the core fuel pins peak at the top of the core and in the blanket pins at the top of the axial blanket.

The nominal and 2σ peak cladding midwall temperatures that result from the four orificing strategies used in this analysis are presented in Table 4.2.4.3.1. The strategies that equalize the peak cladding midwall temperatures yield lower 2σ peak cladding midwall temperatures and between them, the one that is based on pin

Table 4.2.4.1.1

ASSEMBLY COOLANT FLOW RATES
(lb/hr)

Orificing Zone	Assembly Assignment to Orificing Zones Based on Assembly Power			Assembly Assignment to Orificing Zones Based on Pin Power		
	Number of Assemblies	Equal Peak Assembly Coolant Temperatures	Equal Peak Cladding Midwall Temperatures	Number of Assemblies	Equal Peak Assembly Coolant Temperatures	Equal Peak Cladding Midwall Temperatures
1	156	273,360	260,427	156	268,740	263,435
2	114	245,832	245,599	138	244,176	238,972
3	60	220,872	234,584	36	216,477	222,336
4	108	163,062	159,772	126	160,433	161,478
5	36	124,242	128,868	24	115,368	117,395
6	30	86,214	96,105	66	63,720	76,330
7	157	45,852	52,944	115	45,114	47,920
8	198	2,107	2,107	198	2,107	2,107
9	24	10,673	10,673	24	10,673	10,673
Total	883	116,463,258	116,463,258	883	116,463,258	116,463,258

Table 4.2.4.1.2

ASSEMBLY AVERAGE COOLANT VELOCITIES
(ft/sec)

Orificing Zone	Assembly Assignment to Orificing Zones Based on Assembly Power		Assembly Assignment Orificing Zones Based on Pin Power	
	Equal Peak Assembly Coolant Temperatures	Equal Peak Cladding Midwall Temperatures	Equal Peak Assembly Coolant Temperatures	Equal Peak Cladding Midwall Temperatures
1	23.1	22.0	22.7	22.2
2	20.8	20.7	20.6	20.2
3	18.7	19.8	18.2	18.7
4	20.6	20.2	20.3	20.4
5	15.7	16.3	14.6	14.9
6	10.9	12.1	8.1	9.6
7	5.8	6.7	5.7	6.0

Table 4.2.4.2.1

NOMINAL PEAK LINEAR POWER RATINGS
(kW/ft)

Reactor Region	BOL	EOL
Core	14.2	12.2
Internal Blanket	4.8	16.4
Radial Blanket	3.4	9.6

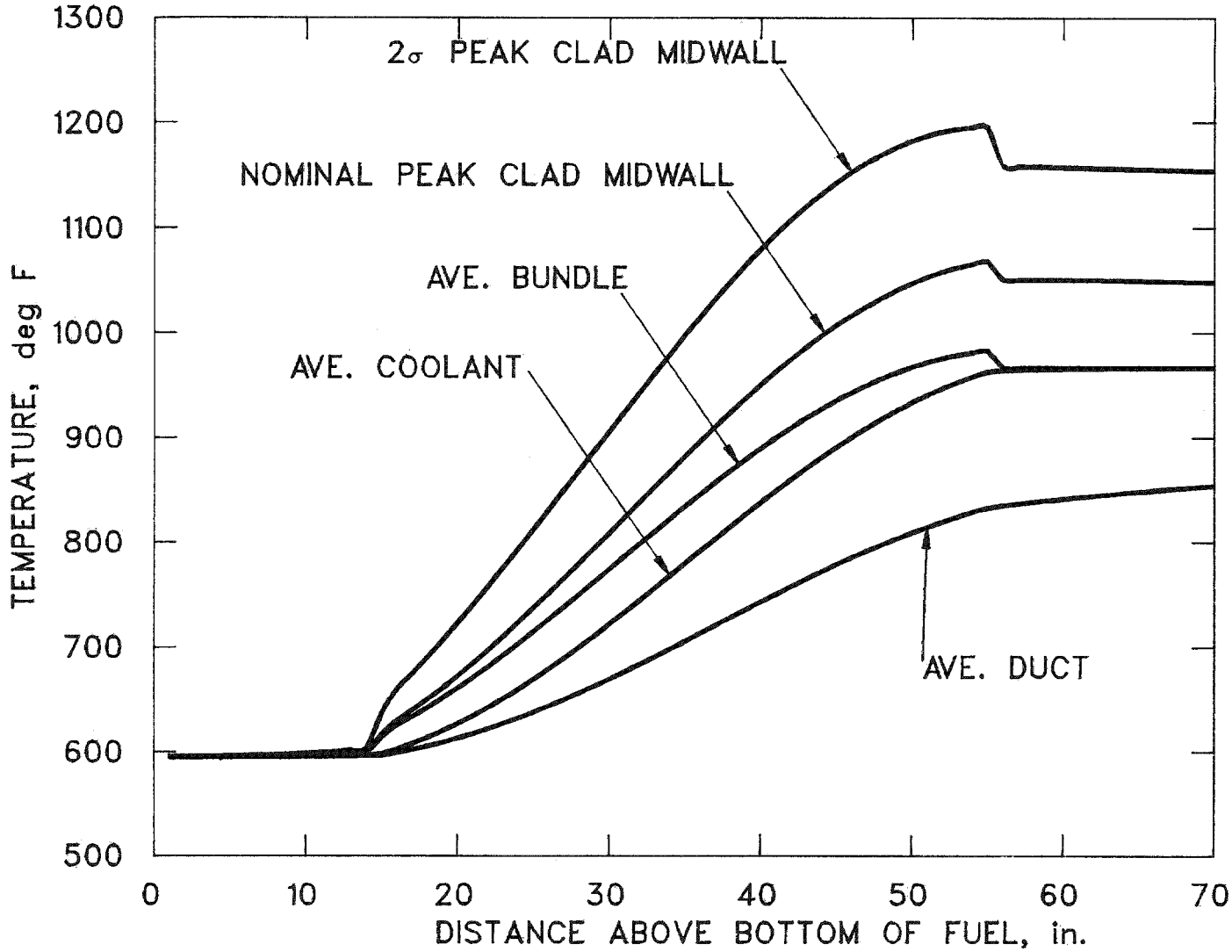

Figure 4.2.4.3.1. Nominal and 2σ peak clad midwall temperatures and average coolant, duct and bundle temperatures. (First orificing zone, orificing based on assembly power and equal peak assembly coolant temperatures.)

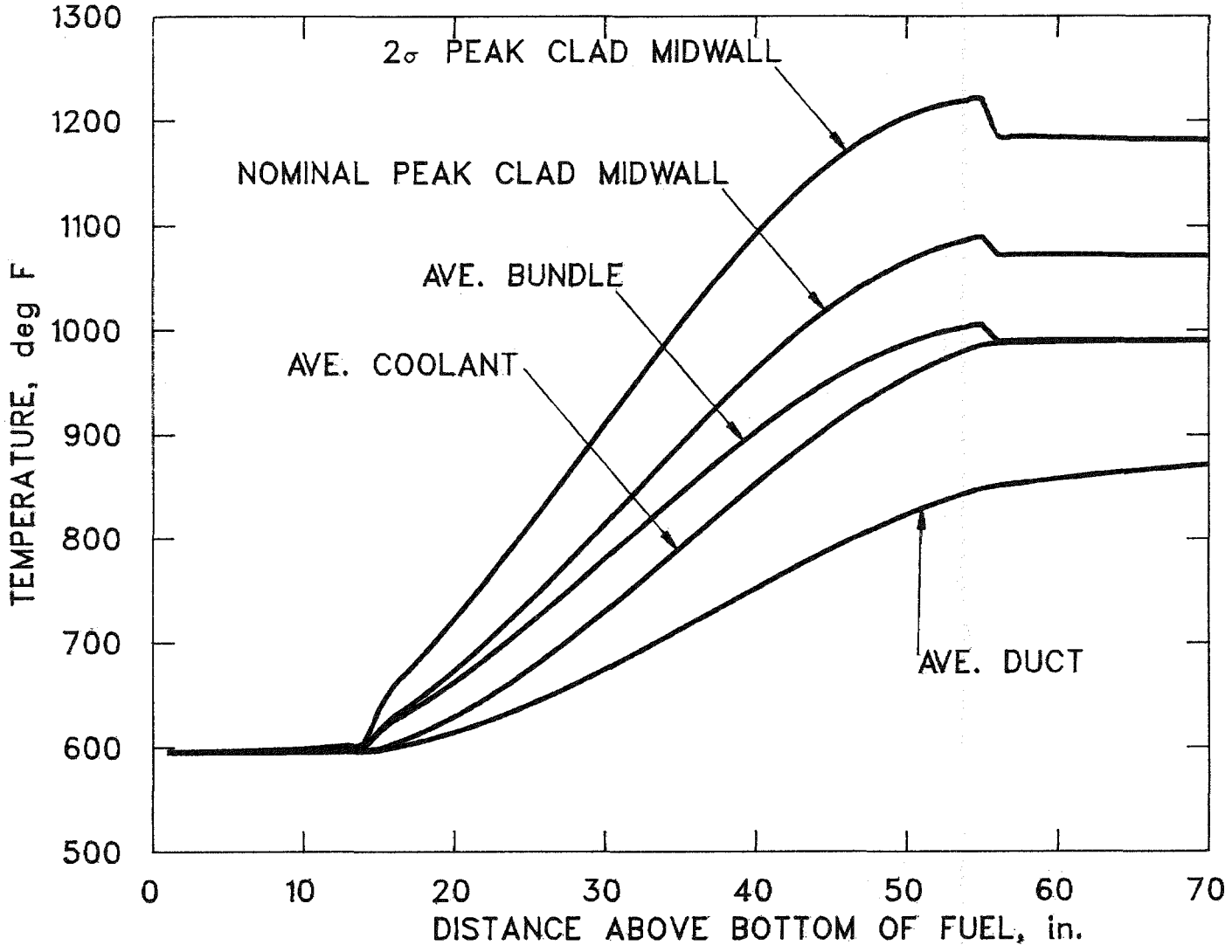

Figure 4.2.4.3.2. Nominal and 2σ peak clad midwall temperatures and average coolant, duct and bundle temperatures. (Second orificing zone, orificing based on assembly power and equal peak assembly coolant temperatures.)

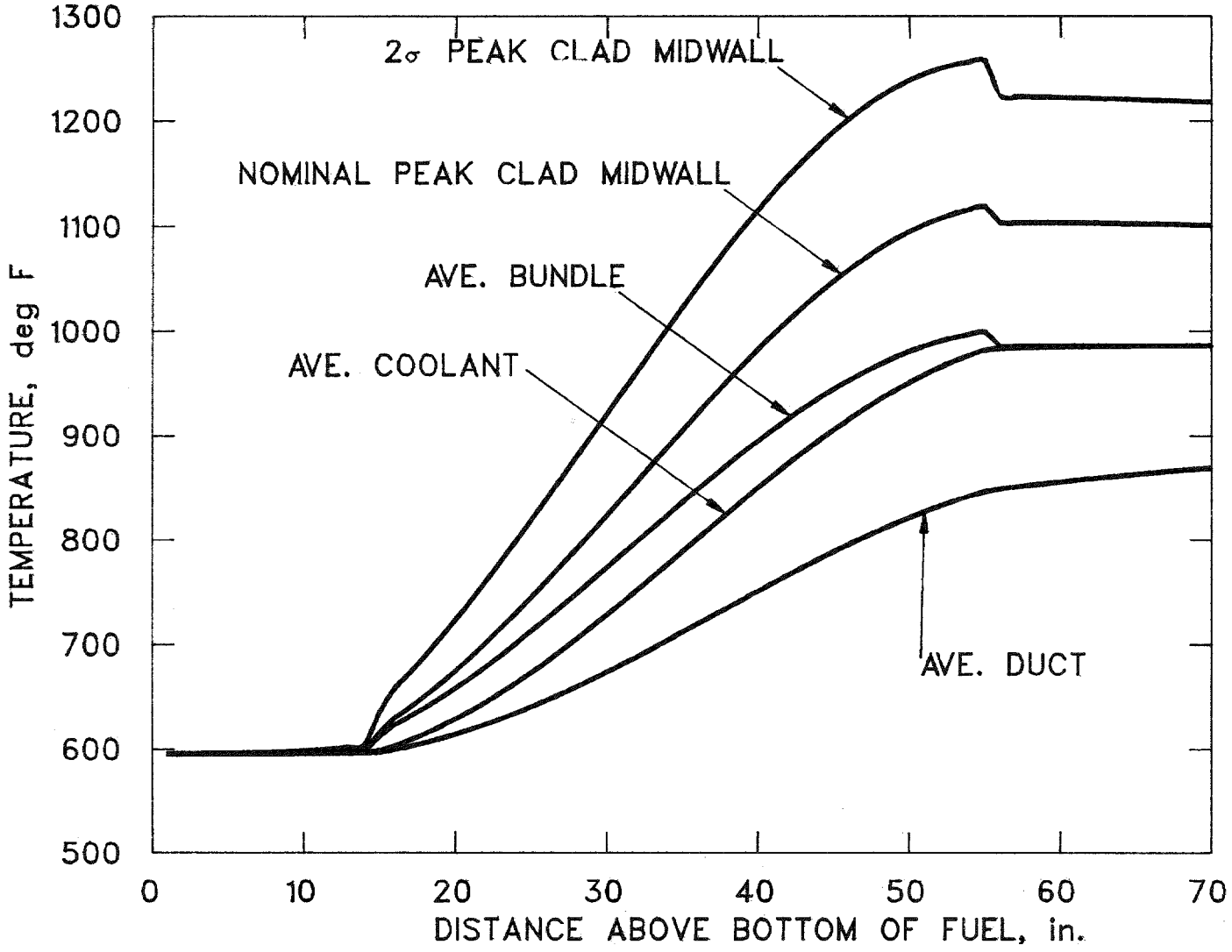

Figure 4.2.4.3.3. Nominal and 2σ peak clad midwall temperatures and average coolant, duct and bundle temperatures. (Third orificing zone, orificing based on assembly power and equal peak assembly coolant temperatures.)

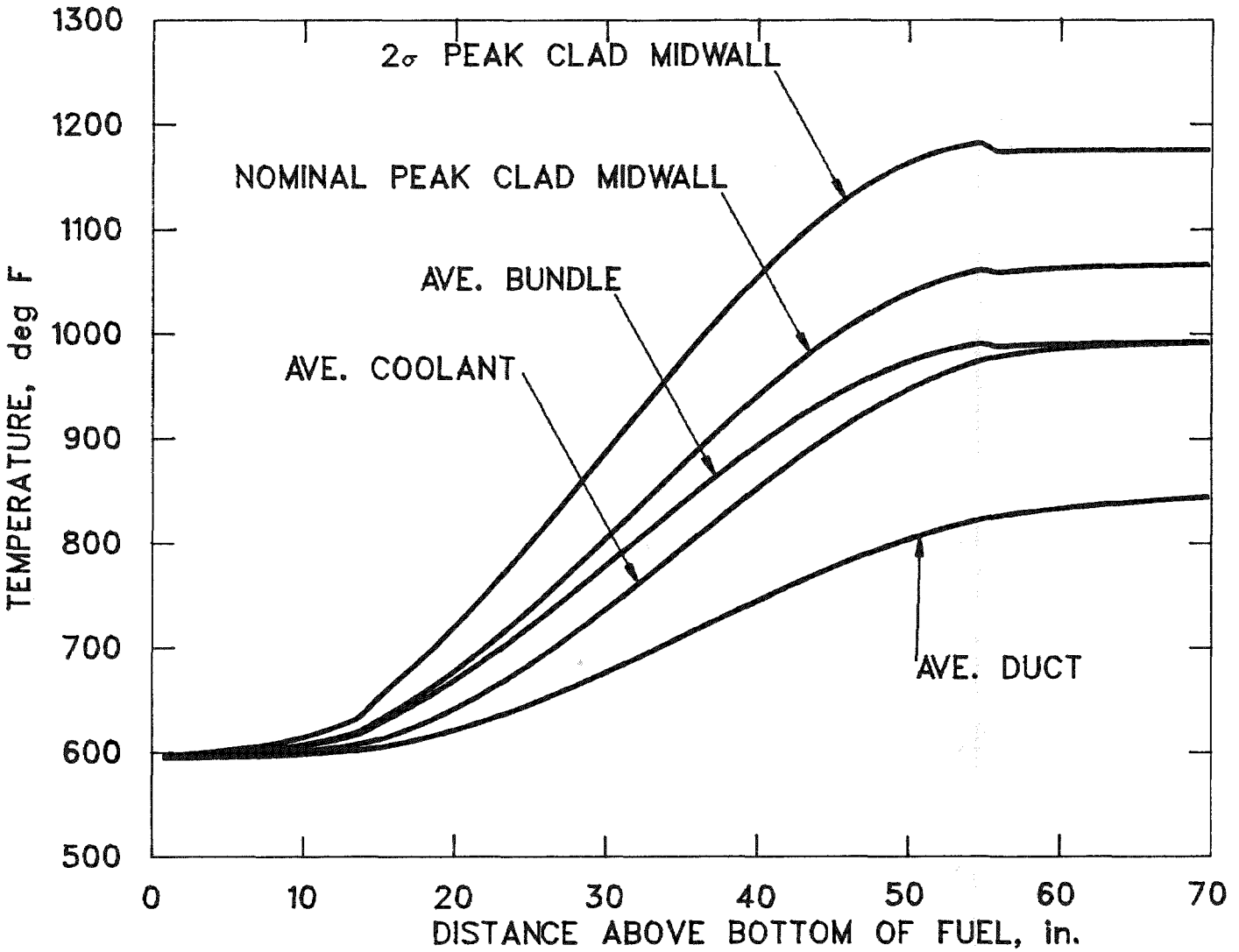

Figure 4.2.4.3.4. Nominal and 2σ peak clad midwall temperatures and average coolant, duct and bundle temperatures. (Fourth orificing zone, orificing based on assembly power and equal peak assembly coolant temperatures.)

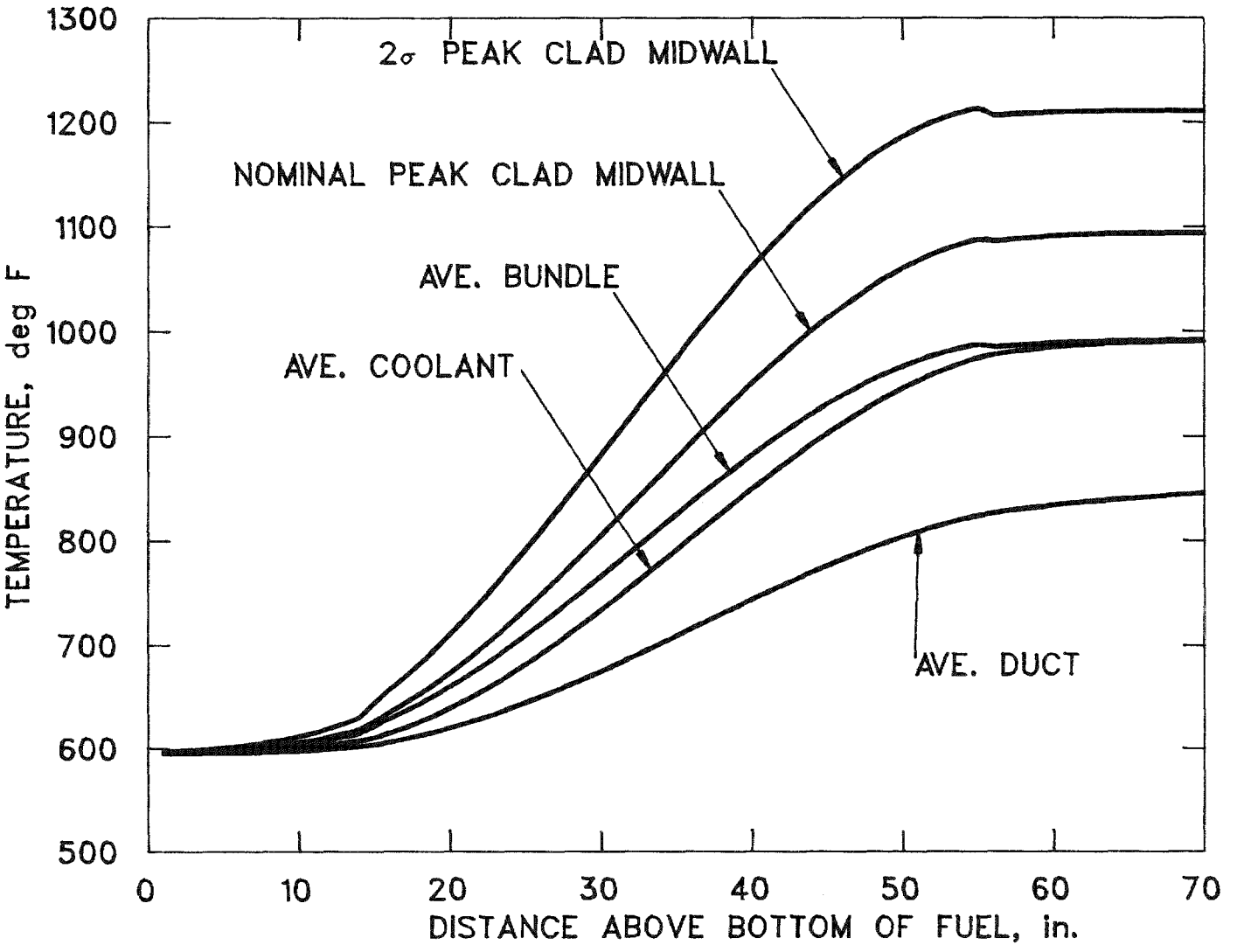

Figure 4.2.4.3.5. Nominal and 2σ peak clad midwall temperatures and average coolant, duct and bundle temperatures. (Fifth orificing zone, orificing based on assembly power and equal peak assembly coolant temperatures.)

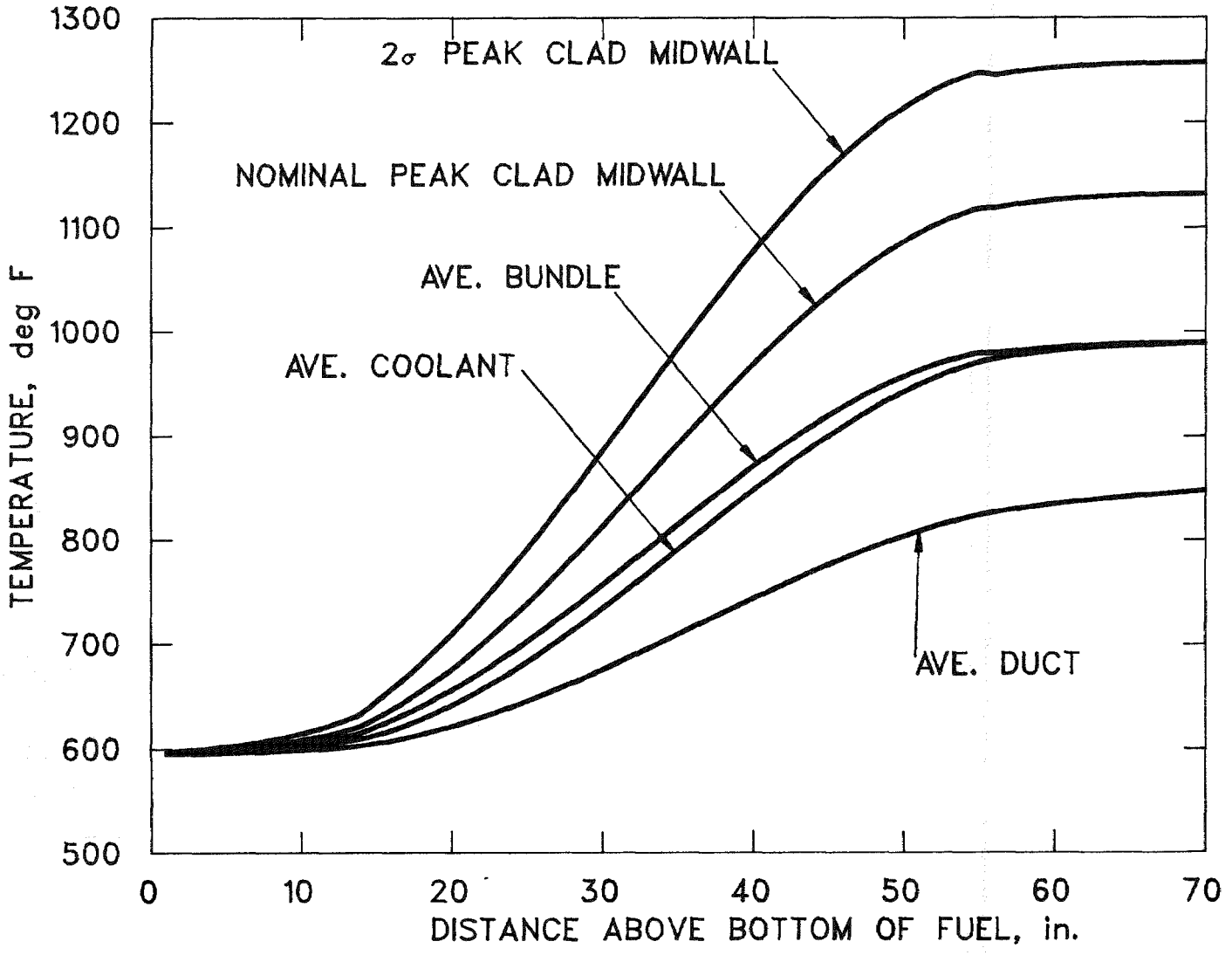

Figure 4.2.4.3.6. Nominal and 2σ peak clad midwall temperatures and average coolant, duct and bundle temperatures. (Sixth orificing zone, orificing based on assembly power and equal peak assembly coolant temperatures.)

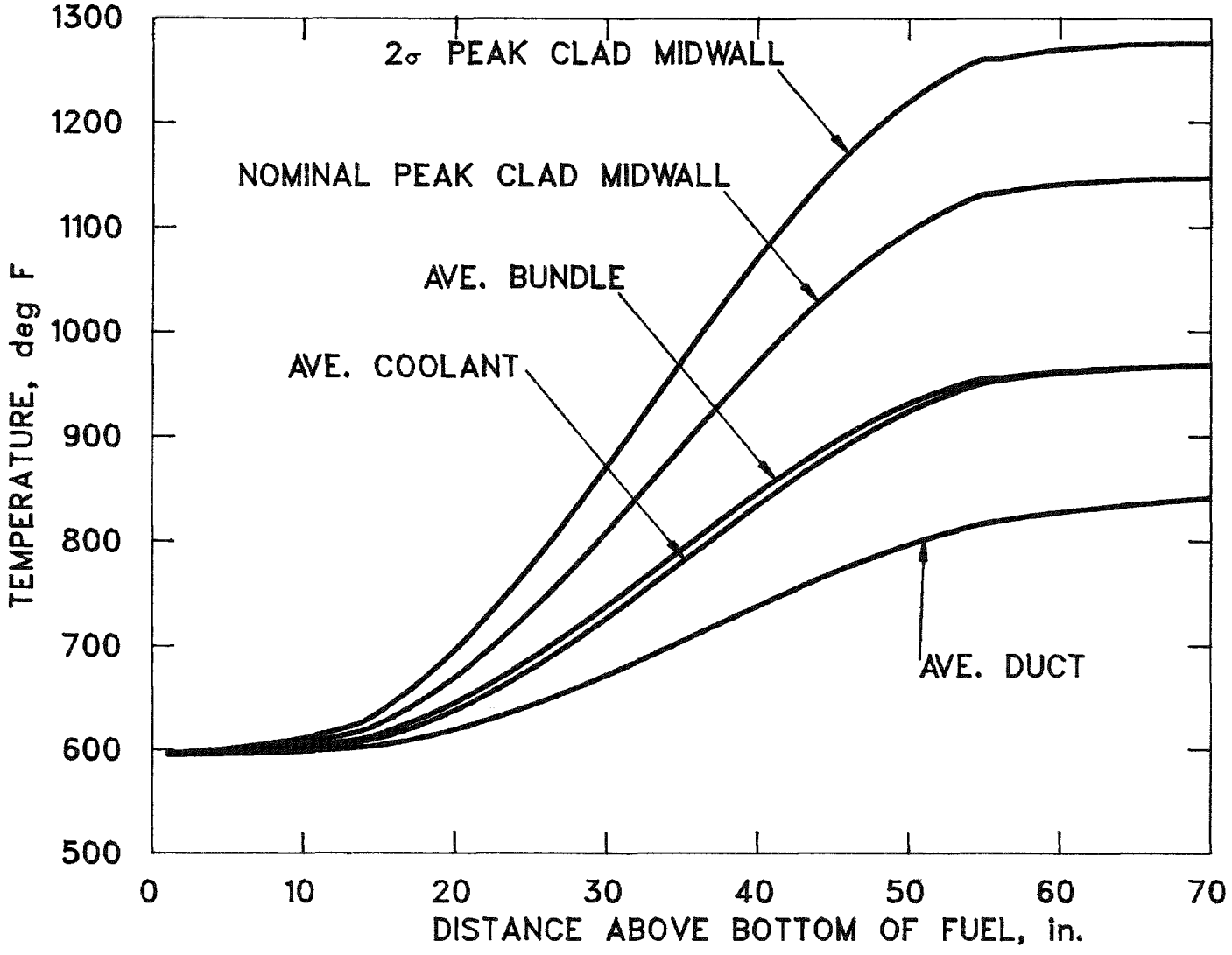

Figure 4.2.4.3.7. Nominal and 2σ peak clad midwall temperatures and average coolant, duct and bundle temperatures. (Seventh orificing zone, orificing based on assembly power and equal peak assembly coolant temperatures.)

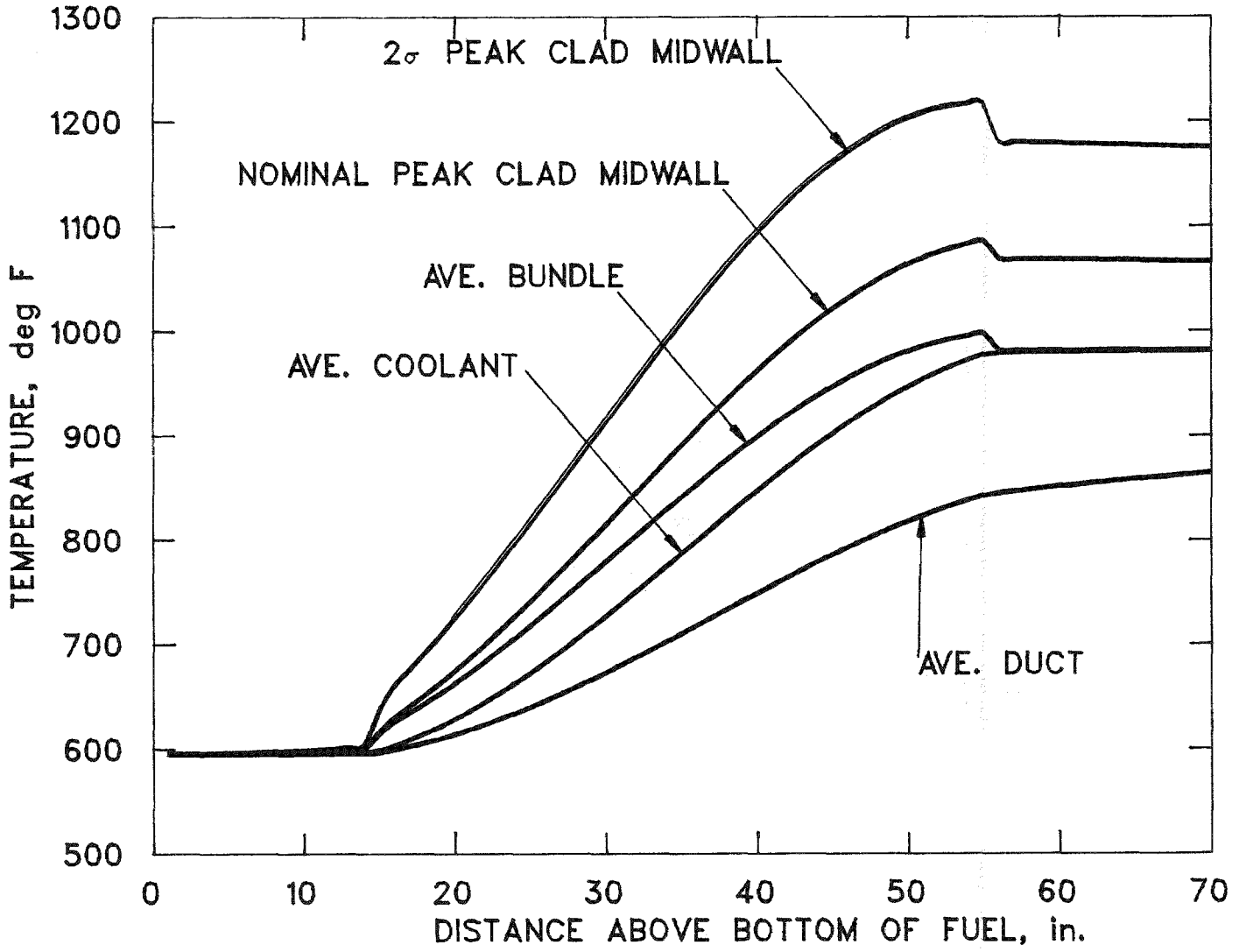

Figure 4.2.4.3.8. Nominal and 2σ peak clad midwall temperatures and average coolant, duct and bundle temperatures. (First orificing zone, orificing based on assembly power and equal peak cladding midwall temperatures.)

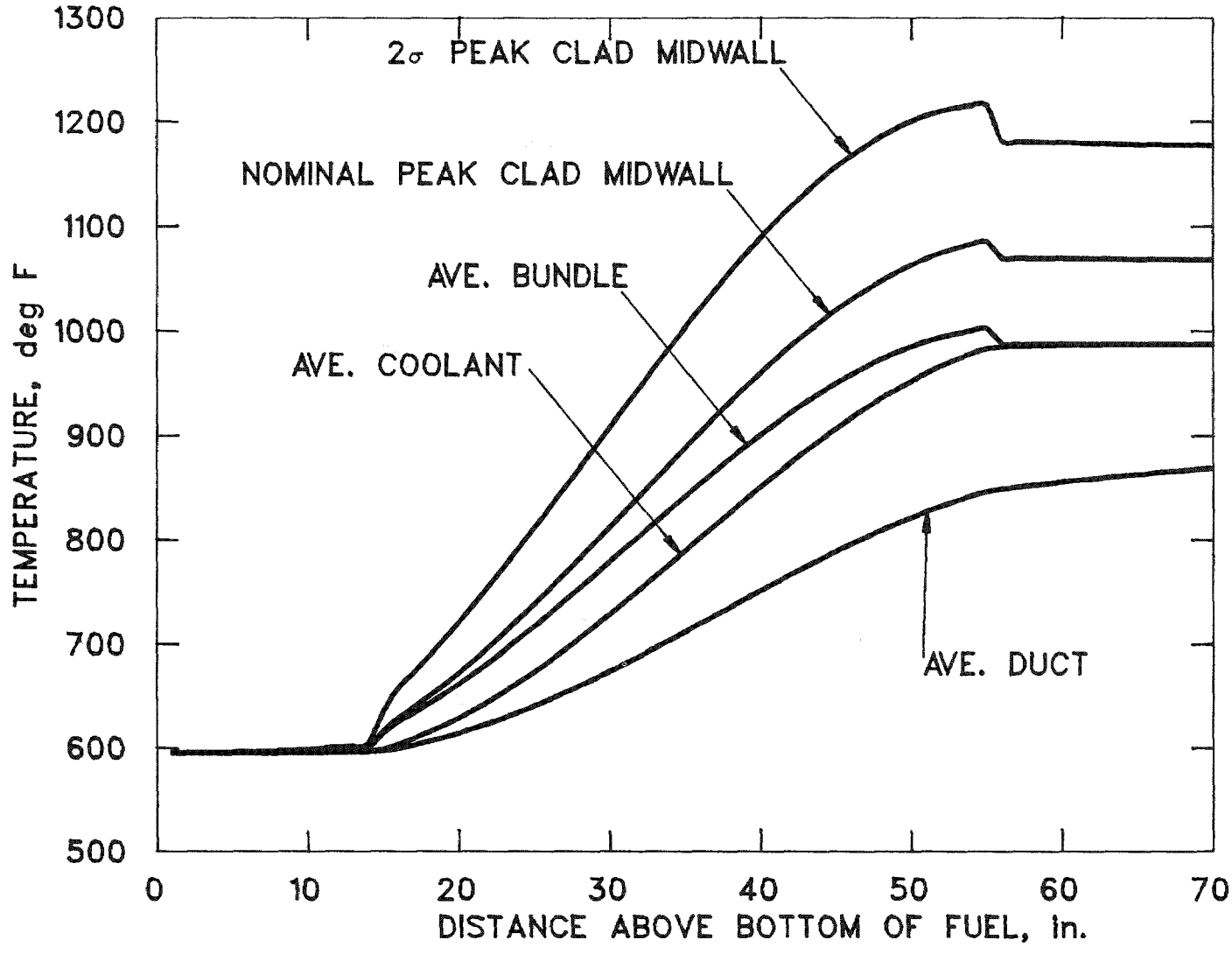

Figure 4.2.4.3.9. Nominal and 2σ peak clad midwall temperatures and average coolant, duct and bundle temperatures. (Second orificing zone, orificing based on assembly power and equal peak cladding midwall temperatures.)

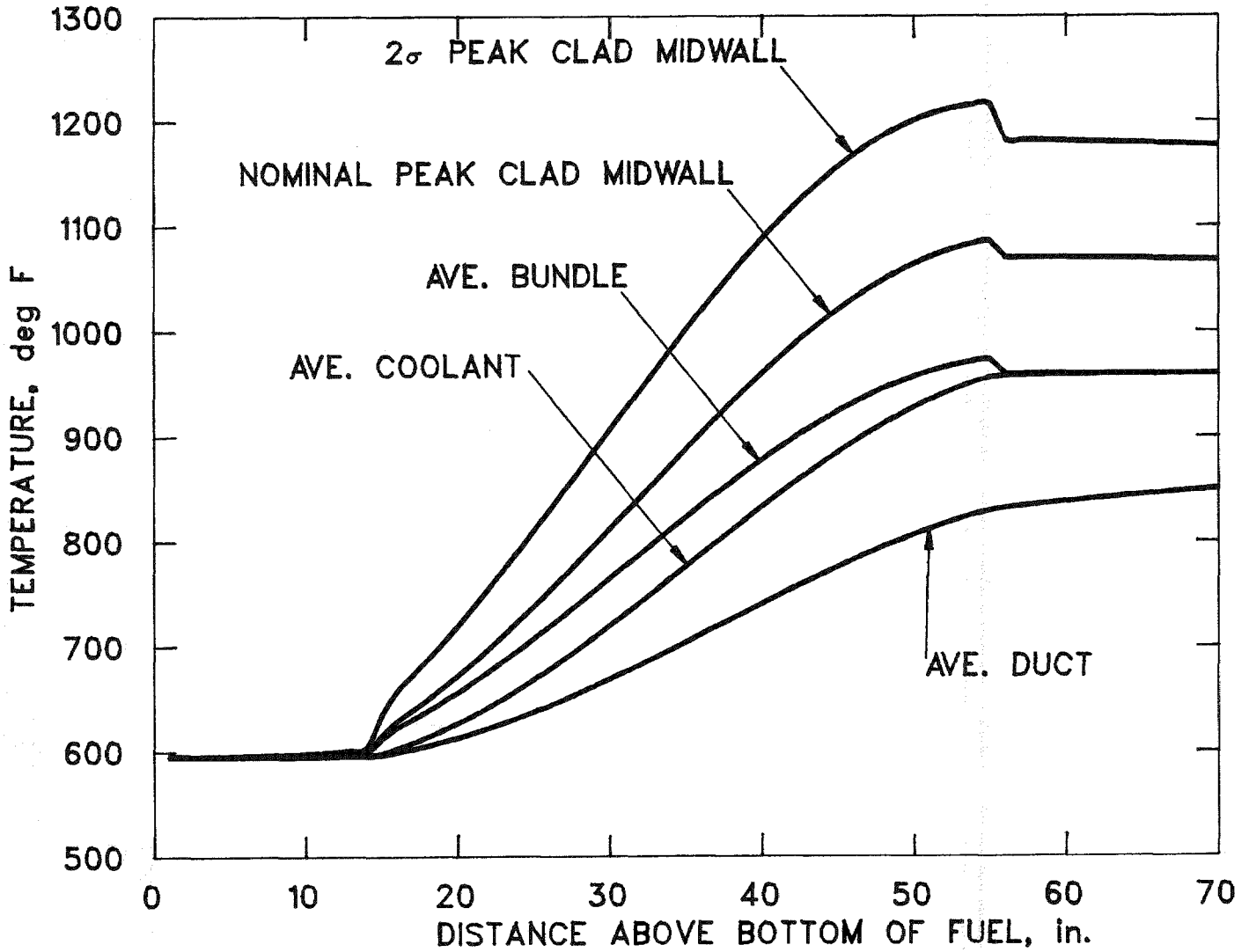

Figure 4.2.4.3.10. Nominal and 2σ peak clad midwall temperatures and average coolant, duct and bundle temperatures. (Third orificing zone, orificing based on assembly power and equal peak cladding midwall temperatures.)

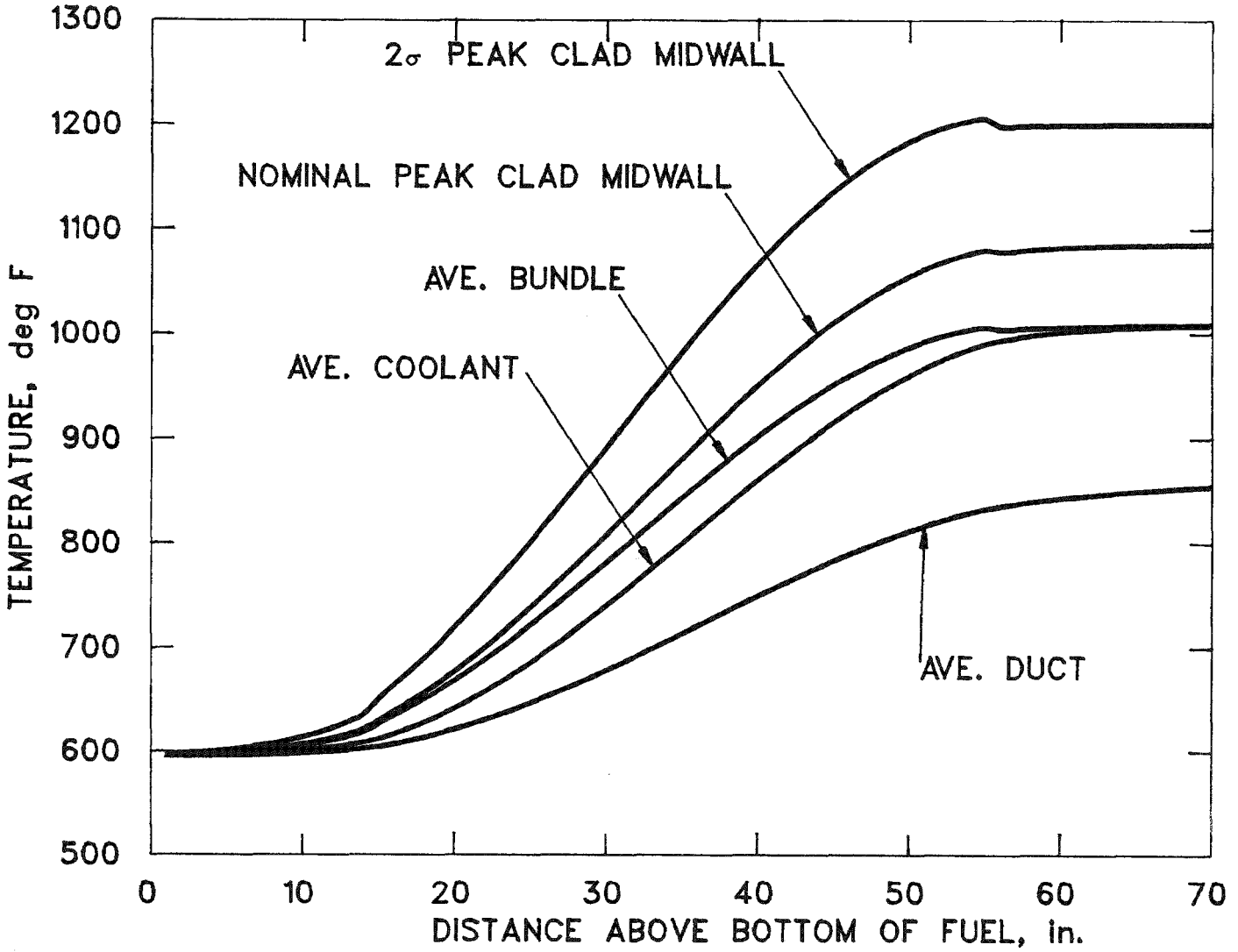

Figure 4.2.4.3.11. Nominal and 2σ peak clad midwall temperatures and average coolant, duct and bundle temperatures. (Fourth orificing zone, orificing based on assembly power and equal peak cladding midwall temperatures.)

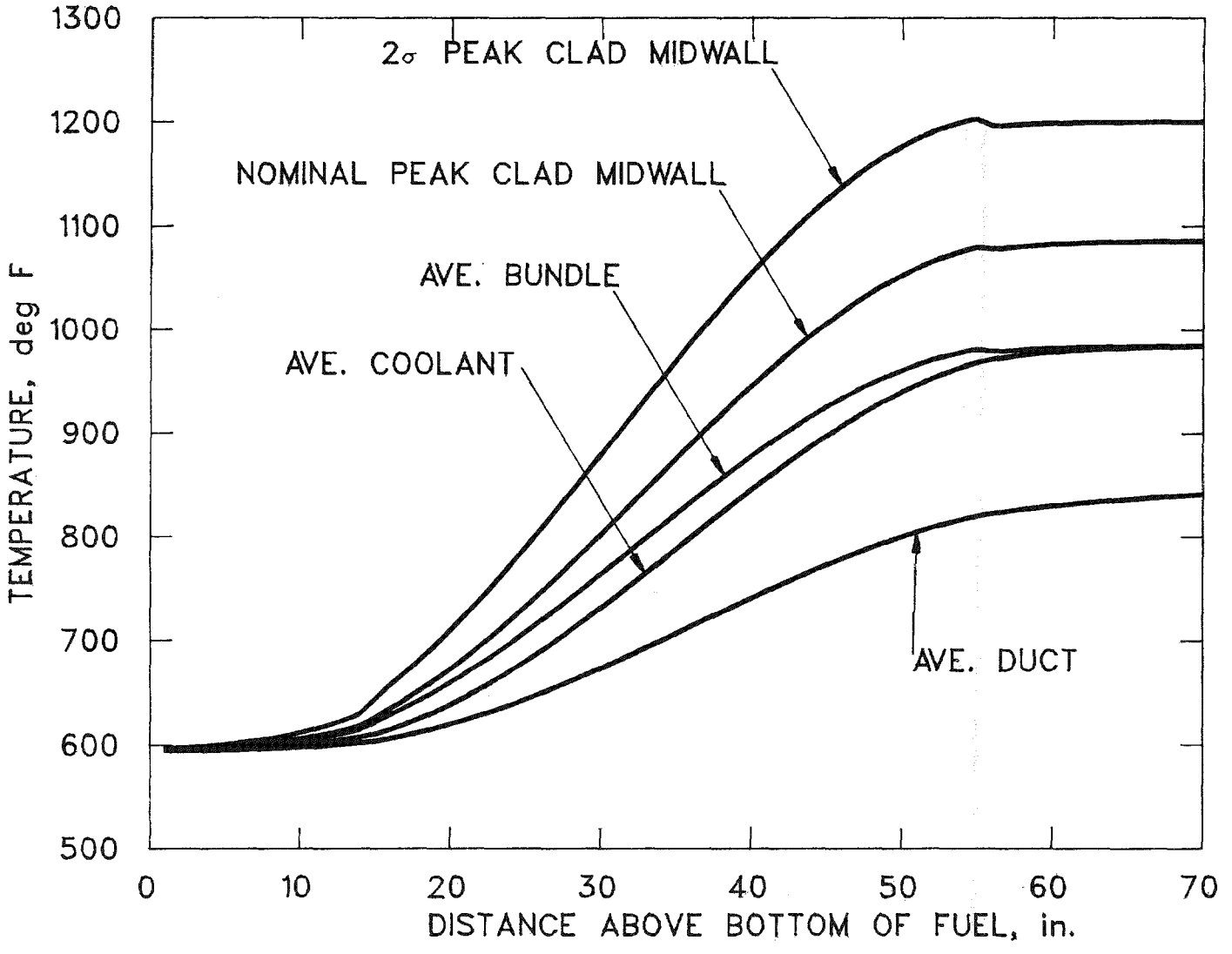

Figure 4.2.4.3.12. Nominal and 2σ peak clad midwall temperatures and average coolant, duct and bundle temperatures. (Fifth orificing zone, orificing based on assembly power and equal peak cladding midwall temperatures.)

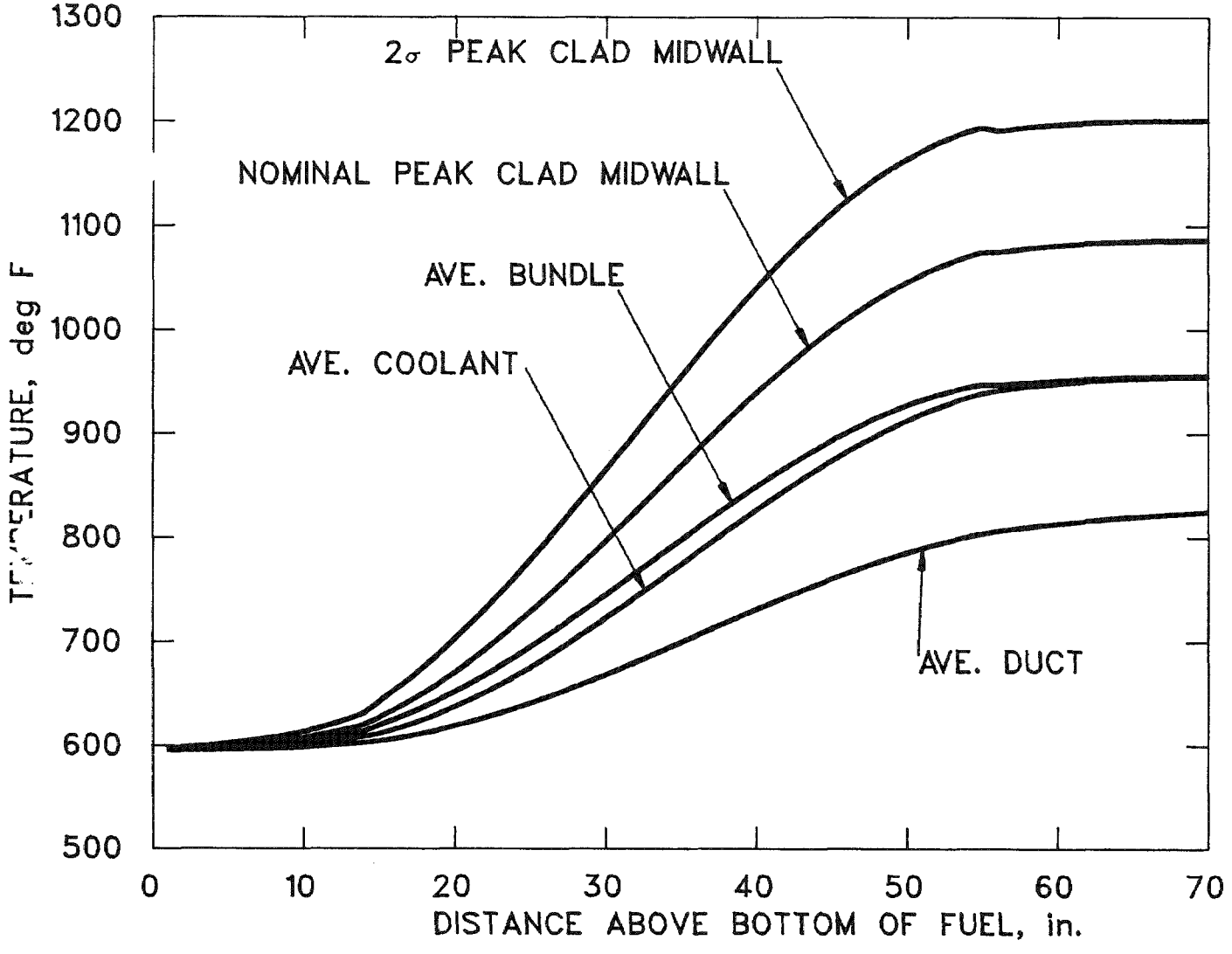

Figure 4.2.4.3.13. Nominal and 2σ peak clad midwall temperatures and average coolant, duct and bundle temperatures. (Sixth orificing zone, orificing based on assembly power and equal peak cladding midwall temperatures.)

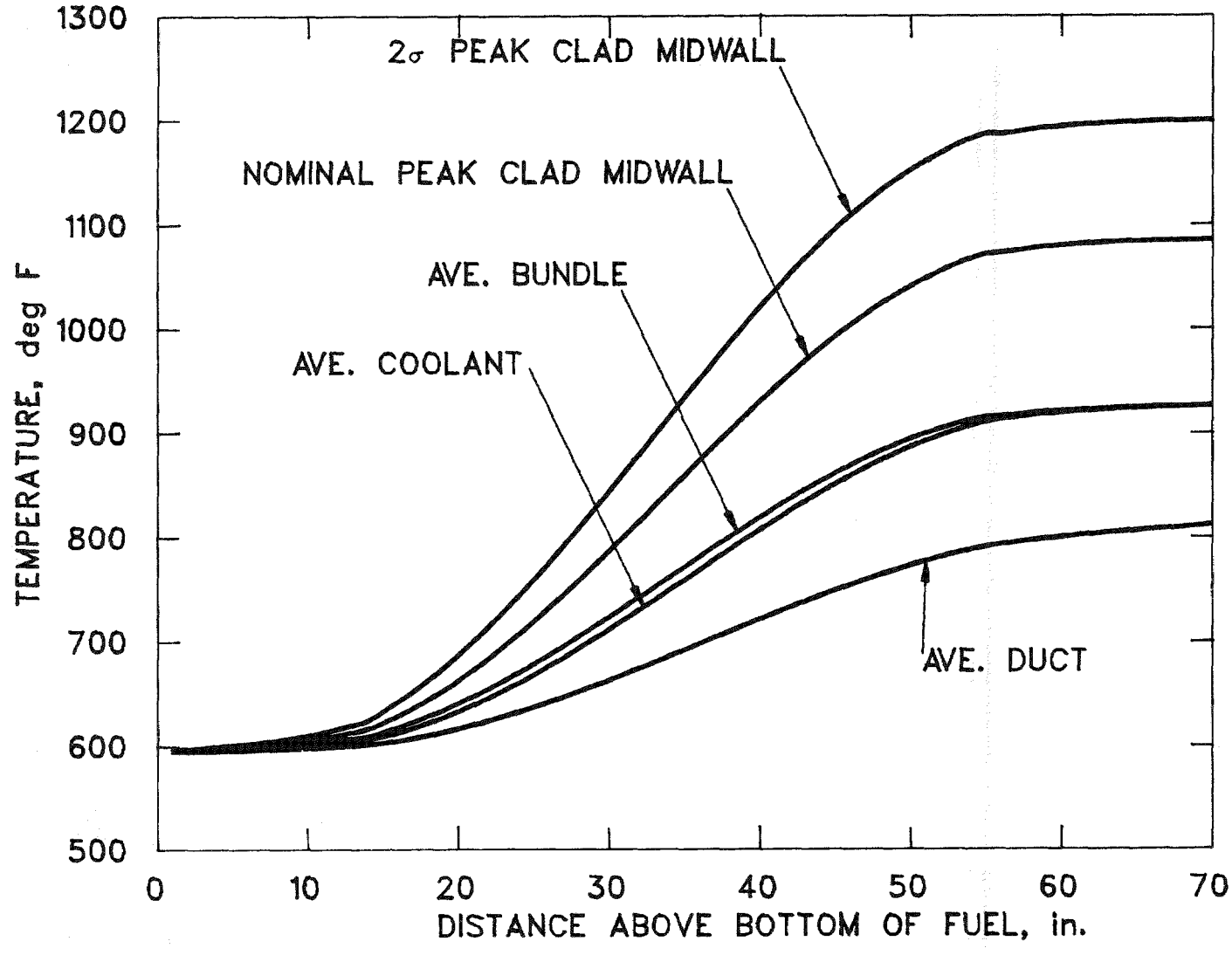

Figure 4.2.4.3.14. Nominal and 2σ peak clad midwall temperatures and average coolant, duct and bundle temperatures. (Seventh orificing zone, orificing based on assembly power and euqal peak cladding midwall tmeperatures.)

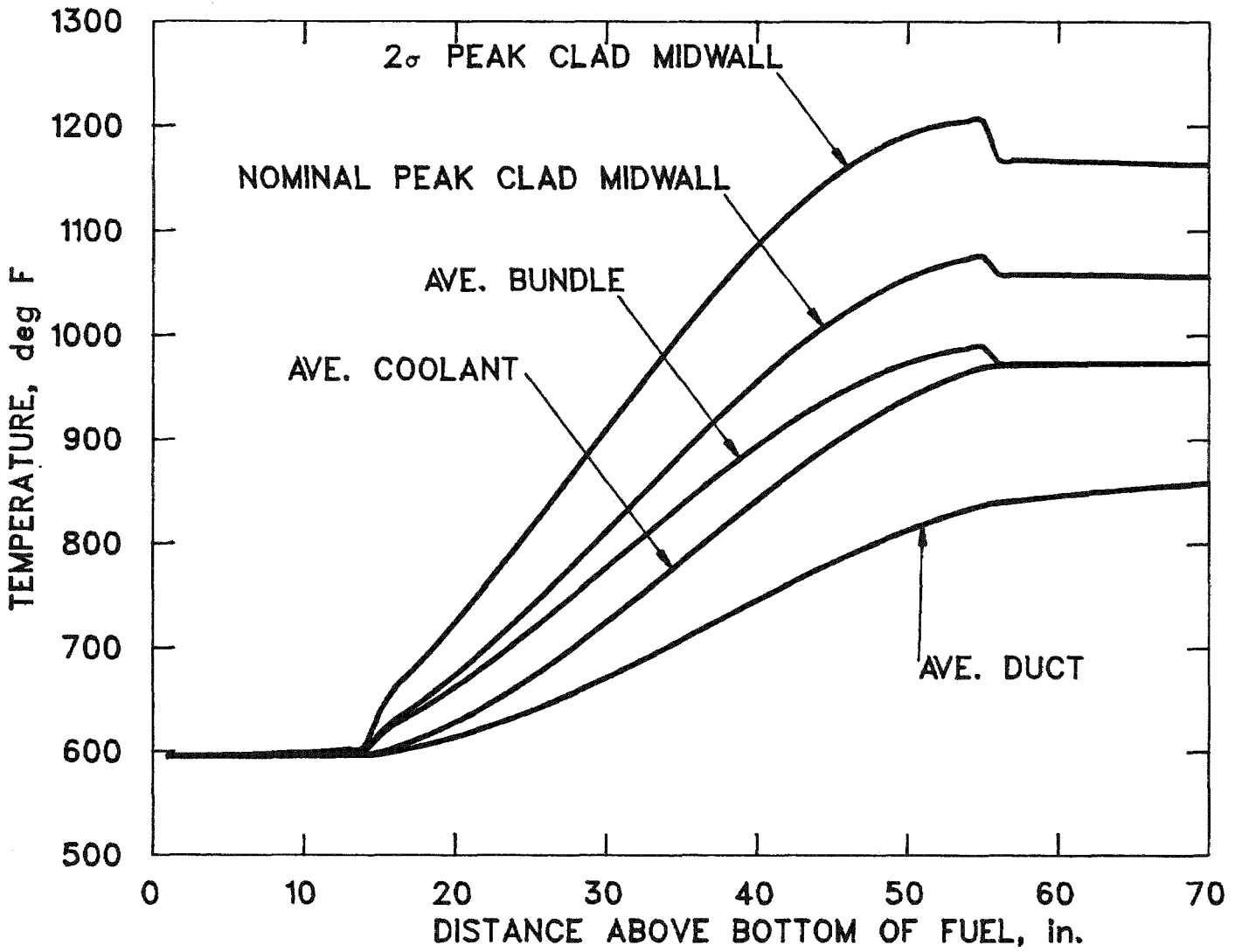

Figure 4.2.4.3.15. Nominal and 2σ peak clad midwall temperatures and average coolant, duct and bundle temperatures. (First orificing zone, orificing based on pin power and equal peak assembly coolant temperatures.)

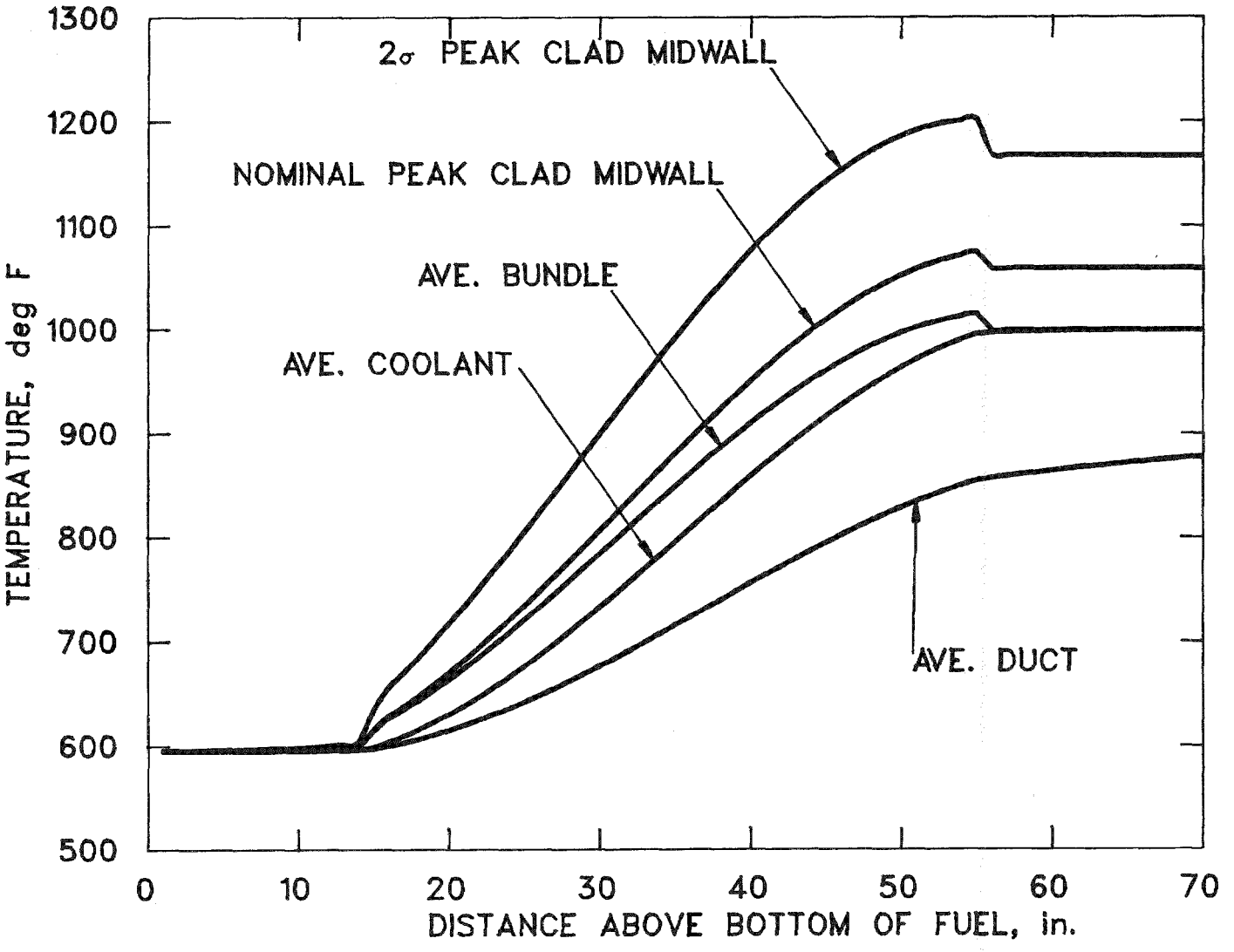

Figure 4.2.4.3.16. Nominal and 2σ peak clad midwall temperatures and average coolant, duct and bundle temperatures. (Second orificing zone, orificing based on pin power and equal peak assembly coolant temperatures.)

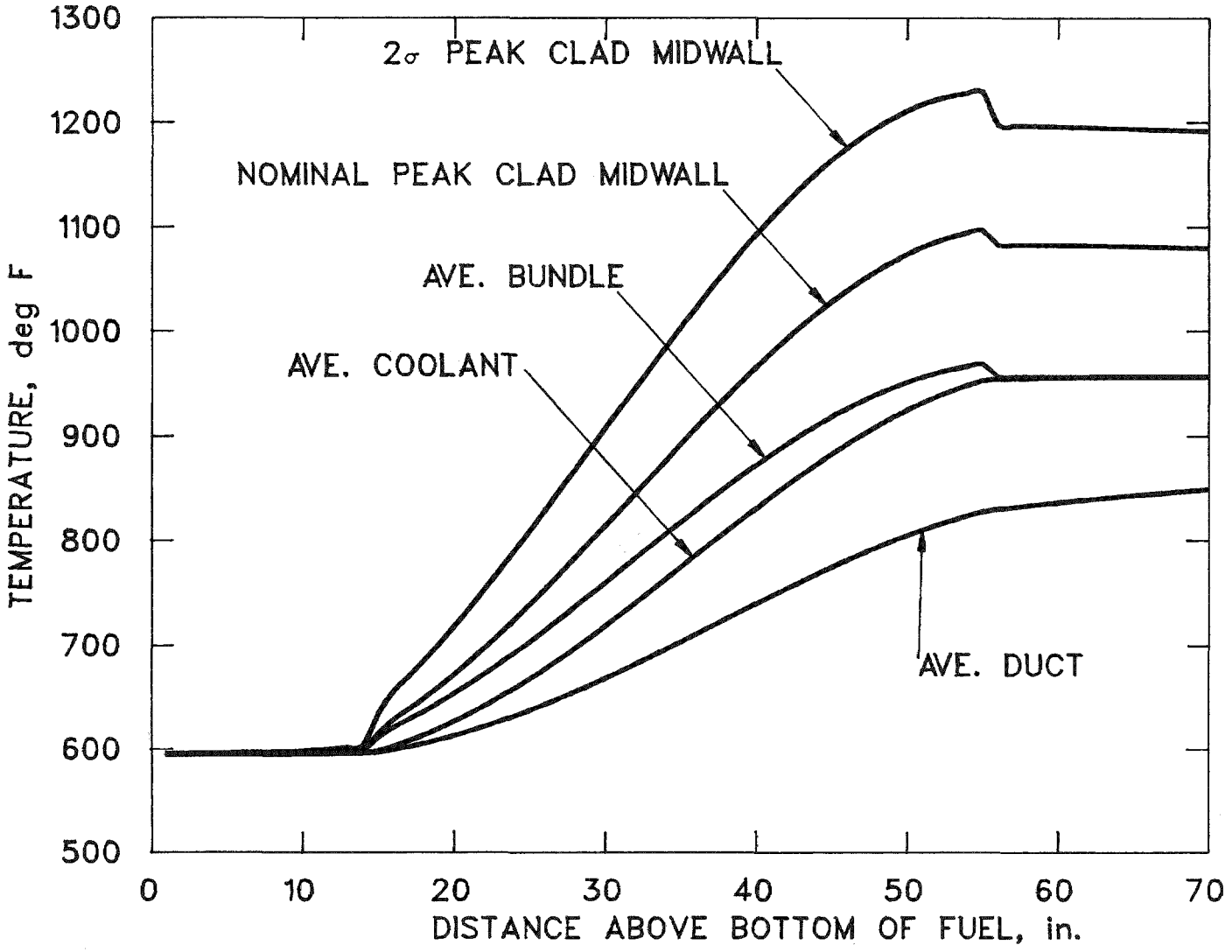

Figure 4.2.4.3.17. Nominal and 2σ peak clad midwall temperatures and average coolant, duct and bundle temperatures. (Third orificing zone, orificing based on pin power and equal peak assembly coolant temperatures.)

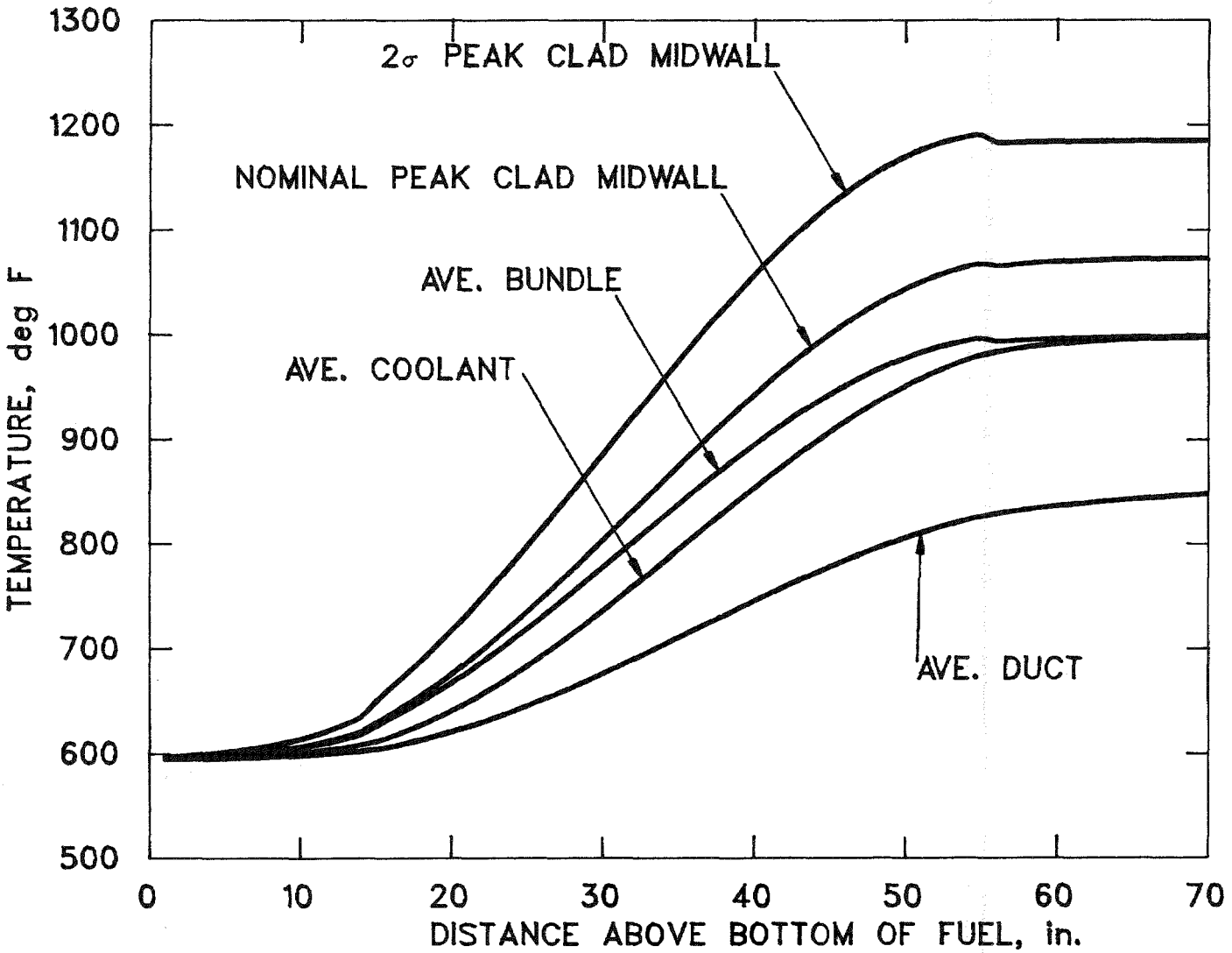

Figure 4.2.4.3.18. Nominal and 2σ peak clad midwall temperatures and average coolant, duct and bundle temperatures. (Fourth orificing zone, orificing based on pin power and equal peak assembly coolant temperatures.)

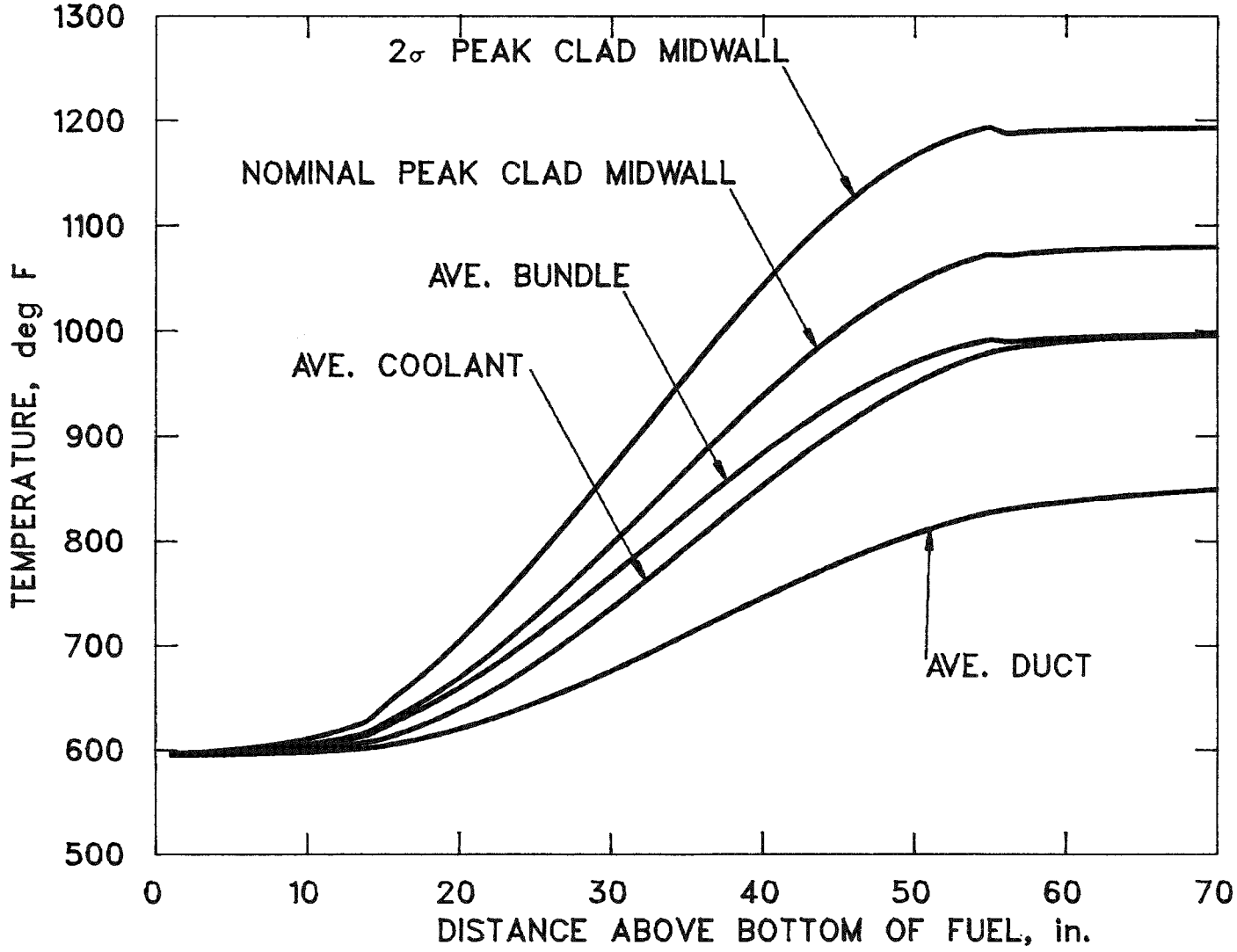

Figure 4.2.4.3.19. Nominal and 2σ peak clad midwall temperatures and average coolant, duct and bundle temperatures. (Fifth orificing zone, orificing based on pin power and equal peak assembly coolant temperatures.)

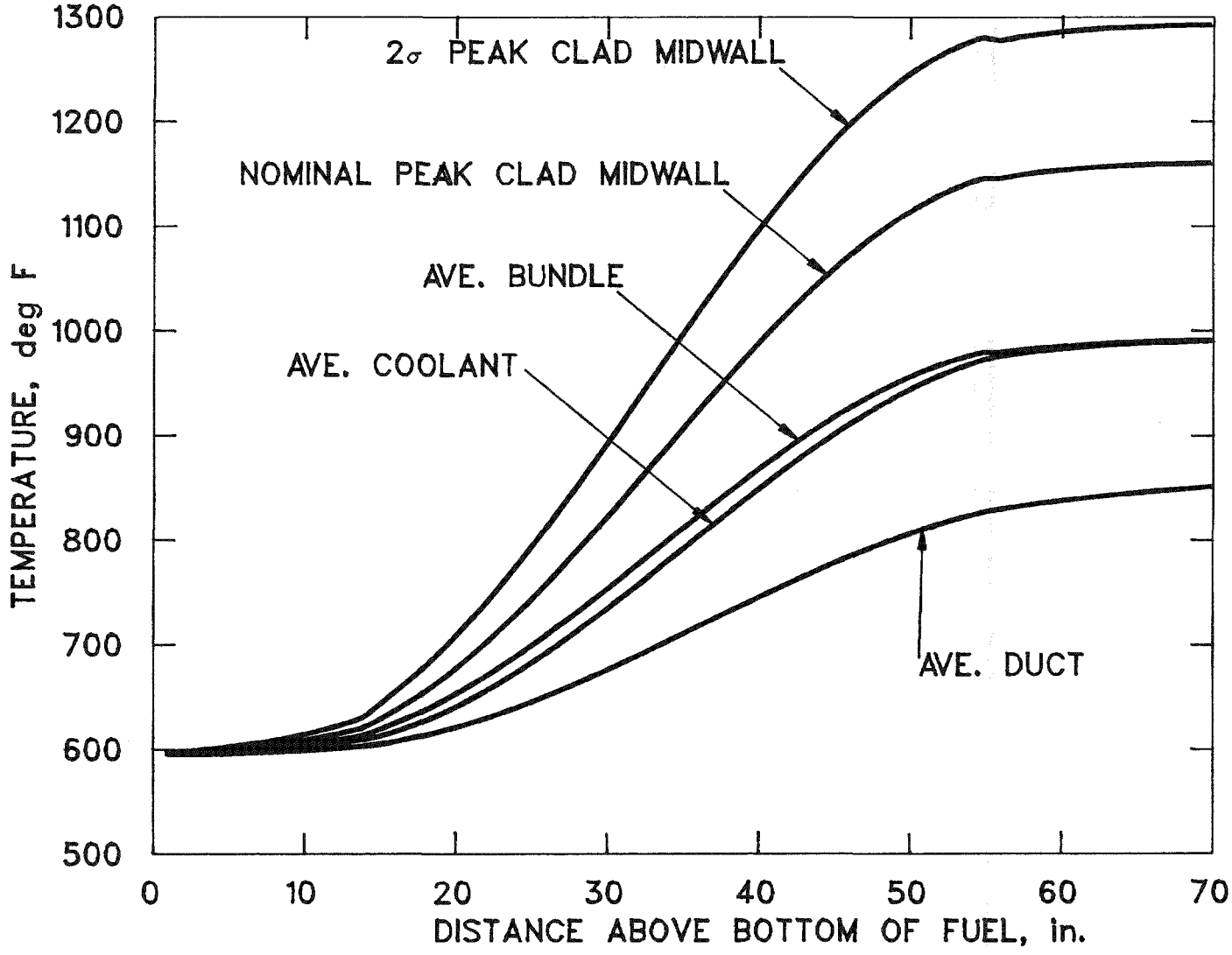

Figure 4.2.4.3.20. Nominal and 2σ peak clad midwall temperatures and average coolant, duct and bundle temperatures. (Sixth orificing zone, orificing based on pin power and equal peak assembly coolant temperatures.)

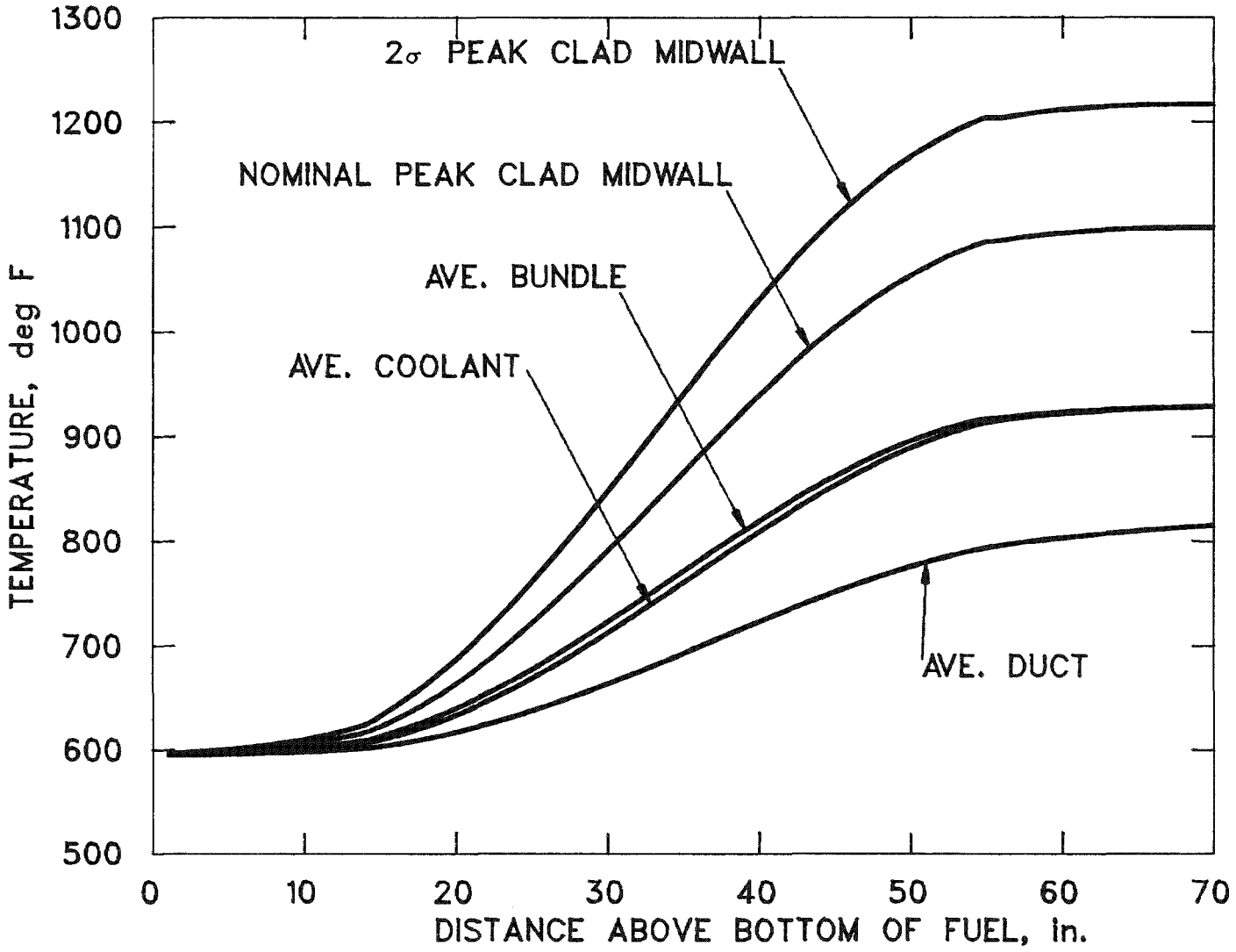

Figure 4.2.4.3.21. Nominal and 2σ peak clad midwall temperatures and average coolant, duct and bundle temperatures. (Seventh orificing zone, orificing based on pin power and equal peak assembly coolant temperatures.)

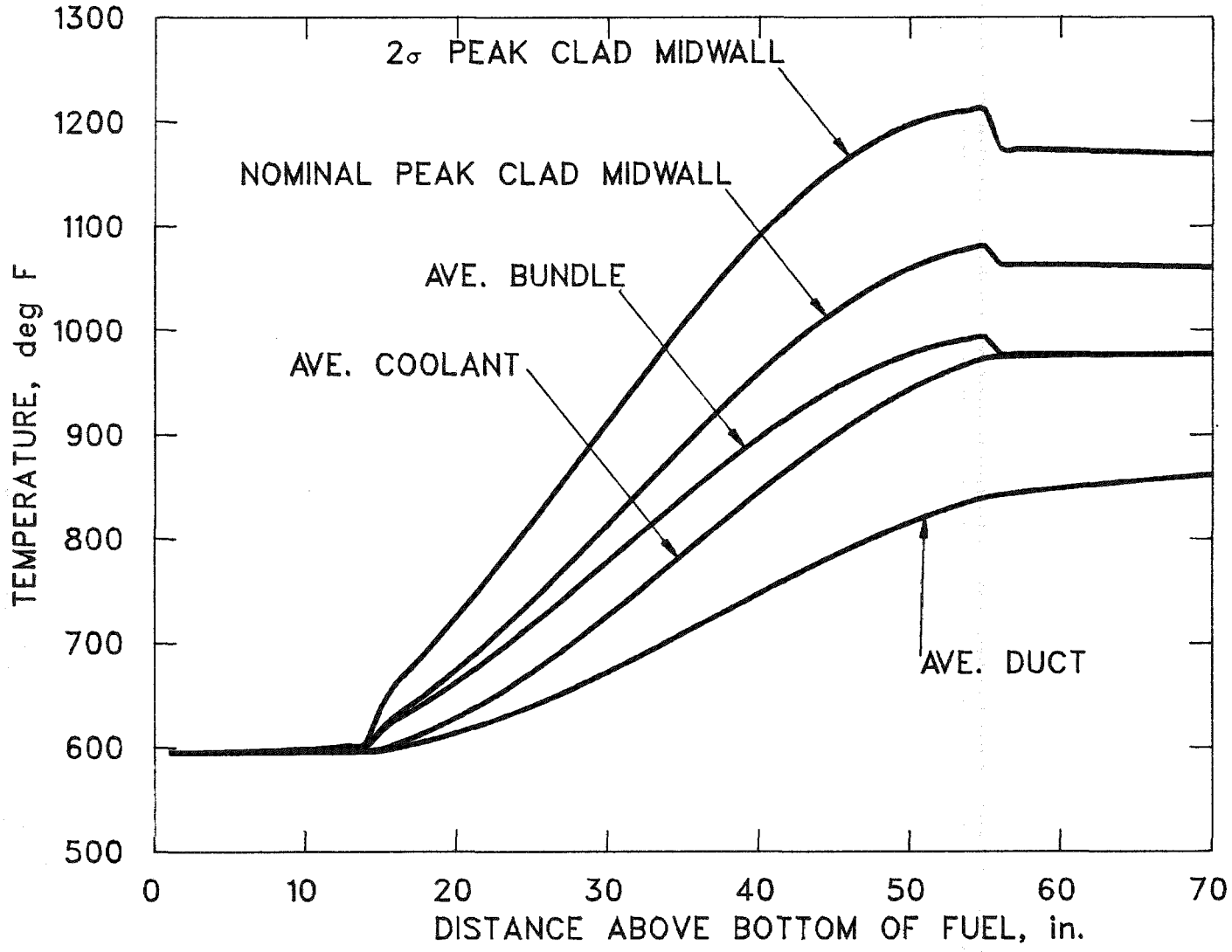

Figure 4.2.4.3.22. Nominal and 2σ peak clad midwall temperatures and average coolant, duct and bundle temperatures. (First orificing zone, orificing based on pin power and equal peak cladding midwall temperatures.)

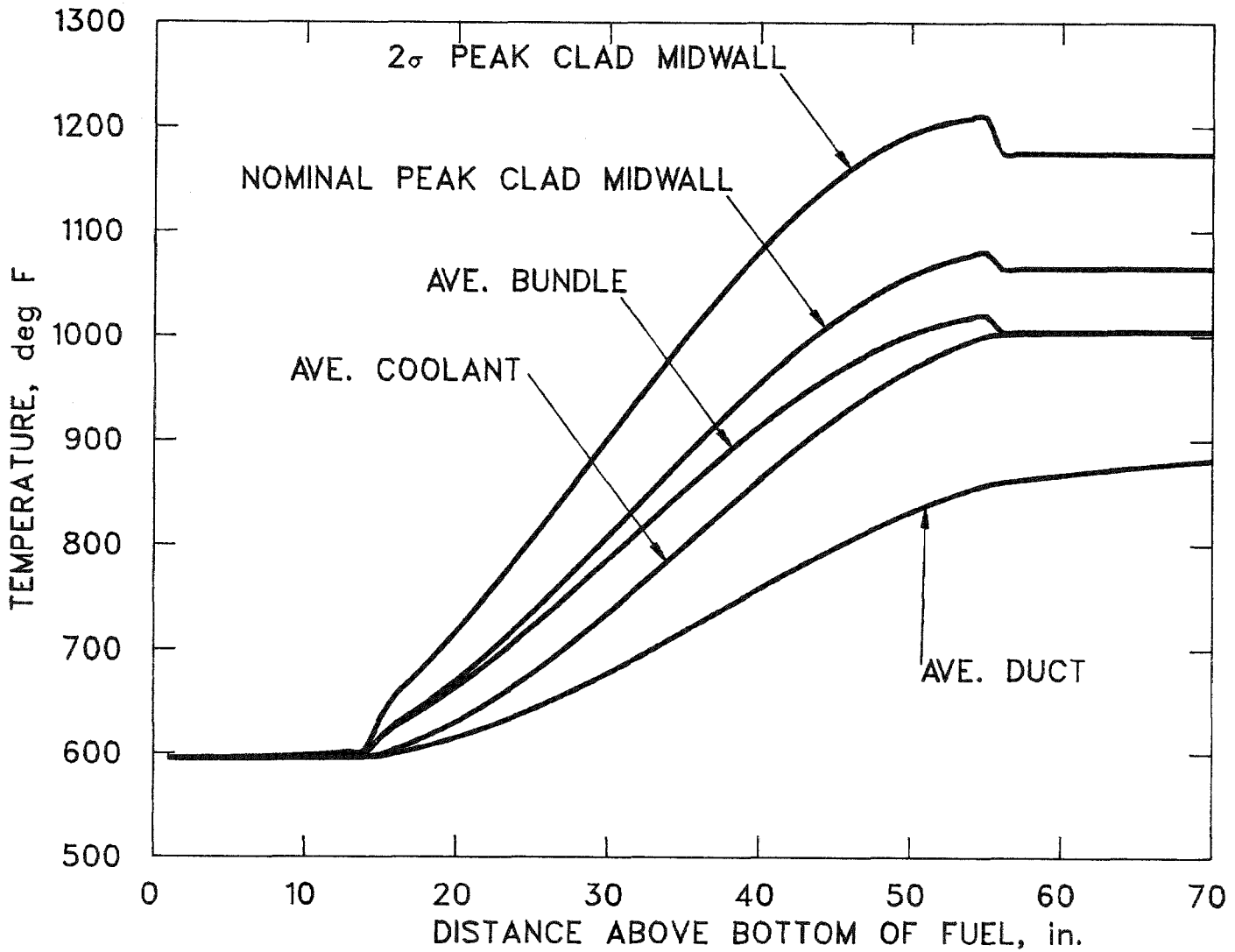

Figure 4.2.4.3.23. Nominal and 2σ peak clad midwall temperatures and average coolant, duct and bundle temperatures. (Second orificing zone, orificing based on pin power and equal peak cladding midwall temperatures.)

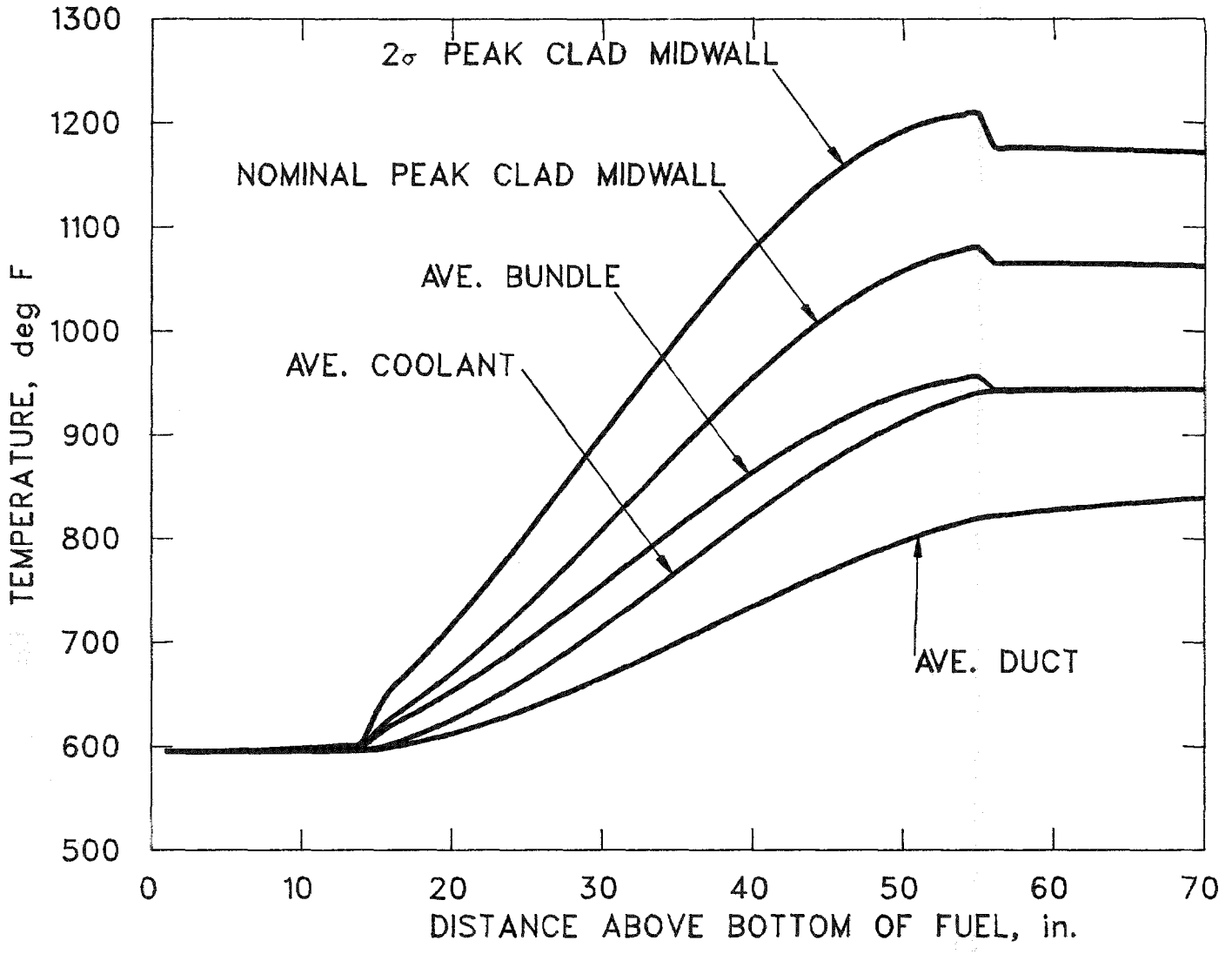

Figure 4.2.4.3.24. Nominal and 2σ peak clad midwall temperatures and average coolant, duct and bundle temperatures. (Third orificing zone, orificing based on pin power and equal peak cladding midwall temperatures.)

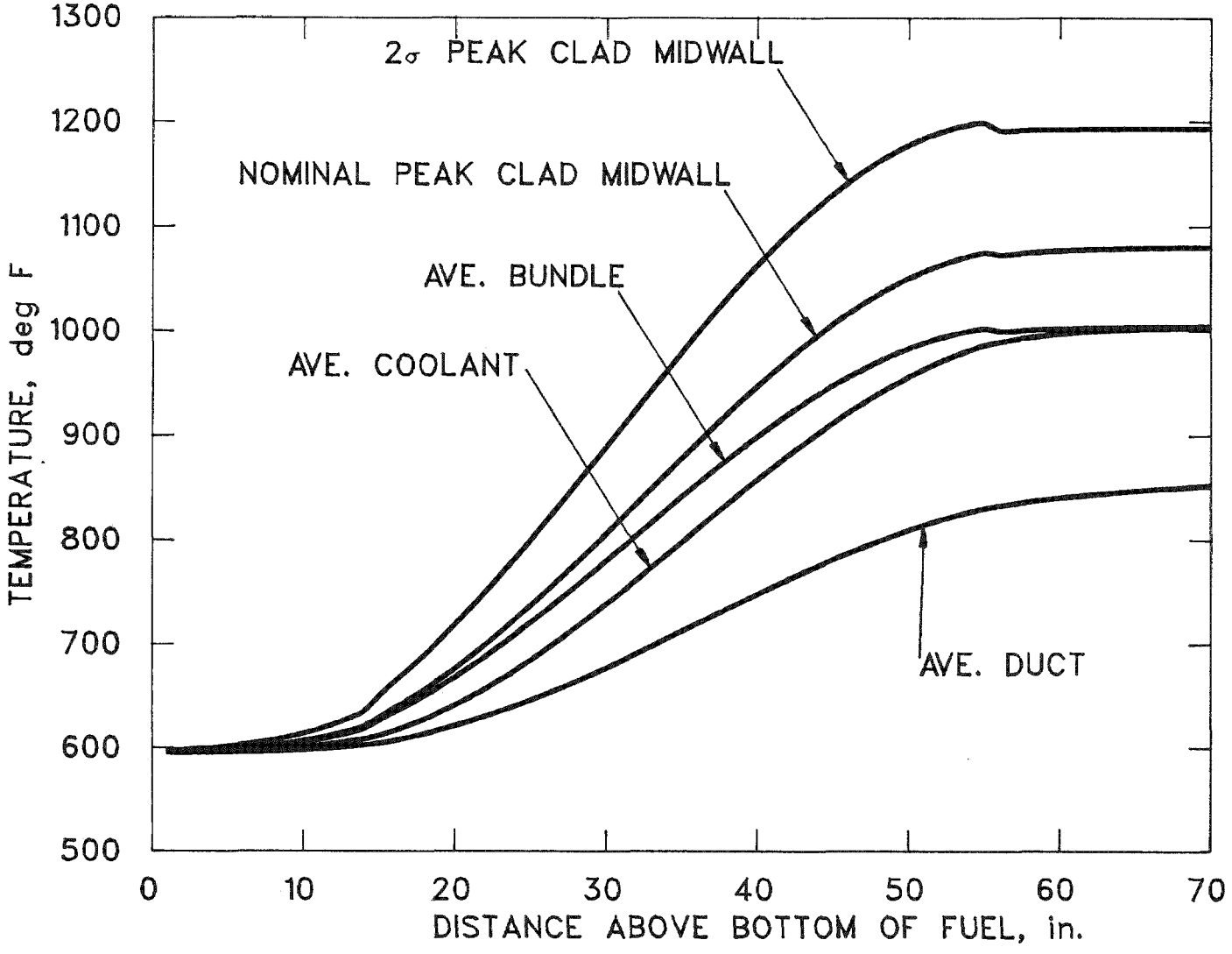

Figure 4.2.4.3.25. Nominal and 2σ peak clad midwall temperatures and average coolant, duct and bundle temperatures. (Fourth orificing zone, orificing based on pin power and equal peak cladding midwall temperatures.)

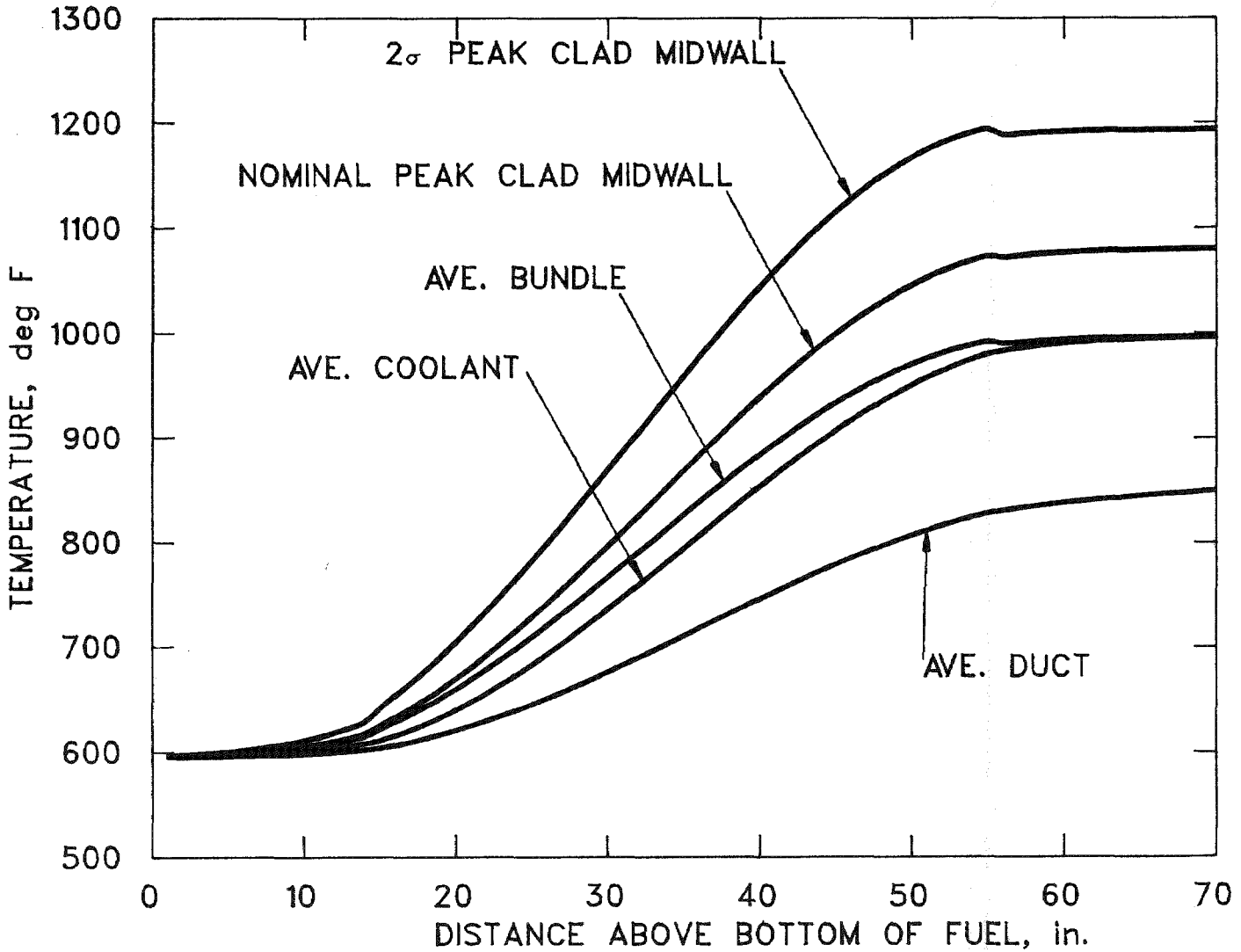

Figure 4.2.4.3.26. Nominal and 2σ peak clad midwall temperatures and average coolant, duct and bundle temperatures. (Fifth orificing zone, orificing based on pin power and equal peak cladding midwall temperatures.)

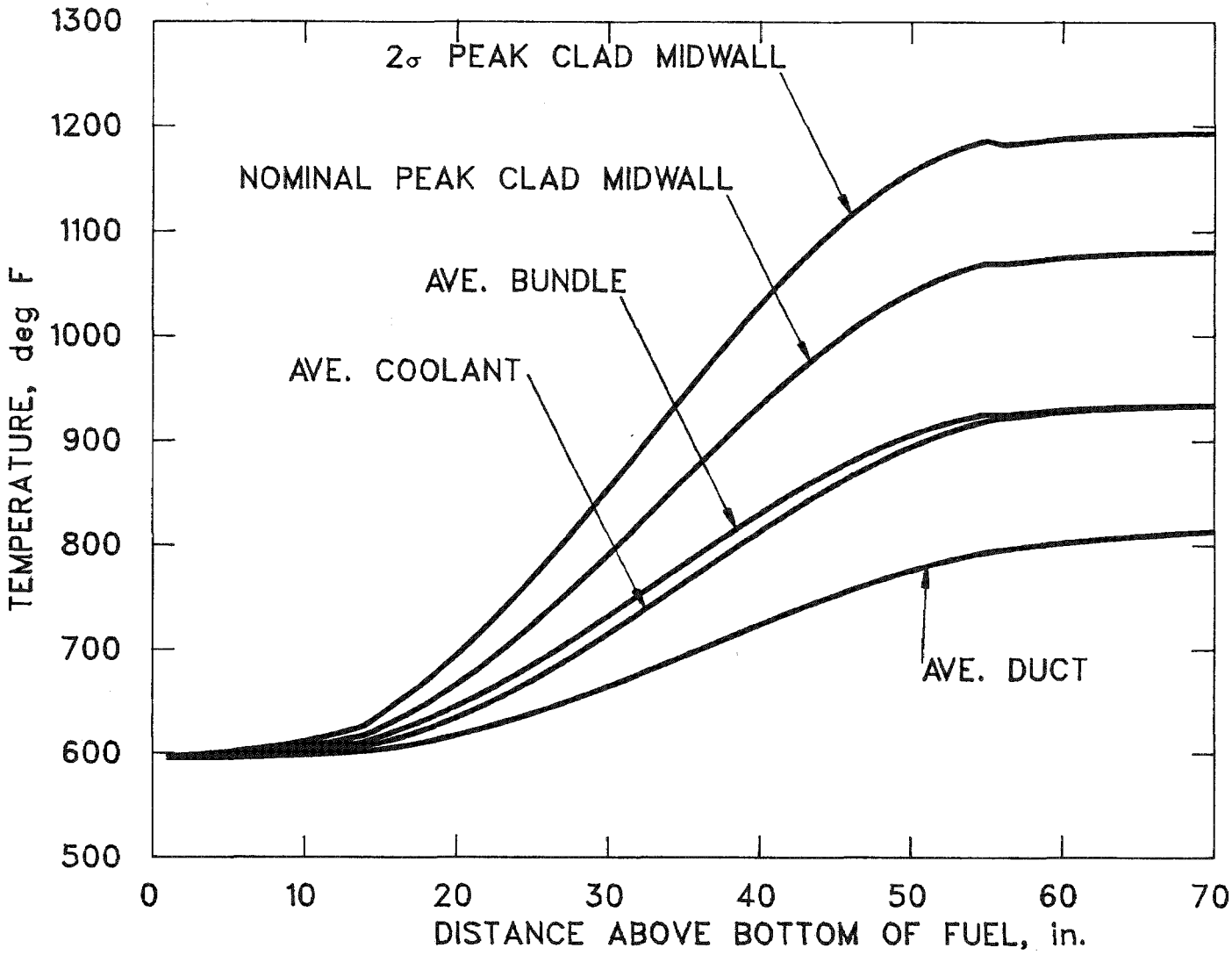

Figure 4.2.4.3.27. Nominal and 2σ peak clad midwall temperatures and average coolant, duct and bundle temperatures. (Sixth orificing zone, orificing based on pin power and equal peak cladding midwall temperatures.)

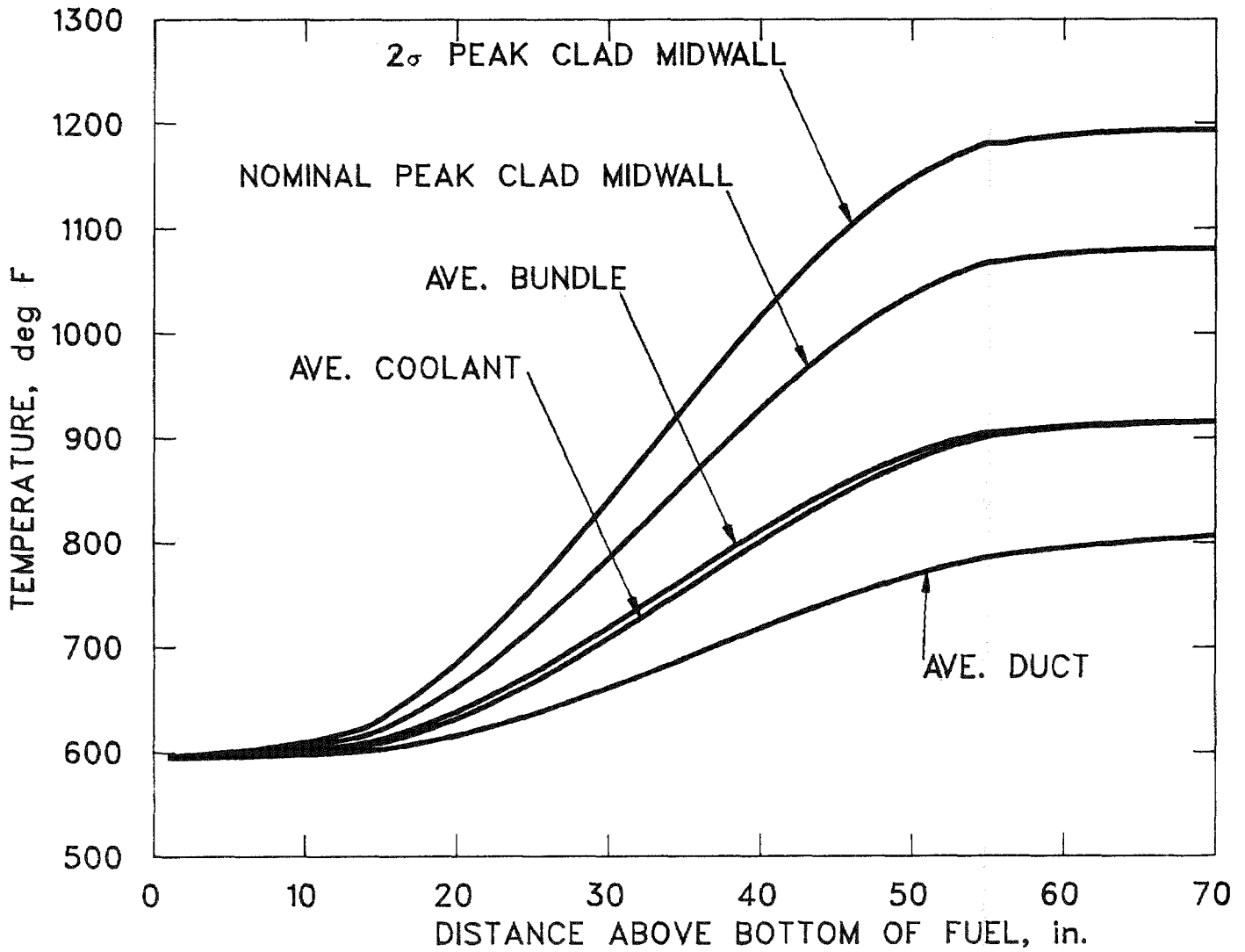

Figure 4.2.4.3.28. Nominal and 2σ peak clad midwall temperatures and average coolant, duct and bundle temperatures. (Seventh orificing zone, orificing based on pin power and equal peak cladding midwall temperatures.)

Table 4.2.4.3.1

NOMINAL AND 2σ PEAK CLADDING MIDWALL TEMPERATURES

Temperatures (°F)	Assembly Assignment to Orificing Zones Based on Assembly Power		Assembly Assignment to Orificing Zones Based on Pin Power	
	Equal Peak Assembly Coolant Temperatures	Equal Peak Cladding Midwall Temperatures	Equal Peak Assembly Coolant Temperatures	Equal Peak Cladding Midwall Temperatures
Nominal	1167	1093	1181	1088
2σ	1300	1227	1318	1220

power yields the lowest 2σ peak cladding midwall temperture which is 1220° F. If orificing is based on assembly power and equal peak assembly coolant temperatures the 2σ peak cladding midwall temperature is raised to 1300° F.

4.2.4.4 Coolant Temperatures

Average assembly coolant temperatures for BOL and EOEC conditions at three axial locations,i.e., core midplane, core-upper axial blanket interface,and top of upper axial blanket, are shown in Figures 4.2.4.4.1 to 4.2.4.4.24. The peak assembly coolant temperatures that result from the four orificing strategies considered are given in Table 4.2.4.4.1. The strategies that equalize the peak assembly coolant temperatures yield lower assembly coolant tempertures. From them, the one that is based on assembly power yields the lowest peak assembly coolant temperature, which is 990° F. However, the difference between the lowest and maximum peak assembly coolant temperatures that result from the four orificing strategies is 16° F.

4.2.4.5 Assembly Bundle Pressure Drops

Rod bundle friction pressure drops have been calculated by Chiu's method for the flow rates resulting from the four orificing strategies used in this analysis. Nominal values for these pressure drops are presented in Table 4.2.4.5.1. The maximum pressure drops are provided either by the first core orificing zone (orificing zone #1) or by the first blanket orificing zone (orificing zone #4) and they vary with the orificing strategy from 51.0 psi to 53.2 psi. To accommodate calculational uncertainties, the pressure drop used to design the fuel assembly (Section 3.1) is well above these values. To balance the pressure losses in the remaining zones with the maximum pressure loss, additional losses have to be taken in the shield/orifice region and in the core support module.

4.2.5 Duct Wall Temperatures

Irradiation induced creep and swelling of the assembly duct walls depend on the temperature of these walls. Assembly bowing is a function of the temperature differences across the assembly duct walls.

Assembly duct wall temperatures have been determined for the different orificing strategies discussed in Section 4.2.2.1 using the code CORE-3D. As it has already been discussed (Section 4.2.4), CORE-3D takes into account interassembly heat

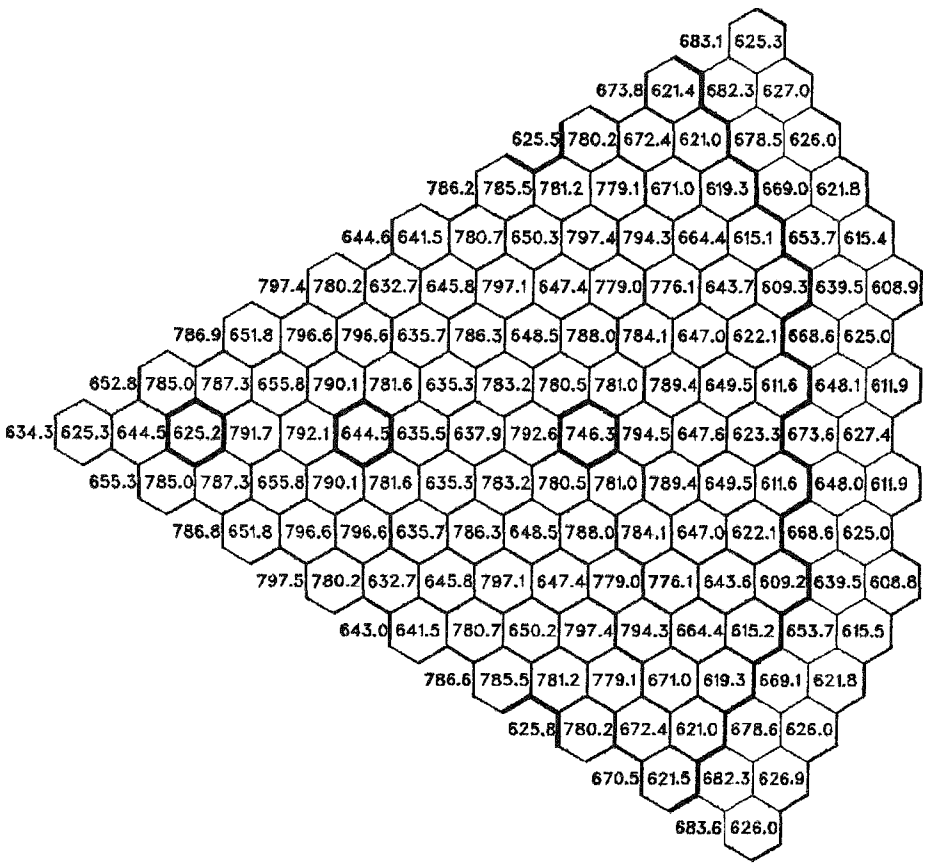

Figure 4.2.4.4.1. Average coolant temperatures (^{o}F) at BOL at core midplane. (Orificing based on assembly power and equal peak assembly coolant temperatures.)

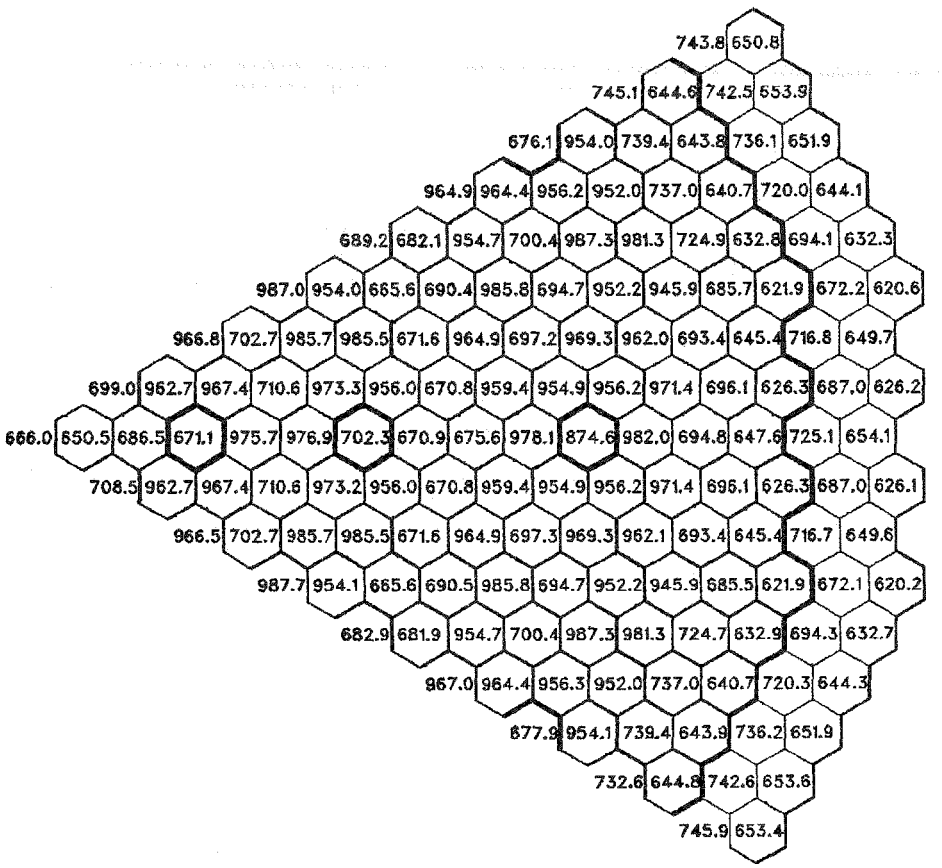

Figure 4.2.4.4.2. Average coolant temperatures (°F) at BOL at core-upper axial blanket interface. (Orificing based on assembly power and equal peak assembly coolant temperatures.)

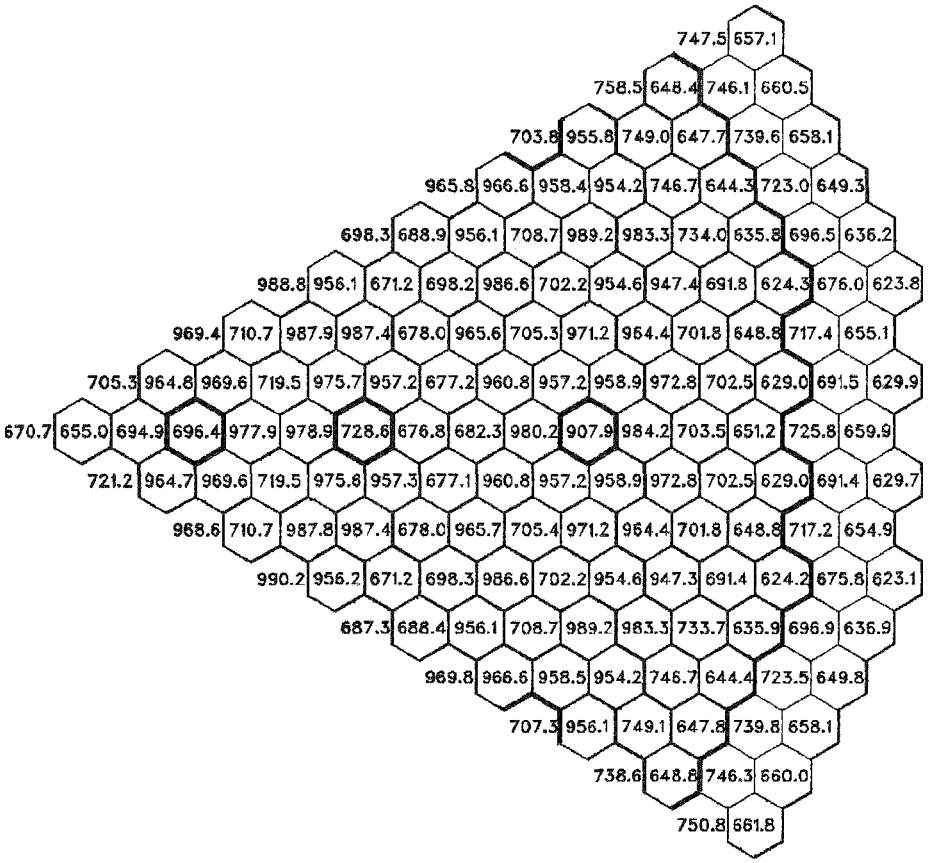

Figure 4.2.4.4.3. Average coolant temperatures (^{o}F) at BOL at the top of the upper axial blanket. (Orificing based on assembly power and equal peak assembly coolant temperatures.)

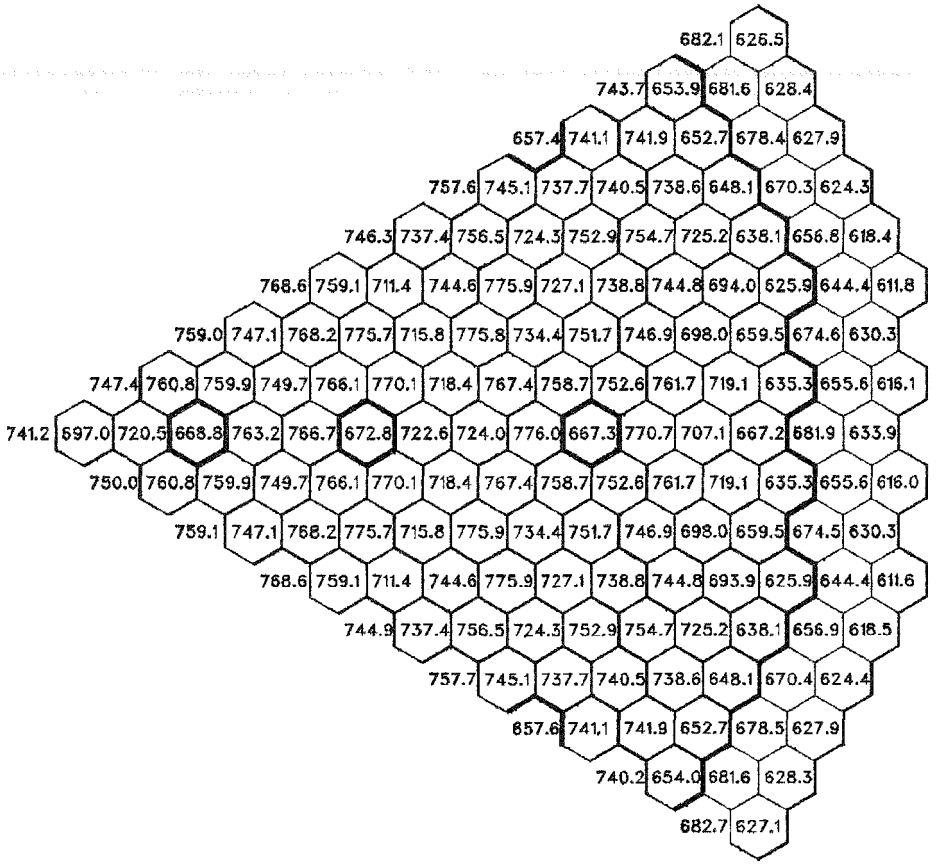

Figure 4.2.4.4.4. Average coolant temperatures (^{o}F) at EOEC at core midplane. (Orificing based on assembly power and equal peak assembly coolant temperatures.)

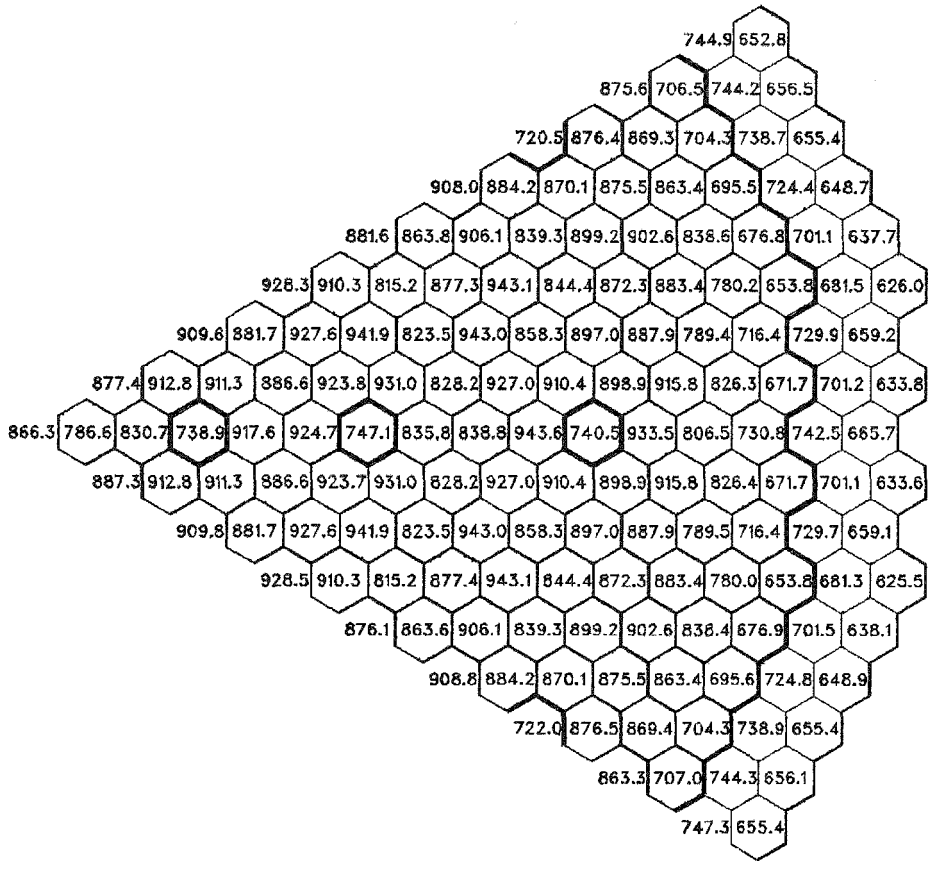

Figure 4.2.4.4.5. Average coolant temperatures (^{o}F) at EOEC at core-upper axial blanket interface. (Orificing based on assembly power and equal peak assembly coolant temperatures.)

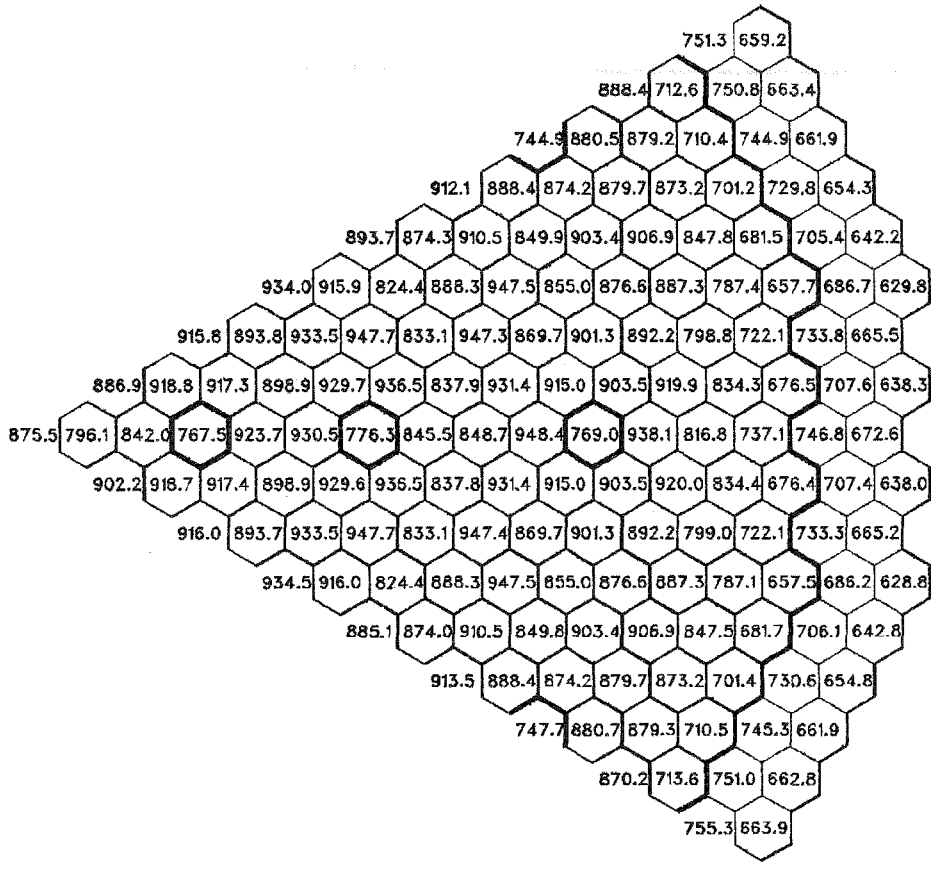

Figure 4.2.4.4.6. Average coolant temperatures (^{o}F) at EOEC at the top of the upper axial blanket. (Orificing based on assembly power and equal peak assembly coolant temperatures.)

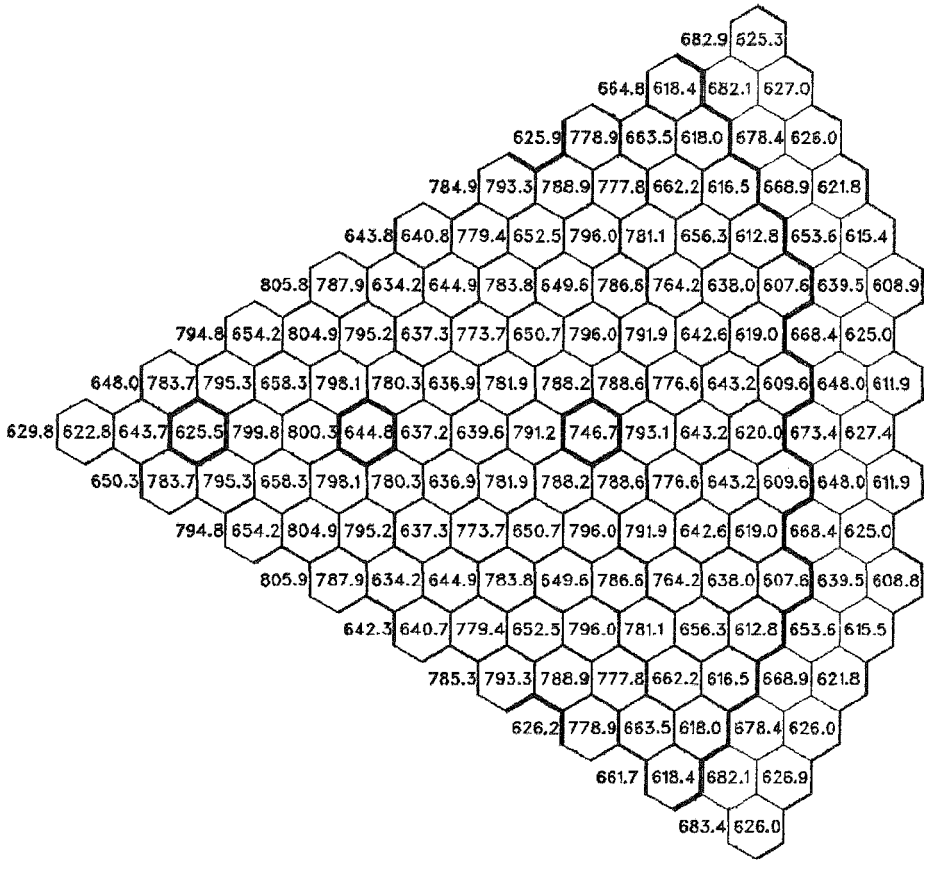

Figure 4.2.4.4.7. Average coolant temperatures ($^{\circ}$F) at BOL at core midplane. (Orificing based on assembly power and equal peak cladding midwall temperatures.)

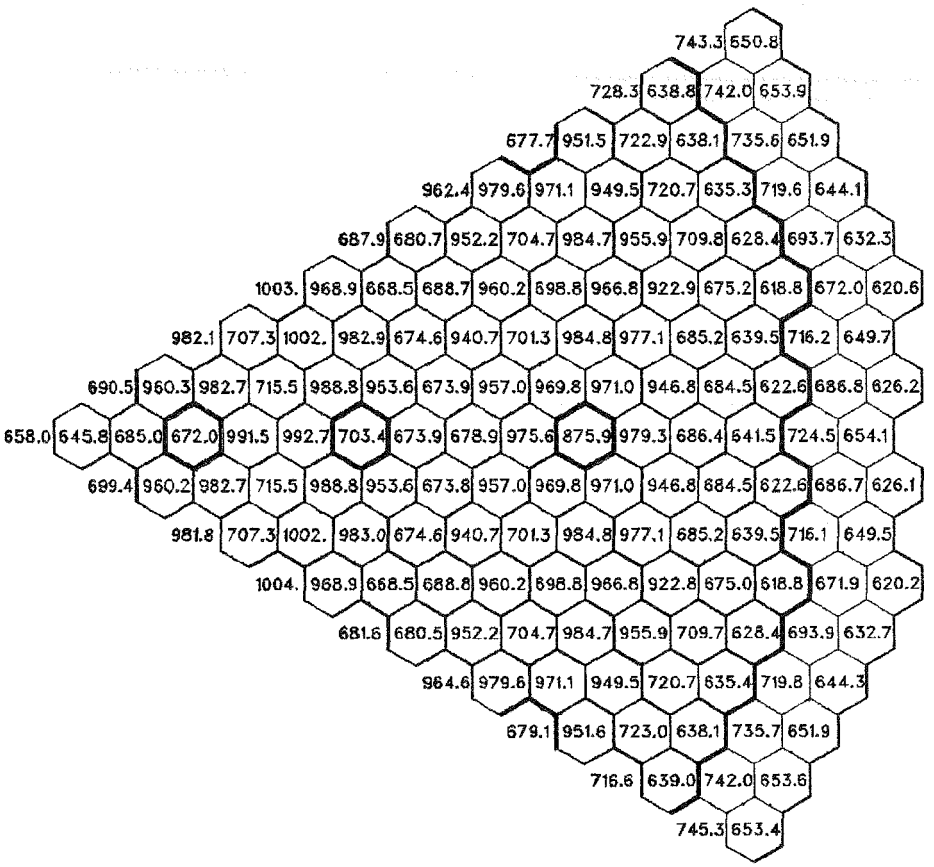

Figure 4.2.4.4.8. Average coolant temperatures (^{o}F) at BOL at core-upper axial blanket interface. (Orificing based on assembly power and equal peak cladding midwall temperatures.)

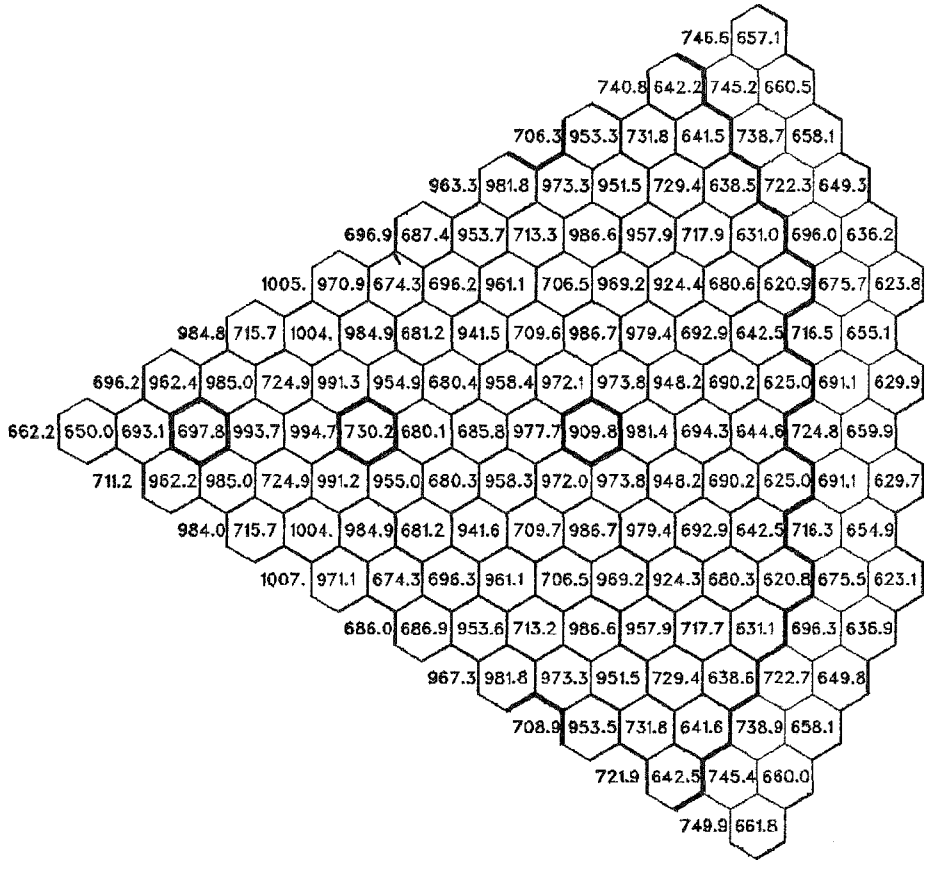

Figure 4.2.4.4.9. Average coolant temperatures (^{o}F) at BOL at the top of the upper axial blanket. (Orificing based on assembly power and equal peak cladding midwall temperatures.)

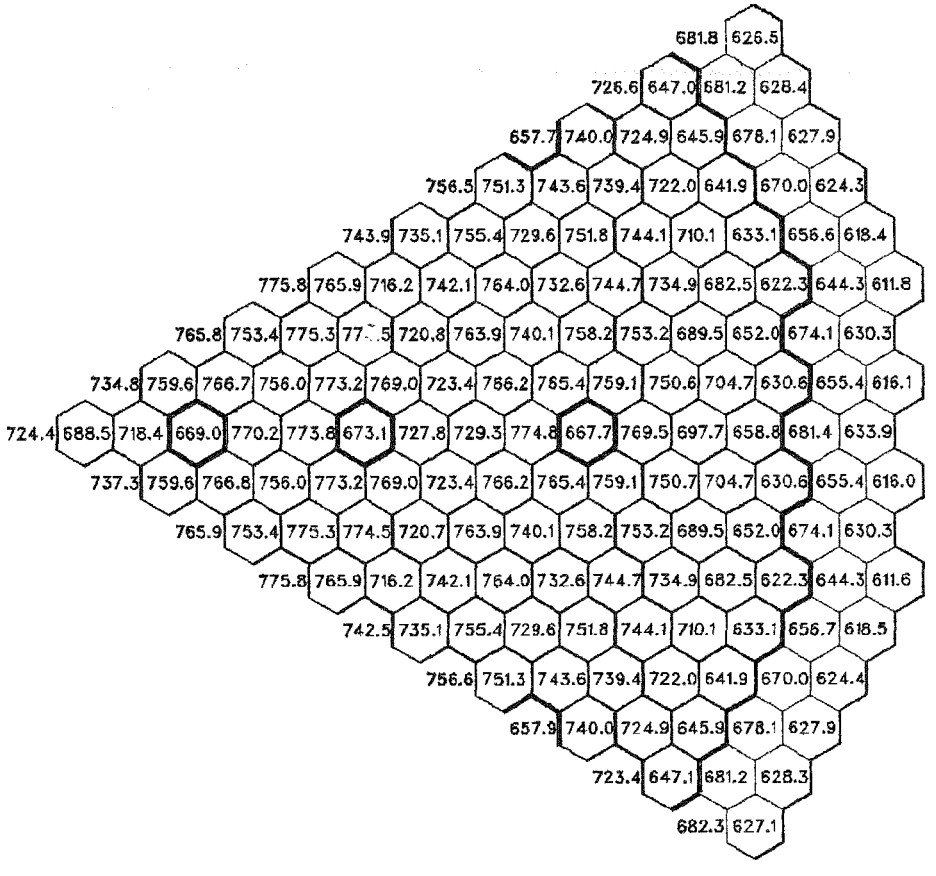

Figure 4.2.4.4.10. Average coolant temperatures ($^{\circ}$F) at EOEC at core midplane. (Orificing based on assembly power and equal peak cladding midwall temperatures.)

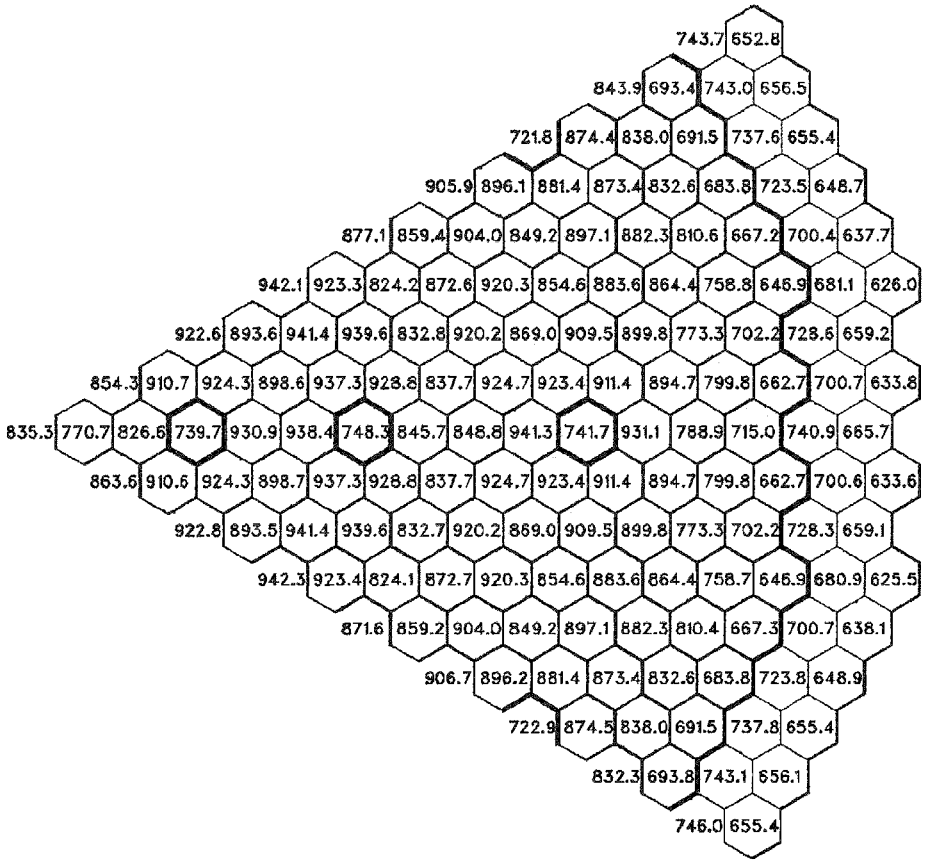

Figure 4.2.4.4.11. Average coolant temperatures (°F) at EOEC at core-upper axial blanket interface. (Orificing based on assembly power and equal peak cladding midwall temperatures.)

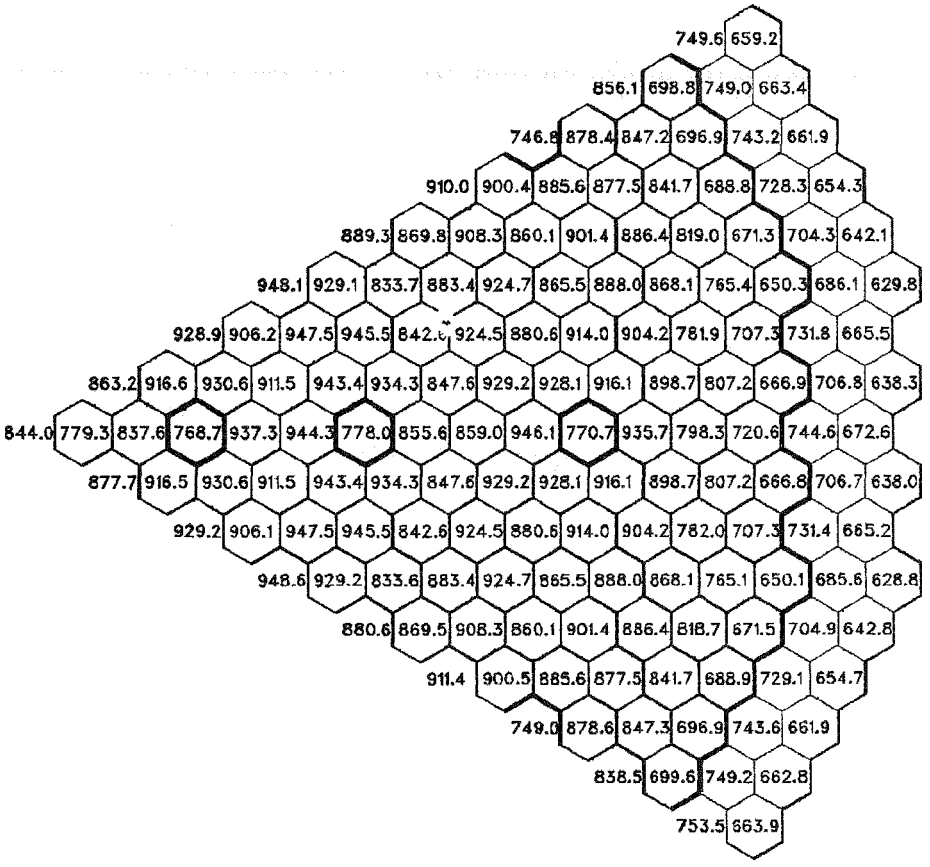

Figure 4.2.4.4.12. Average coolant temperatures (^{o}F) at EOEC at the top of the upper axial blanket. (Orificing based on assembly power and equal peak cladding midwall temperatures.)

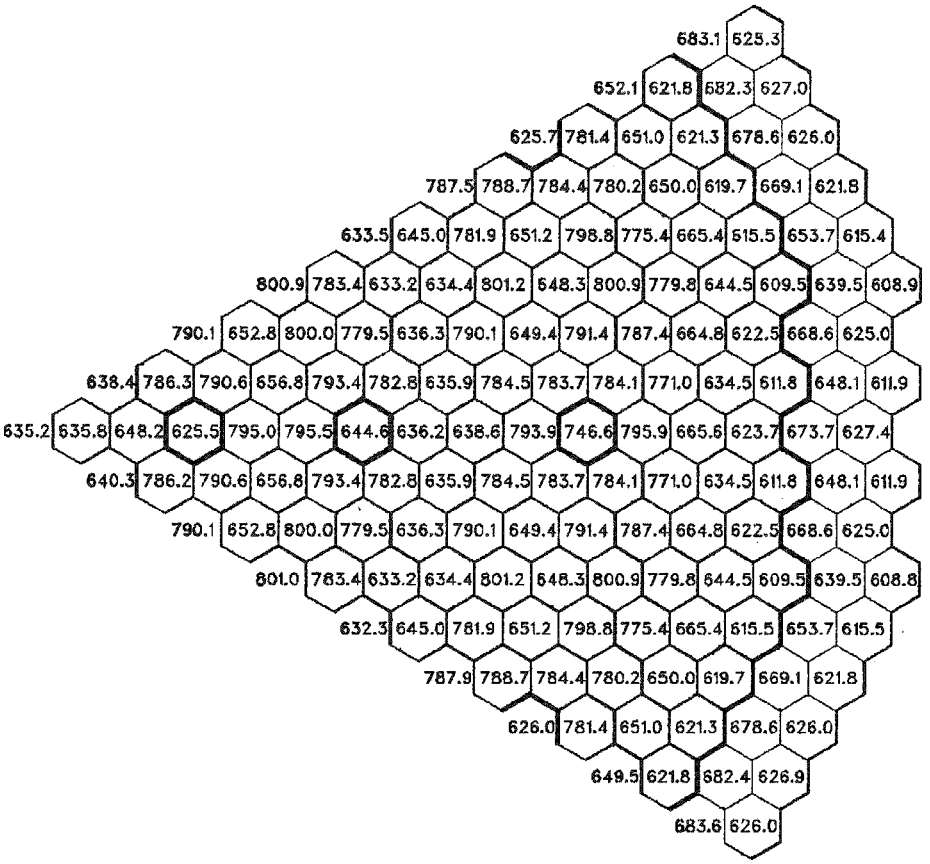

Figure 4.2.4.4.13. Average coolant temperatures (^{o}F) at BOL at core midplane. (Orificing based on pin power and equal peak assembly coolant temperatures.)

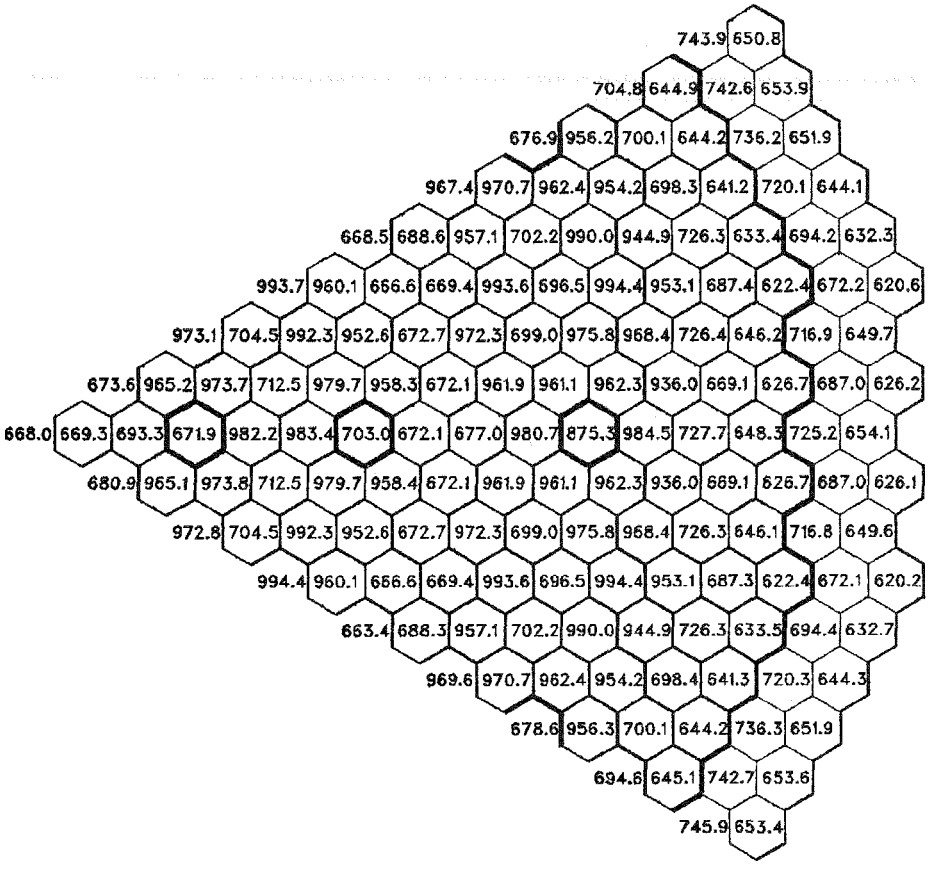

Figure 4.2.4.4.14. Average coolant temperatures (^{o}F) at BOL at core-upper axial blanket interface. (Orificing based on pin power and equal peak assembly coolant temperatures.)

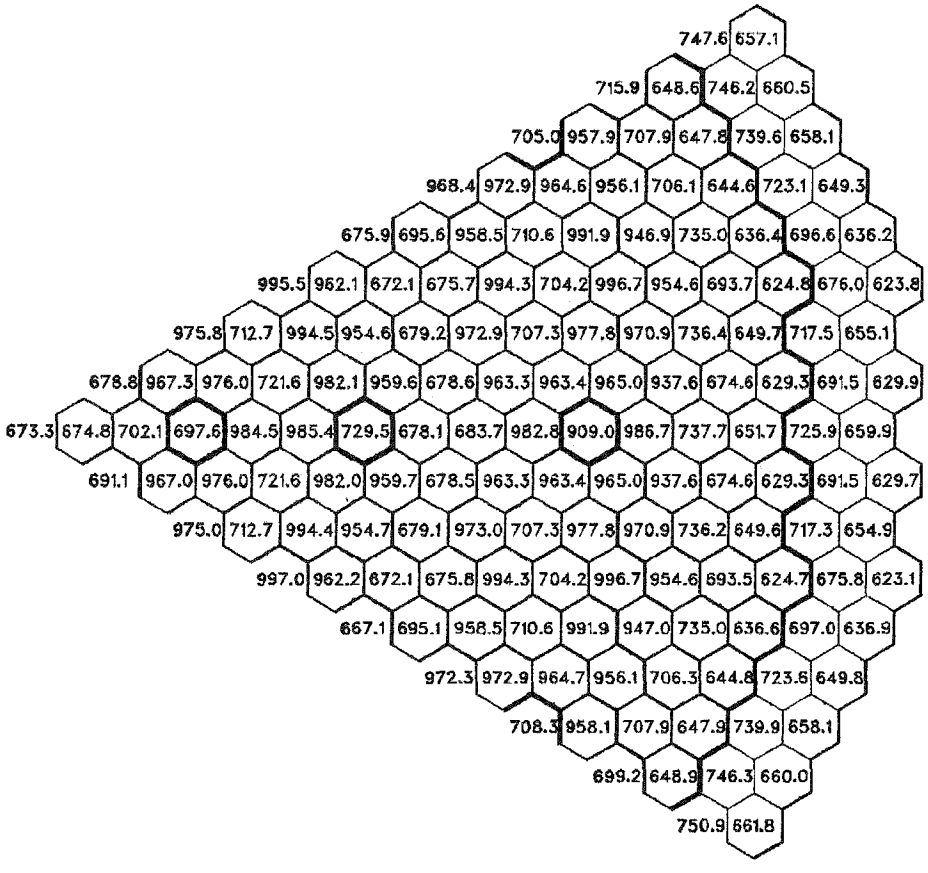

Figure 4.2.4.4.15. Average coolant temperatures (^{o}F) at BOL at the top of the upper axial blanket. (Orificing based on pin power and equal peak assembly coolant temperatures.)

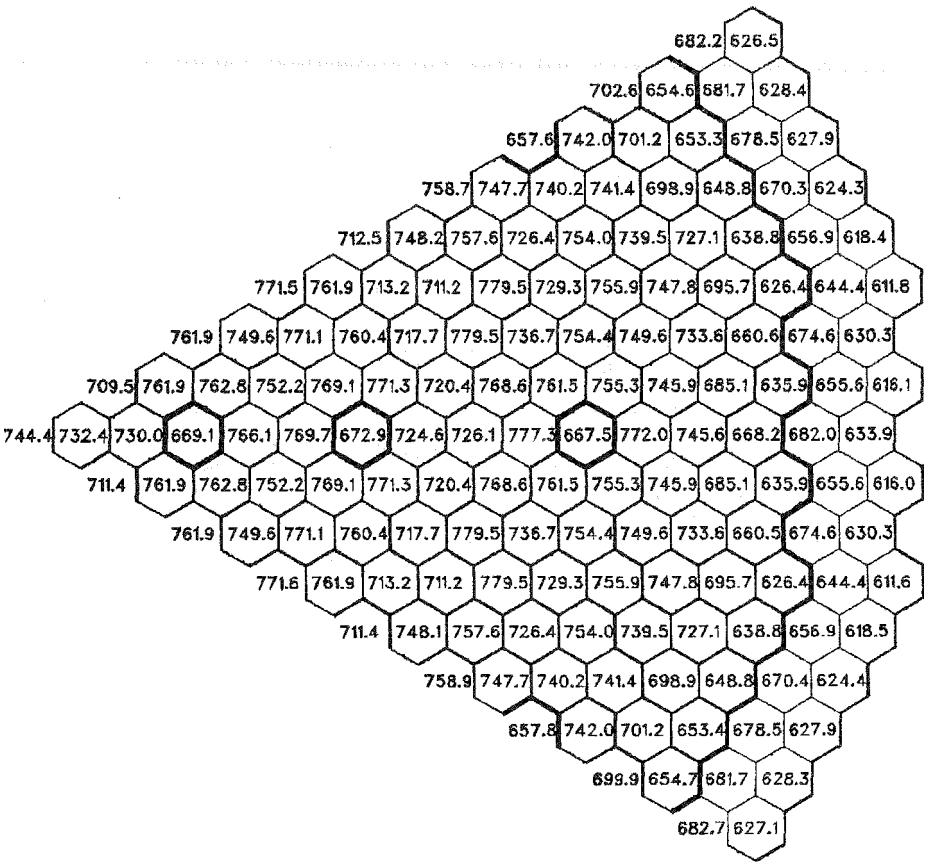

Figure 4.2.4.4.16. Average coolant temperatures (^{o}F) at EOEC at core midplane. (Orificing based on pin power and equal peak assembly coolant temperatures.)

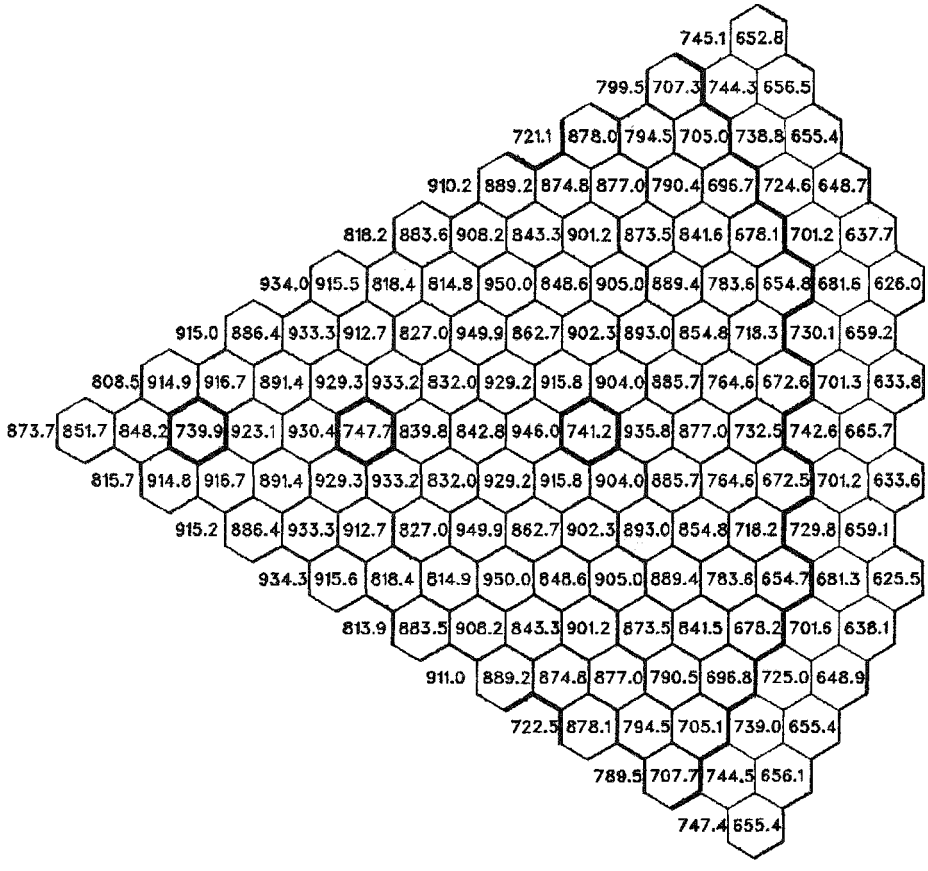

Figure 4.2.4.4.17. Average coolant temperatures (^{o}F) at EOEC at core-upper axial blanket interface. (Orificing based on pin power and equal peak assembly coolant temperatures.)

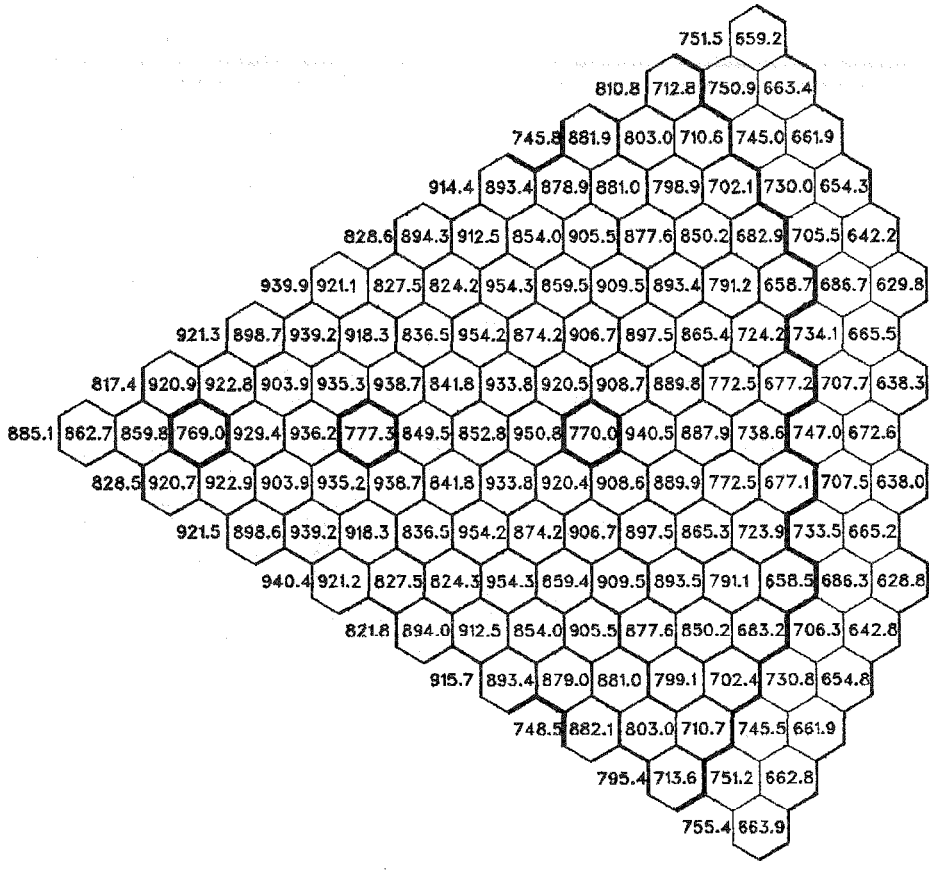

Figure 4.2.4.4.18. Average coolant temperatures (^{o}F) at EOEC at the top of the upper axial blanket. (Orificing based on pin power and equal peak assembly coolant temperatures.)

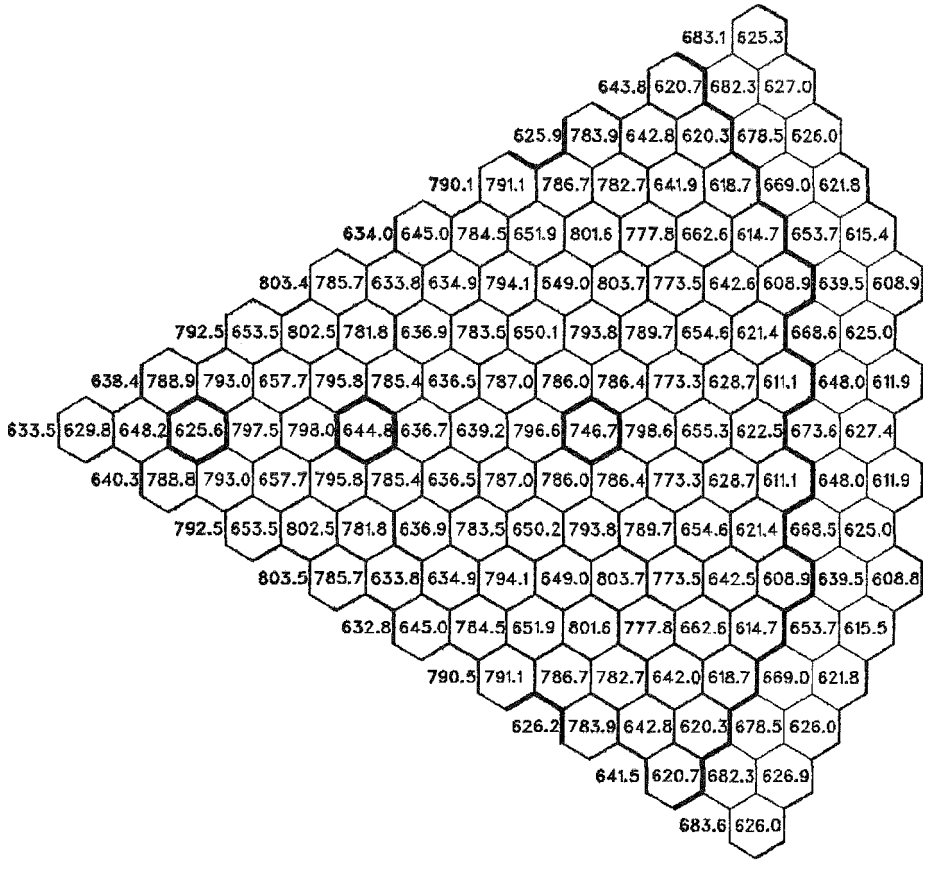

Figure 4.2.4.4.19. Average coolant temperatures (^{o}F) at BOL at core midplane. (Orificing based on pin power and equal peak cladding midwall temperatures.)

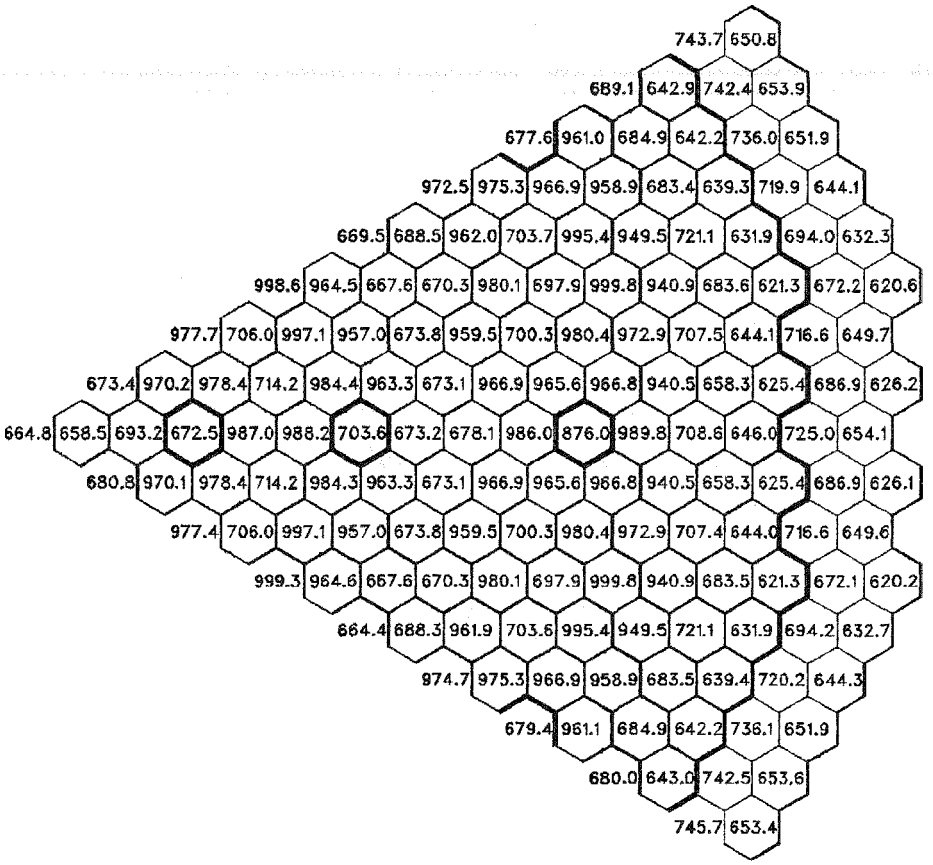

Figure 4.2.4.4.20. Average coolant temperatures (^{o}F) at BOL at core-upper axial blanket interface. (Orificing based on pin power and equal peak cladding midwall temperatures.)

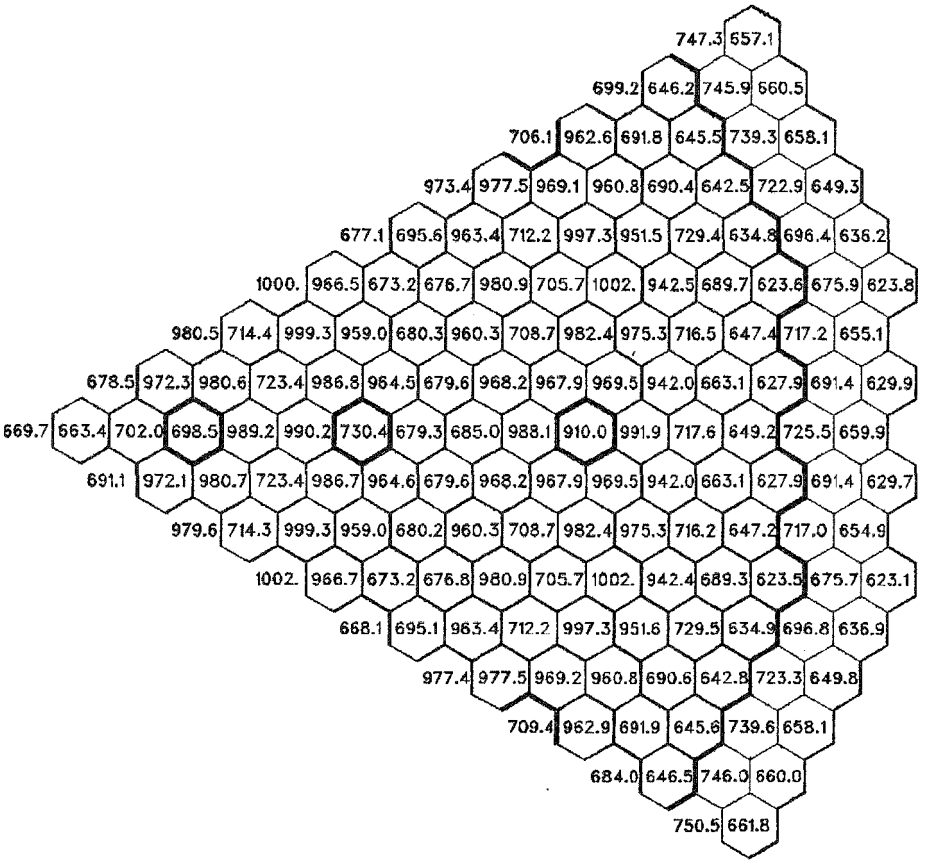

Figure 4.2.4.4.21. Average coolant temperatures (^{o}F) at BOL at the top of the upper axial blanket. (Orificing based on pin power and equal peak cladding midwall temperatures.)

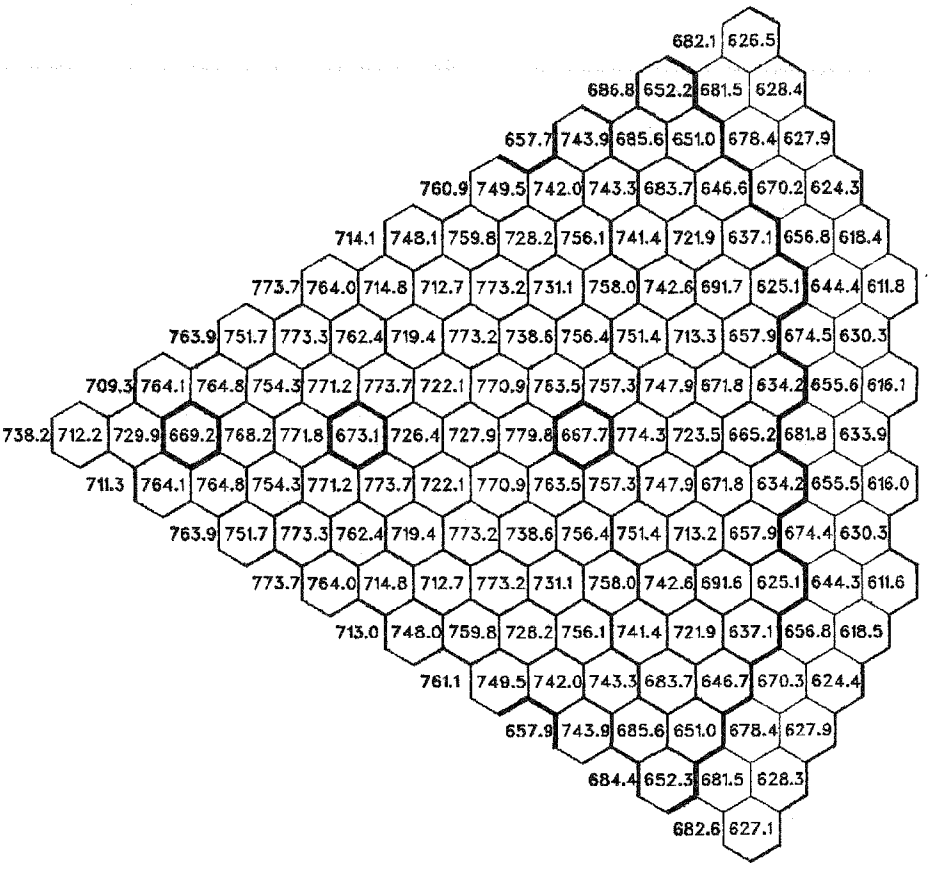

Figure 4.2.4.4.22. Average coolant temperatures (^{o}F) at EOEC at core midplane. (Orificing based on pin power and equal peak cladding midwall temperatures.)

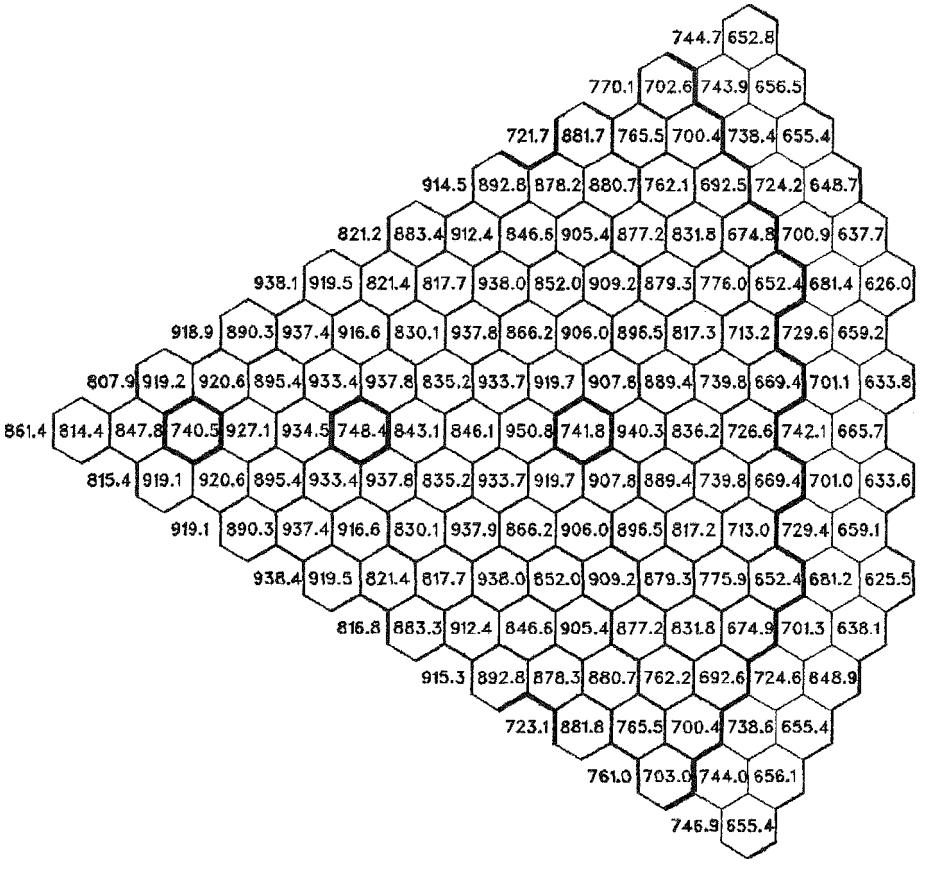

Figure 4.2.4.4.23. Average coolant temperatures (^{o}F) at EOEC at core-upper axial blanket interface. (Orificing based on pin power and equal peak cladding midwall temperatures.)

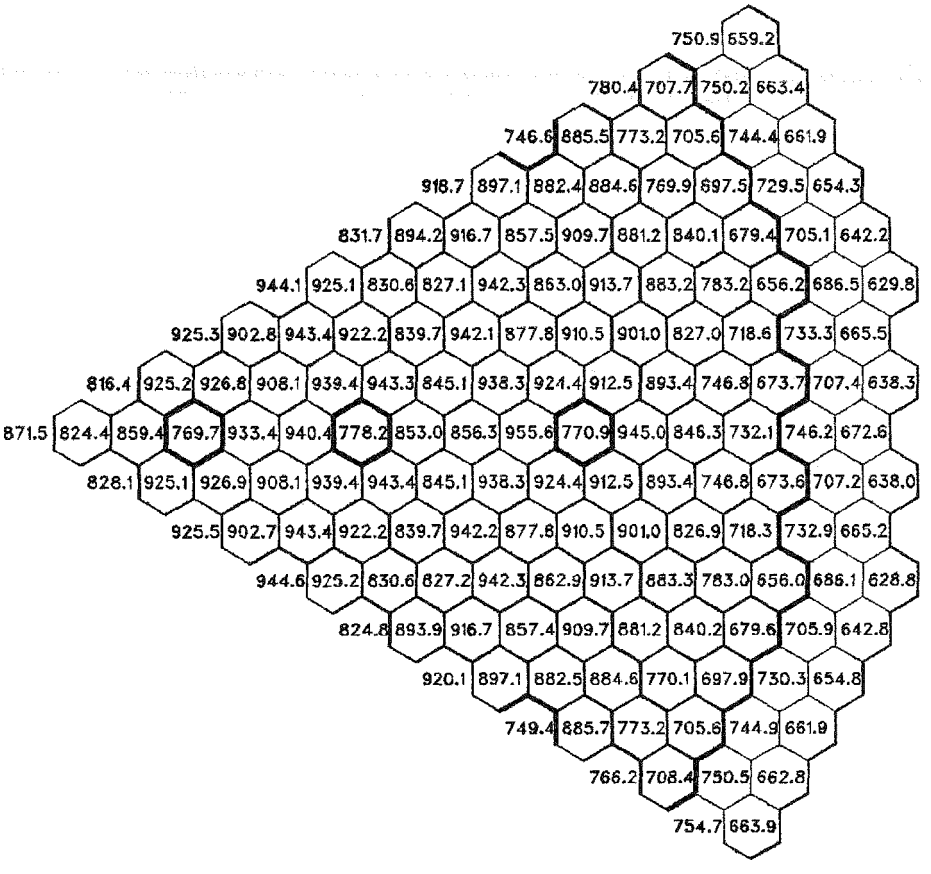

Figure 4.2.4.4.24. Average coolant temperatures (°F) at EOEC at the top of the upper axial blanket. (Orificing based on pin power and equal peak cladding midwall temperatures.)

Table 4.2.4.4.1

PEAK ASSEMBLY COOLANT TEMPERATURES (^{o}F)

Assembly Assignment to Orificing Zones Based on Assembly Power		Assembly Assignment to Orificing Zones Based on Pin Power	
Equal Peak Assembly Coolant Temperatures	Equal Peak Cladding Midwall Temperatures	Equal Peak Assembly Coolant Temperatures	Equal Peak Cladding Midwall Temperatures
990	1006	997	1002

Table 4.2.4.5.1

ASSEMBLY BUNDLE PRESSURE DROPS

(psi)

Orificing Zone	Assembly Assignment to Orificing Zones Based on Assembly Power		Assembly Assignment to Orificing Zones Based on Pin Power	
	Equal Peak Assembly Coolant Temperatures	Equal Peak Cladding Midwall Temperatures	Equal Peak Assembly Coolant Temperatures	Equal Peak Cladding Midwall Temperatures
1	53.2	48.6	51.5	49.7
2	43.7	43.7	43.2	41.5
3	35.9	40.1	34.6	36.4
4	53.0	51.0	51.4	52.0
5	32.2	34.4	28.1	29.0
6	16.5	20.1	9.5	13.2
7	5.3	6.8	5.1	5.7

transfer but at its present state does not calculate individual duct wall temperatures. Instead, average temperatures for the duct walls, that face each other, of adjacent assemblies, are calculated. This may overestimate or underestimate duct wall temperatures and duct wall temperature differences. For example, at BOL: if a core fuel assembly is located between a blanket assembly and another core fuel assembly, the temperature of the wall facing the blanket assembly will be underestimated (the blanket assembly has a low power at BOL) and the temperature of the wall facing the other core assembly will be overestimated (if the other core assembly is hotter). As a consequence, the temperature difference between these walls will be overestimated too.

Assembly duct wall temperatures for the four orificing strategies discussed in Section 4.2.2.1 at BOL and EOEC conditions and at three elevations, i.e., core midplane, core-upper axial blanket interface and at the top of the upper axial blanket are presented in Figures 4.2.5.1 to 4.2.5.24. The corresponding maximum duct wall temperature differences at the top of the upper axial blanket are presented in Figures 4.2.5.25 to 4.2.5.32. It must be pointed out that since the power produced in the control and reflector assemblies is very small, coolant and duct wall temperatures can be easily changed by small changes in the flow assigned to these assemblies. Since a detailed design for these assemblies has not been developed in this work, and since detailed γ-transport calculations have not been performed, the flow and consequently, the coolant and duct wall temperatures, and the duct wall temperature differences in these assemblies have not been optimized.

Maximum duct wall temperatures and duct wall temperature differences per reactor region are presented in Table 4.2.5.1. There is a small variation in these maximum values as the orificing strategy varies. The largest of these maximum duct wall temperatures is 923.1^{o}F in the core, 847.6^{o}F in the internal blankets, and 833.1^{o}F in the radial blanket. Similarly, the largest of these maximum duct wall temperature differences is 161.3^{o}F in the core, 133.8^{o}F in the internal blankets, and 151.6^{o}F in the radial blanket.

4.3 FUEL LIFE ANALYSIS

4.3.1 Introduction

The fuel element performance of the reference fuel pin (0.28 in. o.d. pin with a 14 mil cladding thickness and a 30 inches plenum) has been determined as part of

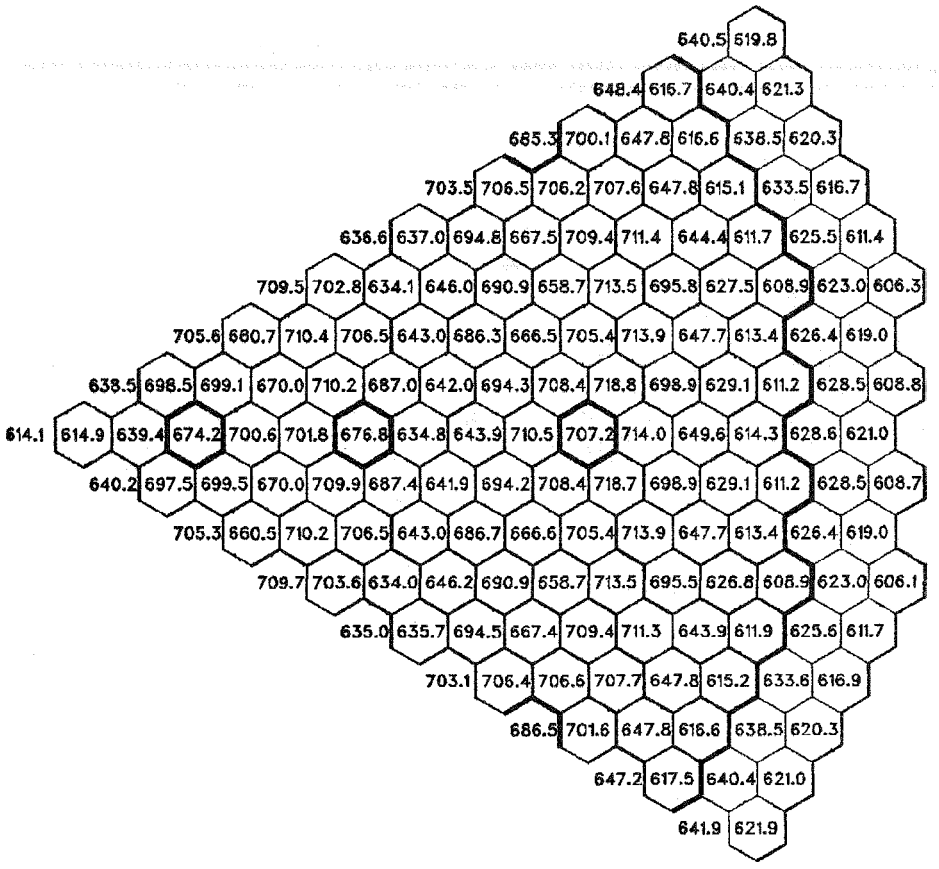

Figure 4.2.5.1. Assembly average duct wall temperatures (^{o}F) at BOL at core midplane. (Orificing based on assembly power and equal peak assembly coolant temperatures).

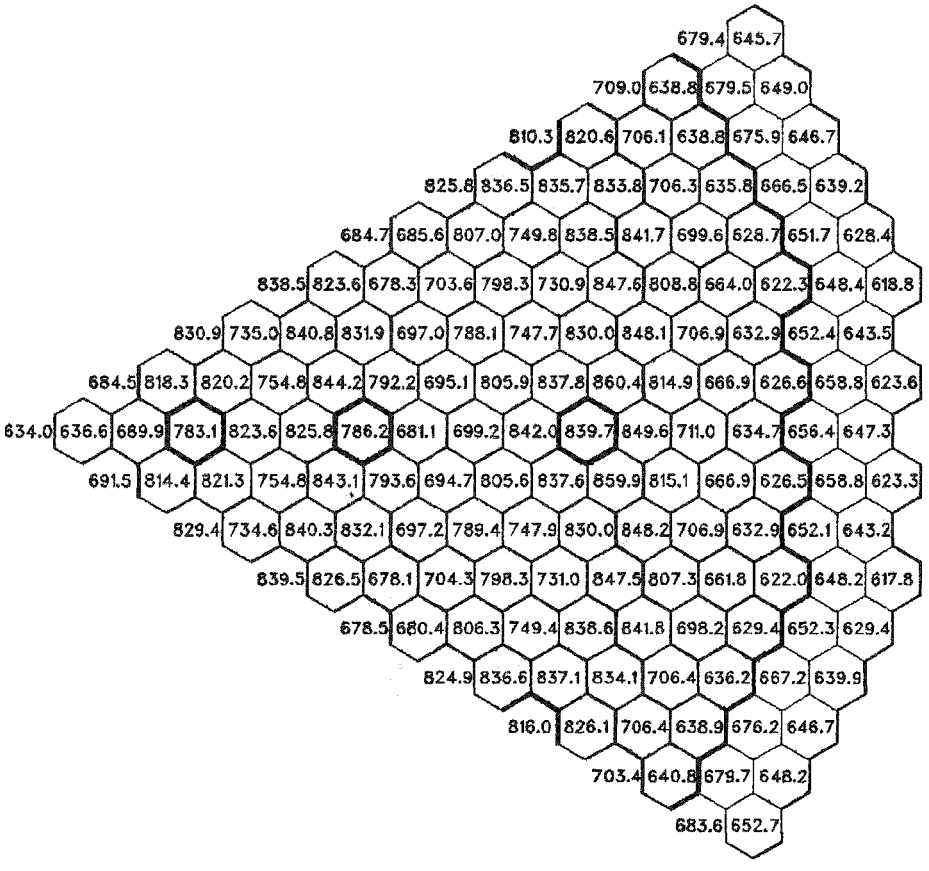

Figure 4.2.5.2. Assembly average duct wall temperatures (^{o}F) at BOL at the core-upper axial blanket interface. (Orificing based on assembly power and equal peak assembly coolant temperatures).

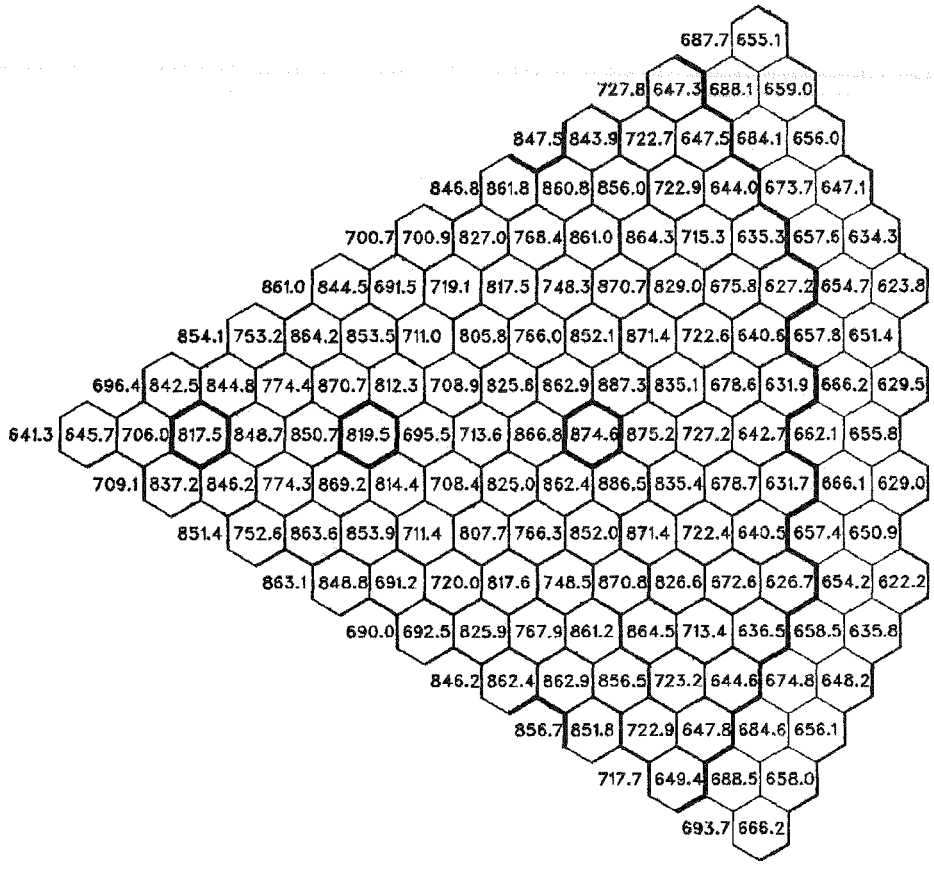

Figure 4.2.5.3. Assembly average duct wall temperatures (^{o}F) at BOL at the top of the upper axial blanket. (Orificing based on assembly power and equal peak assembly coolant temperatures).

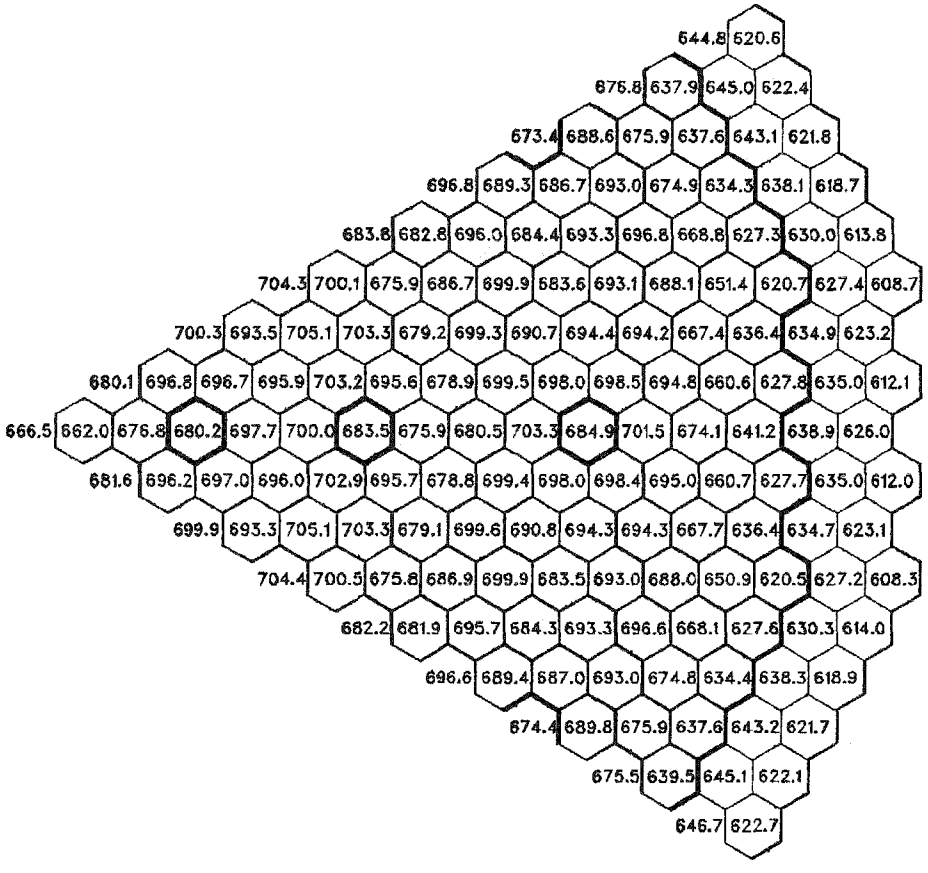

Figure 4.2.5.4. Assembly average duct wall temperatures (^{o}F) at EOEC at core midplane. (Orificing based on assembly power and equal peak assembly coolant temperatures).

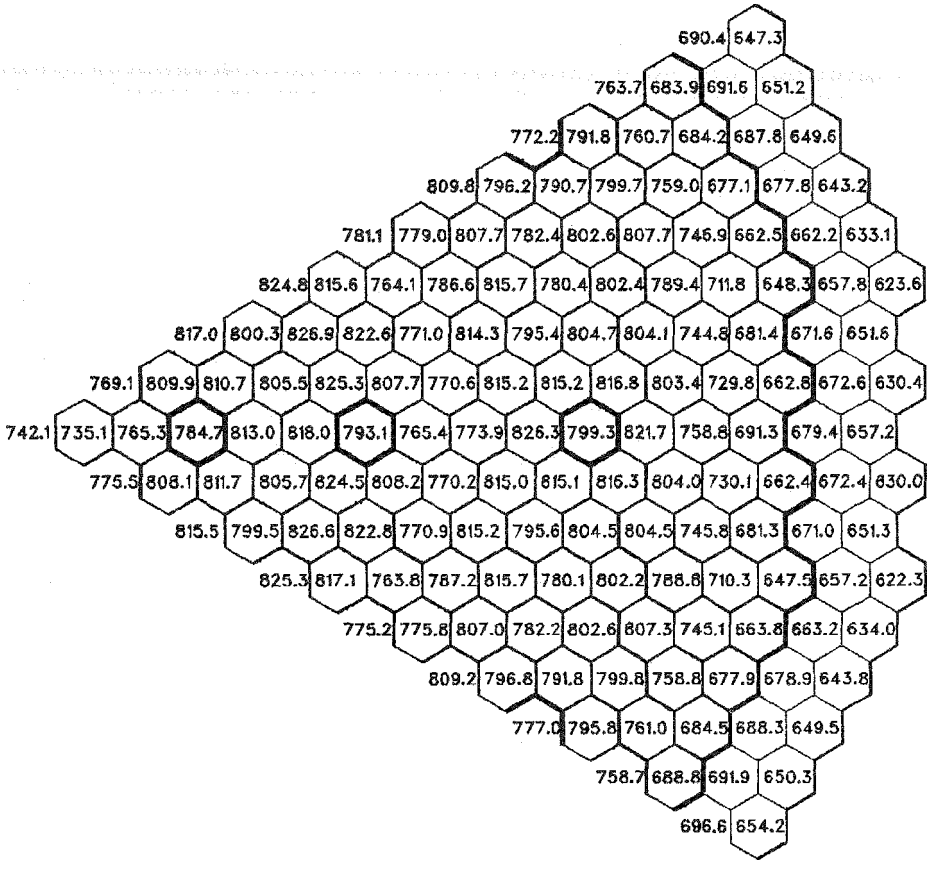

Figure 4.2.5.5. Assembly average duct wall temperatures (^{o}F) at EOEC at core-upper axial blanket interface. (Orificing based on assembly power and equal peak assembly coolant temperatures).

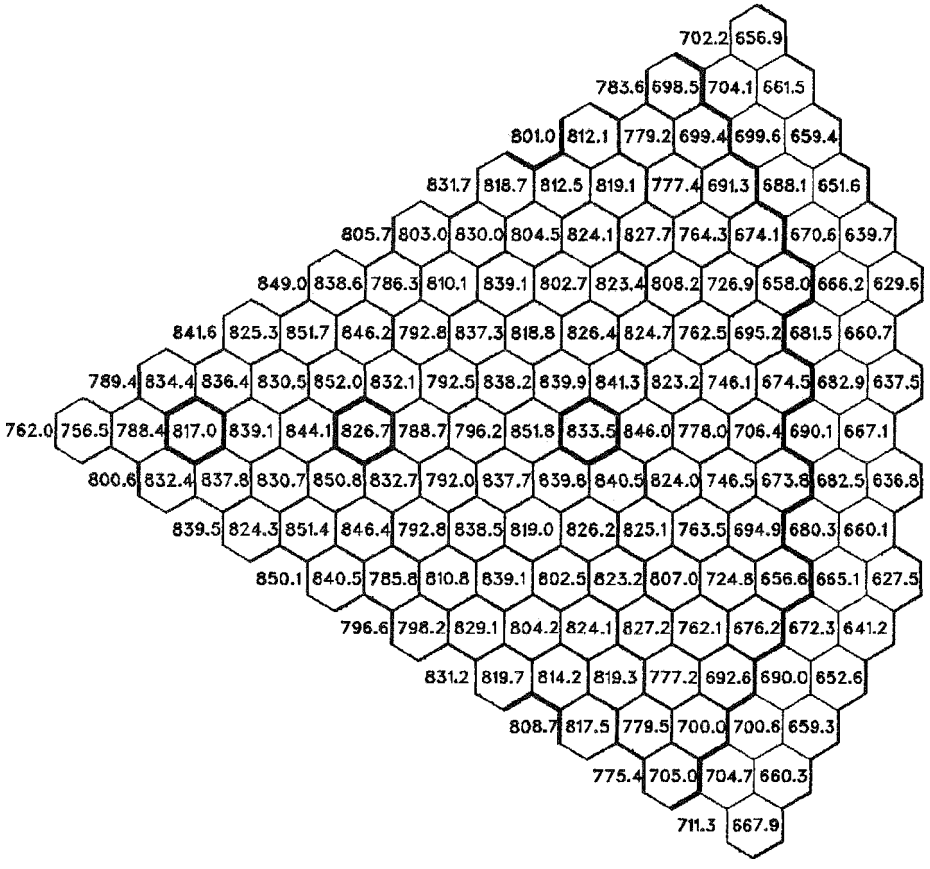

Figure 4.2.5.6. Assembly average duct wall temperatures (^{o}F) at EOEC at the top of the upper axial blanket. (Orificing based on assembly power and equal peak assembly coolant temperatures).

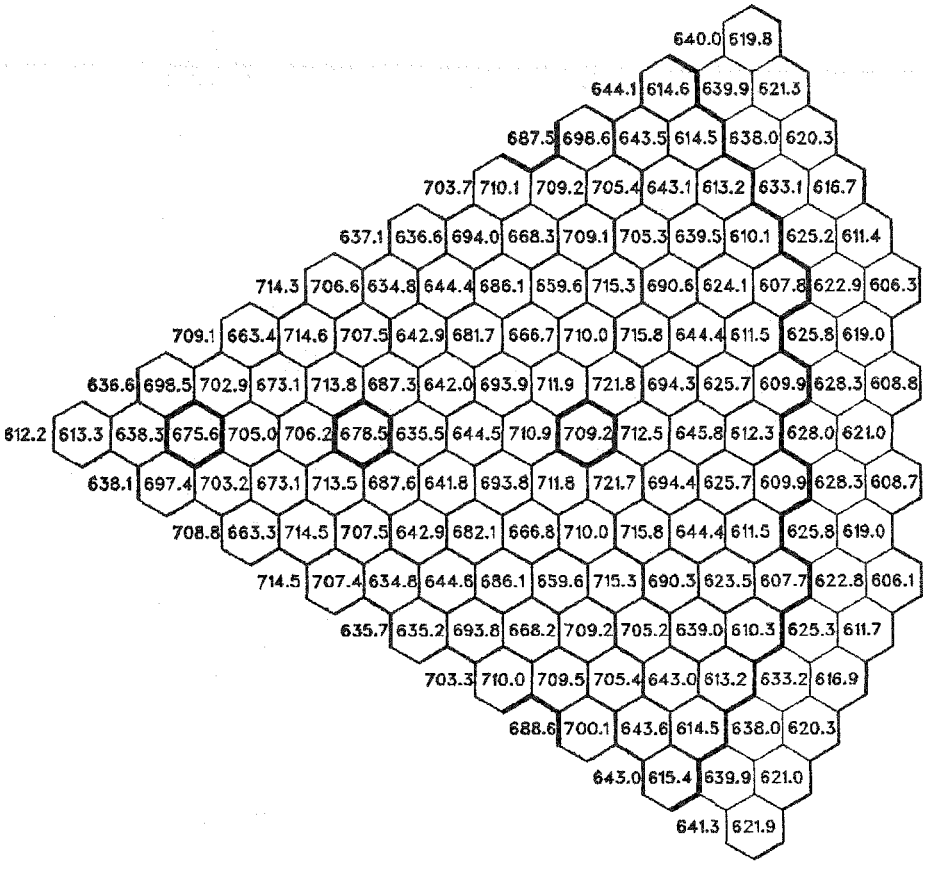

Figure 4.2.5.7. Assembly average duct wall temperatures (^{o}F) at BOL at core midplane. (Orificing based on assembly power and equal peak cladding midwall temperatures).

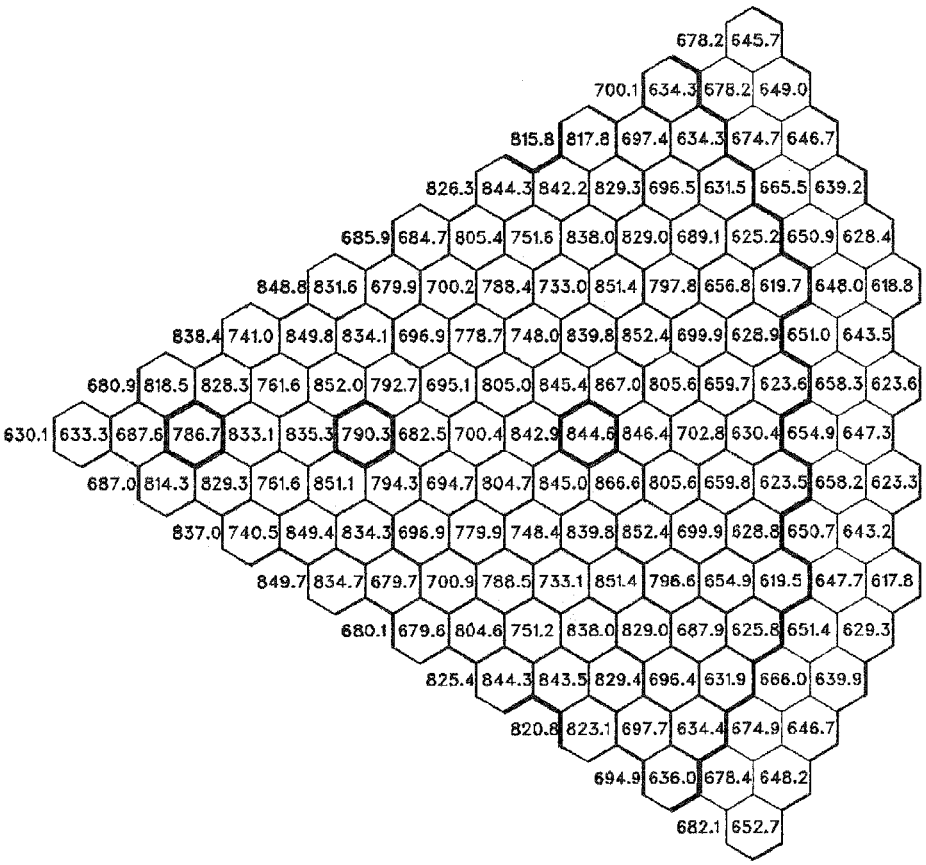

Figure 4.2.5.8. Assembly average duct wall temperatures (^{o}F) at BOL at core-upper axial blanket interface. (Orificing based on assembly power and equal peak cladding midwall temperatures).

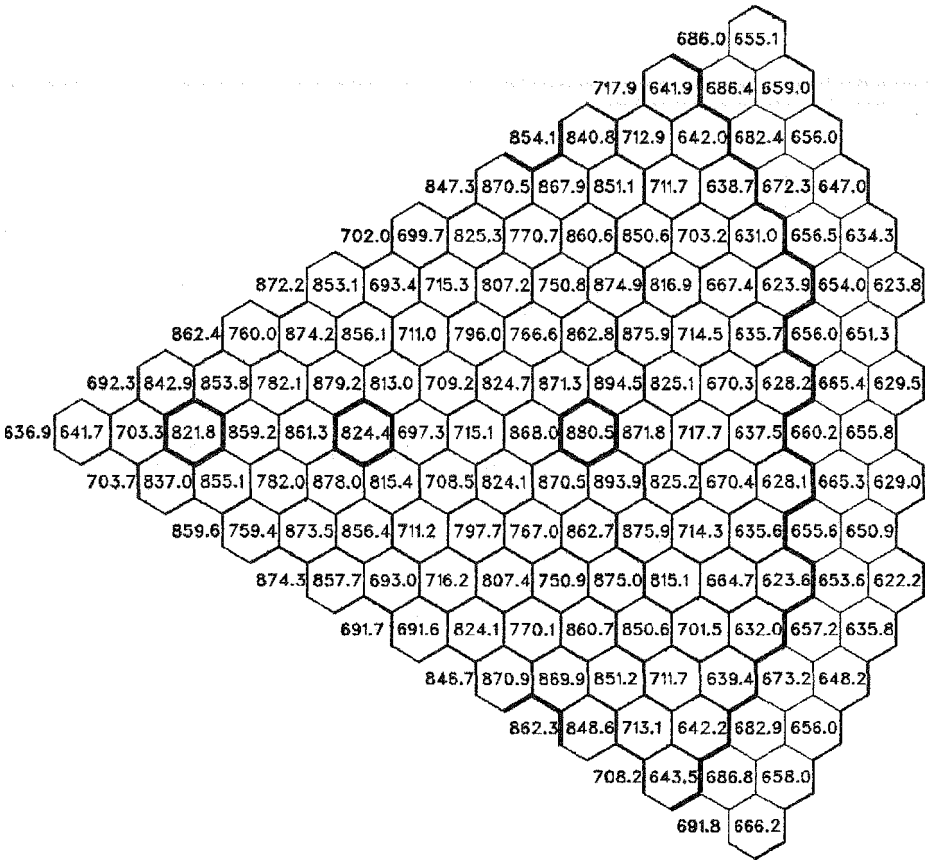

Figure 4.2.5.9. Assembly average duct wall temperatures (^{o}F) at BOL at the top of the upper axial blanket. (Orificing based on assembly power and equal peak cladding midwall temperatures).

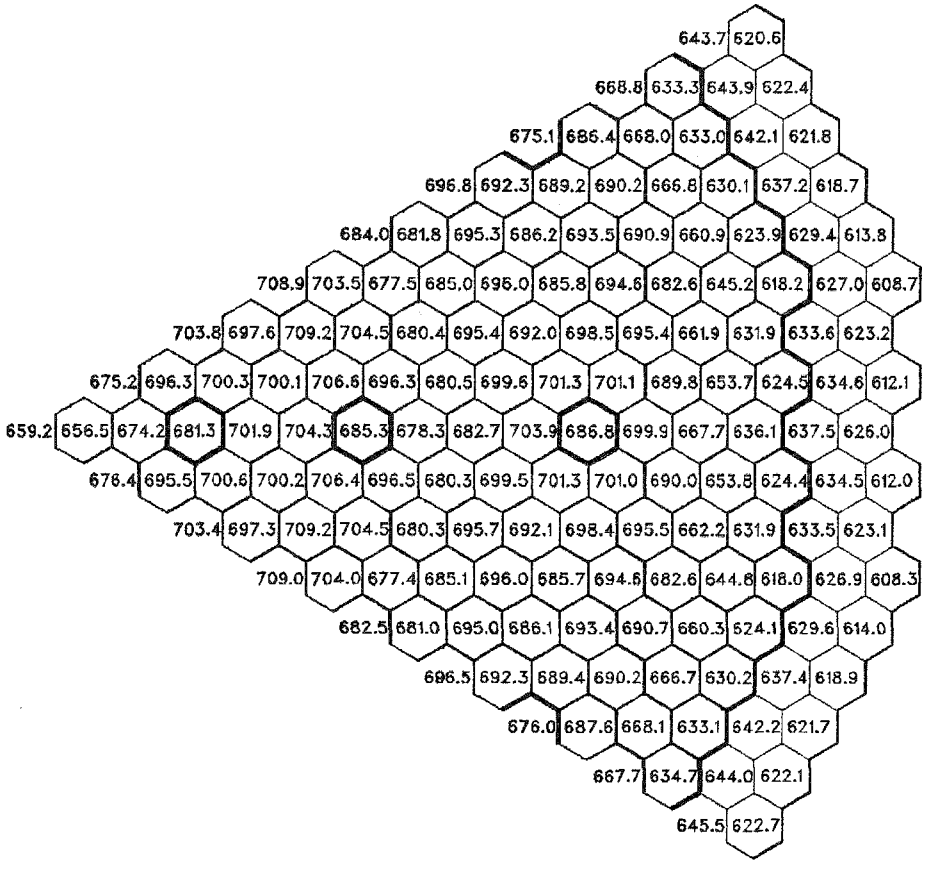

Figure 4.2.5.10. Assembly average duct wall temperatures (^{o}F) at EOEC at core midplane. (Orificing based on assembly power and equal peak cladding midwall temperatures).

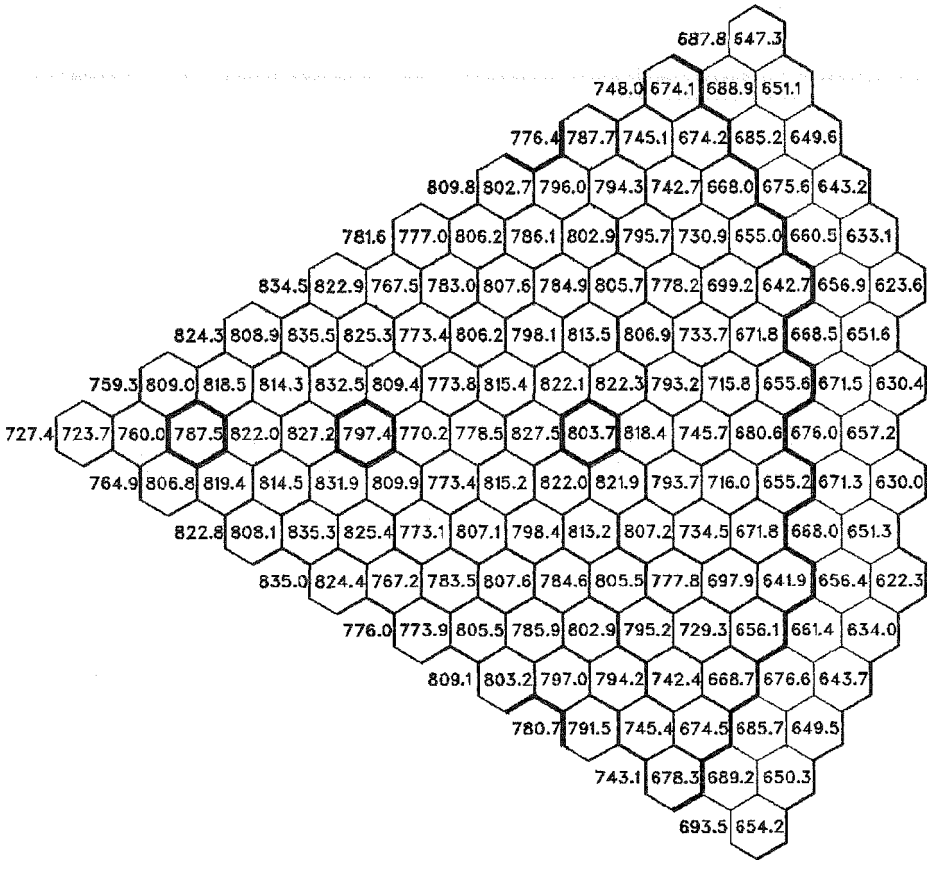

Figure 4.2.5.11. Assembly average duct wall temperatures (^{o}F) at EOEC at core-upper axial blanket interface. (Orificing based on assembly power and equal peak cladding midwall temperatures).

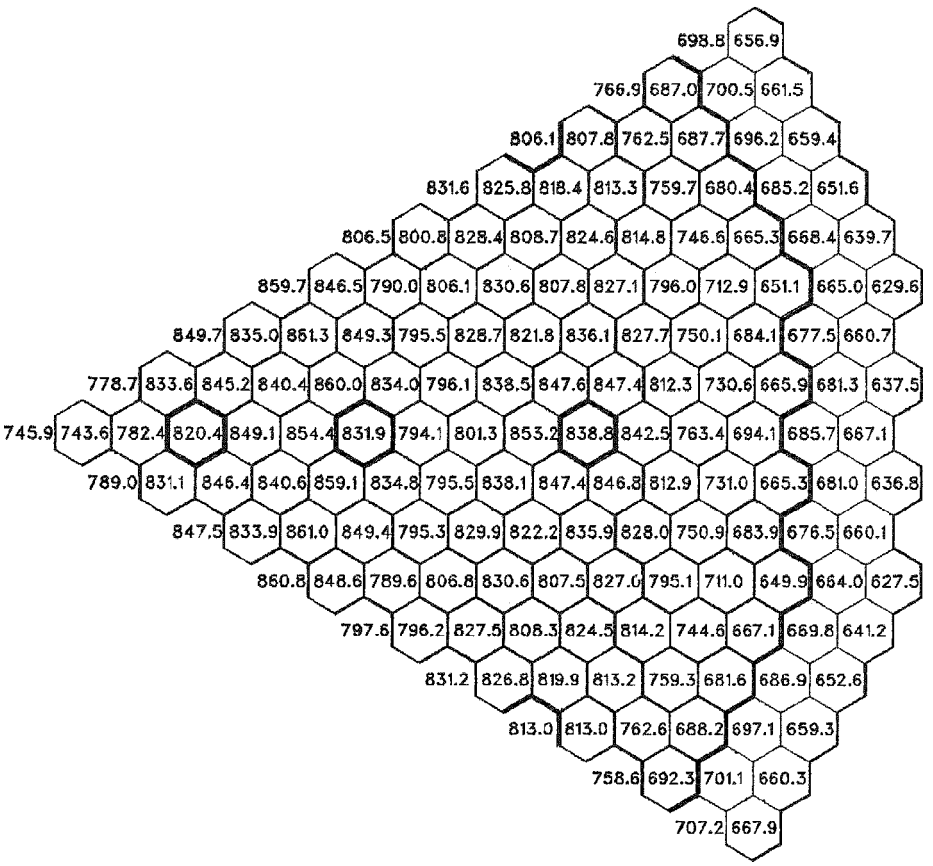

Figure 4.2.5.12. Assembly average duct wall temperatures (^{o}F) at EOEC at the top of the upper axial blanket. (Orificing based on assembly power and equal peak cladding midwall temperatures).

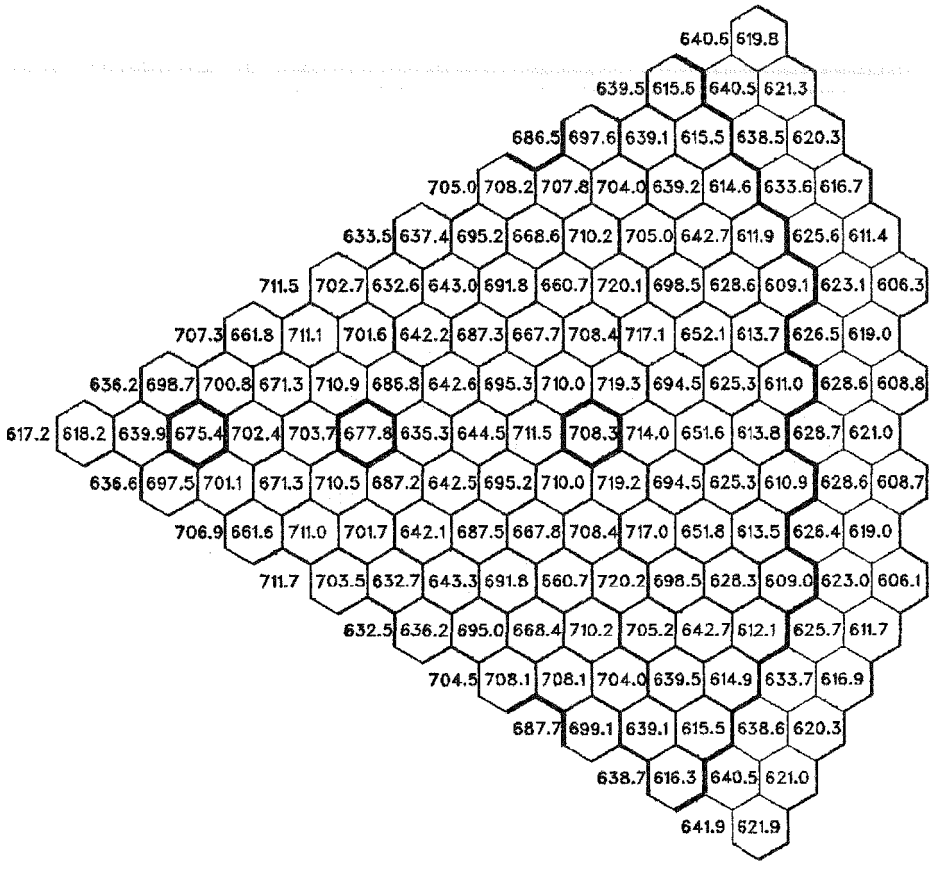

Figure 4.2.5.13. Assembly average duct wall temperatures (^{O}F) at BOL at core midplane. (Orificing based on pin power and equal peak assembly coolant temperatures).

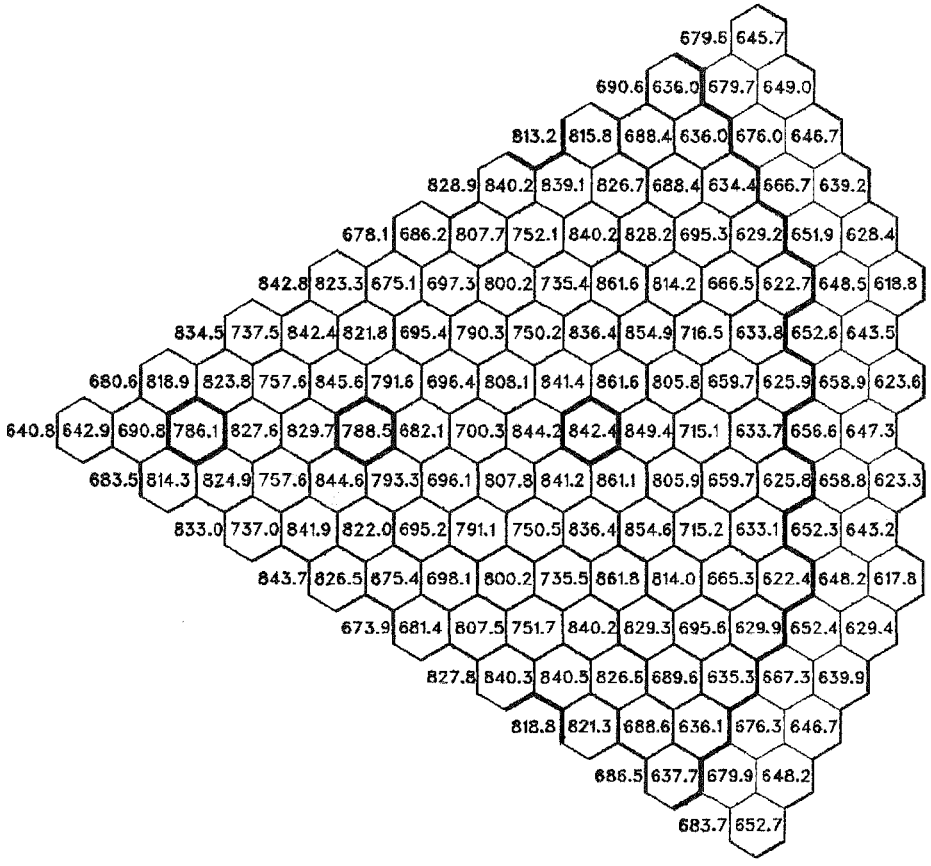

Figure 4.2.5.14. Assembly average duct wall temperatures (^{o}F) at BOL at core-upper axial blanket interface. (Orificing based on pin power and equal peak assembly coolant temperatures).

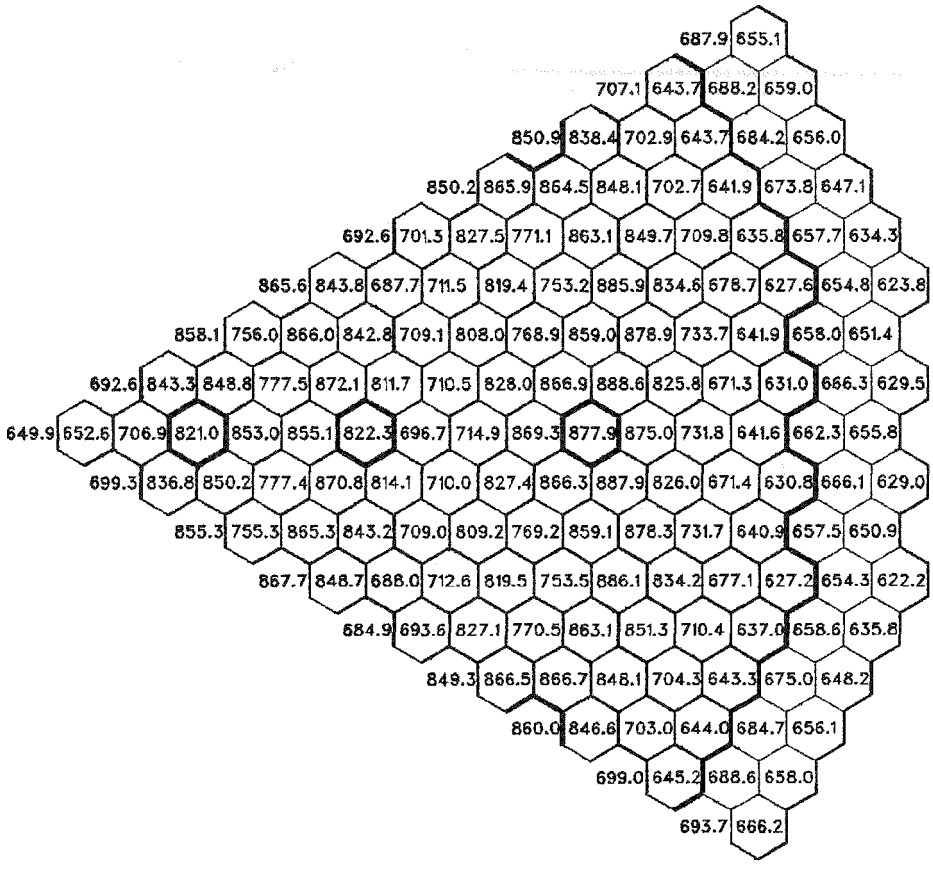

Figure 4.2.5.15. Assembly average duct wall temperatures (^{O}F) at BOL at the top of the upper axial blanket. (Orificing based on pin power and equal peak assembly coolant temperatures).

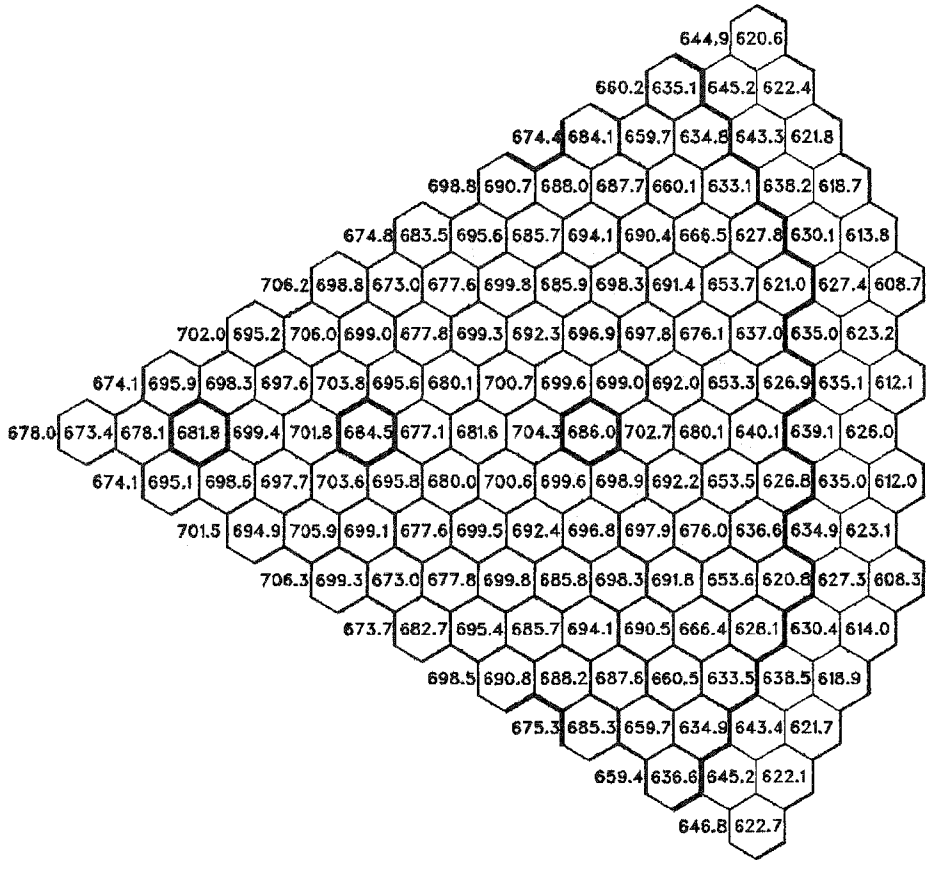

Figure 4.2.5.16. Assembly average duct wall temperatures (^{o}F) at EOEC at core midplane. (Orificing based on pin power and equal peak assembly coolant temperatures).

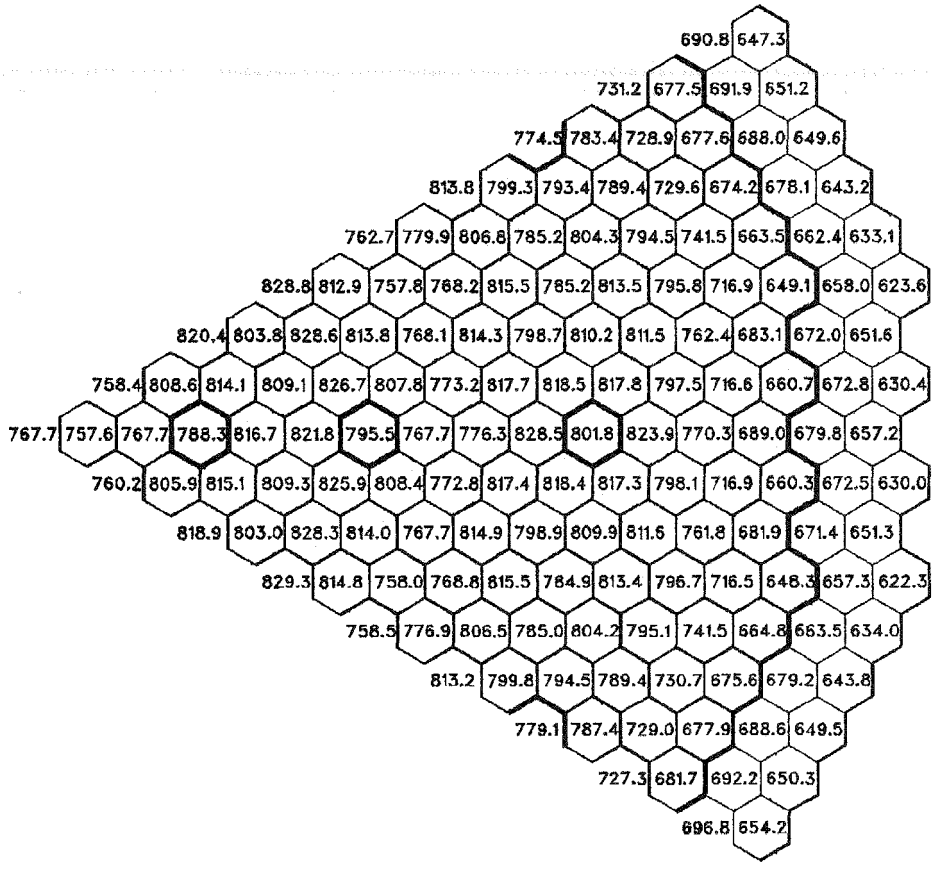

Figure 4.2.5.17. Assembly average duct wall temperatures (^{o}F) at EOEC at core-upper axial blanket interface. (Orificing based on pin power and equal peak assembly coolant temperatures).

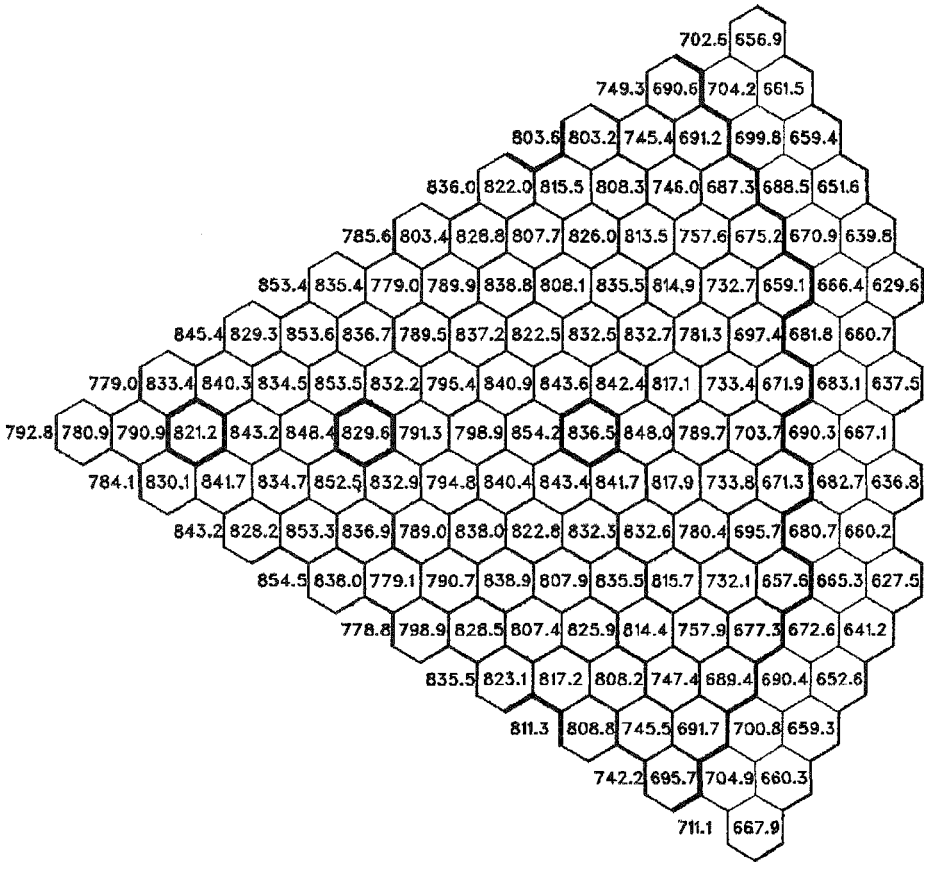

Figure 4.2.5.18. Assembly average duct wall temperatures (^{o}F) at EOEC at the top of the upper axial blanket. (Orificing based on pin power and equal peak assembly coolant temperatures).

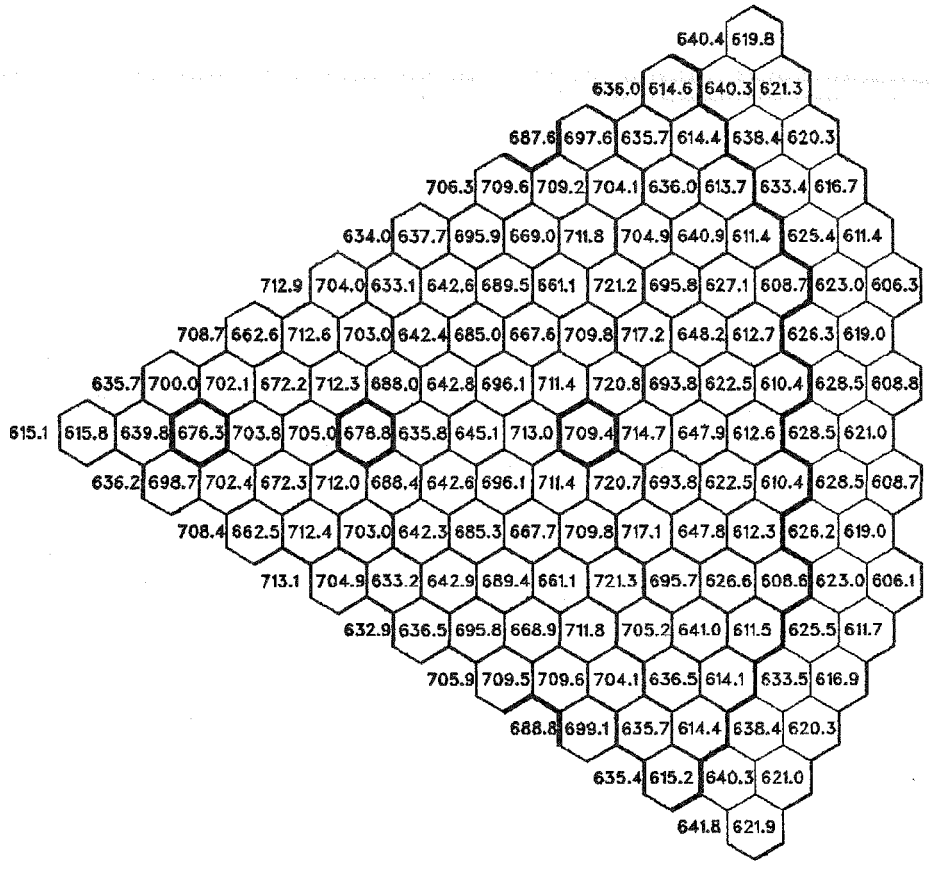

Figure 4.2.5.19. Assembly average duct wall temperatures (^{o}F) at BOL at the core midplane. (Orificing based on pin power and equal peak cladding midwall temperatures).

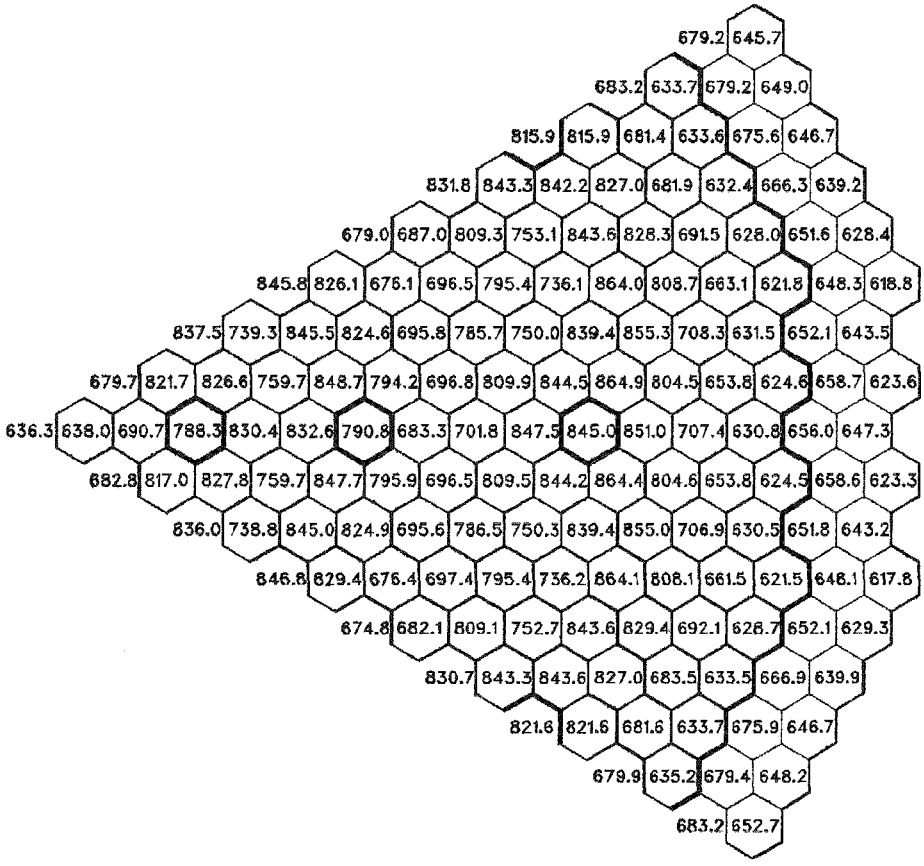

Figure 4.2.5.20. Assembly average duct wall temperatures (^{o}F) at BOL at core-upper axial blanket interface. (Orificing based on pin power and equal peak cladding midwall temperatures).

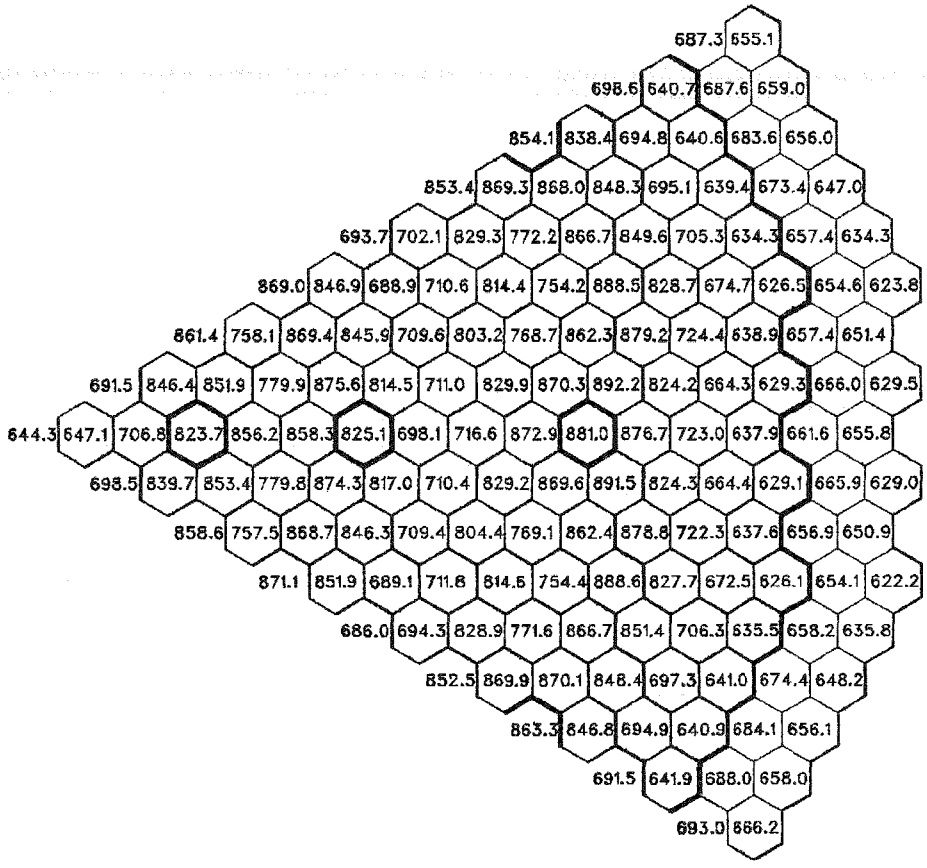

Figure 4.2.5.21. Assembly average duct wall temperatures (^{o}F) at BOL at the top of the upper axial blanket. (Orificing based on pin power and equal peak cladding midwall temperatures).

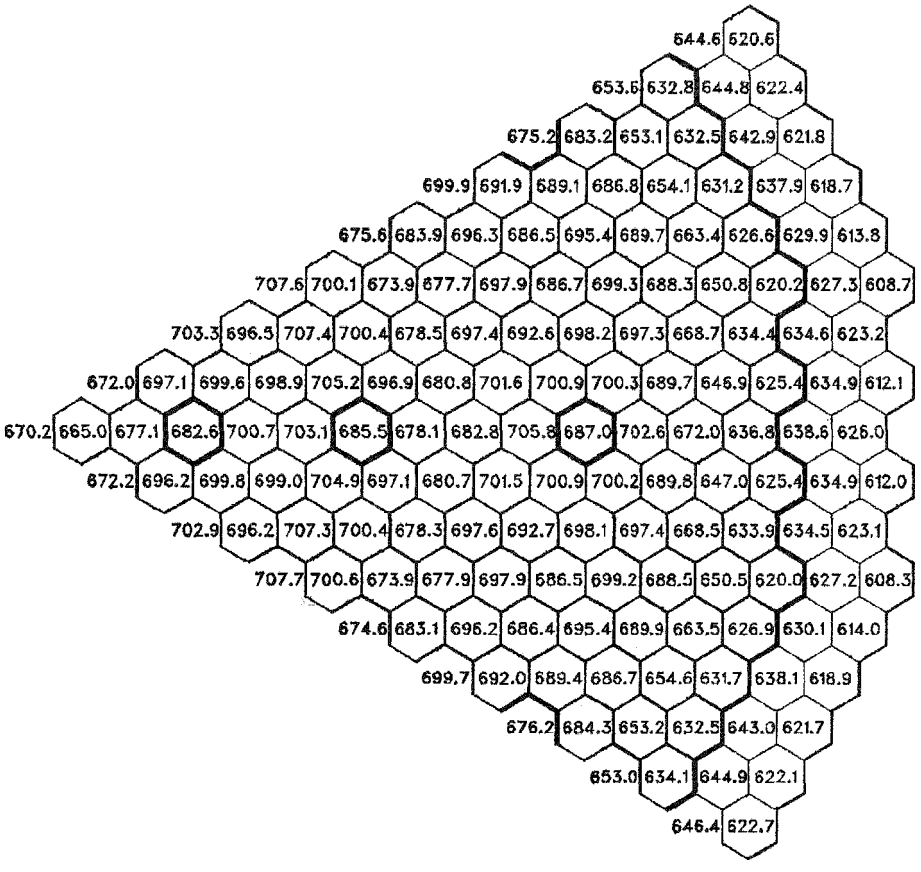

Figure 4.2.5.22. Assembly average duct wall temperatures (^{o}F) at EOEC at core midplane. (Orificing based on pin power and equal peak cladding midwall temperatures).

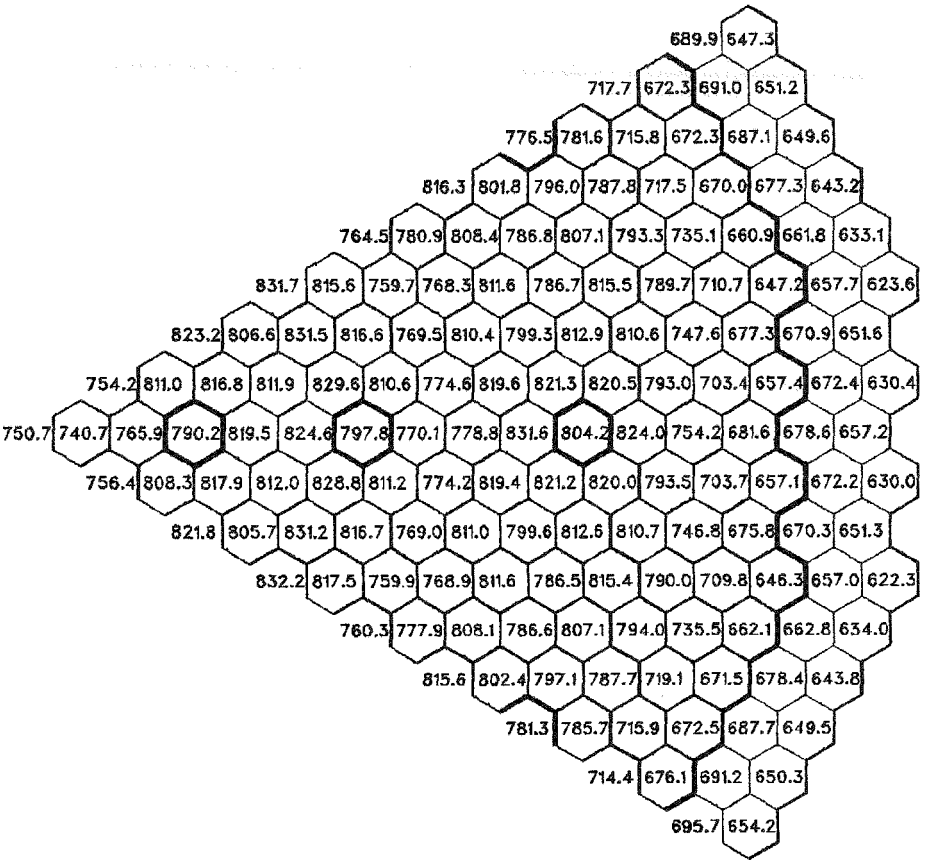

Figure 4.2.5.23. Assembly average duct wall temperatures (^{o}F) at EOEC at core-upper axial blanket interface. (Orificing based on pin power and equal peak cladding midwall temperatures).

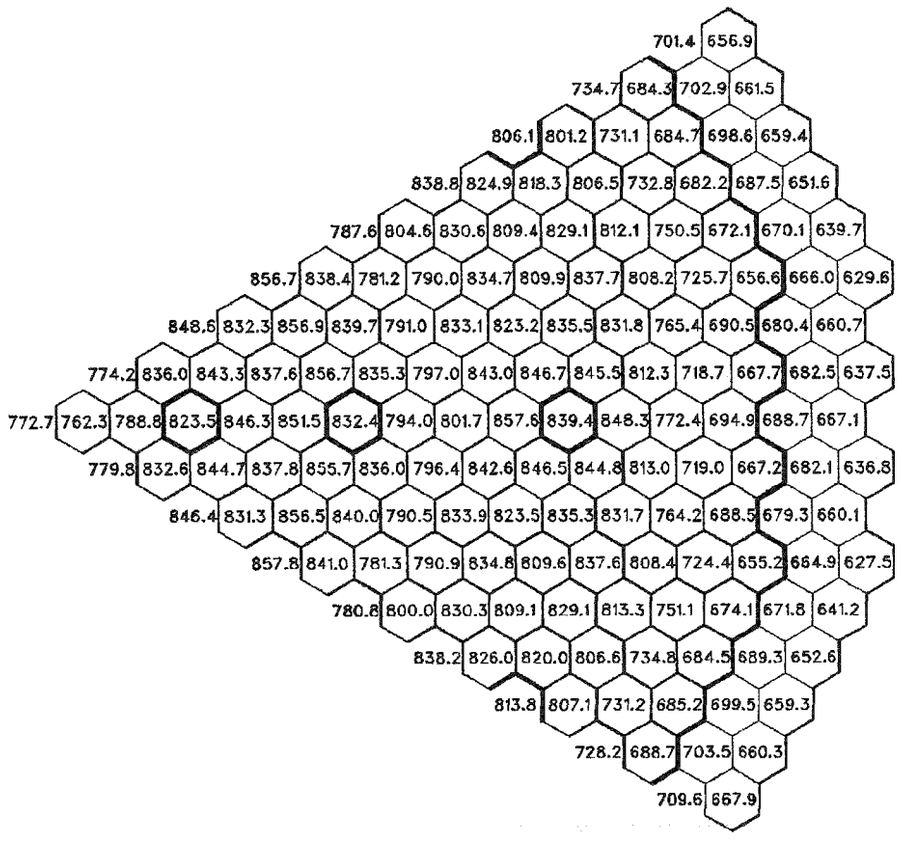

Figure 4.2.5.24. Assembly average duct wall temperatures (^{O}F) at EOEC at the top of the upper axial blanket. (Orificing based on pin power and equal peak cladding midwall temperatures).

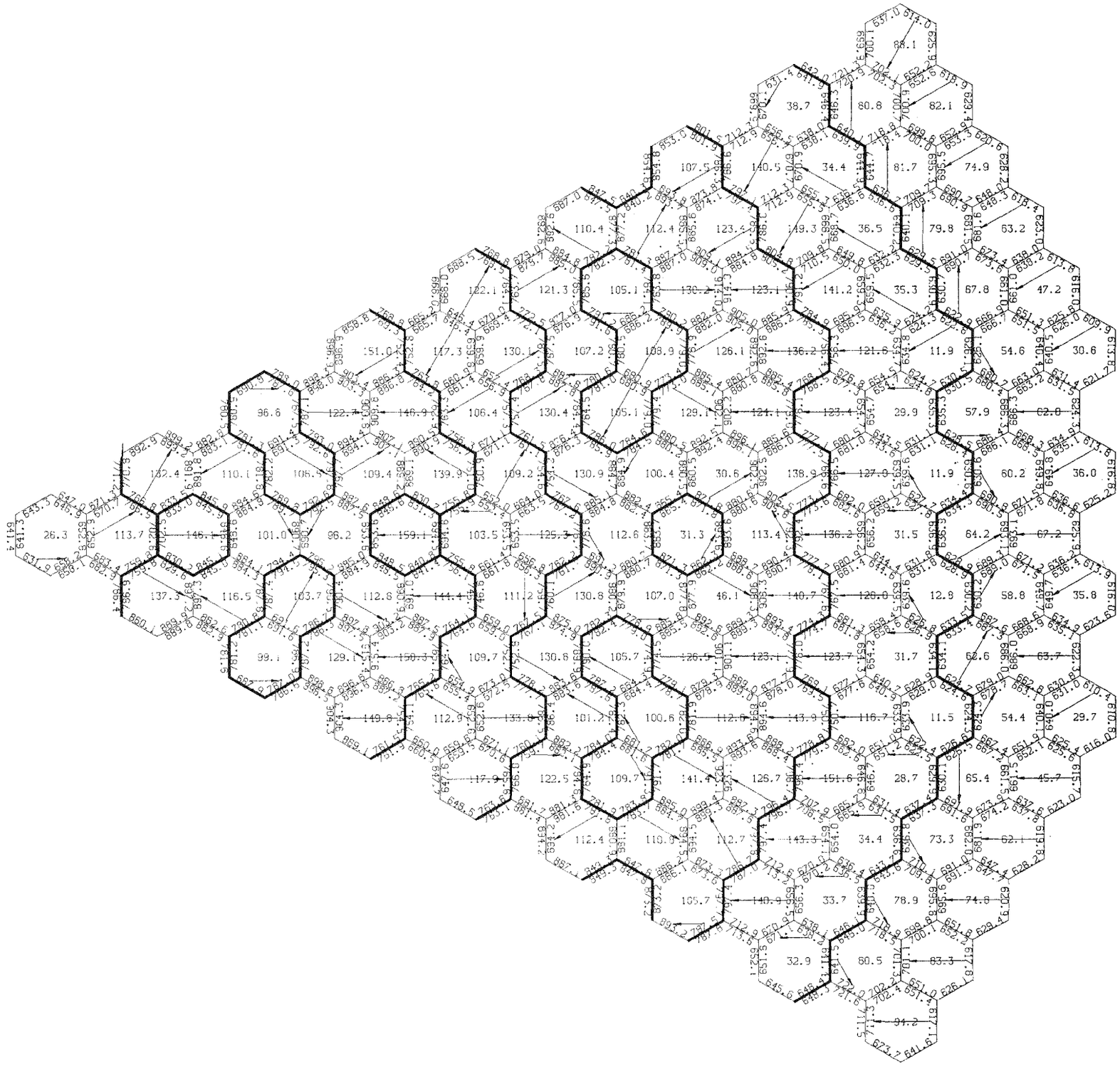

Figure 4.2.5.25. Average duct wall temperatures (^{o}F) and maximum duct wall temperature differences (^{o}F) at BOL at the top of the upper axial blanket. (Orificing based on assembly power and equal peak assembly coolant temperatures.)

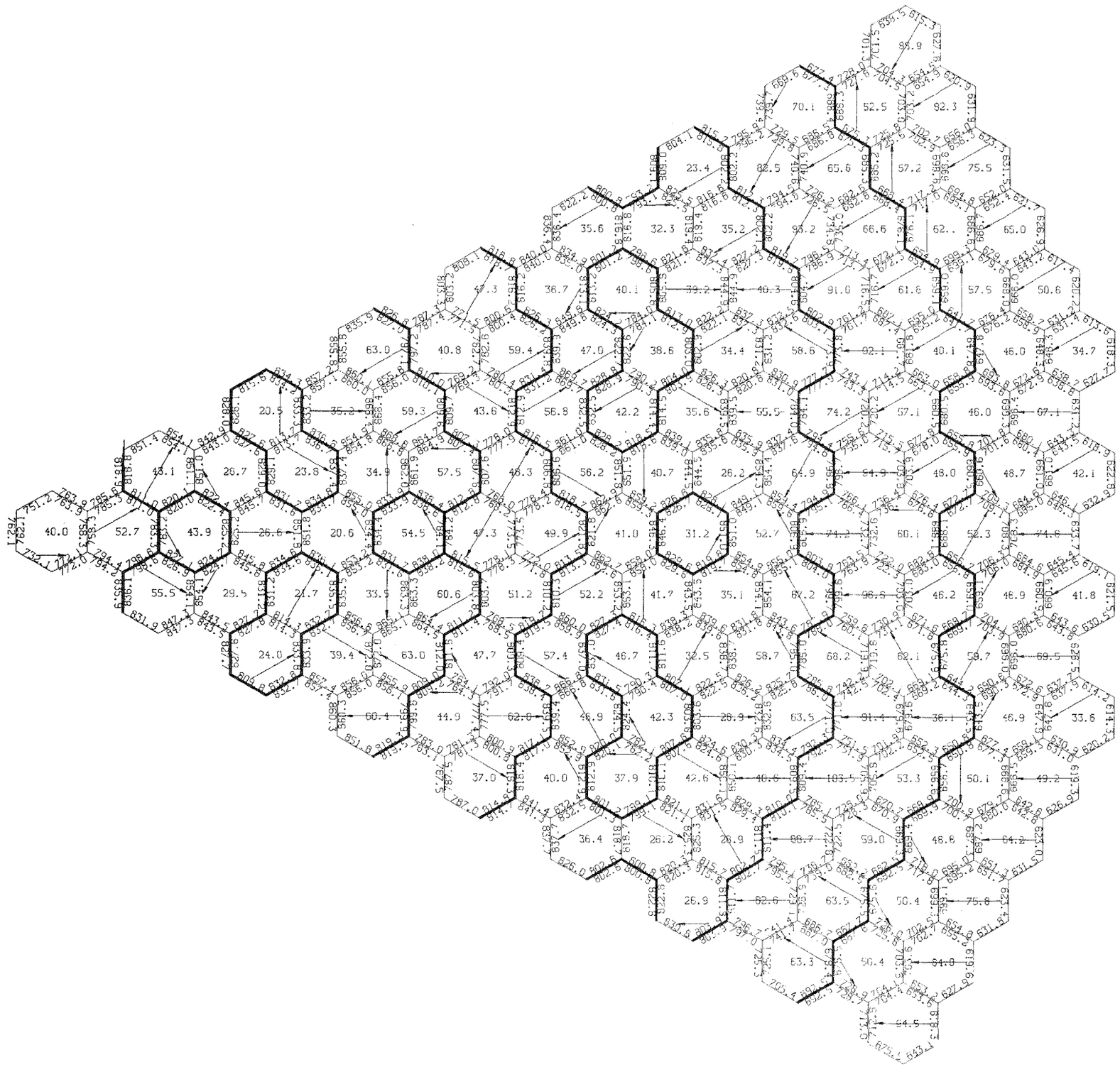

Figure 4.2.5.26. Average duct wall temperatures (^{O}F) and maximum duct wall temperature differences (^{O}F) at EOEC at the top of the upper axial blanket. (Orificing based on assembly power and equal peak assembly coolant temperatures.)

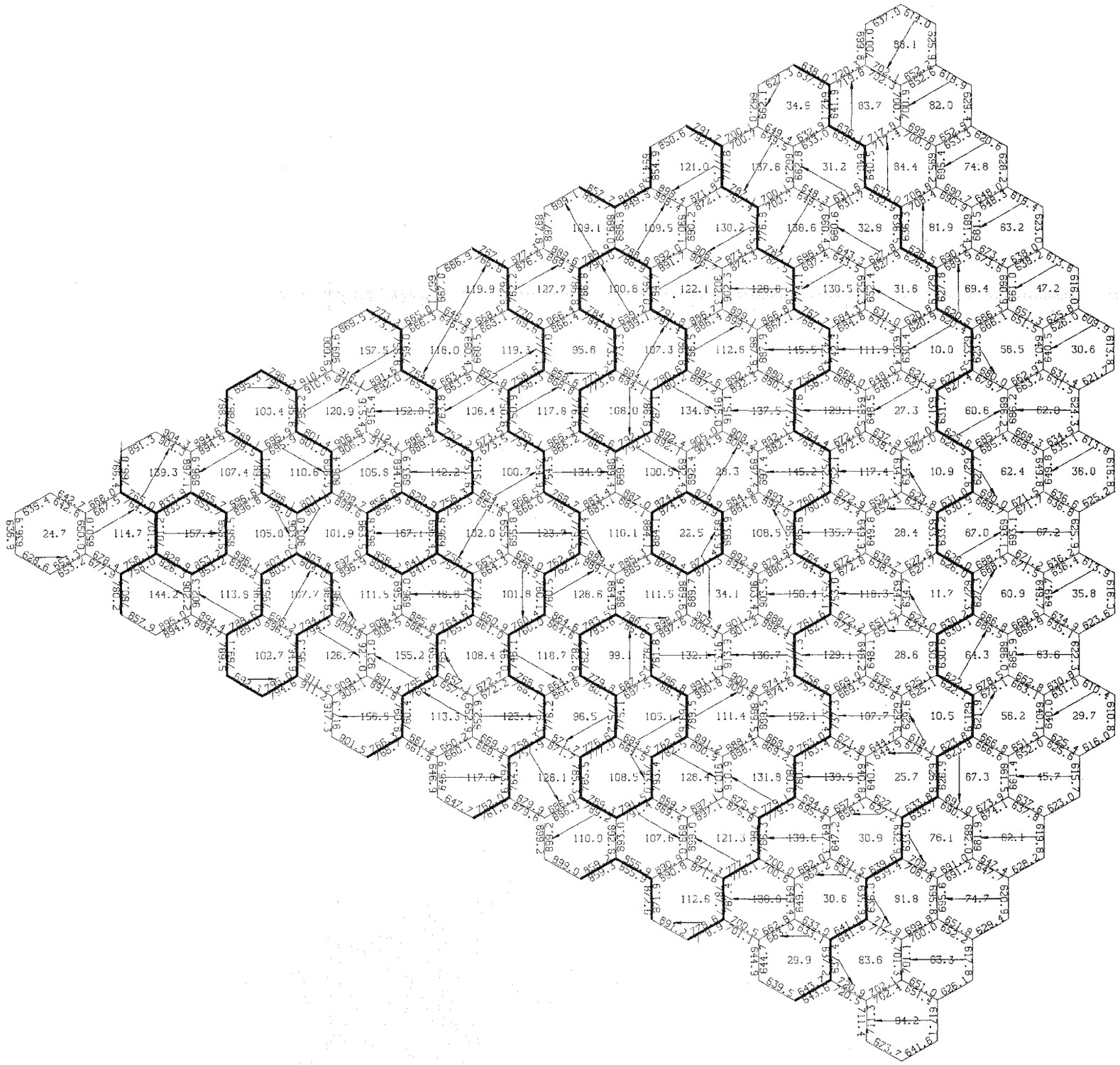

Figure 4.2.5.27. Average duct wall temperatures (^{o}F) and maximum duct wall temperature differences (^{o}F) at BOL at the top of the upper axial blanket. (Orificing based on assembly power and equal peak assembly cladding temperatures.)

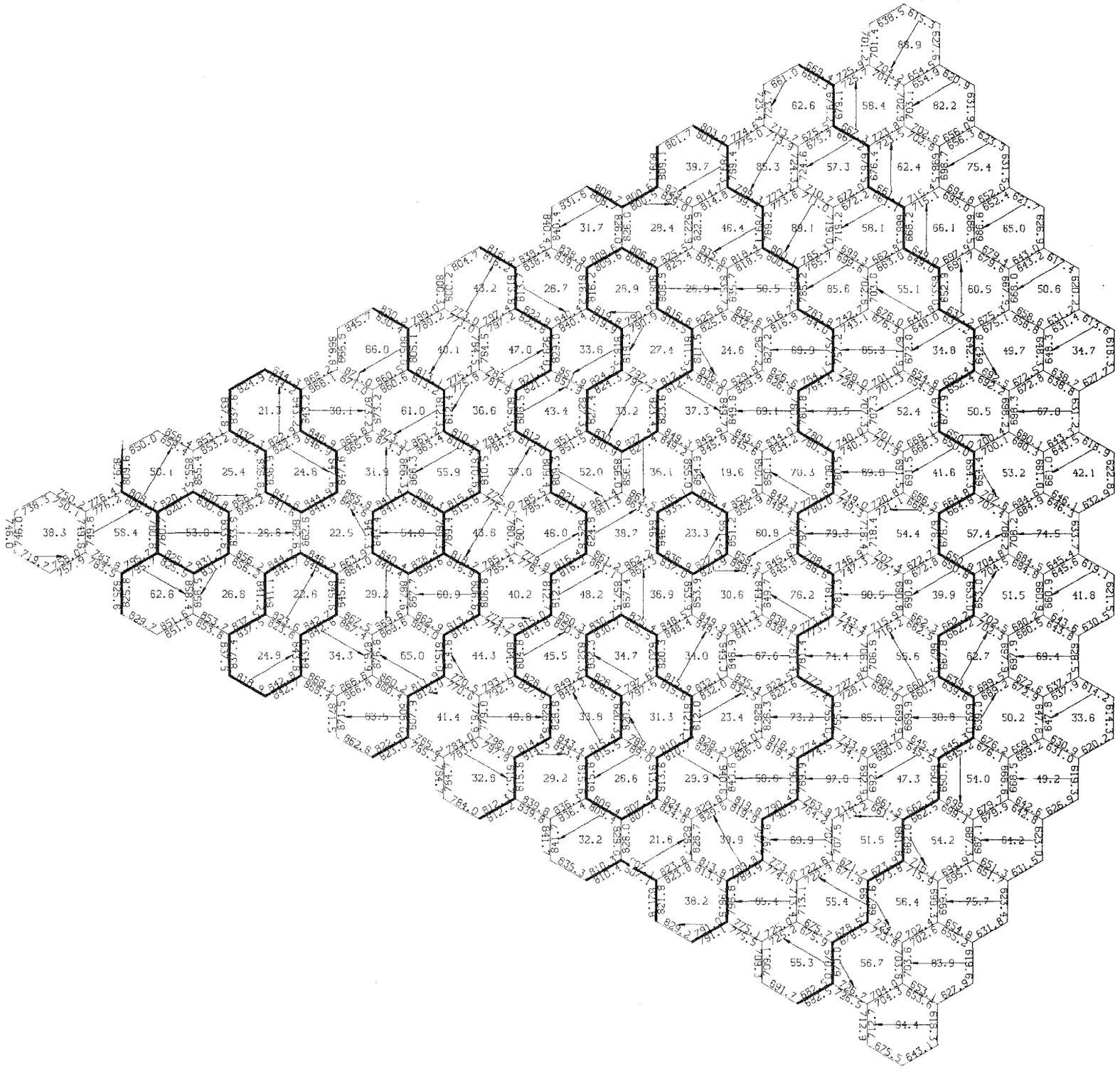

Figure 4.2.5.28. Average duct wall temperatures (^{O}F) and maximum duct wall temperature differences (^{O}F) at EOEC at the top of the upper axial blanket. (Orificing based on assembly power and equal peak assembly cladding temperatures.)

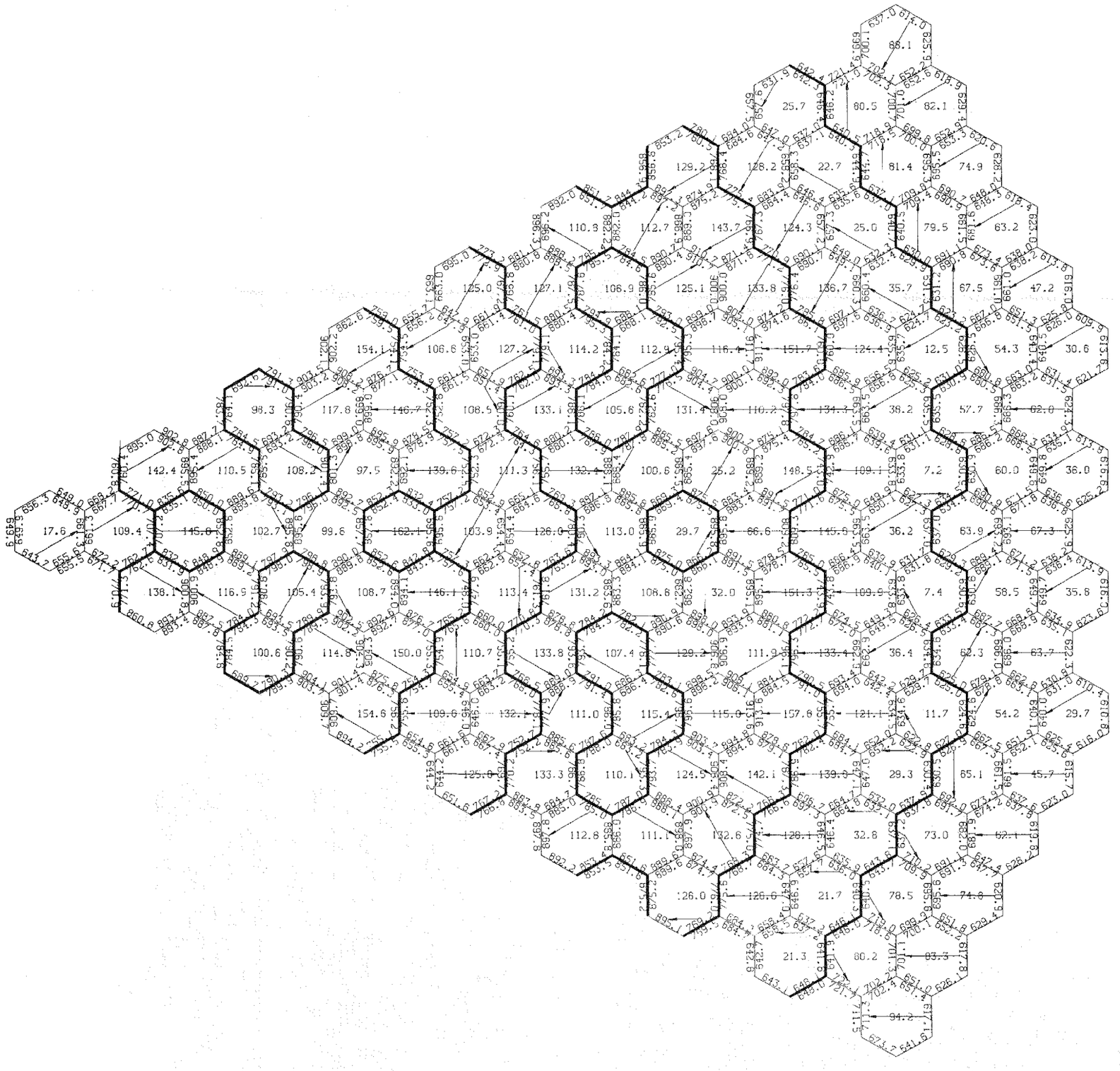

Figure 4.2.5.29. Average duct wall temperatures (^{o}F) and maximum duct wall temperature differences (^{o}F) at BOL at the top of the upper axial blanket. (Orificing based on peak pin power and equal peak assembly coolant temperatures.)

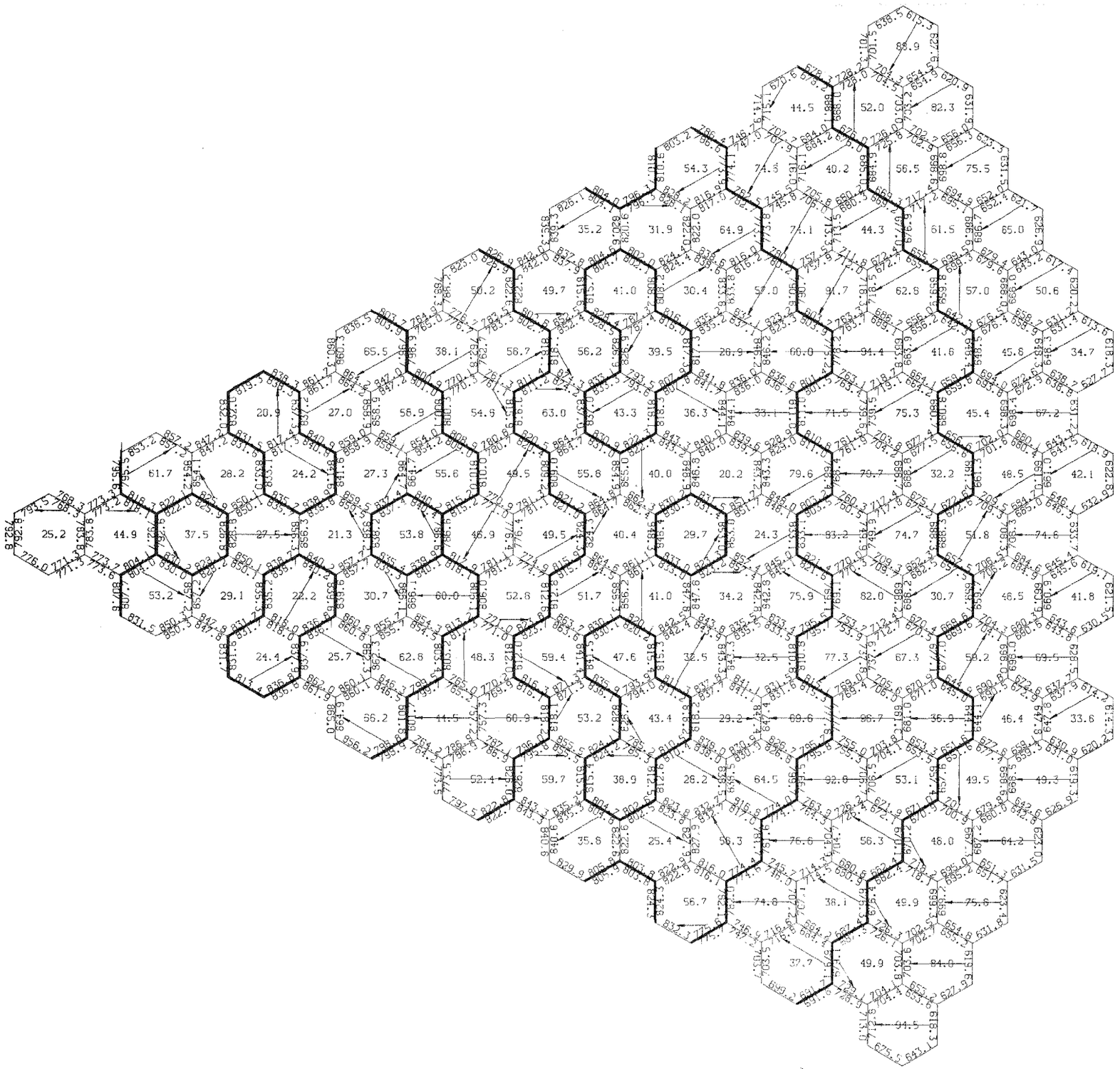

Figure 4.2.5.30. Average duct wall temperatures (^{o}F) and maximum duct wall temperature differences (^{o}F) at EOEC at the top of the upper axial blanket. (Orificing based on peak pin power and equal peak assembly coolant temperatures.)

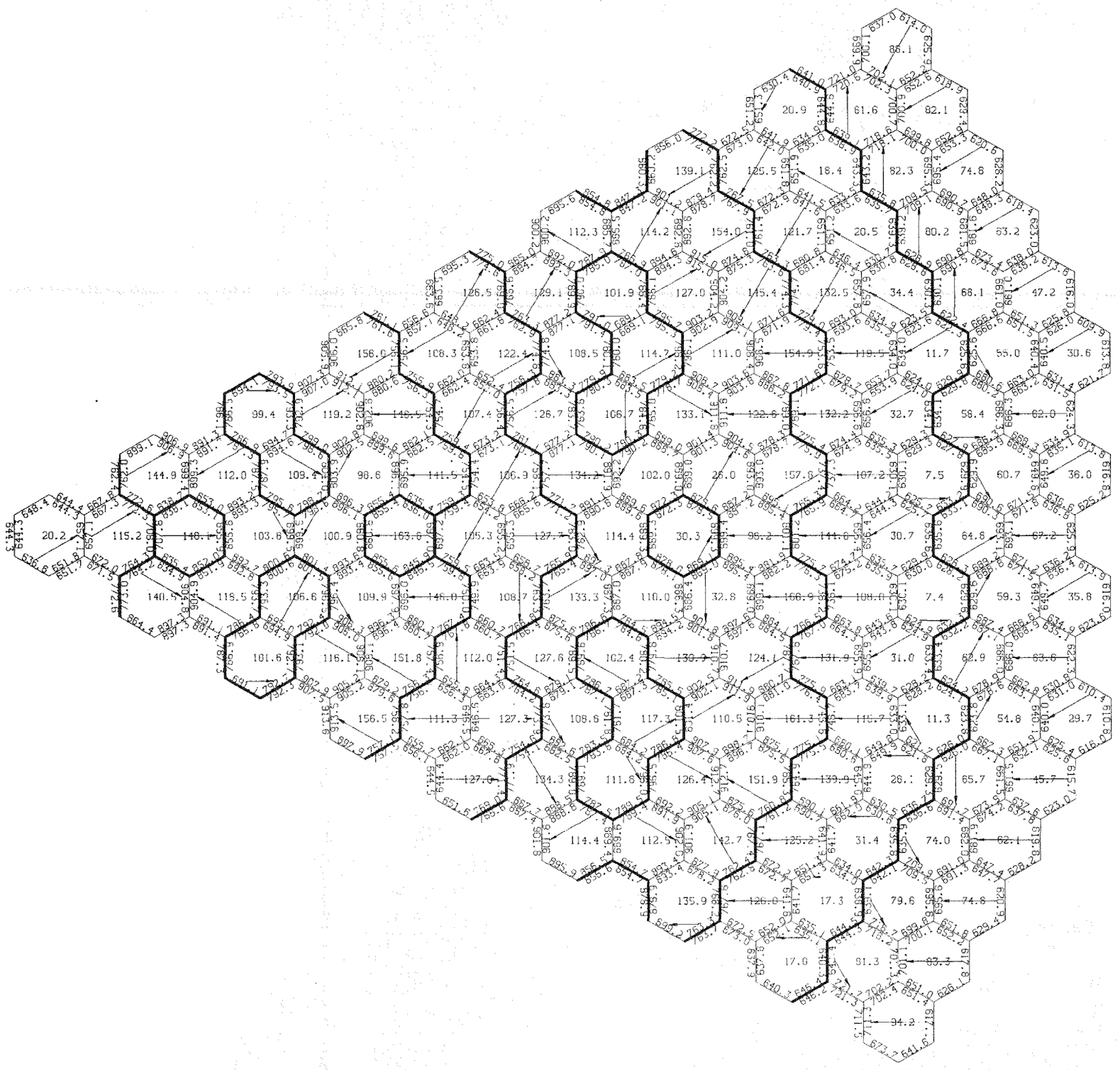

Figure 4.2.5.31. Average duct wall temperature (^{O}F) and maximum duct wall temperature differences (^{O}F) at BOL at the top of the upper axial blanket. (Orificing based on peak pin power and equal peak assembly cladding temperatures.)

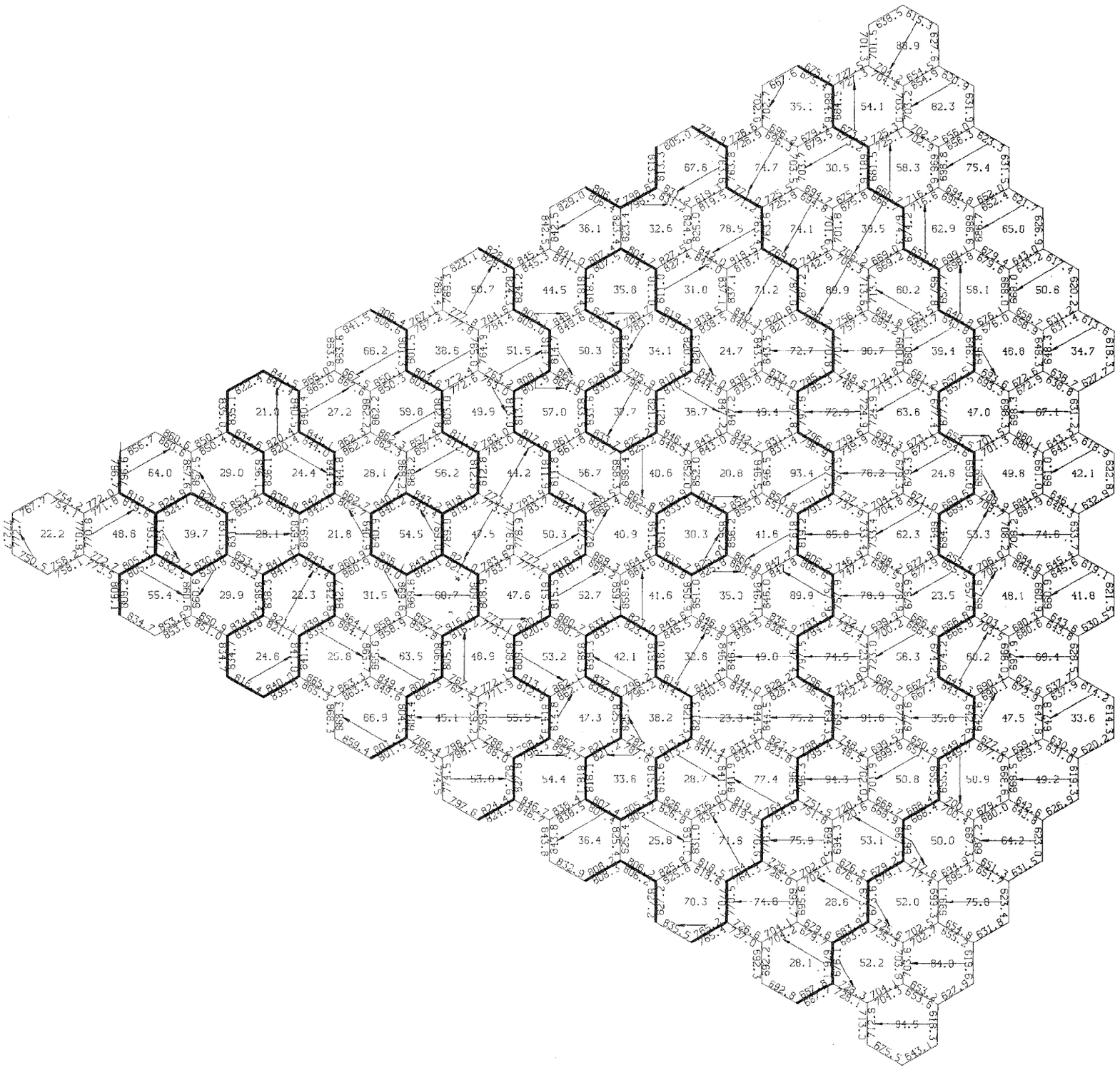

Figure 4.2.5.32. Average duct wall temperatures (^{O}F) and maximum duct wall temperature differences (^{O}F) at EOEC at the top of the upper axial blanket. (Orificing based on peak pin power and equal peak assembly cladding temperatures.)

Table 4.2.5.1

MAXIMUM DUCT WALL TEMPERATURES AND DUCT WALL TEMPERATURE DIFFERENCES

Reactor Region	Assembly Assignment to Orificing Zones Based on Assembly Power		Assembly Assignment to Orificing Zones Based on Pin Power	
	Equal Peak Assembly Coolant Temperatures	Equal Peak Cladding Midwall Temperatures	Equal Peak Assembly Coolant Temperatures	Equal Peak Cladding Midwall Temperatures
	Duct Wall Temperatures (^{o}F)			
Core	923.1[a]	921.0[a]	913.6[a]	915.0[a]
Internal Blanket	839.8[b]	847.6[b]	841.6[b]	844.8[b]
Radial Blanket	819.7[b]	803.0[b]	833.1[b]	819.2[b]
	Duct Wall Temperature Differences (^{o}F)			
Core	151.0[a]	157.5[a]	157.8[a]	161.3[a]
Internal Blanket	133.8[a]	123.7[a]	132.1[a]	127.7[a]
Radial Blanket	151.6[a]	139.5[a]	145.8[a]	139.9[a]

[a] occurs at BOL

[b] occurs at EOEC

a parametric study. Described in Appendix H are the results of this parametric study which assesses the impact on fuel element performance of changes in pin diameter, residence time, plenum volume, cladding thickness, coolant outlet temperature, and power history. The fuel element performance of the reference fuel pin, characterized collectively by complex phenomena such as pressure histories, pellet-cladding gap closure, fuel-cladding mechanical interaction, and cladding stresses and strains ,will be discussed here.

The reference fuel pin is assumed to operate under a constant flux environment using a 1.27% reduction in linear power per atom percent burnup which matches closely the design analysis results. A 3-cycle residence time, with a cycle having 255.5 full-power days, is used. The coolant outlet temperature used is 1050^{o} F, respresenting approximately the coolant outlet temperature for the hottest pin under the orificing criterion of equal peak cladding midwall temperatures. The corresponding nominal peak cladding midwall temperature is 1063^{o} F.

4.3.2 Methodology

The fuel element performance parameters such as fission gas release and pressure, gap closure, fuel-cladding mechanical interaction, cladding stresses and strains were investigated with the LIFE-III[7] code. Detailed descriptions of the analytical models and solution procedures are given in Appendix H and Reference 7.

4.3.3 Performance Analysis

4.3.3.1 Fission Gas Release

The release of fission gas from the fuel pellets into the plenum together with the plenum gas composition as functions of irradiation time are tabulated in Table 4.3.3.1.1. At 50 hours after startup, the fission gas release is 12.5% of total fission gas produced, with a corresponding gas composition in the plenum of 0.5% fission gas. At 1753 hours, the fission gas release reached 68.4% of total fission gas produced, with a corresponding gas composition in the plenum being 64.6% fission gas. Then,both the fission gas release and the plenum gas composition approach slowly their respective asymptotic values of 90 and 96%.

4.3.3.2 Plenum Pressure

The plenum pressure as a function of irradiation time is given in Table 4.3.3.2.1.

Table 4.3.3.1.1

FISSION GAS RELEASE AND PLENUM GAS COMPOSITION

Time, hours	Fission Gas Release, % of total	Plenum Gas Composition, % of Fission Gas
50	12.5	0.5
1753	68.4	64.6
5256	78.1	86.2
8050	80.7	90.8
13050	86.9	94.4
16346	89.7	95.6
18050	90.2	96.0

Table 4.3.3.2.1

PLENUM NOMINAL TEMPERATURE AND PRESSURE HISTORY*

Time, hours	Plenum temperature, ^{o}F	Plenum pressure, psia
50	1050	43.4
1753	1048	125.6
5256	1045	321.8
8050	1039	479.7
13050	1023	773.0
16346	1012	949.3
18050	1006	1030.9

*peak pin

The plenum pressure increases linearly with respect to irradiation time. Starting with a value of 43.4 psia at 50 hours after startup, the plenum pressure increases to 1030.9 psia at 18,050 hours (end-of-life).

4.3.3.3 Fuel-Cladding Gap Closure

The radial gap between the fuel pellet and the cladding is 3.5 mils. Table 4.3.3.3.1 tabulates the radial gaps at five different axial locations with respect to irradiation time. The gap closure occurs at approximately 63 hours after startup at 20 inches above the bottom of active fuel. After 8,800 hours, the gaps at 28 and 36 inches above the bottom of active fuel start to reopen. This reopening is primarily due to enhanced swelling and creep of the cladding relative to fuel swelling. At the end of life (18,050 hours), the radial gaps at 20, 28, and 36 inches above the bottom of active fuel are, respectively, 1.5, 3.6, and 4.7 mils.

4.3.3.4 Cladding Stresses

The cladding hoop stresses at two axial locations (X/L = 0.7 and 0.9, or 28 and 36 inches above the bottom of active fuel) with respect to irradiation time are shown in Figure 4.3.3.4.1. The cladding hoop stresses reach local peak values of 6,500 and 4,000 psia, respectively, at X/L = 0.7 and 0.9, before the fuel-cladding gaps reopen at 8,800 hours. After the reopening of the gaps, the cladding hoop stresses rise monotonically to peak values of 8,500 and 9,000 psia, respectively, at X/L = 0.7 and 0.9. This is due to the fact that after the reopening of the gaps, the only loading on the cladding is from fission gas pressure which exhibits a linearity with respect to irradiation time.

4.3.3.5 Cladding Diametrial Change and Inelastic Strain

The histories of the maximum cladding diametral change and inelastic strain (at X/L = 0.7) are shown in Figure 4.3.3.5.1. The cladding diametral change is measured in % $\Delta D/D$, and the inelastic strain is defined as the cladding diametral change minus one-third of the volumetric swelling.

There is an incubation period of approximately 8,000 hours for both the diametral change and inelastic strain. The maximum diametral change increases slowly from 0.96% at 50 hours after startup to 1.50% at 8,000 hours, then increases more rapidly to 6.16% at 18,050 hours. Similarly, the inelastic strain increases slowly from a zero value to 0.4% at 8,000 hours, then accelarates to 1.96% at

Table 4.3.3.3.1

RADIAL GAPS IN MILS AS FUNCTIONS OF TIME AND AXIAL LOCATION

Time, hours	Axial location, inches above bottom of active fuel				
	4	12	20	28	36
50	2.304	1.108	0.705	1.035	2.335
1753	0.269	0	0	0	0
8050	0	0	0	0	0
8837	0	0	0	0.030	0.011
13050	0	0	0.342	1.511	1.467
16346	0	0	1.123	2.922	3.791
18050	0	0	1.533	3.576	4.709

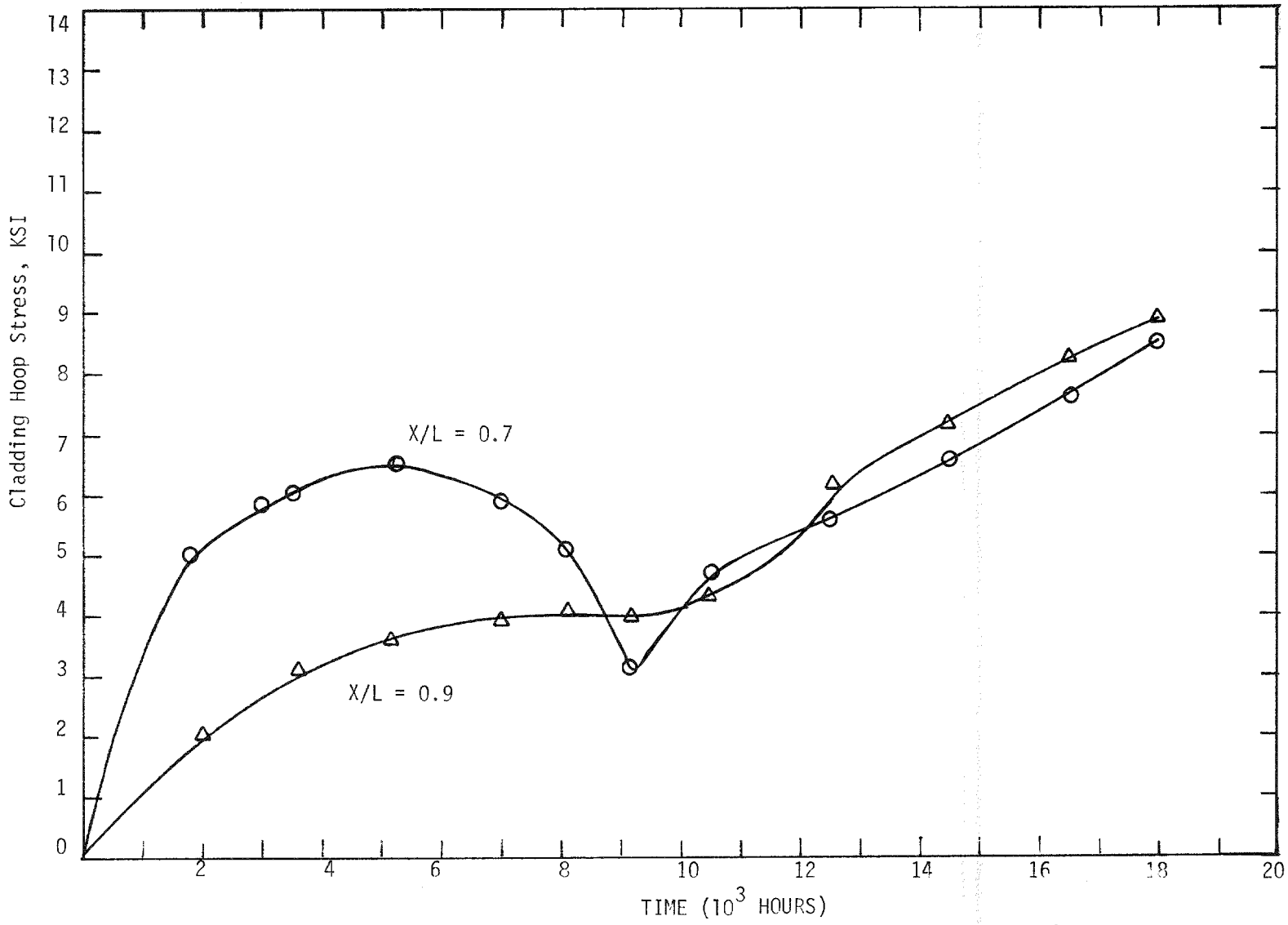

Figure 4.3.3.4.1. Cladding hoop stresses vs irradiation time (0.28" O.D. pin, 1050^{o} outlet temp., 14 mil clad, 30" plenum).

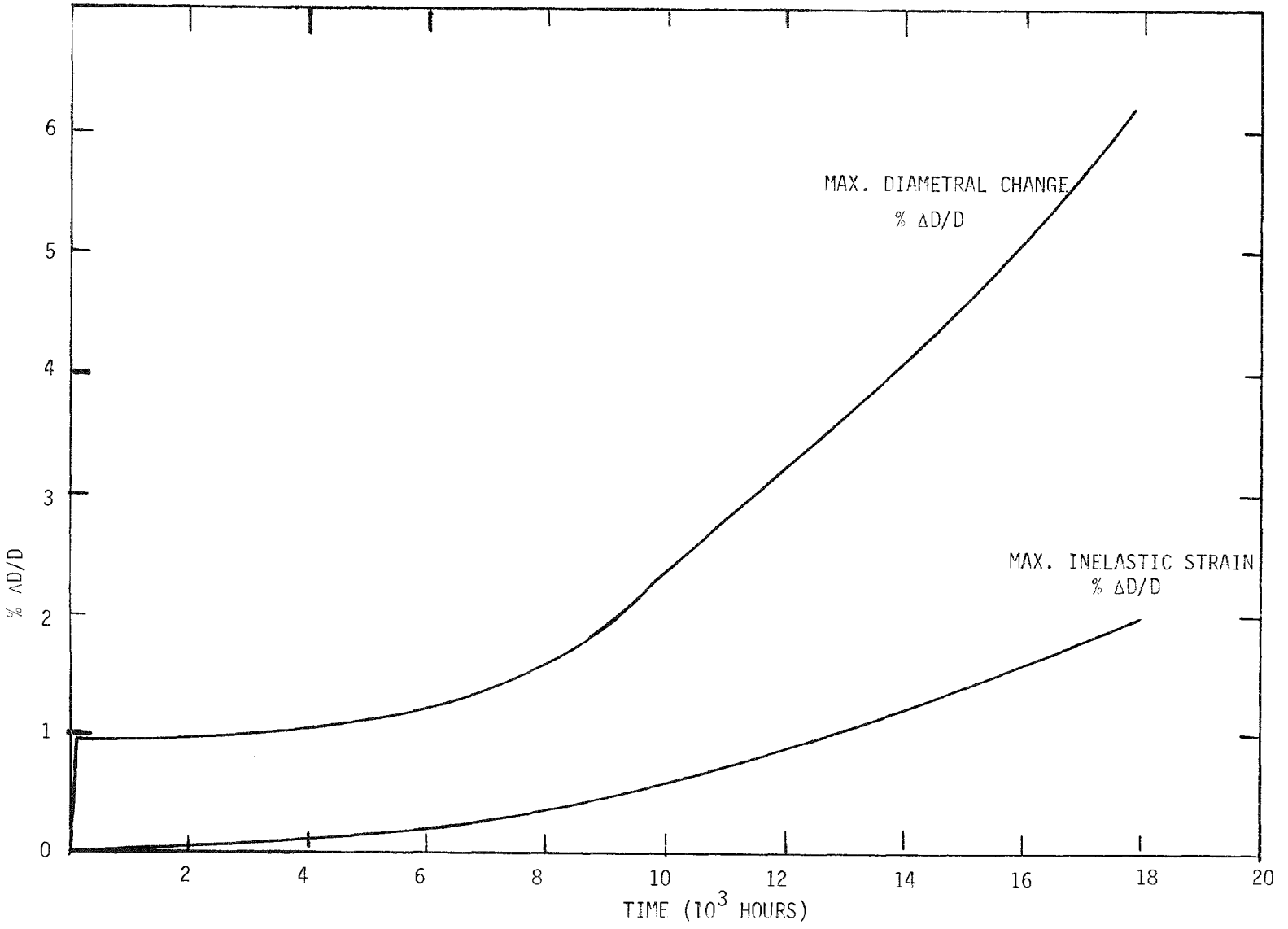

Figure 4.3.3.5.1. Max. diametral change and inelastic strain vs. irradiation time.

18,050 hours.

4.3.4 Fuel Life Criteria

In view of the many extremely complex interacting mechanisms which can cause fuel pin failure via cladding breach, a single fuel life criterion remains to be determined or agreed upon as of today. Three criteria have been extensively studied in the past decade and a brief discussion is given below. The three criteria are:

1. Cumulative damage fraction, CDF
2. Total cladding diametral change
3. Inelastic strain

First of all, the same criticism applies to all three criteria, namely, that it is not clear that there is a well defined range of values for any of these criteria beyond which fuel pins will fail. This may, if at all, be resolved by extensive irradiation programs. The cumulative damage fraction concept is useful to the extent that it is readily calculable. However, since it is not a measurable quantity, it is impossible to determine its value for a failed pin from post-irradiation examinations. One has to reconstruct a failed pin's irradiation history in order to compute its CDF value. This hampers somewhat the experimental correlation of CDF values vs. pin failure data. Furthermore, for the range of temperature and pressure values considered for the current designs, a steady-state CDF limit of 0.5 will allow an exceedingly long fuel life (>30% burnup). Or put in another way, for the current designs utilizing low temperature conditions (coolant inlet at 595^{o} F and 280^{o} F ΔT), the CDF values will be very small (<0.1). This further reduces the effectiveness of CDF as a failure criterion.

The total cladding diametral change criterion had been proposed by the French PHENIX Program. This criterion limits the total deformation the cladding can endure which is caused by a combination of fuel-cladding mechanical interaction, fission gas loading, irradiation swelling and pressure enhanced creep. The basis of the French recommendation of 6% as an operating limit for fuel pins is probably by and large due to T&H and mechanical considerations. The total cladding diametral change is measurable via fuel profilometry.

The inelastic strain, or commonly called mechanical or forced strain, is defined

as the total cladding diametral change minus one-third of volumetric swelling. This serves to indicate how much into the regime of plasticity the cladding has gone. The volumetric swelling is measurable from immersion density experiments before and after irradiation.

Based on the above, it is tentatively proposed that either:

a. A 6% maximum $\Delta D/D$ total diametral change, or
b. A 2% inelastic strain

be used as a fuel failure criterion. This value is further supported by the measurability of these quanties. The 6% $\Delta D/D$ total diametral change is based primarily on the irradiation tests on RAPSODIE[25] Fortissimo core fuel elements. In the absence of other irradiation data which give such a large cladding deformation (>6%), this 6% criterion was used for the current designs. Furthermore, extensive analytical calculations[26] for pins in the EBR-II and FFTF environment give end-of-life values for the maximum cladding diametral changes and inelastic strains in the range of 7 and 2%, respectively. Irradiation of mixed-oxide fuel pins in EBR-II[27,28], Dounreay[29] and JOYO reactor[30,31] has given 3-4% $\Delta D/D$ cladding diametral changes and more than 1% inelastic strains without failure. Preliminary as these data seem to be, they serve to illustrate the difficulties involved in establishing a single fuel life criterion, and to give some credence to the tentatively proposed criteria of 6% $\Delta D/D$ diametral change and 2% inelastic strain for pin failure.

Using the aforementioned 6% total diametral change or a 2% inelastic strain as a tentative fuel failure criterion, the reference fuel pin will not fail.

4.4 TRANSIENT ANALYSIS

4.4.1 Significance of Transient Analysis

The bulk of the heterogeneous core LMFBR study has concentrated upon analysis of the steady-state nuclear, thermal-hudraulic, and structural properties of the core. However, many limitations to systems design occur in the time-dependent response of the reactor to expected and accident events. For example, the placement and worth specifications of a secondary shutdown system must be regarded only as guidelines until it is verified that the shutdown system design keeps

system temperatures within acceptable limits for all transient events in the duty cycle. The resulting peak temperatures depend upon the initiating event, feedback effects, control rod configuration and insertion rate, and a variety of other design details and physical effects. A transient code is necessary to account for the interaction of such a complex collection of phenomena.

Examples of limiting core transients are given in Table 4.4.1.1. Event numbers correspond to the duty cycle of the Clinch River Breeder Reactor[3]. The classifications N, U, E, and F correspond to Normal, Upset, Emergency, and Faulted Events, respectively. The left column of Table 4.4.1.1 describes "up-transients" or events which may lead to unacceptably high core temperature. The right column lists "down-transients" for which the temperature ramp rates are the objects of interest. A single down-transient does not usually have any effect on the plant, but rather of concern is the cumulative damage to fuel and components from many such transients during the plant lifetime. Note that the rod withdrawal transient E-13a falls under both categories, since the down ramp following an overpower trip may cause the most substantial temperature decrease seen during the plant duty cycle.

In that the E-13a event is the fastest of the upset and emergency transients, it provides the means for evaluating the effect of moving the secondary conrol rod parked position from the core-blanket interface to the top of the axial blanket.

As discussed in Appendix A, moving the parked position of the secondary system from the core-upper axial blanket interface to the top of the upper axial blanket reduces the CSDT by about one year. However, this change in the parked position of the secondary system affects the transient performance of the reactor. The time delay between a protection system scram signal and the entry of the secondary control rods into the core, is increased by the time needed for the control rods to cross the upper axial blanket thickness. To determine the impact that the parked position of the secondary control system has on the transient performance of the reactor, uncontrolled rod withdrawal transients have been analyzed for two secondary system parked positions, i.e., control rods parked at the core-upper axial blanket interface and control rods parked at the top of the upper axial blanket. For the analysis, the FX2-TH[32] code has been used in a two-dimensional RZ geometry.

Table 4.4.1.1

LIMITING DUTY CYCLE TRANSIENTS FOR CORE ANALYSIS

SAFETY ("HEATUP") TRANSIENTS		FUEL ROD THERMAL CYCLING STRUCTURAL TRANSIENTS	
E-13a	Trip following rod withdrawal from full power	U-1	Reactor Trip
E-14	Loss of all electrical power (Natural Circulation Event)	U-2b	Trip following rod withdrawal from low power
U-15	Loss of all AC power	E-13a	Trip following rod withdrawal from full power
F-1	Safe shutdown earthquake	N-4	Unloading and loading

4.4.2 RZ Model for Transient Analysis

The FX2-TH code allows core kinetics calculations with feedback in two-dimensional hexagonal or RZ geometry. While hexagonal geometry is desirable in allowing treatment of individual fuel subassemblies, it has the disadvantage of allowing only an adiabatic thermal model for the fuel. Further, a direct representation of control rod motion must involve the Z-direction. While a complete transient hex-Z calculation would be highly desirable, it is beyond the state-of-the-art for transient codes such as FX2-TH and therefore an RZ model of the reactor had to be used.

The power-producing regions of the system are divided into a number of thermal-hydraulic channels summarized in Table 4.4.2.1. The outlet coolant temperature for each channel was obtained as a simple average of the assembly outlet coolant temperatures within that region. The assembly temperatures and assembly flow rates were obtained from the orificing scheme that is based on assembly power and equal peak coolant temperatures (Section 4.2.2).

Boron number densities were adjusted to produce control rod bank worths (Section 4.2.3.6) of 4.28% ΔK and 2.46% ΔK for the primary and secondary banks, respectively.

The dynamics of the secondary shutdown system were treated by an auxiliary code which needs as input the control rod parked position and the time of scram signal. In the FX2-TH model, the secondary control rod ring is divided into 17 axial segments to ensure precise treatment of the axial motion. The auxiliary program produces as output the transient driving function data needed by FX2-TH for each such segment.

The secondary control rod displacement-versus-time curve was taken from the PSAR for the CRBR[3]. Assuming a 200 msec time delay between a scram signal and rod motion, the following piecewise-linear fit was obtained:

$$\Delta X = \begin{cases} 71.12\Delta t, & 0<\Delta t<0.1 \\ 7.112 + 81.23\ (\Delta t-0.1), & 0.1<\Delta t<0.2 \\ 15.24 + 107.95\ (\Delta t-0.2), & 0.2<\Delta t<0.3 \\ 26.035 + 111.125\ (\Delta t-0.3), & \Delta t<0.3 \end{cases}$$

ΔX is rod displacement in centimeters and Δt is the time past beginning of rod

TABLE 4.4.2.1

RZ MODEL FOR TRANSIENT ANALYSIS

ACTIVE THERMAL-HYDRAULIC REGION	TYPE	INNER RADIUS (cm)	OUTER RADIUS (cm)	MASS FLOW RATE PER UNIT AREA (gm/(sec-cm^2))	OUTLET TEMP ^{o}F
1	Blanket (B1)	0.	34.337	115.1	689.9
2	Core (IC)	34.337	43.8693	620.4	966.0
4	Core (IC)	47.9173	61.5256	676.2	971.4
5	Blanket (B2)	61.5256	72.6274	235.3	716.0
6	Core (MC)	72.6274	86.653	619.0	968.0
8	Core (MC)	88.7755	100.574	572.4	968.0
9	Blanket (B3)	100.574	122.292	103.5	682.9
10	Core (OC)	122.292	142.015	639.7	967.2
12	Blanket (B4)	143.319	150.912	275.1	705.2
14	Core (OC)	152.141	178.074	613.2	966.1
15	Radial Blanket	178.074	192.154	80.9	722.2
16	Radial Blanket	192.154	206.175	57.0	639.8

(Channels 3, 7, 11, and 13 are reserved for control rods. Channel 17 is reserved for radial reflector. These thermal-hydraulic channels are not active in the present study.)

motion. The rod motion begins 200 msec past the time at which the protection system senses an overpower trip point and

$$\Delta t = t - t_{scram} - 0.200$$

4.4.3 Uncontrolled Rod Withdrawal Transient

An uncontrolled primary rod withdrawal event has been studied as a severe test of the protection system's ability to protect the core. This transient corresponds to the E-13a event as defined in the duty cycle for the Clinch River Breeder Reactor.

Since the E-13a event is the fastest of the upset and emergency transients, it provides a basis for evaluating the effect of moving the secondary control rod parked position from the core-blanket interface to the top of the axial blanket.

To initiate the event, we assume a maximum credible primary system insertion rate of +13¢/second. This figure was arrived at by assuming:

a. Primary worth of 4.28% Δk distributed among 12 rods,
b. Maximum rod withdrawal rate of 72 inches per minute[3],
c. Interaction factor of 1.785 (Section 4.1.3.6.1.2), and
d. Cosine axial flux shape, leading to a peak-to-average ratio of control worth of $(\pi/2)^2$.

Thus, the upper bound of ramp rate (in \$/sec) due to spurious withdrawal of one primary rod at its maximum speed is:

$$\frac{d\rho}{dt} \leq \frac{(4.28)\ (0.01)\ (1.785)\ (72\ \text{in/min})\ (\pi/2)^2}{(12)\ (0.0036)\ (40\ \text{in})\ (60\ \text{sec/min})} = \$0.13/\text{sec}$$

This may be compared to the assumed ramp-rate of 19¢/second for this emergency event in the Clinch River Breeder Reactor. Because of the inability of the RZ calculation to model individual rod motions, the 13¢/sec reactivity ramp is introduced uniformly throughout the primary system.

The primary control rod system is assumed to be unavailable for scram, so that the secondary (safety) system is initiated on the 130% power-to-flow ratio signal, or

at 130% power for this event. Rod motion begins 200 msec later, and a pump trip occurs 500 msec after the scram signal. The pump coastdown curve is described by:

$$G(t) = G_o\left[1-0.179(t-t_{trip}) + 0.006\ (t-t_{trip})^2\right]$$

as given by Reference 3. Here t_{trip} is the time at which the pump coastdown begins. For a 500 msec delay of pump trip:

$$t_{trip} = t_{scram} + 0.500$$

Figure 4.4.3.1 shows the transient nominal clad midwall temperature as predicted by FX2-TH for an average channel in thermal-hydraulic region 6. This is the region of highest outlet coolant temperature and, since clad temperature follows it very closely, highest clad midwall temperatures as well. The 130% power level is reached at 1.67 seconds, and at 1.87 seconds the secondary rods begin to move. With the rods parked at the core-blanket interface, the transient rapidly turns around as the secondary system enters the core soon after the beginning of rod motion. However, if the rods are parked at the top of the axial blanket, the transient temperatures continue upward for the roughly 0.4 seconds required for the tip of the secondary rods to transverse the axial blanket and enter the core. Maximum region-averaged temperatures of 1019^{o} F and 1046^{o} F are reached, as tabulated in Table 4.4.3.1.

The RZ model does not provide temperature information for individual pins or individual subassemblies. However, CORE-3D and ENERGY calculations (Section 4.2.4) have predicted a steady-state nominal peak assembly clad midwall temperature of 1148^{o} F. This nominal peak clad temperature can be reproduced by applying a factor of 1.406 to the coolant temperature rise obtained in the steady-state FX2-TH calculation for region 6, where the maximum steady-state coolant temperatures are obtained. If this nominal peaking factor is applied to transient temperatures, the nominal peak clad midwall temperature is found to reach 1219^{o} F during the transient, as shown in Table 4.4.3.1 and Figure 4.4.3.2.

The absolute temperature rises, even for the hot channel, differ by less than 50^{o} F for the two parked positions, showing that the increased breeding gain can be achieved without a dramatic degradation of transient performance.

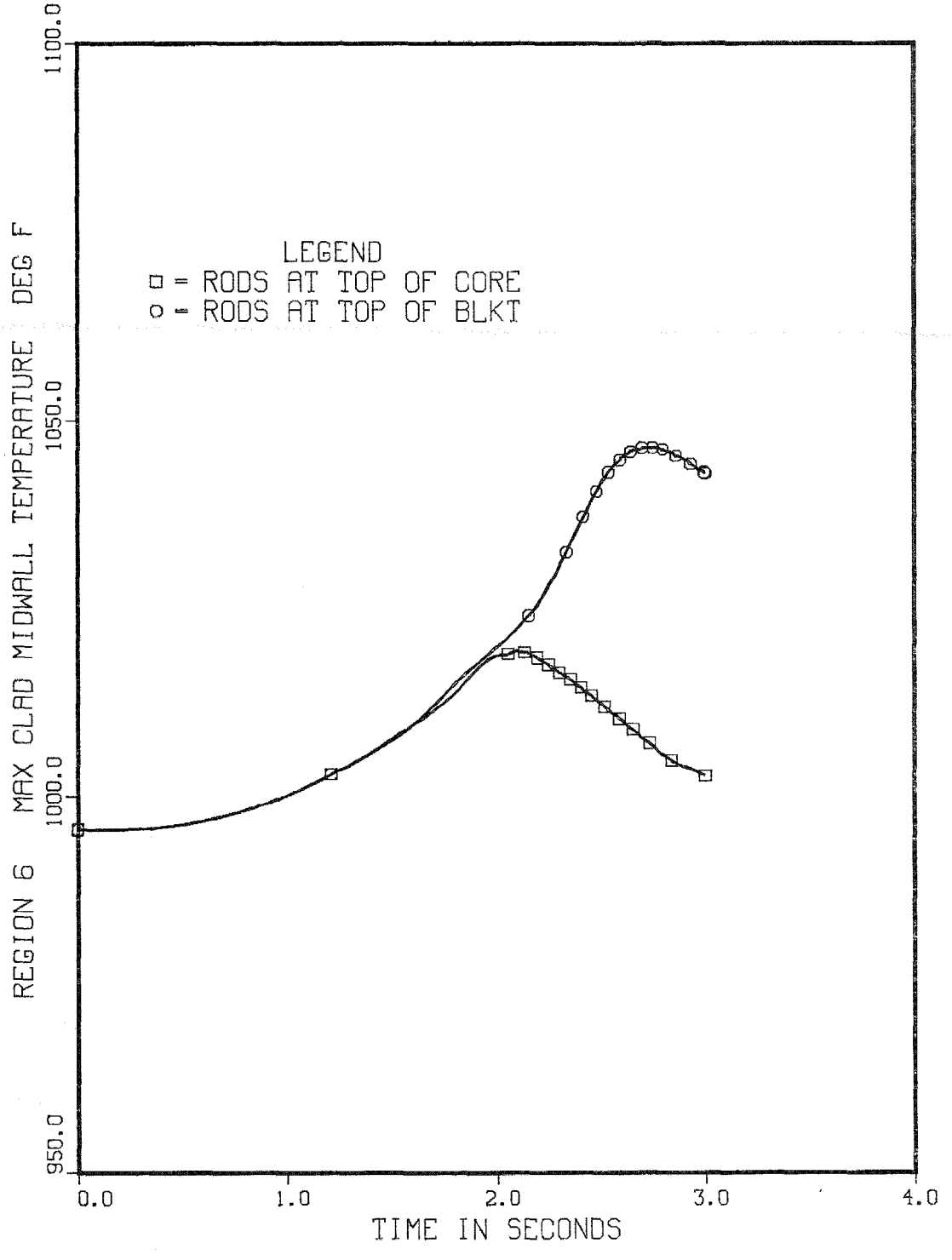

Figure 4.4.3.1. E-13a transient. Region 6 maximum nominal clad midwall temperature versus time.

TABLE 4.4.3.1

UNCONTROLLED ROD WITHDRAWAL TRANSIENT,
BEGINNING-OF-LIFE, 13¢/SECOND INSERTION, SECONDARY SCRAM

MAXIMUM CLAD MIDWALL TEMPERATURE (^{o} F)

	RZ Model Channel 6 (Region-Averaged)	Nominal Peak Channel	3σ-Hot Channel
Steady-State (Beginning of Transient)	995	1148	1295
Maximum Transient Temperature (Control Rods Parked at Core/ Blanket Interface; Pump Trip Delayed 500 msec)	1019	1181	1356
Maximum Transient Temperature (Control Rods Parked at Top of Axial Blanket; Pump Trip Delayed 500 msec)	1046	1219	1404
Maximum Transient Temperature (Control Rods Parked at Top of Axial Blanket; Pump Trip Delayed 900 msec)	1030	1196	1376

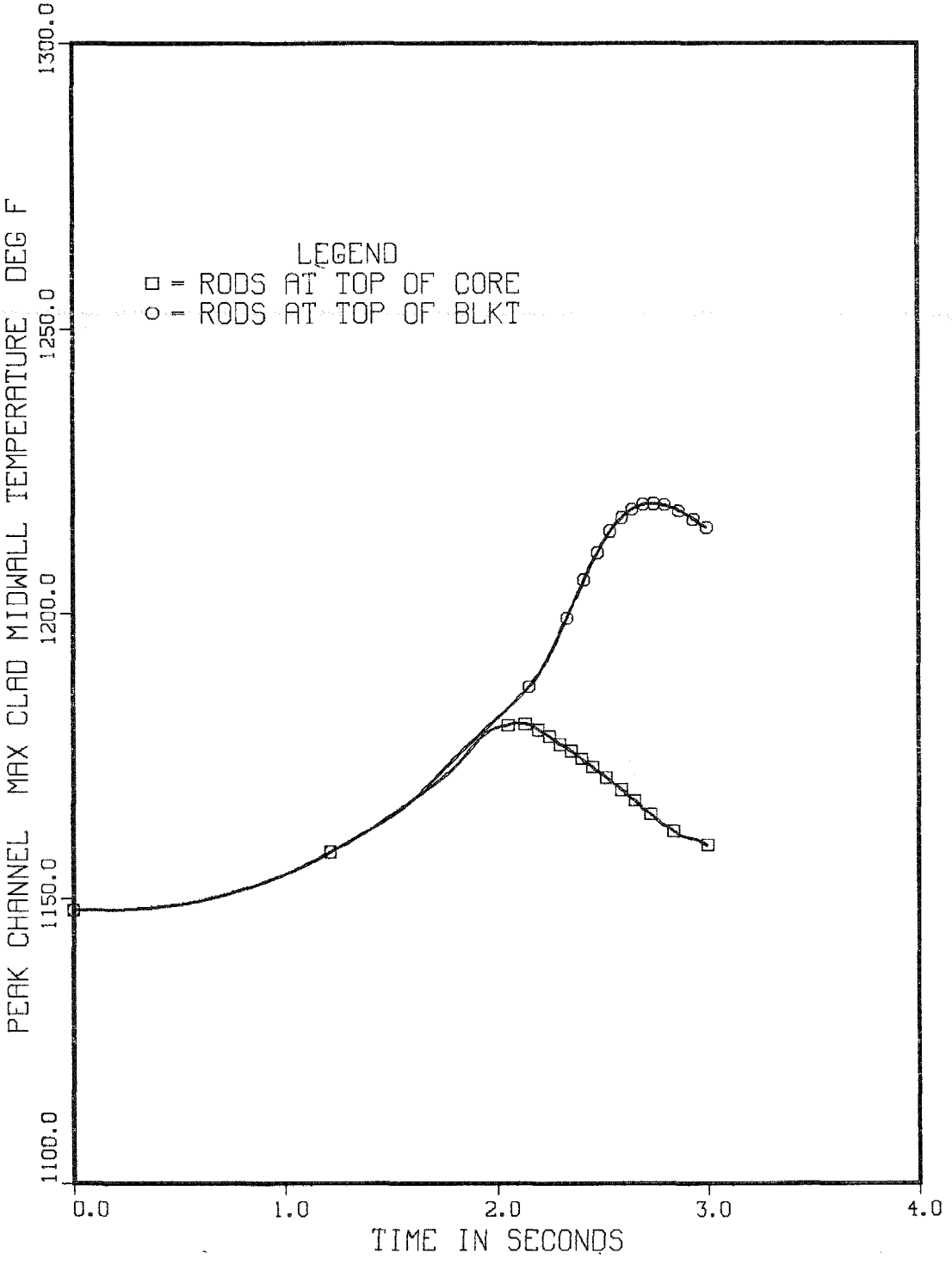

Figure 4.4.3.2. E-13a transient. Nominal peak channel maximum clad midwall temperature versus time.

Hot channel transient temperatures can be obtained by applying 3σ hot channel factors (Section 4.2.3) of 1.264 for the coolant and 1.906 for the clad. The resulting hot-channel clad midwall transients are shown in Figure 4.4.3.3. The above calculations were performed assuming that trip points and delay times are unchanged from the Clinch River Breeder Reactor design. However, moving the secondary parked positions outside the core introduces approximately a 400 msec delay for the rods to enter the core. A consistent design change would then be to delay the pump trip an additional 400 msec as compensation. An additional set of calculations was performed assuming a pump trip delayed 900 msec past the scram signal. The results are summarized in Figures 4.4.3.4 through 4.4.3.6 and in Table 4.4.3.1. Delaying the pump trip reduces the peak temperature difference between the parked positions by about 60%. Such improvement shows the importance of tailoring the protection system design to the core and control designs. Whether such changes to the system could actually be made would depend upon a more complete examination of the transient duty cycle, including a study of the U-1 reactor trip transient (reactor trip from nominal power) and the consequence of a delayed pump trip on temperature ramp-rates due to such down-transients; since reactor upper internals are affected by those rapid temperature changes.

The E-13a transient studied above has assumed a maximum credible rod withdrawal rate of 72 inches/minute. A more complete evaluation of overpower transients should also address both slower insertion rates and also very rapid hypothetical insertion rates proposed for faulted events such as safe-shutdown earthquake transient. Slower transients usually lead to somewhat higher values of peak clad temperature, because more energy can be deposited before the overpower trip point is reached. However, the difference obtained due to a higher secondary rod parked position would be less pronounced than for the faster case studied above. Extremely fast hypothetical insertion rates, such as the 60¢/second introduced during a safe-shutdown earthquake[3], may also involve higher energy depositions than the maximum credible E-13a event examined above.

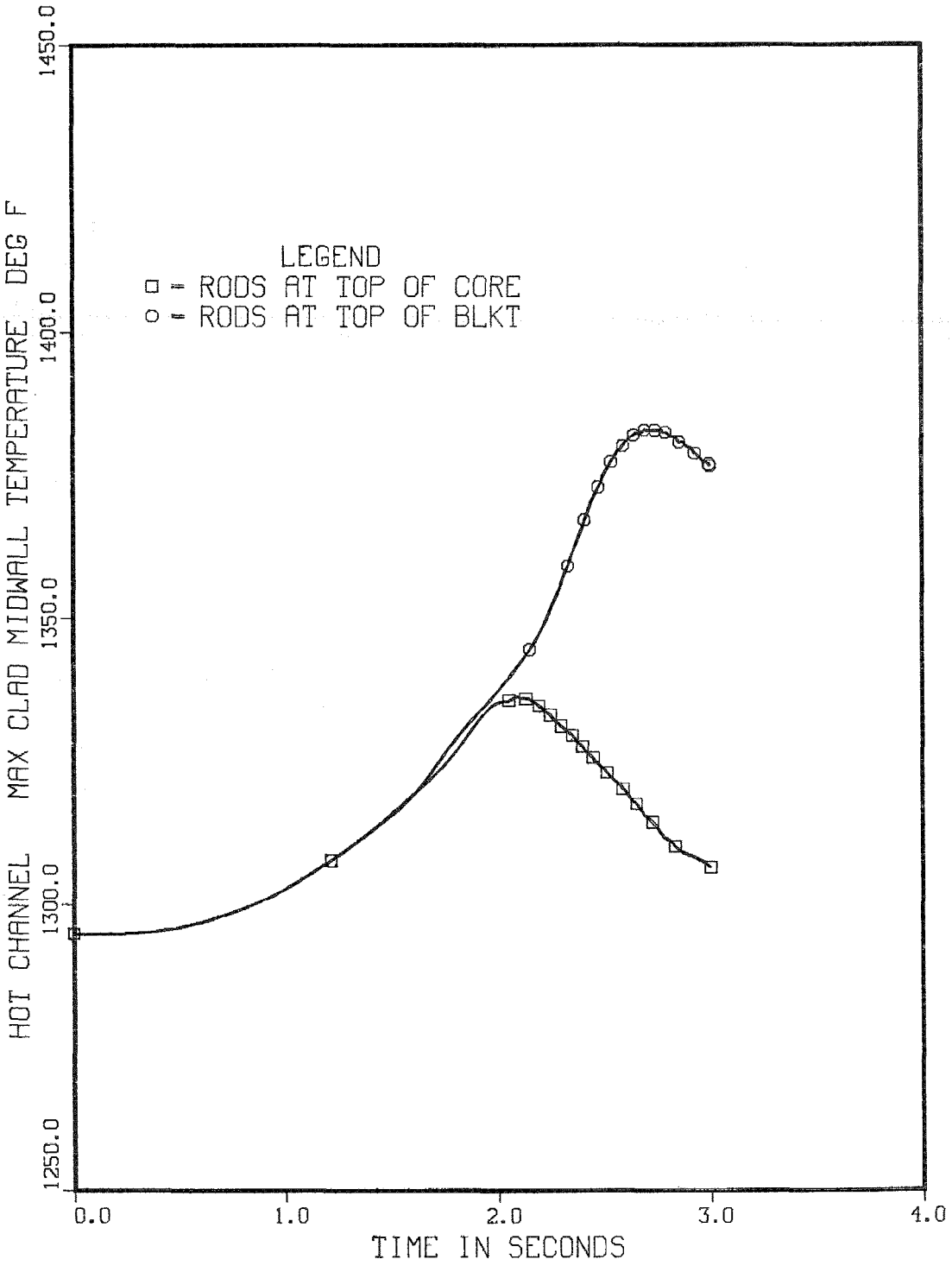

Figure 4.4.3.3. E-13a transient. 3σ hot channel maximum clad midwall temperature versus time.

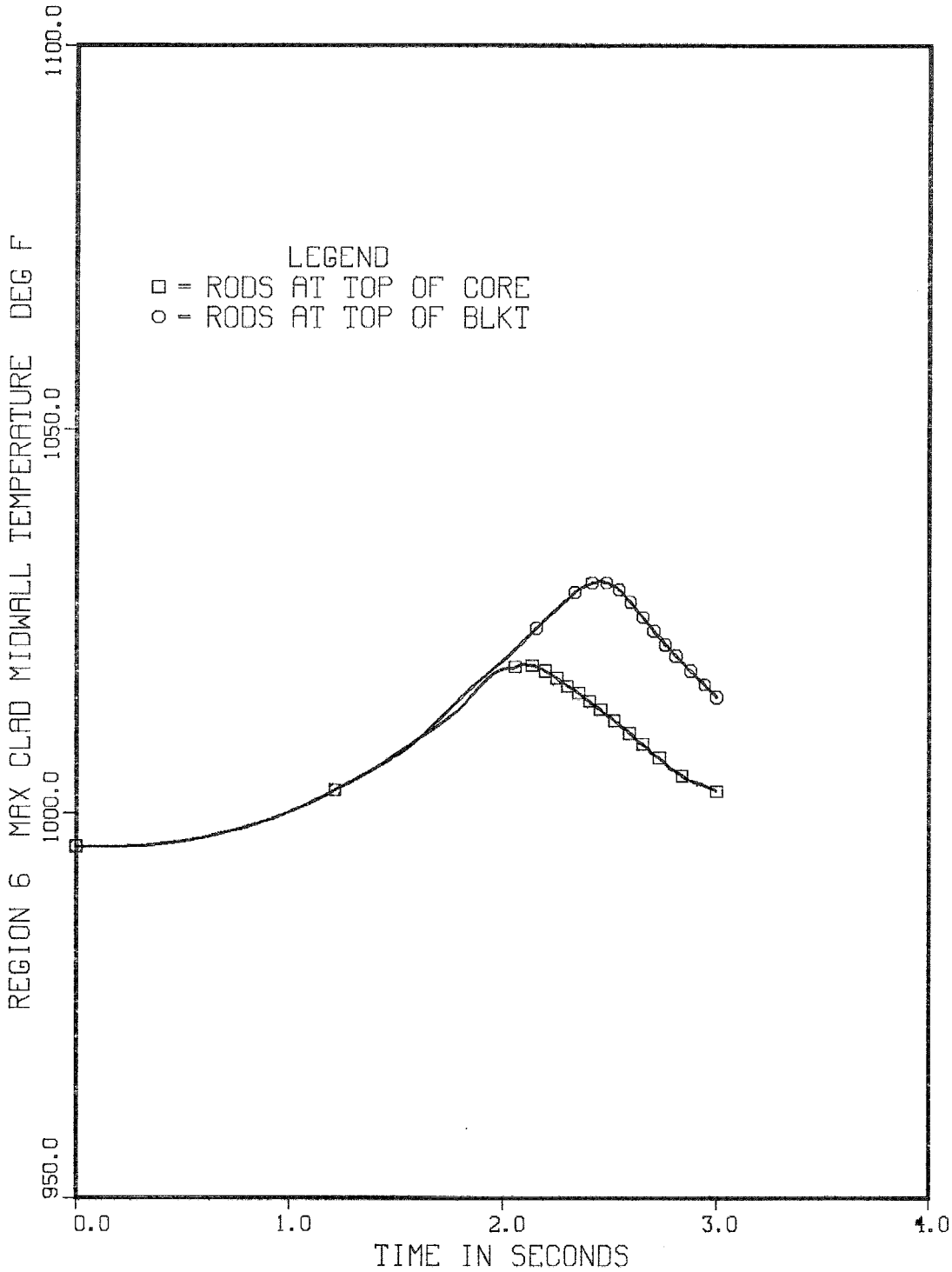

Figure 4.4.3.4. E-13a transient with 900 msec pump trip delay. Region 6 maximum nominal clad midwall temperature versus time

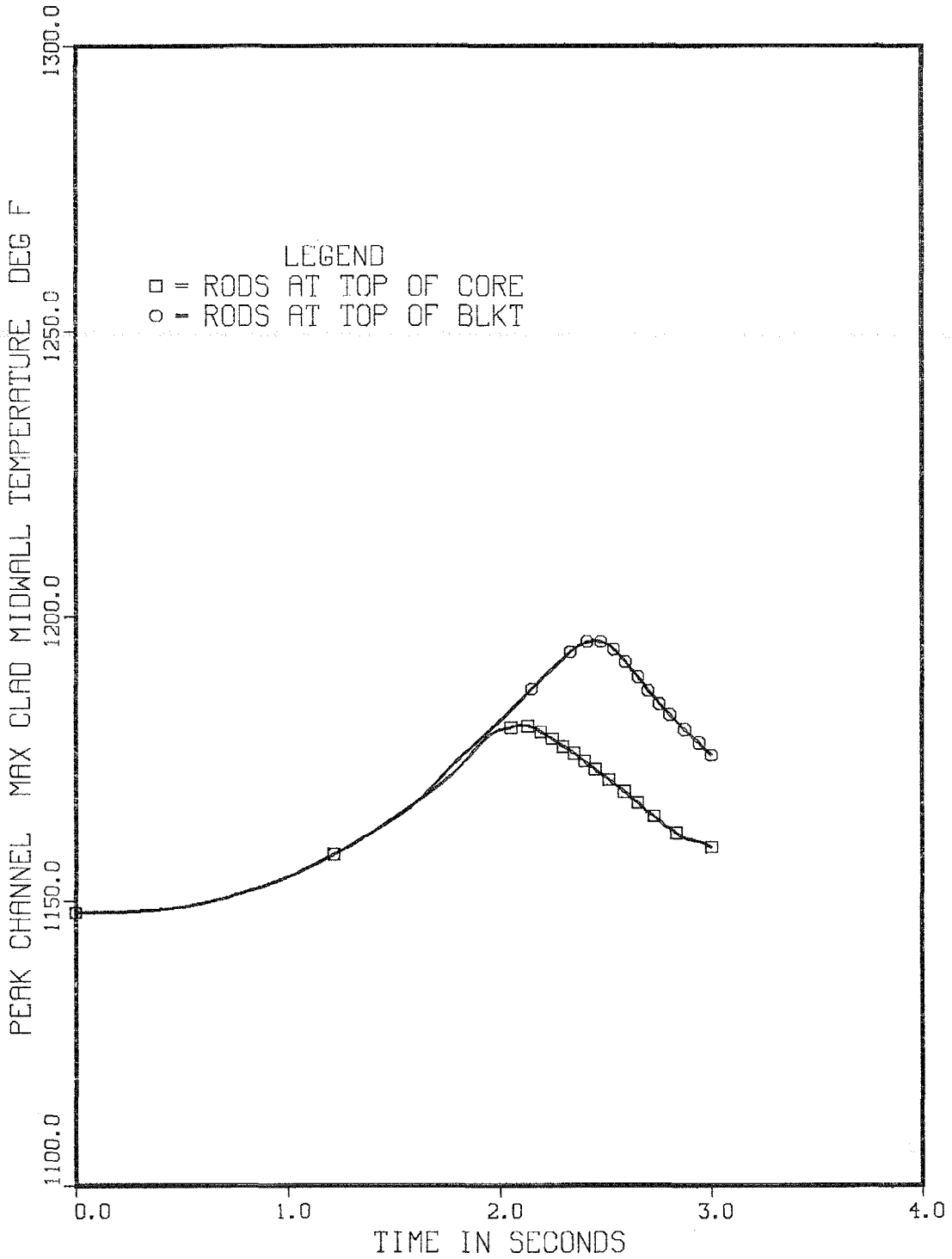

Figure 4.4.3.5. E-13a transient with 900 msec pump trip delay. Nominal peak clad midwall temperature versus time.

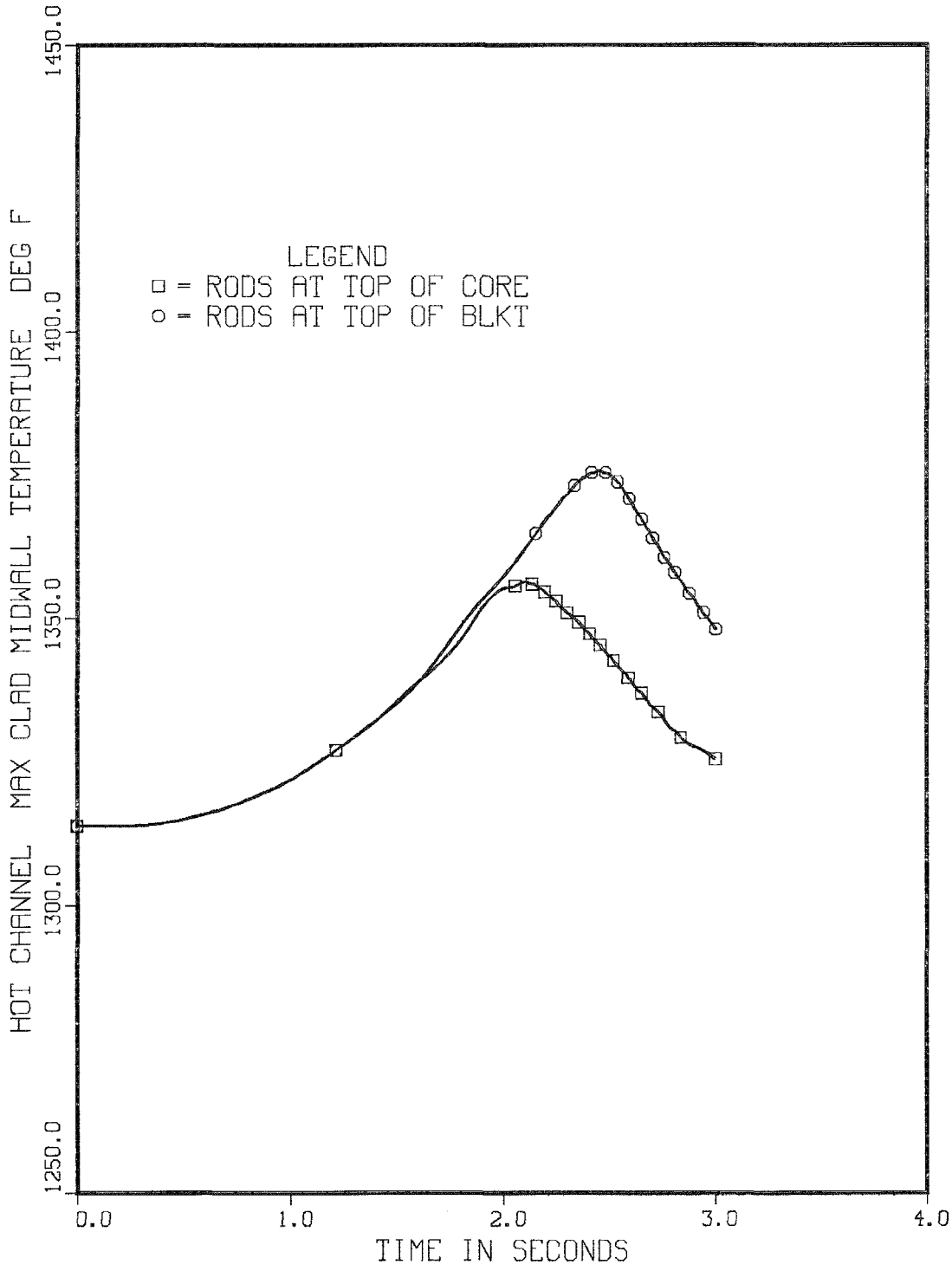

Figure 4.4.3.6. E-13a transient with 900 msec pump trip delay. 3σ peak clad midwall temperature versus time.

5.0. REFERENCES

1. W. P. Barthold et al. Optimization of Radially Heterogeneous 1000-MW(e) LMFBR Core Configurations. EPRI NP-1000 (November 1979).

2. J. C. Chandler et al. The Proliferation Resistant Preconceptual Core Design Study. HEDL TC-1082 (March 1978).

3. Project Management Corporation. CRBRP Preliminary Safety Analysis Report. (1975).

4. W. P. Barthold and C. P. Tzanos. Performance Potential of Reference Fuel in 1200 MWe LMFBRs. ANL FRA-TM-104 (November 1977).

5. W. P. Barthold and Y. I. Chang. Breeding Ratio and Doubling Time Definitions Used for Advanced Fuels Performance Characterization. Trans. Am. Nucl. Soc. 26, 588 (1977).

6. Nuclear Systems Materials Handbook, TID 26666, Hartford Engineering Development Laboratory, Richland, Washington.

7. M. C. Billone, B. L. Harbourne, et. al. The LIFE-III Fuel Element Performance Code User's Manual. Argonne National Laboratory Draft Report, March 1977.

8. W. P. Barthold, J. Beitel, Y. Chang, M. King, Y. Orechwa. Breeding Performance and Pin Diameter Optimization for Mixed Carbide and Nitrides Fuels in 5000 MWt LMFBRs. Part II. ANL Draft Report.

9. R. P. Hosteny. The ARC System Fuel Cycle Analysis Capability, REBUS-2. ANL-7721 (October 1978).

10. T. A. Daly, et al. The ARC System Two-Dimensional Diffusion Theory Capability, DARC2D. ANL-7716 (1972).

11. T. A. Daly, et al. The ARC System Two-Dimensional Adjunct Calculations. ANL-7720 (October 1972).

12. J. C. Beitel and E. U. Khan. CORE-3D - a Computer Program for Predicting Core Wide Coolant and Structure Temperature Distribution in Wire Wrapped LMFBR Assemblies. ANL FRA-TM-100 (April 1977).

13. E. U. Khan. A Porous Body Model for Predicting Temperature Distribution in Wire Wrapped Fuel and Blanket Assemblies of a LMFBR. ScD Thesis M.I.T., June 1975 (also Nuclear Engineering and Design, Vol. 35, Nos. 1 and 2, December 1975).

14. L. J. Koch, Et al. Hazard Summary Report, Experimental Breeder Reactor II (EBR-II). ANL-5719 (May 1957).

15. C. P. Tzanos. Reactivity and Power Shape Control. Nucl. Sci. Eng. 62, 1 (1977).

16. C. P. Tzanos. Enrichment Zoning and Control Rod Programming for Reactivity and Power Shape Control. Nucl. Technol., 41, 195 (1978).

17. A. Mockel, R. de Wouters, S. Pilate, G. Buckel, E. Kiefhaber, A. Polch, D. Thiem and U. Wehmann. Design and Nuclear Analysis of Large Homogeneous and Heterogeneous LMFBR Cores using Multi-Dimensional Diffusion Codes. International Symposium on Fast Reactor Physics, Aix-en Provence, France, 24-28 (September 1979).

18. R. A. Donrals, WARD, Personal Communication

19. FFTF Shielding Design and Analysis Summary Report, WARD-2171-54 (June 1975).

20. M. D. Carelli, A. J. Friedland, C. W. Bach and R. A. Marketly. An Optimization Method for Orificing LMFBR Cores. Trans. Am. Nucl. Soc., 26 437 (1977).

21. E. U. Khan, W. P. Barthold. Flow Orificing of Large LMFBR Cores with Interassembly Heat Transfer. Trans. Am. Nucl. Soc., 26 452 (1977).

22. E. Novendstern, Turbulent Flow Pressure Drop Model for Fuel Rod Assemblies Utilizing a Helical Wire-Wrap Spacer System, Nucl. Eng. Design, 22, 19 (1972).

23. C. Chiu, N. E. Todreas and W. M. Rohsenow. Turbulent Flow Split Model and Supporting Experiments for Wire Wrapped Core Assemblies. Nucl. Tech, 50, 40 (1980).

24. C. Chiu, N. E. Todreas and W. M. Rohsenow. Subchannel and Bundle Friction Factors and Flow Split Models for Laminar, Transition and Turbulent Flows in Wire Wrapped Nuclear Fuel Assemblies. Thermal Hydraulic Working Group 4th Meeting, Argonne National Laboratory, (April 24, 1979).

25. G. Marbach, P. Millet and R. Peray. Cladding Deformations in RAPSODIE and Consequences. International Conference of Fast Breeder Reactor Fuel Performance, ISBN 089448-105-3, 123 (1979).

26. U. P. Nayjak, A. Boltax, R. J. Shalka, and A. Biancheria. An Analytical Comparison of the Irradiation Behavior of Fast Reactor Carbide and Oxide Fuel Pins. Advanced LMFBR Fuels Proceedings, ERDA 4455, 537 (1977).

27. R. D. Leggett, E. W. Heck, P. J. Levine, and R. F. Hilbert. Steady-State Irradiation Behavior of Mixed Oxide Fuel Pins Irradiated in EBR-II. International Conference of Fast Breeder Reactor Fuel Performance, ISBN 089448-105-3, 2 (1979).

28. P. J. Levine, U. P. Nayjak, et al. Irradiation Performance of WSA-3 -4 and -8 Mixed-Oxide Fuel Pins in Grid-Spaced Assemblies. International Conference on Fast Breeder Reactor Fuel Performance, ISBN 089448-105-3, 143 (1979).

29. E. Edmonds, W. Stloss, et al. Mixed Oxide Fuel Performance. International Conference of Fast Breeder Reactor Fuel Performance. ISBN 089448-105-3, 53 (1979).

30. K. Ulmatsu, Y. Ishida, et al. Irradiation Performance of Mixed Oxide Fuel Pins-Japanese Experience. International Conference of Fast Breeder Reactor Fuel Performance, ISBN 089488-105-3, 16 (1979).

31. K. Ulmatsu, U. Ishida, et al. Experience and Future Plans of Fast Reactor Oxide Fuels Irridiation in Japan. Advanced LMFBR Fuels Proceedings, ERDA 4455, 110 (1977).

32. R. S. Shober, T. A. Daly, and D. R. Ferguson, FX2-TH: a Two-Dimensional Nuclear Reactor Kinetics Code with Thermal-Hydraulic Feedback. ANL-78-79 (October 1978).